Synthesis Towards Spherical Molecules

Inauguraldissertation

zur

Erlangung der Würde eines Doktors der Philosophie

vorgelegt der

Philosophisch-Naturwissenschaftlichen Fakultät

der Universität Basel

von

Manuel Hugo

2024

Genehmigt von der Philosophisch-Naturwissenschaftlichen Fakultät

auf Antrag von:

Erstbetreuer: Prof. Dr. Marcel Mayor

Zweitbetreuer: Prof. Dr. Christof Sparr

externer Experte: Prof. Dr. Michel Rickhaus

Basel, den 14. November 2023

Prof. Dr. Marcel Mayor (Dekan)

_____

„Haraka haraka haina baraka; one step back and two steps forth"

„Eile, Eile bringt kein Glück; tu es Schritt für Schritt"

Acknowledgement

I would like to thank very much to Prof. Dr. Marcel Mayor for giving me the opportunity to perform my PhD-work in his laboratories, allowing me to research with only very little limits and for all the precious counsels he gave me in these four years.

Many thanks to my Co-supervisor Prof. Dr. Christof Sparr, who always came up with a feasible idea especially when the project route was closely impassable.

I would like to express my gratitude to Prof. Dr. Michel Rickhaus for taking over the role of the external expert.

It was always a great pleasure to work in Lab 8 with people who formed me in countless positive aspects. Adriano and Camiel, who I spent the longest time with, I would like to thank you very much for all the funny, instructive and fruitful discussions we had. Thousand thanks to Ksenia for working next to me, having not only chats about science but also fictive stories. A big thank back to you Flo and who knows, maybe we will meet a third time in life somewhere. I would like to thank to Ramon; I have seldom seen such a nearly perfect working mate. Thanks to Linda, who organized not only my interview but also my comfortable start smoothly. Sudhakar, thanks for the support and collaboration especially after lockdown months. Thanks to Tomaš for valuable tips and the gas pistol.

So many thanks to Brian, starting his Wahlpraktikum literally in my fume hood and pursuing his MSc thesis under my supervision. I can say we have grown together during this period. Thanks to my Nano-Blockkurs student Jonathan, it was great to conduct the electrochemical experiments with you.

Many thanks to people from Luv Lab 6: Lolo, my predecessor and Zwicky who are both fathers of the Moon lander project. Thanks to Eric, especially when we tried to hit the thiaspherophane and thanks to Max for all the nice walks we had and to Charlotte for her extra dose of power.

Thanks the people from Rock Lab 4: Laurent, for his calm and super professional attitude and Juraj for all his direct, sarcastic jokes. To Luise and Salome as very cheerful coworkers and Henrik and Hua for their extraordinary humor. Also to Cristian for his gentle being.

I would like to thank people from Park Lab 2: Tim, not only for his IT-support, also for his informative facts; Alfredo, Almu and Hervé, bringing southern power to the group and being the hub for all unforgettable park events. Thanks to Chris, Jia and Valentin for their charm and Raj for his tips.

Thanks to people from Satellite Lab E: To Joël, one of the most pleasant persons I ever worked with and David, representing most how one imagines a chemist. Many thanks to Jesus for his enjoyable working attitude. Also to Loïc and Thomas for their help, whenever needed.

Special thanks to Camiel, Joël, Brian and Adriano for proofreading this work.

Further appreciation to all students in our laboratories during this time. Also to all the students at Uni Basel I was allowed to teach. It was a great pleasure with you!

Big thanks to the NMR-team around Prof. Dr. Daniel Häussinger who I always consulted to solve sophisticated NMR problems. Further I would like to thank Sylvie Mittelheisser, Dr. Michael Pfeffer and Jonas Zurflüh for supporting me whenever I faced analytical challenges concerning molecular masses. Collaborations with Dr. Kate Wolfer and Simon Berlanda from other departments was an additional great help to verify molecules.

And of course to those who keep the institute working: Olaf Lips, Brigitte Howald, Nathalie Plattner-Longhi and Marina Mambelli-Johnson for all the organizational duties. Oli Ilg for making sure the deliverer fulfills and the Werkstatt team around Markus Ast, Andreas Sohler, Andy Koller and Hisni Meha, fixing everything reliably in very short time.

… And many others walking around in the corridors at Uni Basel, it was an awesome time mainly…

In the end, I would like to thank my friends and family, in particular my parents Urs and Margareta and my siblings Andrea and David. I really have the luck to reckon on dozens of helping souls whenever I need help in my life.

And for the very end, I will thank my better half Nicole for all the moments we spent together during this time, and all the moments that follow.

Abstract

Highly symmetric molecules have fascinated scientists in organic chemistry since this research field was established in the middle of the 19th century. Not only because of unknown physical behavior upon perturbation of the electronic shell of such highly ordered compounds, but also overcoming the synthetic challenges by finding appropriate strategies for these extraordinary molecular architectures provides this work a unique character.

This work is divided in two parts A and B, whereby part A focuses on the aimed synthesis of spherical shaped molecules, called **spherophanes**. The closest known molecule which was synthesized is buckminsterfullerene C_{60}, reported in the 1980s. Part B describes the approach towards a **square pyramidal shaped cage molecule**, which combines the hemisphere of a calix[4]arene unit with a flat porphyrin.

Part A: The novelty of synthesizing and isolating this sort of spherical molecules with rigid Ar-bridge-Ar units and hence unpredictable physical behavior was addressed in a variety of target structures (Figure A). Our synthetic methods included dimerization approaches, bottom-up strategies and also one-pot reaction attempts. Elaborated results in this work will guide and support future chemists in their approach to successfully achieve spherophanes.

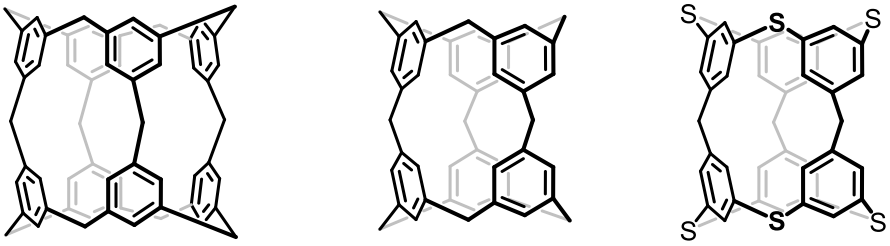

Figure A. Our 3 aimed target structures in this work. All of them consist of Ar-bridge-Ar moieties.

Part B: Combination of the two supramolecular classes of calixarenes and porphyrins resulted in a design where the flat porphyrin unit could optionally be adsorbed on a surface while the calix[4]arene protrudes in a perfect 90° angle. In this work, the synthesis of the molecule (Figure B) was accomplished only when electrochemical reaction technique was applied, which is not often seen in organic synthesis.

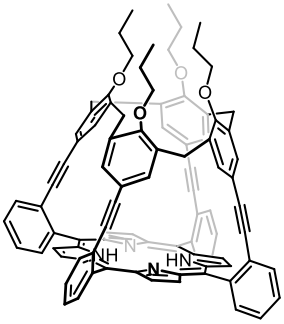

Figure B. Structure of envisioned square pyramidal shaped cage molecule.

Table of Contents

1 Introduction

1.1 Supramolecular Compounds

When Charles J. Pedersen reported alkali metal binding to crown ethers in 1967[1], a milestone was laid for the field of supramolecular chemistry. This branch of science is defined best in terms of considering chemistry beyond a molecule, whereas intermolecular bonds and molecular assemblies are investigated. Donald J. Cram later[2] described interactions between a cavity bearing "host" molecule to recognize its smaller "guest". Thus, for the first time in organic chemistry, the link to biochemical processes (enzyme-substrate complex) was revealed. A facile example of a host-guest system is the trapping of an ammonium cationic species (guest) into an 18-crown-6 ether molecule (host), whereby a two dimensional 2D complex (Figure 1, **1**) is formed. By replacing an ethylene group of the 18-crown-6 compound with a binaphthyl which includes a carboxylate side chain and then applying bulky *tert*-butyl ammonium as cationic guest, a more stable three dimensional 3D complex (Figure 1, **2**) is reported. Important to notice: all host-guest complexes always exhibit a total net charge of zero, which is obtained upon opposing a negative charged counteranion to the positive ammonium charge in the above described example.

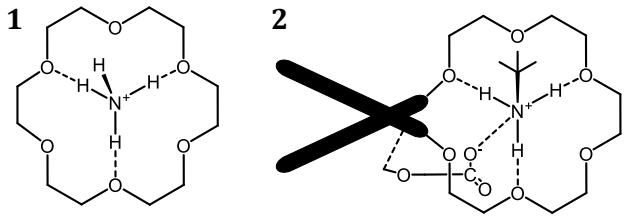

Figure 1. Schematic representation of 2D (**1**) and 3D (**2**) host guest systems. The binaphtyl in **2** is shown as two dark crossed bars for clarity reason.[2]

These initial findings led to the discovery of more supramolecular classes. Cryptands (Latin: *crypta* = cavity) were described first in 1969[3], representing a facile form of 3D host-guest systems where a positively charged metal guest is bound by a bi- or polydentate ligand which has nucleophilic character (Figure 2). The newly formed complex then demonstrates novel characteristics compared to its starting materials and is highly stable under non-acidic conditions. Depending on the lone-pair position of the nitrogen atoms (pointing towards the inside or outside), different conformational equilibria are observed for **3** (Figure 2; **EE**, **NN** or **EN**). These findings substantiate the complexity of investigating supramolecular[4] systems already for small molecules. Noteworthy is the fact to have no cavity in the crystal structure of the pure host, unless guest species move inside. This detail could not be resolved until considering torsion angles in crystal structures of cryptands[5].

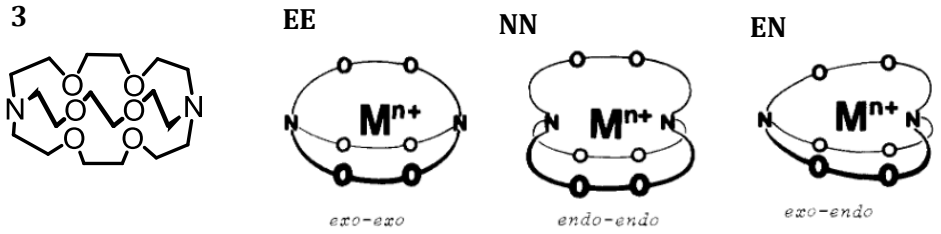

Figure 2. Cryptand host (**3**) and all of its possible conformational equilibrium arrangements upon inserting cationic metals are depicted; **EE**) exo-exo, **NN**) endo-endo, **EN**) exo-endo. Reprinted with permission from Dietrich *et al.*[3], Copyright 1969 Pergamon Press.

More elaborate forms of host-guest systems were pursued to improve the hosts structural recognition for its particular guest[6]. Interesting application fields emerged, as for example having the host as a scavenger for small molecules for purification purposes. Based on all this, by slightly modifying host structures, a high variety of different guests are allowed to enter. Besides crown ethers and cryptands, especially the rigid class of spherands and their hybridization with cryptands (which results in cryptaspherands) or crown ethers (forming hemispherands) were investigated (Figure 3) in the early era of host-guest chemistry.

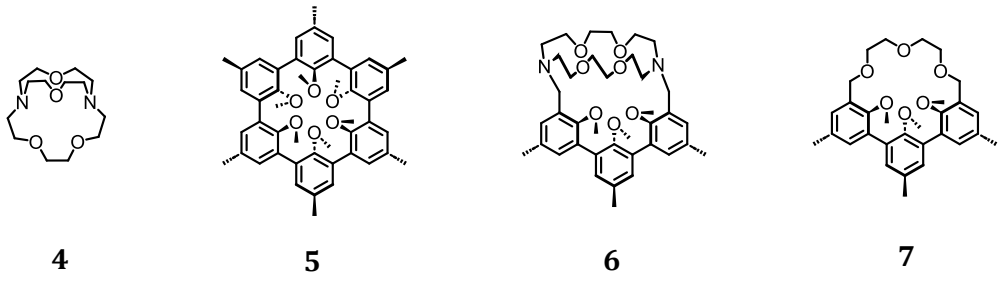

Figure 3. Different subgroups of supramolecular hosts (crpytand **4**, spherand **5**, cryptaspherand **6** and hemispherand **7**) are depicted. The structure resembles the final 3D host-guest form; guest species are omitted for clarity.[6]

In general, the supramolecular class of spherands was synthesized first in 1979[7] to perform higher host-guest performance due to preorganization. These non-rigid spherand systems follow the principle of a quasi-folded electron-rich host without any cavity, but exhibiting a void upon engulfing an electron-poor metal (guest). This is recognized as a shared similarity with crown ethers and cryptands, where without availability of any guest the hosts do not comprise empty cavities since they rather fill themselves intramolecular by folding inwards.

A common framework for spherands are derivatives of cyclohexa-meta-phenylene ([6]-CMP) derivatives (Figure 4, **8** and **9**), which contains six heteroatoms (oxygen) as electron donor and lipophilic methyl groups. In addition to the oxygen to metal dative bond, the carbohydrate moieties avoid cations from passing through the nonpolar sleeve. Hence, Li^+ and Na^+ ions are highly susceptible to be quasi-irreversible scavenged, even at very low concentration from a KOH bulk due

to their better fitting. Complexation using **9** as host molecule has even led to the very fascinating result that no other metal apart from Li^+ and Na^+ is bound to the particular host-guest system[8].

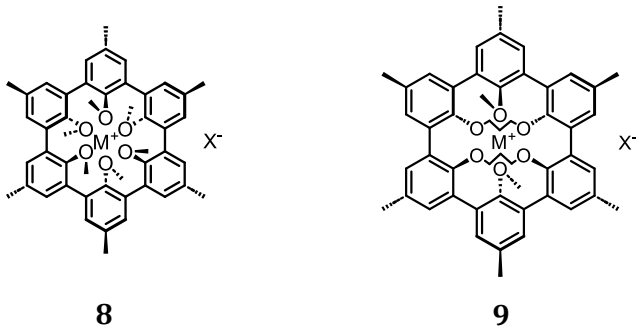

8 **9**

Figure 4. Spherand molecules which consist of a [6]-CMP-framework, depicted without (**8**) and with (**9**) lipophilic bridge. M^+ represents a lithium or sodium cation, X^- a respective counteranion.[8]

While the group of spherands only possesses cavities which are large enough to trap species in the order of magnitude of alkali metals, the desire to synthesize molecules with wider voids then led to the discovery of cavitands. They are represented best by calix[n]arenes, described first by C. David Gutsche[9]. The name refers to the Greek word *calix* for chalice and *arene*, indicating the belt of aromatic rings. First published in 1952[10], ring sizes from calix[4]arene to calix[8]arene (Scheme 1) were obtained in a simple base catalyzed one-pot polymerization reaction of different *p*-alkylphenols in formaldehyde. Upon their first synthesis and purification, the widely applicable cavitand-characteristics of calixarenes were not recognized, since only crystal analysis and physical data was measured instead.

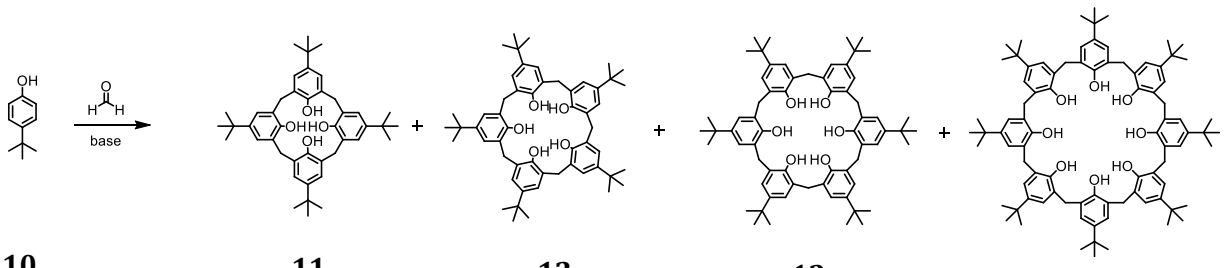

10 **11** **12** **13** **14**

Scheme 1. Reaction equation for conversion of *p-tert*-butylphenol in formaldehyde to *tert*-butylcalix[n]arenes according to Zinke *et al*.[10]

The best known calixarene representatives are calix[4]arene, which is readily obtained by a *retro-Friedel-Crafts* reaction of *p-tert*-butylcalix[4] arene **11** and *p*-methylcalix[4]arene, synthesized first 1957 in a 10 step synthesis[11]. Spectroscopic ^{1}H-NMR measurements of the latter have resulted in different conformational states for the calixarene chalice[12]. Referring to host-guest interactions of calix[4]arenes cavitands, the binding efficiency is determined by its prevalent conformational structure. For this reason, especially the cone conformation (Figure 5, **C**) is of great in-

terest. Unlike seen for spherands – which are strongly limited to trap monoatomic species – calix[4]arenes form complexes with small solvent molecules as chloroform, benzene or toluene with very high tenacities. Disassociation processes were only observed upon prolonged heating at high temperatures and low pressure[13].

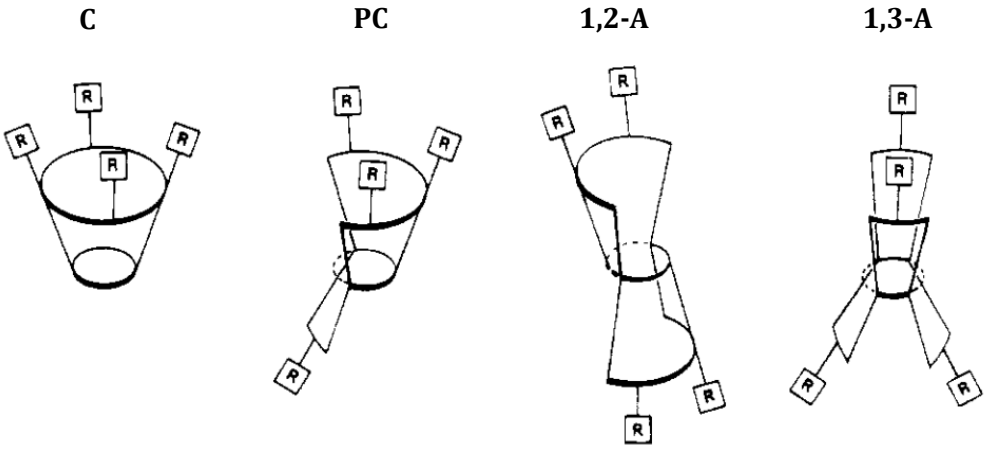

Figure 5. Schematic representation of calix[4]arene conformations; cone (**C**), partial cone (**PC**), 1,2-alternate (**1,2-A**) and 1,3-alternate (**1,3-A**) forms are shown. R refers to an undefined rest. Reprinted with permission from Gutsche *et al.*[12], Copyright 1983 ACS.

The above stated conformational changes of calixarene molecules can be avoided by fixing the upper rim with interlinking bridges. Most prominent example is the etherification of all phenyl groups in calix[4]resorcinarene. The resulting structure (Figure 6, **15**) now resembles a fixed bowl shape[14], hosting small solvent molecules such as sulfur dioxide, acetonitrile or dichloromethane. These findings could be proofed by crystal structure analysis.

So far, all described host molecules have shown characteristics to undergo reversible complexation processes, even when therefore required harsh conditions such as low pH or high temperatures were applied. Since all of these examples have one face side opened like hemispherical objects, the interior species is not ultimately trapped. Carcerands (Figure 6, **16**) represent the interlinkage of two hemispheres to a proper sphere where guests are captured irreversibly (*carcer* refers to prison in Latin). The first carcerand published by Donald J. Cram contains two resorcinarene units[15]. Resorcinarenes represent with calixarenes a common class of starting material for the synthesis of spherical compounds. As Aristotle stated: "*nature abhors a vacuum*" applies as well to the here presented carcerands. FAB (fast atomic bombardment) mass analysis has shown the encapsulation of several organic and inorganic species (Figure 6, **Guests**) in Cram's compound **16**. These carcerand-guest complexes can be found in certain literature as carceplex and show low solubility in commonly used solvents. In recent years, carcerands were used in a number of studies as for example the purification of C_{60} and C_{70} fullerenes[16] and the removal of toxic arsenic via imprisoning[17].

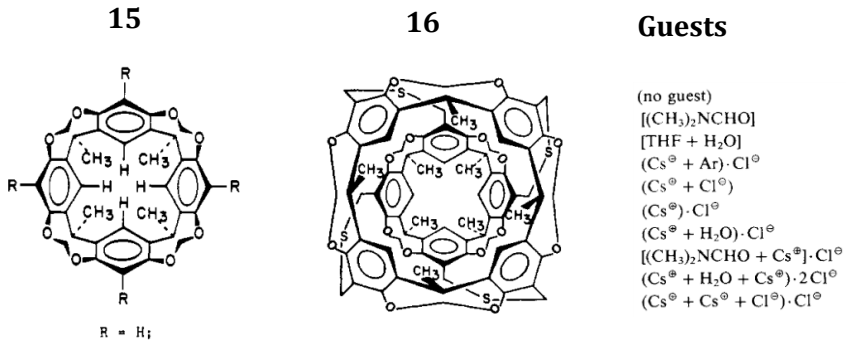

Figure 6. 3D structures of resorcinarene cavitand (**15**) and resorcinarene based carcerand (**16**). Identified guests by fast atomic bombardment (FAB) spectrometry (**Guests**). Reprinted with permission from Cram *et al.*[14], Copyright 1985 ACS.

The original idea to simulate biochemical processes with supramolecular systems has been achieved to a certain extent thanks to all of the successfully synthesized and isolated cavity bearing host-guest systems. A step further towards mimicking enzymes is the autoencapsulation through intermolecular forces[18,19], where the cavity size is varied depending on guest solvation and assembly of the dimeric host. Moreover, the application of arenes as a catalytic shell eventually was established when selective acetal hydrolysis[20] and unprecedented terpenoid skeleton synthesis[21] was reported.

1.2 Fullerenes and Phanes

The synthesis and characterization of the highly spherical carbon allotrope buckminsterfullerene C_{60} **25** (also known as buckyball) was reported first in 1985 by Harold W. Kroto *et al.*[22] The techniques involved carbon vaporization into a helium stream for synthesis whereas analysis was conducted by time of flight (TOF) mass spectrometry. Its icosahedral symmetry group I_h offers the possibility to exhibit unusual properties when placing an atom in its interior, as for example remarkable NMR shifts due to ring currents. C_{60} was characterized as a new form of carbon in a solid form first in 1990 by mass and infrared spectrometry in addition to X-ray diffraction[23]. The synthesis of fullerene C_{60} usually resulted in a mix of fullerenes with a higher molecular weight as byproducts (e. g. fullerene C_{70}). In a 12 step synthesis[24] (Scheme 2) the first rational organic reaction towards C_{60} was published, whereby the last step included a flash vacuum pyrolysis at 1100 °C.

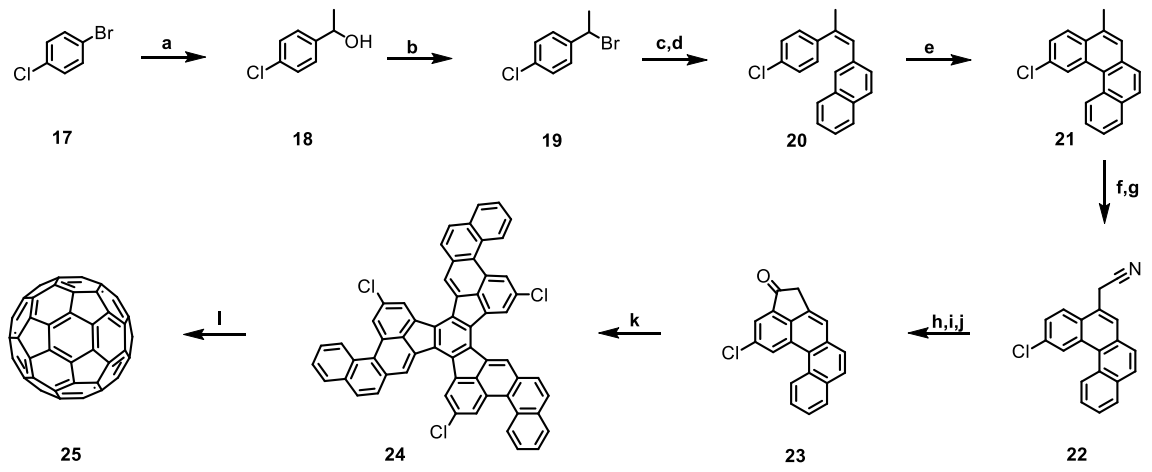

Scheme 2. 12 step reaction pathway to fullerene C_{60} **25** according to Scott *et al.*[24] Conditions: **a**) 1. Mg, ether, 2. acetaldehyde, 97% **b**) PBr_3, benzene, 86% **c,d**) 1. $P(C_6H_5)_3$, toluene; 2. $LiOCH_2CH_3$, 2-naphthaldehyde, EtOH/DCM, 71% **e**) I_2, propylene oxide, UV_{254}, cyclohexane, 92% **f,g**) 1. NBS, benzoyl peroxide, CCl_4; 2. KCN, tetrabutylammonium hydrogensulfate, water/DCM, 93% **h,i,j**) 1. KOH, ethylene glycol; 2. $SOCl_2$; 3. $AlCl_3$, DCM, 51% **k**) $TiCl_4$, orthodichlorobenzene, 85% **l**) flash vacuum pyrolysis, 1100 °C.

Higher fullerenes as for instance C_{70}, C_{76} or C_{84} were then synthesized under identical conditions as C_{60} and isolated upon derivatization with *ortho*-quinodimethane from the crude mixture using either column or HPLC chromatography[25]. These larger fullerene representatives show deviating degrees of local curvature of the fullerene spheroid and hence no perfect I_h symmetry is attained. As a consequence, asymmetric osmylation experiments using OsO_4 as reagent have shown greater strain relief and therefore a higher kinetic reactivity for these larger spheres[26].

To step into supramolecular chemistry, possible host-guest interactions for fullerenes (also known as endohedral complexes) were investigated. Low yielding results were published over laser vaporization[27] (insertion of metals) or high pressure conditions[28] (insertion of noble gases).

Techniques to open fullerenes in a controlled manner have developed from 1995 when Fred Wudl presented (Scheme 3) controlled opening of fullerenes[29]. One sp^2-sp^2 bond of the hardly soluble C_{60} fullerene[30] was broken upon addition of azides[31] and the adjacent double bond was oxidized under irradiating conditions. This intermediate was prone to be cleaved to final diketone (Scheme 3, step b).

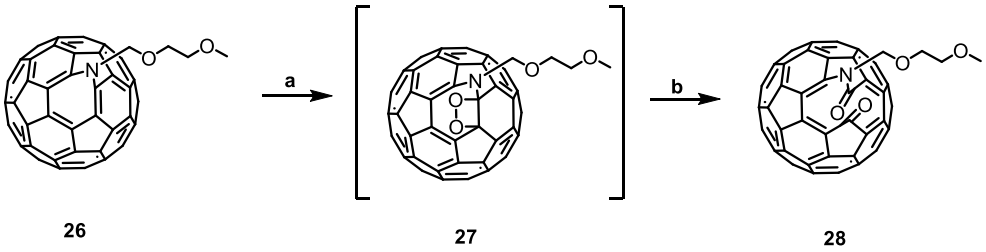

Scheme 3. Controlled opening of fullerene C_{60} derivative **26** is shown. Starting material was synthesized by exposing fullerenes to azides according to Prato *et al.*[31] Conditions: **a**) hν (500HN filtered flood lamp), 1,2-dichlorobenzene, 25-30 °C, 3 h **b**) subsequent reaction 64%.

Molecular surgery became an adequate expression for the opening and closure of fullerenes. The latter was conducted the first time when one H_2 molecule was fully encapsulated in the C_{60} sphere[32] and following purification was accessible by conventional physical methods. Before that, the deposit of one H_2 molecule in an opened C_{60} cage, resembling a cavitand with guest insertion, was reported[33]. Of great interest is the formation of additional endohedral fullerenes, as for example the first synthesis and characterization (^{1}H-NMR, exact mass *m/z*) of a CH_4 molecule which is encapsulated in a C_{60} shell, defined as CH_4@C_{60} (Figure 7)[34]. The CH_4 proton signal in the CH_4@C_{60} ^{1}H-NMR spectrum was found at an immense upfield shift, lower than -5.5 ppm, due to strong ring currents of C_{60} (Figure 7, left).

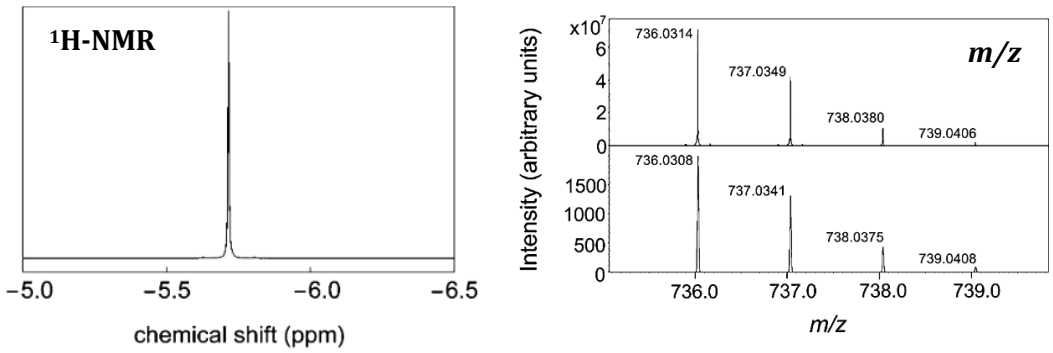

Figure 7. ^{1}H-NMR chemical shifts of CH_4 (left) and high resolution atmospheric pressure photoionization (APPI) mass spectrum (right) are shown. Reprinted with permission from Bloodworth *et al.*[34], Copyright 2019 Wiley.

Furthermore, when C_{60} is doped with alkali metals, physical measurements could prove the first existence of a 3D organic conductor[35]. Soon afterwards, superconductivity was observed at a transition temperature of 18 K by applying potassium as dopant (K_xC_{60}) which was validated by magnetic field dependent microwave absorption and resistivity experiments (Figure 8)[36]. Additional investigations using K_3C_{60} resulted in a large transition temperature decrease upon higher applied pressures[37].

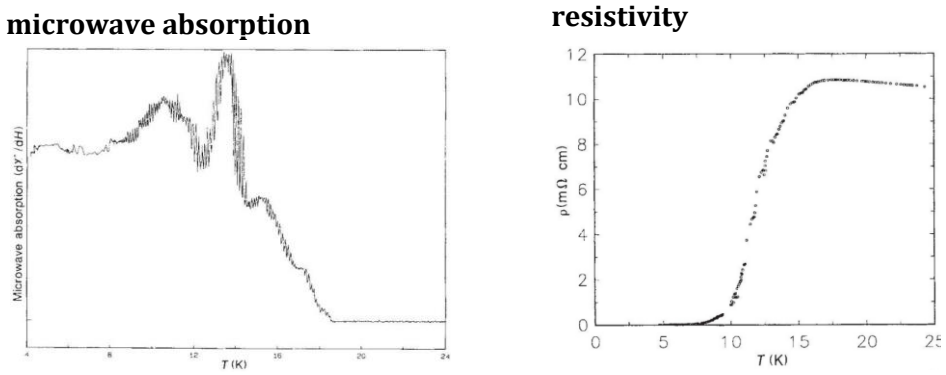

Figure 8. Proof of superconductivity onset at 18 K. Reprinted with permission from Hebard *et al.*[36], Copyright 1991 Nature Publishing Group.

Since C_{60} is a strong electron acceptor, it intercalates electron donors such as alkali metals which gives fulleride salt stoichiometries with the general formula of A_xC_{60}. Thereby, X can vary from 1 (e.g. CsC_{60}) to 12 (e.g. $Li_{12}C_{60}$), while C_{60} is reduced to oxidation states between –I and –VI. Mainly A_3C_{60} salts show metallic composition and therefore exhibit superconducting characteristics. The direct comparison among various alkali metals incorporated into fullerene C_{60} indicates a tendency to grand influence of the formed lattice[38]. As an example, Rb_3C_{60} exceeds the transition temperature T_c (Curie temperature) of K_3C_{60} by 10 K (Figure 9, left). Superconductivity is explained reasonably by assuming a high alkali metal doping together with $(C_{60})^{n-}$-species exerting partial occupation of the t_1g state (LUMO+1) (Figure 9, right).

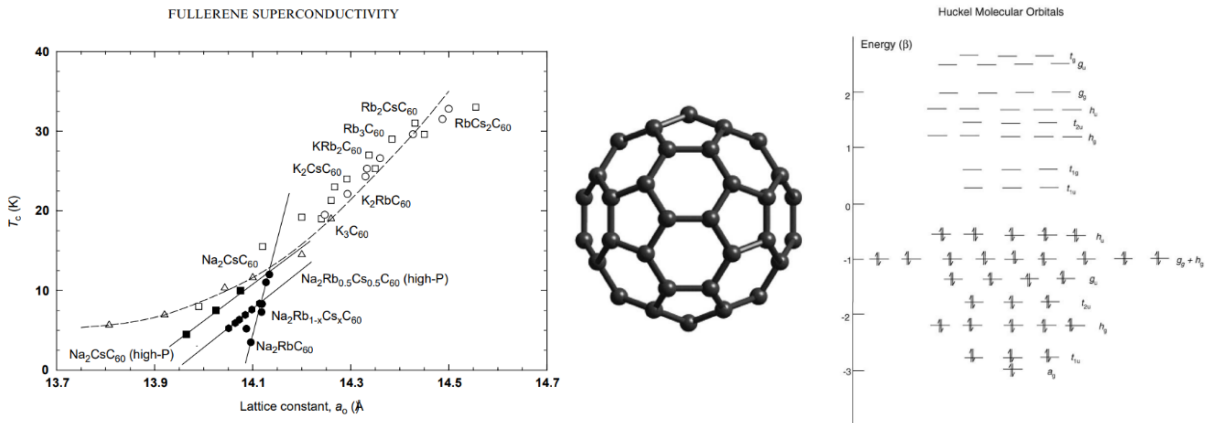

Figure 9. Transition temperature dependence T_c of lattice constants of different A_3C_{60} compounds is shown on the left. Hückel molecular orbital of C_{60} is shown on the right. Reprinted with permission from Margadonna *et al.*[38], Copyright 1991 Nature Publishing Group.

Calculations even predict the existence of $(C_{60})^+$ upon charge separation, when F_2 donates an electron to build endohedral fullerene $F_2^-@C_{60}^+$.[39]

In co-crystallization experiments of C_{60} with organic donor tetrakis(dimethylamino)ethylene (TDAE), air sensitive black crystals $C_{60}(TDAE)_{0.86}$ were isolated[40]. Measurements in magnetic fields from 0.1 to 1000 Oe have validated it as a truly organic ferromagnet with a high Curie temperature T_c of 16.1 K.

At this point, the molecular class of phanes is introduced, which is defined by an aromatic unit interlinked with an aliphatic chain. Unlike fully sp^2 hybridized fullerenes but similar to calixarenes, sp^2 and sp^3 hybridized carbon atoms are present in these molecules. The cyclic form cyclophane is well known in chemical research. A popular example is [2.2]paracyclophane **31**, which is used increasingly as a scaffold in molecular design, due to application possibilities in organic photonics and electronics[41]. Recent work in our group has shown quantum interference effects which were controlled by the substitution pattern of [2.2]paracyclophane[42]. Its synthesis and discovery was achieved first in 1949 after low pressure pyrolysis of *p*-xylene[43], but named and synthesized in controlled manner in 1951 (Scheme 4)[44] by *Wurtz*-coupling of benzylic dibromides.

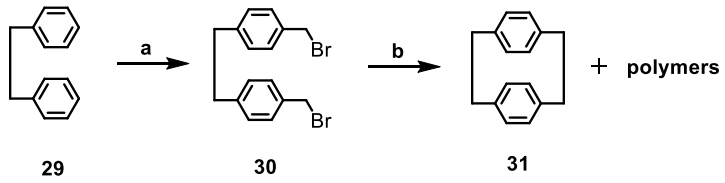

Scheme 4. Synthetic route of [2.2]paracyclophane **31** according to Cram *et al.*[44] is depicted Conditions: **a**) HBr, HCOH **b**) Na.

The synthesis of more strain relieved [6]paracyclophane **35** is synthesized from spiro compounds in a *Bamford-Stevens* type reaction[45], followed by a pyrolysis rearrangement at 250 to 400 °C (Scheme 5). These benzene derivatives with meta- or para-bridged macrocyclic systems are also called *ansa* (Latin: handle) compounds.

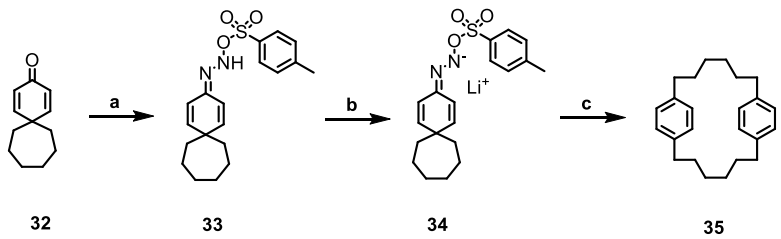

Scheme 5. Synthesis of [6]paracyclophane **35** according to Kane *et al.*[45] is depicted Conditions: **a**) tosyl hydrazine **b**) lithiation **c**) flash pyrolysis at 250 to 400 °C; overall GC-yield of 5-10%.

Other *ansa* compounds have been reported recently in our group when pyrene was interlinked to pyrenophane via aliphatic chain[46].

A further example in cyclophane chemistry is cage-like superphane **46**, published first in 1979.[47] The synthesis was accomplished in ten steps under high temperature and low pressure conditions (Scheme 6). Recent calculations[48] explain structural changes of endohedral cation-superphane complexes, which is illustrated best by the swelling process of the phane cage. Charge and radius of the trapped monoatomic cation determine the stability of the complex. In addition, exohedral cation-superphane complexes were calculated, where the cation is either located above the benzene ring (in front of the superphane window) or in equatorial position (centered to C-C spacer bonds).

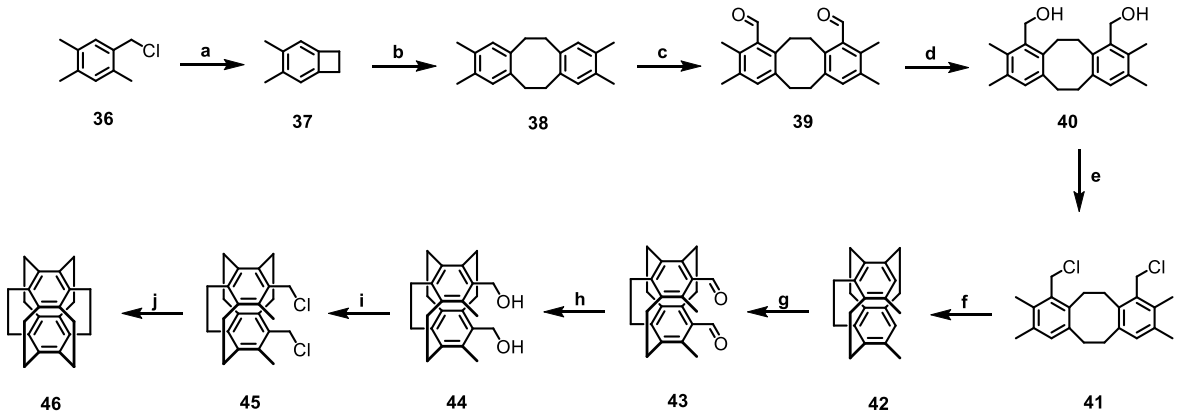

Scheme 6. Superphane **46** synthesis in a ten step reaction path according to Schirch *et al.*[47] Conditions: **a**) 710 °C, 10^{-2} Torr, 48% **b**) diethyl phthalate, 300 °C, 50% **c**) formylation, 49% **d**) $NaBH_4$, quant. **e**) $SOCl_2$, quant. **f**) 700 °C, 10^{-2} Torr, 40% **g**) formylation, 75% **h**) $LiAlH_4$, quant. **i**) $SOCl_2$, quant. **j**) 650 °C, 10^{-2} Torr, 40%.

1.3 Spherophanes

As most of the so far described supramolecular molecules are possible to synthesize, isolate and characterize, we now focus on the synthesis of strained spherical molecules, which are scarce in literature.

While spherands and cavitands demonstrate how (small) guests are trapped by their hemispherical host conformations to change characteristics such as polarization, they all remain limited to a hemispherical shape. On the other hand, fullerenes are eligible as well to incorporate small species and exhibit, in case of C_{60}, a perfectly icosahedral I_h symmetry. But their operative spectrum is limited due to challenging synthetic routes. Two years before Harold W. Kroto published fullerenes[22], Donald J. Cram inspired chemistry community by presenting a hypothetic new class of cavitands[49] in 1983: "closed spherical cavitands" with a hypothetic centered guest molecule, filling its void. When these syntheses succeed, physical properties of the shell (host) and the guest can be compared to the entire host-guest system. The proposed structures consist of either 6 or 12 aromatic units, each bearing 2 hydrogens in para position and are interlinked by 9 (**47**) or 24 (**48**) simple bridging groups (e.g.: $-CH_2-$, -0-, -S-, -NH-, C=O, $-CH_2-CH_2-$, $-0-CH_2-O-$). $-CH_2-$ was chosen for the model compounds (Figure 10), as it is the most strain releasing of all mentioned bridges, which only contain one atom between the aromatic units.

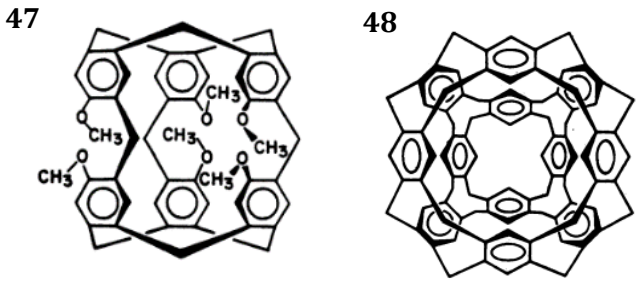

Figure 10. Envisioned closed spherical cavitands containing either 6 (left) or 12 (right) aromatic rings. Reprinted with permission from Cram *et al.*[49], Copyright 1983 AAAS.

First accomplishments towards this vision were achieved by Gabard *et al.*[50], whereby the synthetic strategy was adapted in a way that $-O-CH_2-CH_2-O-$ bridges led to appropriate feasibility to synthesize his target compound **49** (Figure 11). The presence of one equivalent chloroform as guest was detected by elemental analysis and verified by NMR-techniques and mass spectrometry.

49

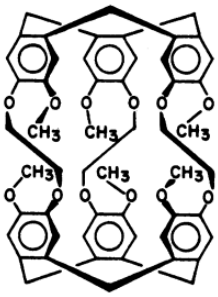

Figure 11. Synthesized spherical cavitand according to Gabard *et al.*[50], Reprinted with permission from Cram *et al.*[49], Copyright 1983 AAAS.

In 1992, R. Ross *et. al*. proposed the molecular class of spherophanes[51] in their publication "*Polarizabilities of Hollow Spherical Organic Molecules with Encapsulated Cations*". Target molecule is a cuboctahedral compound, which consists of 8 benzene rings interlinked via 12 bridges (heteroatomic: -S- or -O-; homoatomic: $-CH_2-$) in a 1,3,5-substitution pattern on the aromatic ring (Figure 12, left). The chosen name spherophane derives from two word definitions: cyclophane as it is the main characteristic unit of the structure and the word sphere, referring to its shape. Assuming spherophanes as 3D organic metals, expectations arose of unpredictable counterion effects. This is explained best in Figure 12 (right) where a "traditional" organic salt is compared to a charged heterospherophane. The former appears in a stacked form (bearing a positive or negative charge) with having the respective counterions next to it while the spherophane is expected to engulf the ion alike a host-guest system. Thereby the spherophane shell itself remains neutral in charge.

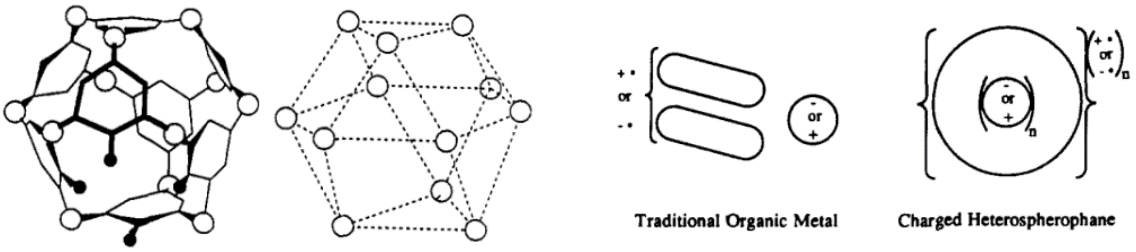

Figure 12. Left: Dreiding model of a spherophane whereby the open circles represent heteroatomic bridges. In the right model, benzene rings are omitted to indicate cuboctahedral structure. Right: comparison between a traditional organic metal and charged spherophane, where the charged counterion is engulfed in the neutral shell. Reprinted with permission from Ross *et al.*[51], Copyright 1992 ACS.

Permanent dipole moments and electric and thermal polarizabilities were calculated for neutral heterospherophanes (thiaspherophane for -S- or oxaspherophane for -O-) bearing a charged encapsulated singly ionized cation. While thiaspherophane exhibits a low permanent dipole at low temperatures and none at high temperatures, oxaspherophane possesses a strong permanent dipole moment at any temperature. High temperatures result in high polarizability for thiaspher-

phane (contribution through electronic and ionic motion) and low polarizability for oxaspherophane (contribution only through ionic motion). Interestingly, at low temperatures polarizability values are reversed for both heterospherophanes. Inspired by the highly symmetrical architecture and its eventual electrochemical behavior, spherophanes are the main topic of this thesis.

Computational studies suggest lower energetic barrier for H_2 insertion in spherophanes compared to fullerenes[52,53]. Therefore, the diameter pore between four adjacent aromatic hydrogens of four different model-spherophanes (spher1 = no bridge; Meth2 = -CH_2- bridge; Oxa3 = oxaspherophane; Thia4 = thiaspherophane) was calculated (Figure 13, left). Once H_2 is inserted into spherophanes, a stabilizing effect of H_2@Spher1, H_2@Meth2, H_2@Oxa3 and H_2@Thia4 has resulted from computational modelling. The H_2 insertion was studied and energy-levels are shown in Figure 13 (right), indicating a stabilizing effect especially when H_2 is found in the center of the spherophane. Not only because of low insertion energy, but also a finally very stable H_2@spherophane host-guest system along with low releasing energy values, makes Meth2 and Thia4 to possible candidates for H_2 storage cages.

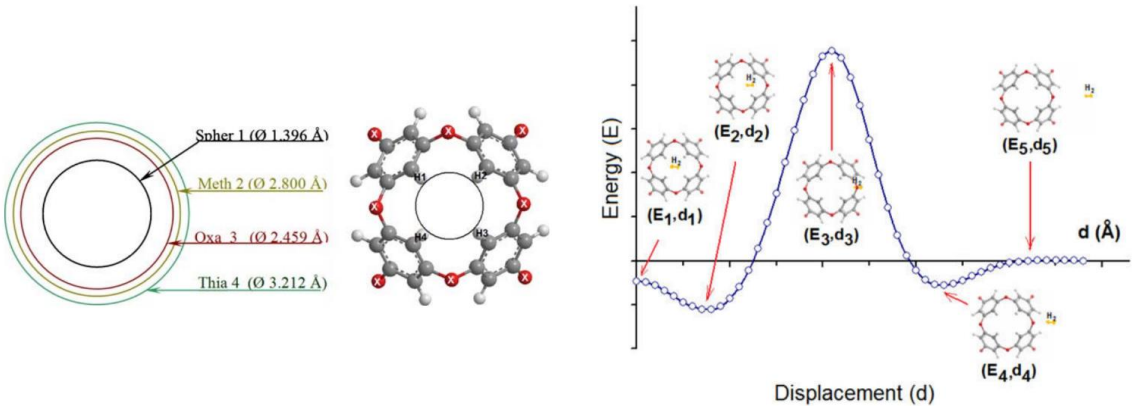

Figure 13. Left: Pore diameters of four different spherophanes, the entrance for H_2 insertion is marked with a circle. Reprinted with permission from Saal *et al.*[52], Copyright 2009 Springer. Right: Dependence of H_2 displacement for the particular energy level. Reprinted with permission from Saal *et al.*[53], Copyright 2009 Elsevier.

So far, spherophanes remain a fully hypothetic model and its stability is not guaranteed. Known issues are its conformational rigidity and its unidentified physical behavior. Calculations[51] indicate approximate diameters of 5 Å for oxaspherophane and 7 Å for thiaspherophane. This is close to the known C_{60} fullerene diameter of 7 Å,[54] which characteristics one aims to mimic by the first synthesis of spherophanes. In previous work, thiaspherophane has been chosen as target molecule, since it is expected to potentially show interesting electrochemical properties upon removing one electron from the shell, due to perturbation of the fully conjugated, highly ordered symmetry. Furthermore, the synthesis of a cavitand consisting of *meta*-substituted diphenyl sulfide moieties has already been achieved in only two reaction steps[55] by West *et al*. Recently, Lorenzo Delarue Bizzini[56] described the most concise evidence for a thiaspherophane derivative (Scheme 7), where the *m/z* of **54** was measured by high resolution ESI spectrometry (Figure 14).

The superimposed isotope pattern of the mass spectrum fits for singly deprotonated **55** and hydrodehalogenated **56** forms of **54**.

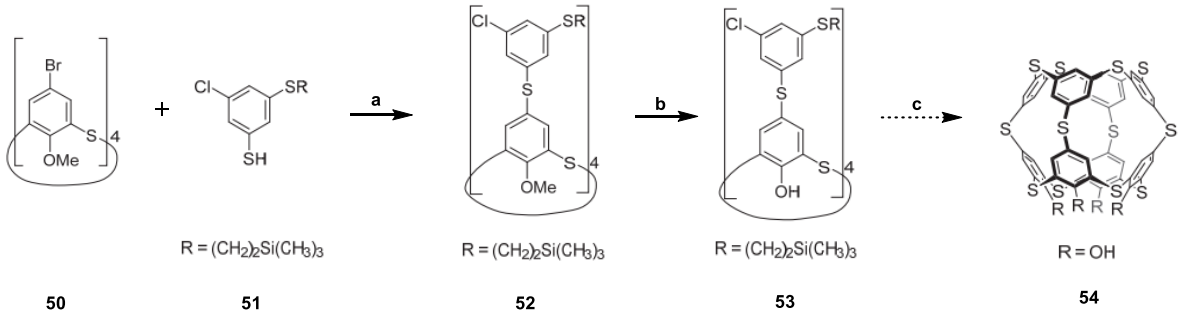

Scheme 7. Last three reaction steps to possible thiaspherophane derivative **54** according to Bizzini[56] are shown. Conditions: **a**) xantphos, $Pd_2(dba)_3$, t-BuONa, toluene, 110 °C, 5h, 79% **b**) BBr_3, DCM, -78 °C to rt, 16 h, 98% **c**) CsF, N,N-dimethylacetamide, 170-200 °C, 2 h, only traces seen by high resolution ESI and MALDI-TOF.

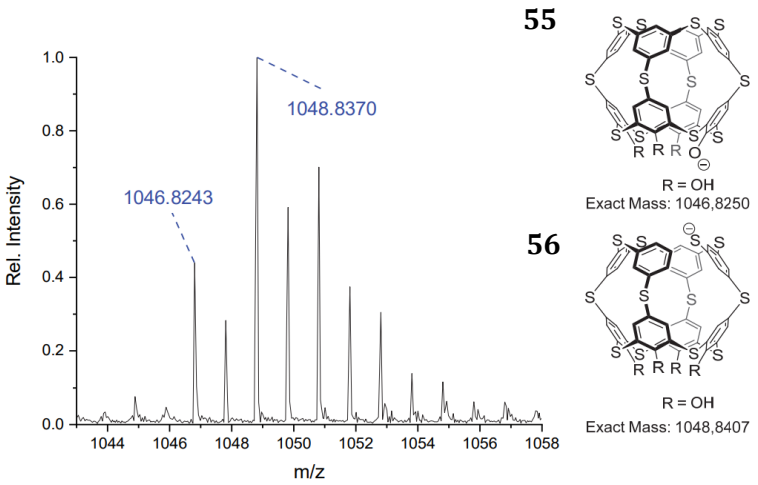

Figure 14. High resolution ESI with superimposes isotope pattern of molecules **55** and **56**.[56]

Previous attempts to isolate thiaspherophane were performed by Markus Gantenbein[57] in a wrap approach to eventually synthesize this spherical compound. Thereby, a thiacalix[6]arene precursor **57** containing two functionalized aromatic rings was exposed to undergo S_NAr reaction (Scheme 8). Overall, four new S-Ar sulfide bonds were planned to be formed by thiolate attack to the Ar-F bond. Even after extensive screening, no thiaspherophane was detected by TLC, DART-MS and ^{1}H-NMR measurements. Nevertheless, this project shows the first reported experiment to synthesize thiaspherophane from a precursor which comprises all atoms present in the desired target compound.

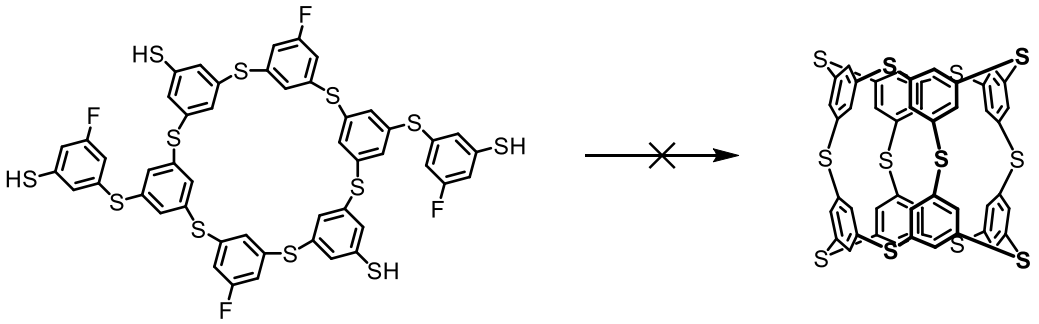

57 **58**

Scheme 8. Asymmetric sphere closing attempts from **57** by fourfold S_NAr attack of thiolates to aryl fluorides according to Gantenbein[57], with thiaspherophane **58** as target compound is shown. Screening conditions: $NaN(SiMe_3)_2$, DMA, 90 °C, 3 d; $NaN(SiMe_3)_2$, DMI, 90 °C, 3 d; K_2CO_3, DMSO, 90 °C, 3 d; NaH, DMI, 90 °C, 3 d.

As explained above, the synthesis and full characterization of spherophanes (with thiaspherophane as aimed target compound) remained hypothetical. When examining state of the art of small molecular cages, research tends to larger molecules, which resemble spherophanes only in regard to have a high symmetry, cavities and spherical shape. But their number of bridging units and hence, the diameter is considerably larger. In the following section some of these structures are presented:

A commercial available starting material for synthesizing spheres are hemispherical shaped calixarenes, well investigated by C. David Gutsche[58]. Before spherophanes were defined in the early 1990s, cavitand was the common expression for such molecular systems. An easy strategy for synthesizing cavitands is the mono-,double- or fourfold linkage of easily accessible hemispherical starting material as for example calixarenes[59] by Böhmer *et al*. Different aliphatic chains were applied (-$C(CH_3)_2$-, -$(CH_2)_5$-, -$(CH_2)_8$-, -$(CH_2)_{12}$-) as interlinking bridges, whereby the shortest -$C(CH_3)_2$- linkage **61** resembles most our desirable narrow sphere with a cage diameter of 5-10 Å. Its synthesis is shown in Scheme 9. Reaction path **a** using tetrabromomethylated diphenol yielded higher spherical product **61** than path **b**, albeit reaction conditions were same.

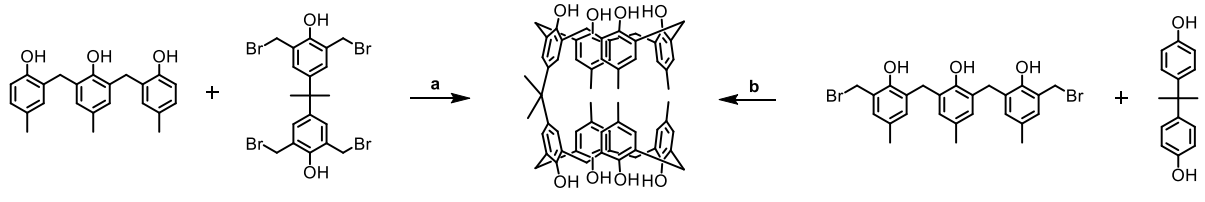

59 **60** **61** **62** **63**

Scheme 9. Synthesis of mono linked calix[4]arene dimer **61** from easy accessible starting materials, according to Böhmer *et al*.[59] **a**) $TiCl_4$, dioxane, reflux, 10-13% **b**) $TiCl_4$, dioxane, reflux, <10%.

Applying the same reaction conditions as in Scheme 9, double (**64**) and fourfold (**65**) interlinked calixarenes were isolated (Figure 15). Both of them represent the molecular class of cavitands and from a synthetic point of view, indicate a preference for longer interlinkage chains upon increasing number of bridges.

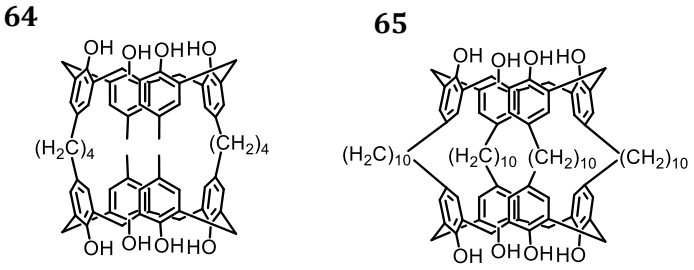

Figure 15. Cavitand consisting of two Calix[4]arenes which are linked via two isobutyl chains **64** or their fourfold interlinked version via isodecyl chains **65**.[59]

In a work, which focuses closer on reversible host-guest interactions, two calix[4]resorcinarene derivatives were dimerized via self-assembly reaction in propan-2-ol[60]. Initial incentive was the better understanding of biological models, resulting in a cavity bearing sphere by simple hydrogen bonding of two concave monomers. Eight propan-2-ol molecules are involved in the resulting donor-acceptor system **66**, stabilized by resorcinarene-O-H-O-propan-2-ol hydrogen-bonds (Figure 16).

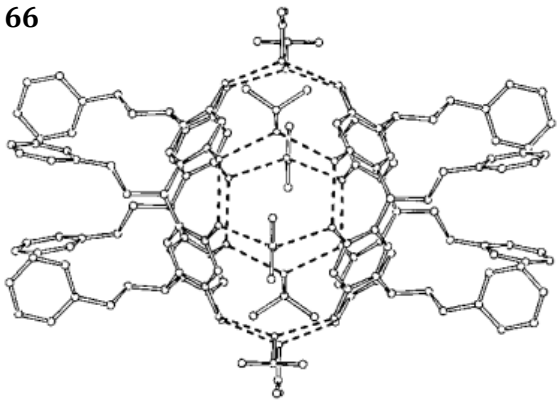

Figure 16. Spherical cage **66** is formed upon solvent mediated dimerization of two calix[4]resorcinarene derivatives. Hydrogen atoms are omitted for clarity. Reprinted with permission from Rose *et al.*[60], Copyright 1998 RSC.

Michael Mastalerz and his group reported a cuboctahedral cage[61], consisting of 12 triptycene tetraol molecules **68** and 8 1,3,5-benzenetriboronic acid **69** units to form 48 boronic ester bonds **70** (Figure 17). While the cuboctahedral Archimedean solid structure of this new compound resembles the complexity of spherophanes in a sense of architecture, its synthesis is greatly straightforward by simply heating the starting materials in chloroform (Figure 17, left). Also the inner diameter of 26 to 31 Å exceeds calculated spherophane cavities by a four- to sixfold dimension (Figure 17, right). Due to solubility issues of non-alkylated triptycene tetraol **67**, no respective cage is formed.

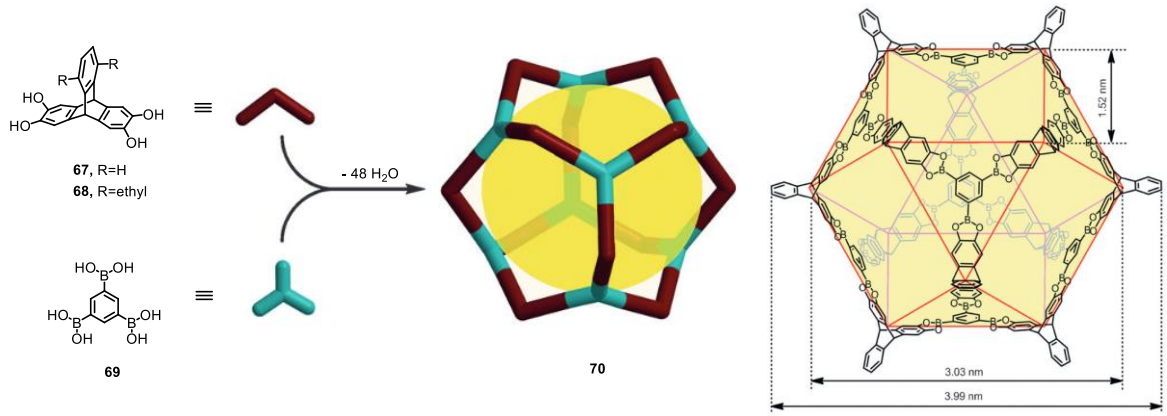

Figure 17. Simple synthesis of the cuboctahedral cage (left). The inner diameter lies between 26 Å at minimum and 31 Å at maximum. The ethyl groups in the molecular cage (right) are omitted for clarity. Reprinted with permission from Zhang *et al.*[61], Copyright 2014 Wiley.

The group then synthesized a smaller cage molecule **73** with smaller diameter (11 to 12 Å)[62]. Shape persistence was kept by covalent imine bond formation and its cuboctahedral form is guaranteed by 8 benzene rings interlinked via 12 imine bridges. The synthesis is conducted as an imine condensation in acetonitrile at room temperature from triethyl-substituted triamine **71** and triethylbenzene-tricarbaldehyde **72** (Scheme 10). Hence, an analogue to spherophanes in regard to the amount of aromatic rings, number of bridging units and diameter was accomplished.

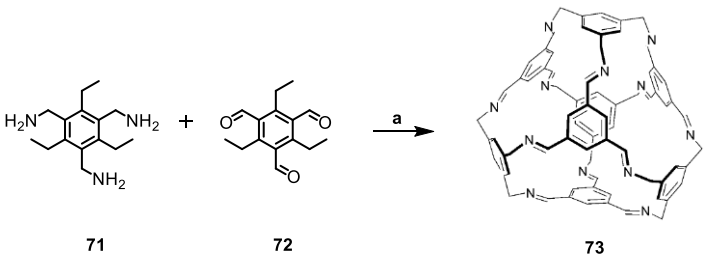

71 72 73

Scheme 10. 12-fold imine condensation to target structure **73** according to Lauer *et al.*[62] Ethyl groups are omitted for clarity. Conditions: a) acetonitrile, rt, 3 d, 47%.

1.4 Introduction of Porphyrins

One of the most fascinating natural products which is absolutely required for countless of key processes in living organisms represents the class of porphyrins. As a component of hemoglobin, cytochrome c and chlorophyll it is involved in oxygen transport, electron transport and photosynthesis[63]. Besides its biochemical functions, also its physical behavior at interfaces is of great interest[64]. A related structure to porphyrins is corrin[65], which is a main component of the well investigated vitamin B_{12}, a very demanding vitamin which ensures formation of blood cells and neural shells. The isolation and description of porphyrin-derivatives from biological everyday objects reaches back at least to Greek philosopher Hippocrates. A well-known characteristic of porphyrins was discovered in 1883, when Jacques-Louis Soret analyzed blood samples to find a strong absorption maximum at around 400 nm, the so called Soret band[66]. The investigation of the first proper laboratory synthesis was published by Paul Rothemund in 1935.[67] Therein, four pyrroles condensate with four molecules of formaldehyde to a porphyrin **77** or in case of acetaldehyde to meso-tetramethylporphyrin **78**, both detected by absorption spectroscopy. Addition of oxidizing agents such as $CaCO_3$/MgO or $PbCrO_4$ led to an increased yield (Scheme 11).

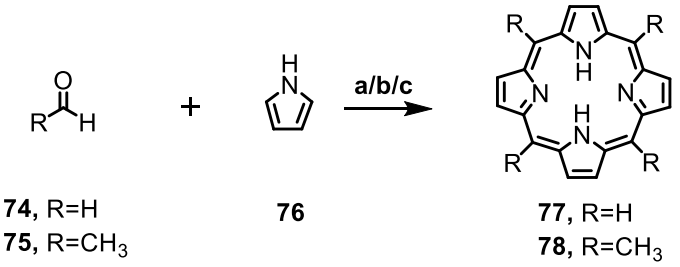

Scheme 11. Rothemund porphyrin synthesis from fourfold condensation of four pyrrole units with aldehyde (formaldehyde or acetaldehyde). Conditions: **a)** aldehyde, MeOH, rt, weeks **b)** aldehyde, MeOH, 65 °C, 25 h **c)** aldehyde, MeOH, 90 °C, 20 h.[67]

Similar reaction conditions and the usage of a variety of aldehyde starting materials then allowed the formation of a number of *meso*-substituted porphyrins including tetraphenylporphyrin[68]. Improvements to that procedure was not made before 1967[69], when less harsh reaction parameters were used by refluxing the reaction mixture only for 30 min. in propionic acid. However, the yield did still not exceed 20%.

This issue overcame Jonathan S. Lindsey in 1986 [70] by condensation of pyrrole and benzaldehyde in an equilibrium reaction to tetraarylporphyrinogen **81**. By subsequent addition of an oxidant he formed the respective porphyrin irreversibly. Condensation was supported by a Lewis acid catalyst (BF_3 or TFA) and oxidation performed after 1 h reaction time by 1,4-benzoquinone derivatives[71] (Scheme 12). Formation of porphyrinogen **80** strongly depends on concentration, showing only little ring closure in either highly diluted or concentrated experiments. Purification of a broad scope of porphyrin derivatives was achieved after performing short chromatography.

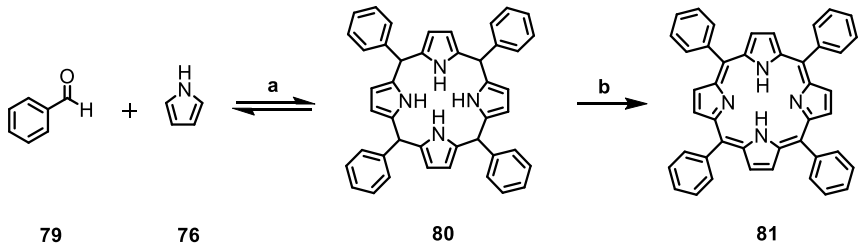

Scheme 12. Lindsey porphyrin **81** synthesis by *in situ* oxidation of porphyrinogen **80**. Conditions: **a)** triethyl orthoacetate, BF_3 etherate, DCM, rt, 1 h **b)** *p*-chloranil, 39 °C, 1 h, 40-45%.[71]

As an alternative route to obtain *trans*-porphyrins, pyrrole can be added in excess to synthesize dipyrromethanes first. These react further with an aldehyde to the respective porphyrin[72].

Apart from above mentioned *in vivo* functions of porphyrins, electrical properties are of great interest, such as applications in optical devices or material science. One example is the electric charge transport over long distances, well known that conductivity decreases upon increasing length. Exceptionally, by fusing porphyrins, the opposite effect was observed when the porphyrin-oligomers were employed in break junctions to function as molecular wires[73]. Other monomeric[74] and dimeric porphyrin molecules were applied in break junction experiments[75,76]. Furthermore, the role of porphyrins on clean solid surfaces has been investigated intensively in recent decades. After the technique of scanning tunnel microscopy (STM) to determine conformation of large molecules (e.g. porphyrins) on surfaces has been established[77], porphyrin sublimation on Au(111) has shown nonplanar adsorption behavior[78]. Another irregularity was reported upon vapor deposition of iron triphenylcorrole on Cu(111), which resulted in restricted symmetry on the functionalized surface[79].

1.5 Electroorganic Synthesis

A raised demand for sustainability in chemical processes moved scientists interest to develop the field of electroorganic synthesis. In principle, all moieties in an organic molecule which can undergo redox-chemistry are addressable for this reaction technique. It roots in the invention of the first reported battery by Alessandro Volta[80] in 1800 and ensuing results by Michael Faraday[81]. On a laboratory scale experiment, either a divided (Figure 18 A) or an undivided cell (Figure 18 B) are chosen for conducting electrochemical reactions[82]. Since a divided cell causes an immense voltage drop within the cell, the undivided cell is preferred unless stability of the components demands for cell division. The reaction itself takes place directly at the electrode, which supports the substrate to overcome kinetic hurdles to either gain or lose electrons (Figure 19).

Benefits as the ability of working under mild reaction conditions and the avoidance of aggressive and hazardous reagents has led to numerous publications in recent decades[83,84] in electroorganic synthesis. Even when examples of organic molecules synthesized electrochemically on large scale are rather scarce, as for example the *Baizer* or *Lysmeral* processes[85], electrochemical late-stage modification to attain large functional compounds has been established[86].

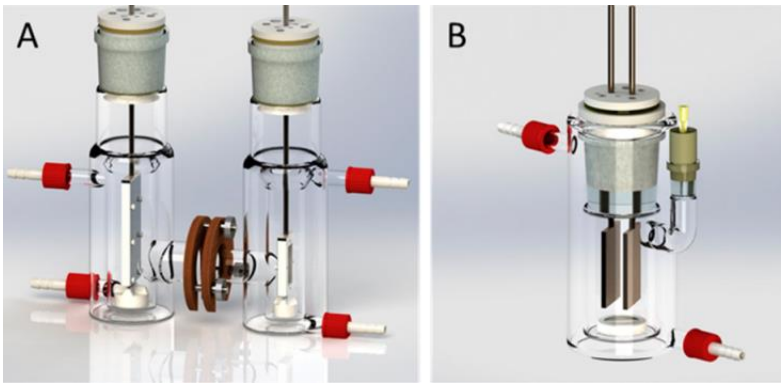

Figure 18. Setup to perform electroorganic reactions. Left: **A**, a divided cell design is shown. Right **B**, an undivided compartment is shown. Reprinted with permission Waldvogel *et al.*[82], Copyright 2018 ACS.

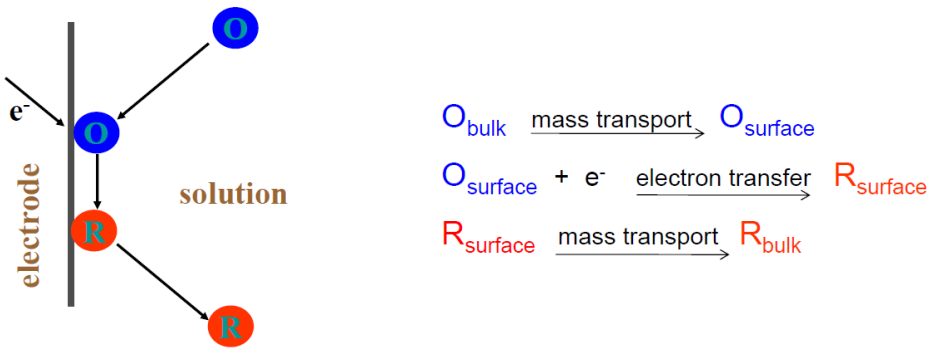

Figure 19. Schematic overview of a reduction process occurring on an electrode surface. Species $\mathbf{O_{bulk}}$ adsorbs on the electrode to become $\mathbf{O_{surface}}$ (mass transport). In a next step, $\mathbf{O_{surface}}$ gains an electron $\mathbf{e^-}$ to become reduces species $\mathbf{R_{surface}}$ (electron transfer) before desorbing the electrode as $\mathbf{R_{bulk}}$ (mass transport).

Substantial efforts towards electroorganic synthesis were made in 1849, when Hermann Kolbe described the CO_2-loss of a carboxylic acid and hence, the formation of a radical which can undergo recombination reaction[87]. Additionally, upon extended electron contact, the radical oxidizes to the carbenium ion (*Hofer-Moest*-reaction) which is susceptible to nucleophilic attack[88] (Scheme 13).

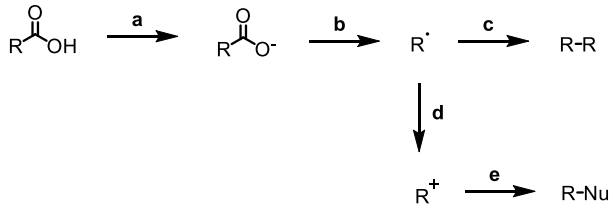

Scheme 13. Early electroorganic discoveries of trivial carboxylic acids are shown. Processes: **a)** deprotonation **b)** first oxidation step on Pt anode and CO_2-loss **c)** recombination of the formed radical **d)** second oxidation step on Pt anode **e)** nucleophilic attack (or elimination as side reaction).[88]

Meanwhile, sterically hindered dialkyl ether synthesis has been established using electrochemical *Kolbe* reaction conditions[89]. On a side note in this work (but bearing broad application potential), 1-adamantanecarboxylic acid **82** undergoes *Hofer-Moest* chemistry first before nucleophilic attack by a nitrile group to the carbenium ion results in amide **83** formation upon aqueous workup. This is known as *Ritter* reaction (Scheme 14).

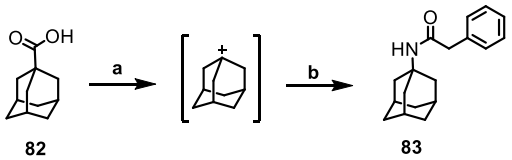

Scheme 14. *Hofer-Moest* reaction step **a)** of 1-adamantanecarboxylic acid **82**, followed by an intermolecular *Ritter* reaction **b)** by nucleophilic attack of 2-phenylacetonitrile forming amide **83**.[89]

A step towards applying electroorganic synthesis to supramolecular chemistry was laid by the conversion of porphyrinogen to porphyrin in an undivided cell. Thereby, yields were obtained in equal amounts as with standard chemical oxidation methods[90]. In a first step, porphyrinogen was formed under *Lindsey* conditions (see also chapter 1.4) from pyrrole and fluorinated benzaldehyde derivatives; in some of the experiments, the pyrrole was fluorinated as well (Figure 20). Then, in a second step, the preorganized porphyrinogen moiety was oxidized electrochemically to the porphyrin by loss of six electrons and six protons (Scheme 15). Interestingly, electron poor porphyrinogen systems did proceed the oxidation in absence of catalytic amounts of mediating oxidizing agent (quinone derivative, Table 1).

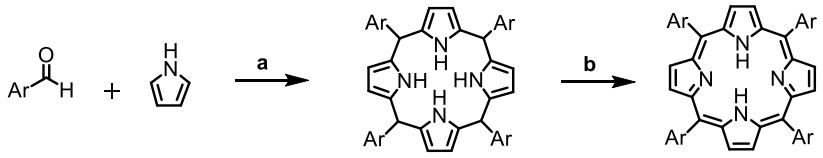

Scheme 15. Formation of porphyrinogen from aldehyde and pyrrole under classical Lindsey conditions and subsequent oxidation in the electrochemical cell to the porphyrin. Conditions: **a)** BF_3-etherate, DCM, rt, 1 h **b)** Loss of 6 e^- and 6 H^+.[90]

The obtained yields varied from 21 to 41%, which is not exceeded by experiments which are conducted exteriorly of an electrochemical cell (Table 1) in conventional laboratory vessels.

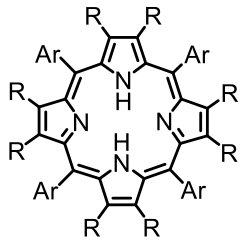

R= 8 H; Ar= C_6H_5 (**$TPPH_2$**); Ar= C_6F_5 (**$TPFPPH_2$**)

R= 4 F, 4 H; Ar= C_6H_5 (**$4FTPPH_2$**)

R= 8 F; Ar= C_6H_5 (**$8FTPPH_2$**); Ar= C_6F_5 (**$8FRPFPPH_2$**)

Figure 20. Depiction of formed porphyrin according to Bondon *et al.*[90]. The degree of fluorination on the porphyrin scaffold and the aromatic rings determines the necessity of mediating auxiliaries and the value of the applied potential in the final electrochemical oxidation step.

Table 1. Isolated yields of porphyrins, which are obtained by either conventional chemistry (chemical yield) or by electrochemical settings (electrochemical yield). The oxidation is performed on the respective preformed porphyrinogen as starting material.[90]

Porphyrin	Chemical yield (%)	Electrochemical yield (%)	Mediator	Potential E vs. SCE (V)
$TPPH_2$	38	36	Chloranil	0.8
$4FTPPH_2$	38	35	DDQ	1.1
$TPFPPH_2$	26	22	DDQ	1.2
$8FTPPH_2$	40	37	DDQ	1.45
$8FTPPH_2$	40	41	None	1.2
$8FTPFPPH_2$	18	21	None	1.45

2 Aim of This Work and Synthetic Strategy (Part A)

2.1 Aim of This Work

Herein we describe our efforts towards the synthesis of a series of spherical molecules (Figure 21). Our ultimative object is methylenespherophane **84** which was predicted[51] first in 1992 and is the central focused target structure in this work. Since the discovery of fullerenes in the 1980s, no further synthesis of such a highly symmetrical ball shaped compound has been achieved, what makes the attempts to synthesize and isolate this molecule to a very interesting task. Thereby, establishing the synthetic strategy towards these highly symmetrical compounds is of great interest and the extraordinary architecture of 8 benzene rings interlinked via 12 methylene bridges is incentive enough to isolate this molecule. Physical properties are expected mainly upon disturbing the high symmetry. Once we have methylenespherophane in hand, upon electrochemical oxidation of the shell, one electron e^- could be removed and the resulting perturbation is expected to show interesting redox behavior. In addition, published[53] predictions highlight the potential use of the methylenespherophane cage as a hydrogen storage container as one of the physical properties.

Previous attempts [57,56] in our group have endeavored to synthesize and isolate thiaspherophane **58**. This spherophane analogue differs from **84** by interlinking the 8 benzene units via 12 sulfide bridges instead of -CH_2-, while the symmetric aspects resemble methylenespherophane. Thiaspherophane is believed to show even additional physical characteristics such as thermal polarizability but its synthesis adds an additional challenge due to the lability of the Ar-S bond. A major issue in synthesizing thiaspherophane has been found in the increasing degree of strain towards the final reaction steps of this spherical compound, especially when starting from small and flat building blocks. Furthermore, apart from preorganizing approaches, polymerization as side reaction remains a serious drawback when forming the spherical spherophane.

Besides envisioned cuboctahedral molecule **84**, we designed smaller spherical target compounds **85** and **86**, which both exhibit D_{3h} symmetry. Thereby we expect entropic benefits for the desired trimerization reaction and less oligomeric side products, since a lower number of new bond formations is required when starting from monomeric units. Once we have one of these highly symmetrical molecules in hand, we established for the first time –to the best of our knowledge– a spherical compound, consisting of truly Ar-(monoatomic)bridge-Ar moieties.

While the first of these D_{3h} symmetry spherophane models consists of 6 benzene units interlinked via 9 methylene bridges (**85**), the second model is a hybrid of Ar-CH_2-Ar and Ar-S-Ar linkages (**86**). For simplicity, we decided to define model compound **85** as **small methylenespherophane** while **86** will be named **hybrid spherophane**. Albeit their D_{3h} symmetry is not precisely spherical but rather shaped like a rugby ball.

The above mentioned structures, the previous attempted thiaspherophane as well as the three target compounds that are aimed in this work, are depicted in Figure 21.

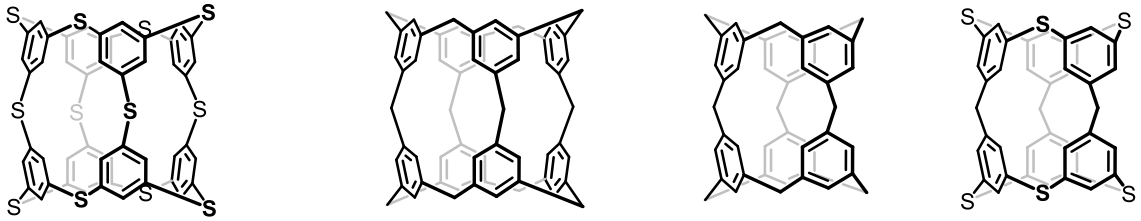

58 **84** **85** **86**

Figure 21. Target structure of thiaspherophane **58** and the addressed structures for this work: methylenespherophane **84**, small methylenespherophane **85** and hybrid spherophane **86**.

2.2 Retrosynthetic Analysis for Methylenespherophane **84**

The synthetic pathway for methylenespherophane was elaborated in three potential routes, that were explored in parallel:

First Approach: Dimerization

As shown in Scheme 16, target compound **84** is expected to be obtained upon reduction of aromatic and benzylic carbon atoms of **88**. For practical reasons, benzylic alcohols of **87** are reduced in a very last reaction step since they are considered to undergo reduction more readily than phenols. This reduction process is either boron[91], phosphorous[92] or silicon[93] mediated. The removal of the *n*-propoxy groups of **88** is assumed to cost high effort, since electron rich Ar-O bonds are considered to be cleaved only when harsh reducing conditions are applied. Most of the proposed alkoxybenzene reductions in literature are under elevated temperatures and high pressure of hydrogen gas (e.g. in an autoclave), which we preferably avoid to not reduce any of the aromatic rings[94,95]. Other methods to reduce aromatic alkoxy groups were found either by using *Birch*-type reaction conditions[96] or working nickel catalyzed under oxygen exclusion in the glovebox[97]. These *n*-propoxy tails were introduced for previous steps, where their hydrophobic interaction guaranteed the stability of a cone-like structure and hence are necessary in the design of the synthetic sequence. **88** represents the first stage of a methylenespherophane derivative, wherefore its isolation and characterization is considered an absolute key step in this work. Dimerization experi-

ments using a variety of *Grignard*-conditions in highly diluted reaction mixtures to avoid polymerization as side reaction, starting from either building block **89** or **90** is expected to result in **88**. **89** and **90** are synthesized from commercially available 4-*tert*-butylcalix[4]arene in four and six steps respectively.

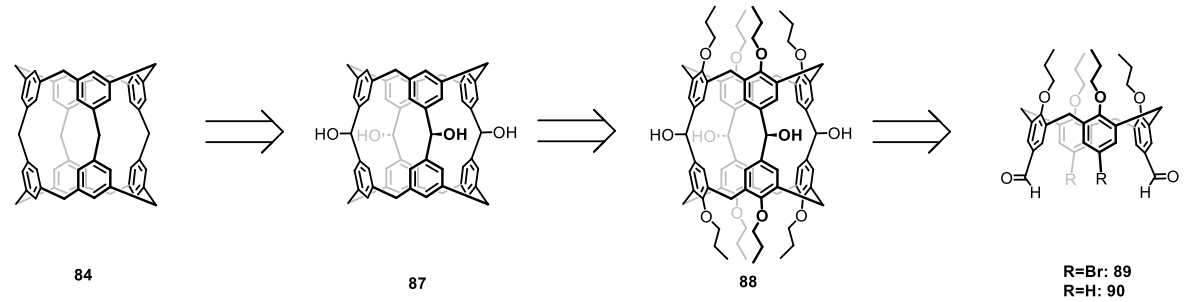

Scheme 16. Retrosynthetic pathway for target molecule methylenespherophane **84** and key building blocks is depicted.

Second Approach: *Suzuki*-Type Reaction

Target structure **84** is obtained from *Suzuki*-type cross coupling of preorganized arylboronic calix[6]arene building blocks **91-92** with 1,3,5-tris(chloromethyl)benzene (Scheme 17). In this approach, a 6 benzene units and 6 methylene-bridges bearing precursor is expected to exhibit a *zig-zag* form due to sterically demanding boronic groups. Hence, the para positions of the first, third and fifth aromatic unit in the calix[6]arene point out of plane while the other benzene rings are twisted the other way round in plane. In this arrangement, two 1,3,5-tris(chloromethyl)benzene units, one from each side, are coupled [98,99,100] to **91** or **92** to form **84**. Boronic moieties are introduced by Ir-catalyzed reaction using $(Bpin)_2$ as agent[101] and to avoid steric clash, functionalization occurs at the para-position of calix[6]arene **93**. Synthesis of the latter is the key step for this approach, since completely reduced calix[6]arene compounds are not found in literature. **93** is attempted to synthesize by complete Ar-OH reduction of **119**.

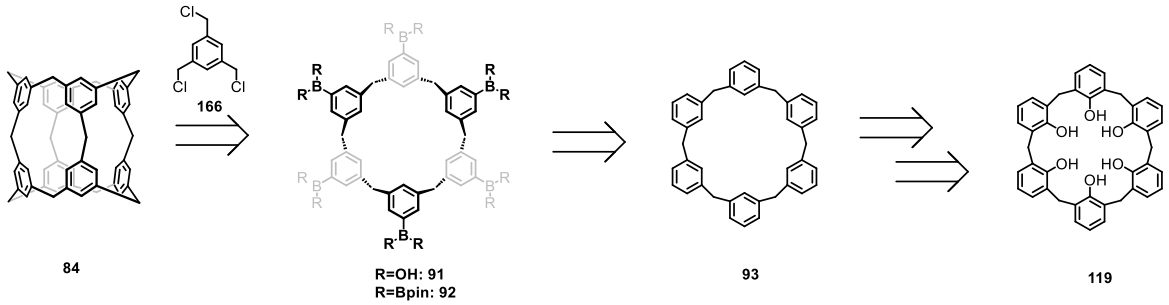

Scheme 17. Retrosynthetic pathway for target molecule methylenespherophane **84** from Ar-B functionalized groups, which are synthesized from **119**.

Third Approach: *Vollhardt* Ring Closure

As a third option, we designed a precursor comprising all required atoms for target molecule **84** (Scheme 18), which is found in the fully silyl-deprotected structures of **94** and **95**. Alike in the second approach, a *zigzag* form due to steric effects is expected, which can undergo aromatic ring closure in a *Vollhardt*–type cobalt mediated [2+2+2]-cycloaddition[102] reaction step. Thereby, six terminal alkynes –three point in plane and the other three out of plane– form two benzene rings. Therefore, precursors **94** and **95** are synthesized in an asymmetric calix[6]arene ring closing reaction followed by benzylic alcohol reduction from building blocks **96-99**. These are obtained from flat, monoaromatic precursors **100-103**. This is the most concise bottom-up approach we considered for methylenespherophane **84** synthesis, which leads over numerous reaction steps, starting from very small commercially available compounds.

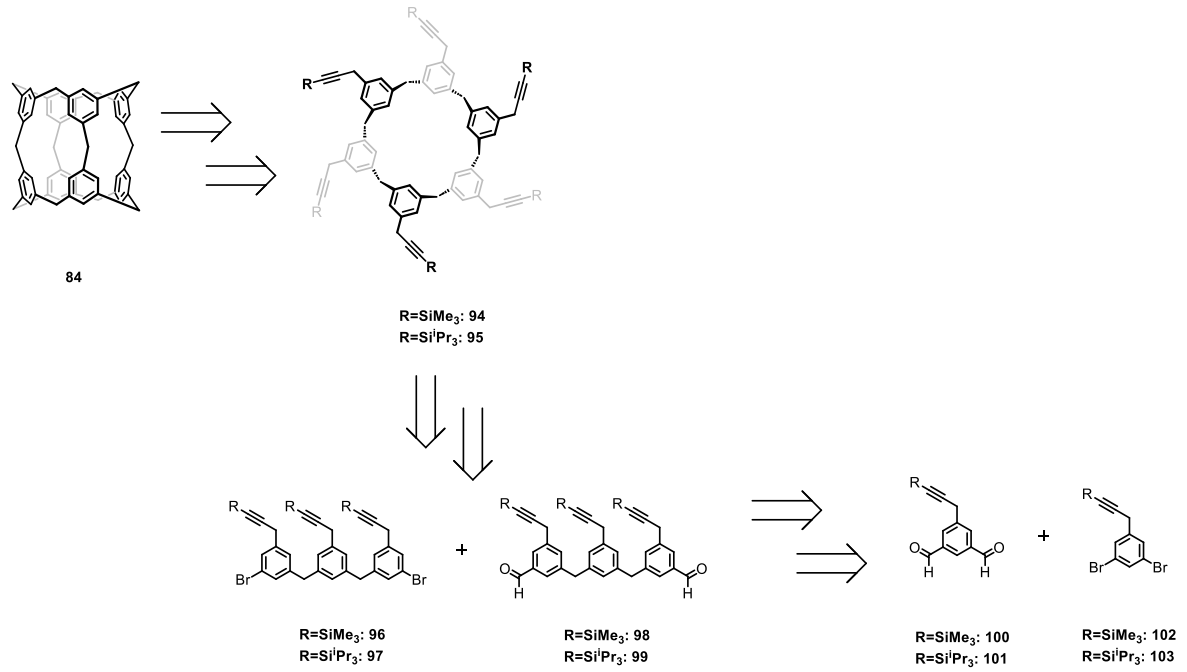

Scheme 18. Retrosynthetic pathway for target molecule methylenespherophane **84** via *Vollhardt* reaction.

2.3 Retrosynthetic Analysis for Small Methylenespherophane **85**

Target compound **85** is expected from reducing all benzylic alcohol groups of **104** (Scheme 19). By applying highly diluted conditions and exposure of **105** to butyllithium conditions, oligomerization reaction occurs. Side product formation such as linear polymerizations is inevitable but kept as small as possible with the given dilution. The focus is laid on the trimer product in this synthetic route, even when other oligomers with spherical shape can be formed as well. Since the number of binding events, symmetry and cavity size are all decreased for trimer **104** formation compared to its particular tetramer, we consider its formation in this one-pot reaction sequence as more likely. Especially the required binding events are expected to have a substantial influence on the formed products when considering statistic reaction under highly diluted conditions. Regardless of which spherical oligomer of **105** is isolated in the end of this work, the information for the synthesis and characterization of other spherophane molecules is an enormous benefit for future approaches.

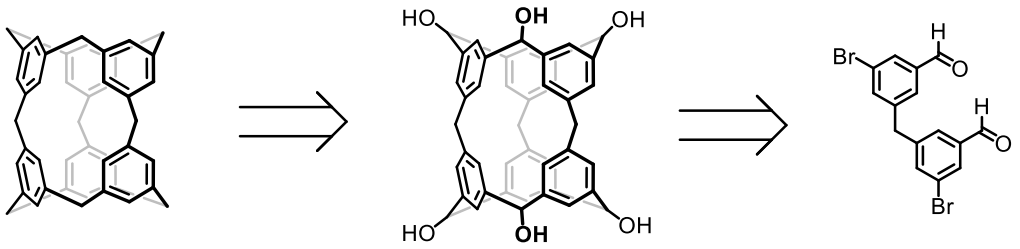

85 **104** **105**

Scheme 19. Retrosynthetic pathway for target molecule small methylenespherophane **85** with a one-pot trimerization reaction as key step.

2.4 Retrosynthetic Analysis for Hybrid Spherophane **86**

In previous dissertations[57,56] efforts were made towards thiaspherophane **58**, representing the class of heterospherophanes which does not consist only of C and H atoms. A decreased bonding angle in Ar-S-Ar bonds leads to higher strain and more reactivity which makes the isolation of this class even more difficile. In this work, we decided to simulate at least some of the arylsulfide characteristics in choice of **86** as a target structure. As a last step, 6-fold phenol reduction of **106** is required (Scheme 20), which is not trivial especially due to the electron rich system. The parallels to **85** in chapter 2.3 are extensive. Also for this work we assume **107** to form trimeric oligomer **106** most likely in a one pot double S-arylation of double halides[103]. The assumption of forming trimer rather than tetramer derives from research of the late 1980s, when the synthesis of cyclotris(*m*-phenylene sulfide) was discussed[104]. Since *ortho*-substituents as the phenol moiety to Ar-Br has afforded diaryl sulfides in excellent yield[103], **107** was the building block of choice to attempt trimerization.

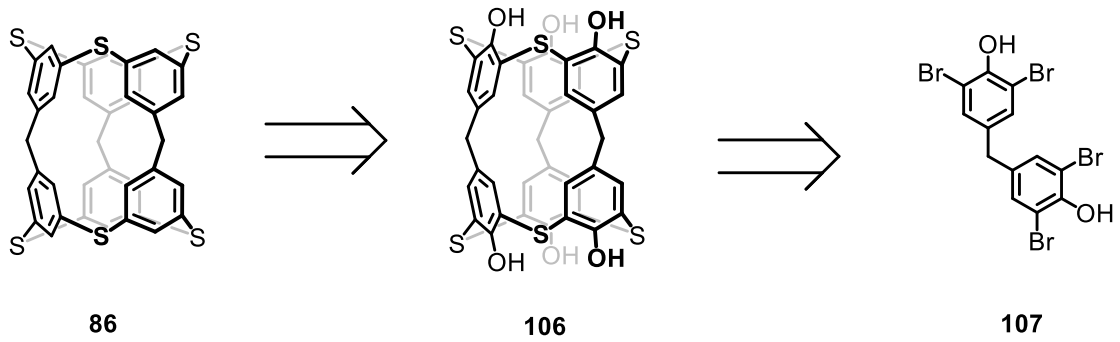

Scheme 20. Retrosynthetic pathway for target molecule hybrid spherophane **86** with a one-pot trimerization reaction as key step.

3 Results and Discussion

3.1 Methylenespherophane **84**

First Approach: Dimerization

For this approach we started from commercially available 4-*tert*-butylcalix[4]arene **111** to first remove *tert*-butyl groups in a *retro-Friedel-Crafts* reaction[105,106]. Long reaction times, vigorously stirring and elevated temperatures favored the liquid-liquid heterogeneous reaction mixture to reach completion. Phenols of **112** were then protected with an *n*-propoxy tail by applying S_N2 reaction conditions, whereby replacing THF with DMF increased the yield from 40 to 86%. Isolated **113** was fourfold brominated using NBS[107]. Interestingly, when using **113** slightly wetted with MeOH, we observed best conditions for the complete bromination. Monomer **89** was then already our aimed starting material for dimerization experiments. Its synthesis was performed by aryl bromide to lithium exchange, followed by DMF quenching. Even when an excess of *n*-BuLi is added to **114**, lithiation stops at the dilithiated stage. Additionally, of great advantage for our strategy, the 5' and the 17' positions of the calix[4]arene are lithiated in good yields, which can be rationalized by charge distribution of the two negative charges. Hemispherical shaped compound **89** was used as starting material for a series of spherophane closing dimerization attempts by using butyllithium and *Grignard* reagents. By adding butyllithium reagents to **114**, two of the four bromine atoms in opposed position on the upper calix[4]arene rim was substituted by two hydrogens, resulting in compound **115**. In a second reaction, the remaining two Ar-Br in **115** are converted to aldehydes upon quenching Ar-Li with DMF to obtain **90**.[108] For this step, yields increased considerably by replacing *n*-BuLi with *t*-BuLi, since none of the alkyl-bromide species is formed,

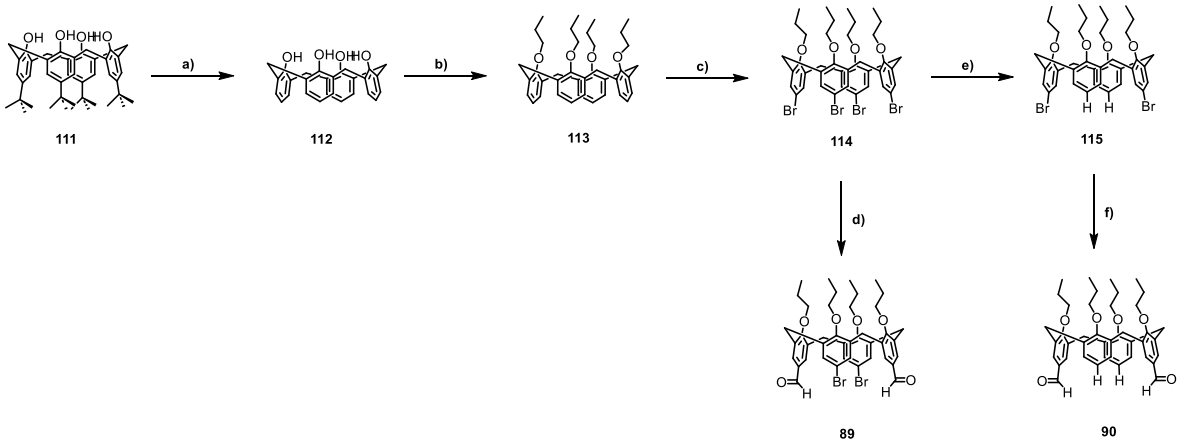

Scheme 21. Synthesis of calix[4]arene monomers **89** and **90** from commercially available **111**. Conditions: **a)** $AlCl_3$, toluene, 60 °C, 72 h, 83% **b)** NaH, C_3H_7Br, DMF, 0 °C to rt, 2 h, 86% **c)** NBS, 2-butanone, rt, 24 h, 82% **d)** 1.) *n*-BuLi, THF, -78 °C, 30 min. 2.) DMF, -78 °C to rt, 1.5 h, 68% **e)** 1.) *n*-BuLi, THF, -78 °C, 30 min. 2.) MeOH, -78 °C to rt, 1.5 h, 88% **f)** 1.) *t*-BuLi, THF, -78 °C, 30 min. 2.) MeOH, -78 °C to rt, 2 h, 76%.

which could undergo hydrodehalogenation reaction with ArLi (furthermore, nucleophilic addition was observed when using *n*-BuLi). Building block **90** lacks halide atoms and is therefore not suitable for conventional halide-to-metal exchange experiments, which then transforms the respective aromatic carbon atom to a good nucleophile. But as a promising alternative, recently reported *Turbo-Hauser* bases[109] open the possibility to deprotonate the Ar-H in the sterically least hindered position[110], especially with a functional group in *para* position, to introduce a highly nucleophilic Ar-MgCl*LiCl moiety.

Initial dimerization approaches (Scheme 22) from **89** using the common lithiation agents *n*-BuLi and *t*-BuLi have resulted in full conversion of starting material with observing the mass for **88** only in traces by measuring LC-MS (ESI). Side products by using *n*-BuLi were found in the nucleophilic attack of *n*-butyl-chain to the aldehyde, verified by NMR-techniques. Other unintended species as hydrodehalogenation products of **89** and higher oligomers were detected by using MALDI measurements. Hydrodehalogenated side product was responsible for the detection of *m/z* **88** in LC-MS (discussed below in Figure 22). *Barbier-Grignard* type procedures by adding zinc dust and applying ultrasonic frequencies[111] have not resulted in more than 50% conversion of **89** without any mass detection of **88**. $NiCl_2$-mediated approaches conducted under glovebox conditions including sacrificial $CrCl_2$-salts (*Hiyama-Nozaki-Grignard* type reaction)[112] in DMF did not result in any conversion of **89** at room temperature but a complex mixture of compounds was obtained at elevated microwave reaction temperatures of 150 °C.

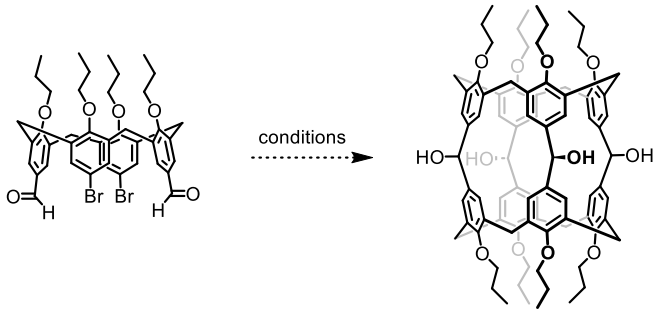

89 **88**

Scheme 22. Symmetric dimerization experiments to **88** from dibromo-dicarbaldehyde monomer **89**.

To overcome the so far seen insufficient Ar-Br *Grignard*-activation without the necessity of applying functional group intolerant reagents, **90** was used as starting material for dimerization attempts (Table 2). As described above, Ar-H is activated by a 2,2,6,6-tetramethylpiperidinylmagnesium chloride lithium chloride complex solution by deprotonation and subsequent Ar-MgCl*LiCl formation. This reactive intermediate undergoes nucleophilic attack on the aldehyde moieties. To prevent undesirable competing oligomerization reactions, diluted reaction conditions were applied (Scheme 23).

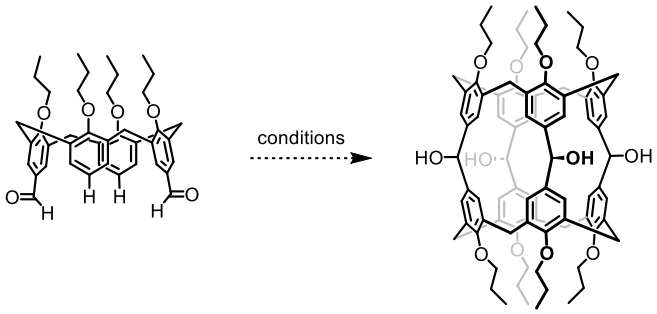

90 88

Scheme 23. Symmetric dimerization experiments to **88** from dicarbaldehyde monomer **90** reacting with an excess of 2,2,6,6-tetramethylpiperidinylmagnesium chloride lithium chloride complex solution (1.0 M in THF/toluene). Conditions: see Table 2.

Table 2. Reaction conditions for the dimerization approach of monomer **90** to target structure **88**.

#	m / mg	c / mM	T / °C	t	conversion	*m/z* of 88	comment or output
1	100	30	-78 to rt	16 h	full	no	
2	150	100	150	10 min.	full	yes	microwave
3	100	200	-10 to rt	72 h	partial	yes	
4	150	115	-10 to rt	16 h	partial	yes	T-gradient
5	1500	90	-10 to 30	20 h	partial	yes	2 mg
6	240	3.5	-10 to 30	16 h	partial	yes	30 mg
7	240	41	-10 to 65	2.5 h	partial	yes	
8	240	62	-10 to 120	30 min.	full	no	microwave

A drawback of using **90** instead of **89** reacting to **88** is the absence of bromine atoms, which are easy recognizable by mass spectrometry measurements due to its characteristic isotope pattern. The highest challenge to identify target structure **88** in these dimerization approaches emerged by having absolutely identical *m/z* of 1296.69 Da signals not only in comparison to **90** but also compared to all other dimeric side products, which are assumed to be formed as intermediates of the reaction (Figure 22). To give some examples: we consider the same *m/z* when two monomers of **90** fly together in the ESI detector as for dimer **88**, since exactly the same chemical formula is obtained then. When one aldehyde of **90** undergoes nucleophilic addition, substrate **116** is formed and upon attacking two aldehydes, molecule **117** is formed. Both of them show *m/z* 1296.69 Da.

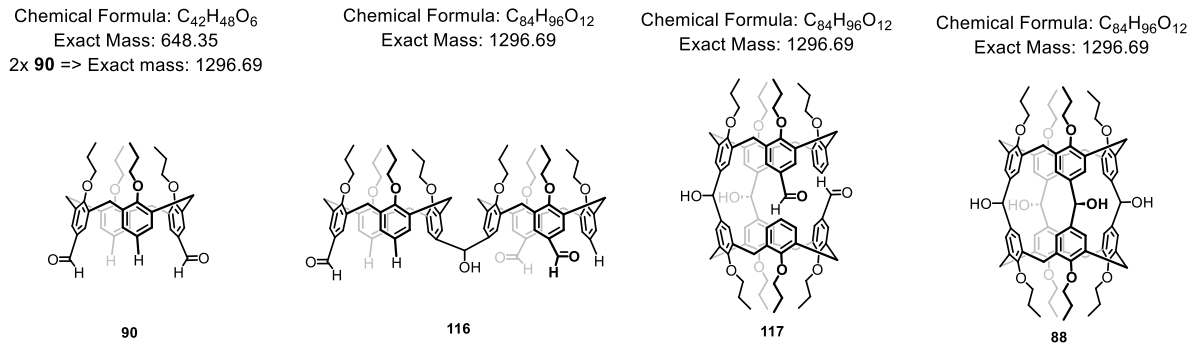

Figure 22. Possible products of dimerization attempt of **90** is shown. Substances **116** and **117** are considered as intermediate in this reaction, rather than side products. Exact mass of *m/z* 1296.69 can be found in any of the depicted structures, due to identical chemical formula.

Apart from the highlighted mass uncertainty for target structure **88**, its inherent void is guaranteed only in theory, when all of the four hydroxyl groups point towards the outer phase of the sphere. As a result, different stereoisomers with varying NMR-signals could eventually be considered as the desired product.

In principle, expected intermediate **117** attributes characteristics to a truly cavitand and is due to representing an almost perfect sphere of synthetic interest as well. Especially, since it would be a perfectly preorganized starting compound for a final sphere closure.

Experiments were conducted according to Table 2. While no product mass was found upon performing the halogen-metal exchange at -78 °C (entry 1), high temperature exposure (entry 2) has led to a multi component mixture. This challenge was addressed best by applying a slow gradient of the reaction temperature, starting with an ice bath at -10 °C followed by slowly warming up to room temperature. In most of the experiments, the reaction mixture was diluted with freshly distilled THF, except for entries 3-5, where **90** was dissolved directly in the commercial 1.0 M 2,2,6,6-tetramethylpiperidinylmagnesium chloride lithium chloride complex solution in THF/ toluene.

As seen in Figure 22, starting material **90**, several intermediate compounds and desired product **88** do all show *m/z* 1296.69 by measuring ESI under prevalent conditions. Therefore, we found an adequate solution: by isolating compounds from crude mixtures with focus on ^{1}H-NMR spectra without aldehyde signal, we make sure to obtain possible **88**. This criterion accounted for two fractions (Table 2, entries 5 and 6), which were isolated after exhaustive column chromatography, preparative TLC and GPC purification steps. On a large scale reaction step, starting with 1.50 g of **90** we isolated 2 mg of milky residue (entry 5). To our delight, this fraction was identified as possible **88** by measuring high resolution mass spectrometry using an ESI source (Figure 23) and by measuring an ^{1}H-NMR spectrum (Figure 24) without any aldehyde signals.

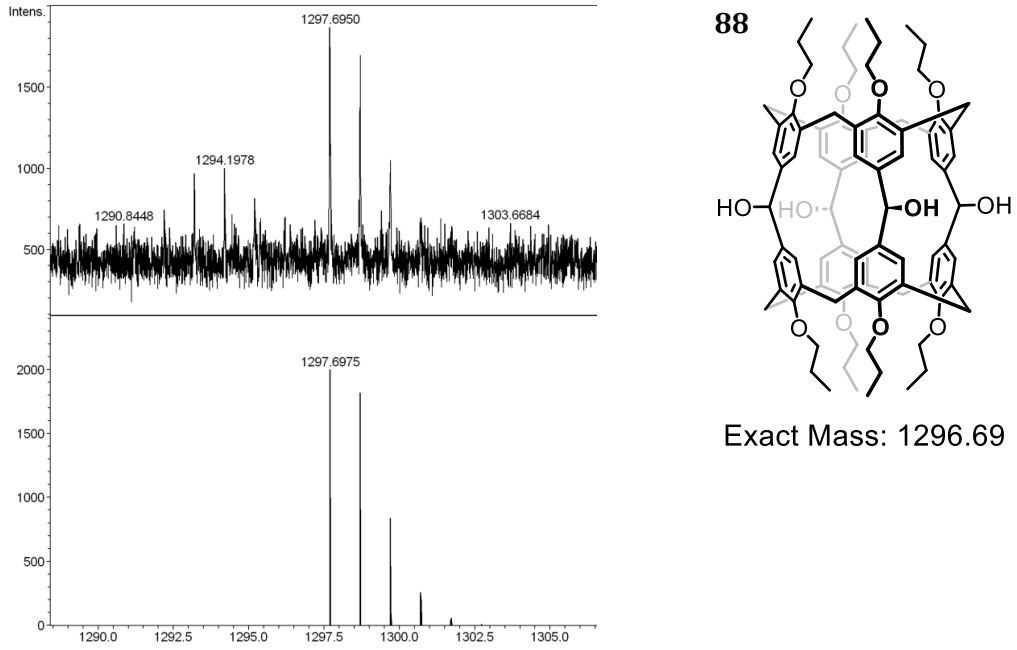

Figure 23. Intensity vs. *m/z* in Da is shown (Table 2, entry 5). *m/z* +1 calculation (bottom) as well as the expected isotope pattern fit for measured **88** sample (top). Measurements were performed by direct ESI on a high resolution instrument.

Since no aldehyde signal was observed and adequate integral distribution was measured in the ^{1}H-NMR experiment (96 H-atoms found), further analyses were performed to verify **88**. DOSY (Figure 25) has identified all signals of the ^{1}H-NMR spectra as components of a single species. We then found all the aromatic ^{1}H-signals being bound to an aromatic C-atom, which was verified via HSQC analysis (Figure 26, left). Hence, we found 20 hydrogen atoms with an aromatic shift, whereby for **88** only 16 are intended. One explanation would be if the 4 benzylic Ar-CH(OH)-Ar hydrogen atoms refer to the triplet at δ 6.73 ppm. This is, to our regret disproved since the benzylic ^{13}C carbon is expected for δ 70 to 80 ppm, but measured HSQC indicates a shift of δ 122 ppm. NOESY and HMBC (appendix, Figures 157 and 158) measurements determine the 3 aromatic proton signals other than δ 6.73 ppm as possible part of the aromatic calixarene. Another reasonable explanation is to allocate the 4 hydroxyl protons to this triplet at δ 6.73 ppm. Nevertheless, this is not compatible with the mentioned HSQC signal of δ 122 ppm. Second signal of conflict is the singlet at δ 4.51 ppm, having an integral of 4 protons. Assigning them to the 4 hydroxyl signals contradicts the found HSQC coupling signal of a δ 66 ppm ^{13}C-shift, extracted from the HSQC spectrum (Figure 26, right). When this singlet is assumed to be the 4 benzylic Ar-CH(OH)-Ar protons, the respective carbon atom in the HSQC fits for the benzylic ^{13}C-region indeed, but the protons would be strongly upfield-shifted, since Ar-C(OH)H-Ar benzylic protons are expected above 6 ppm. Either way, NMR-analyses do not verify desired compound **88**.

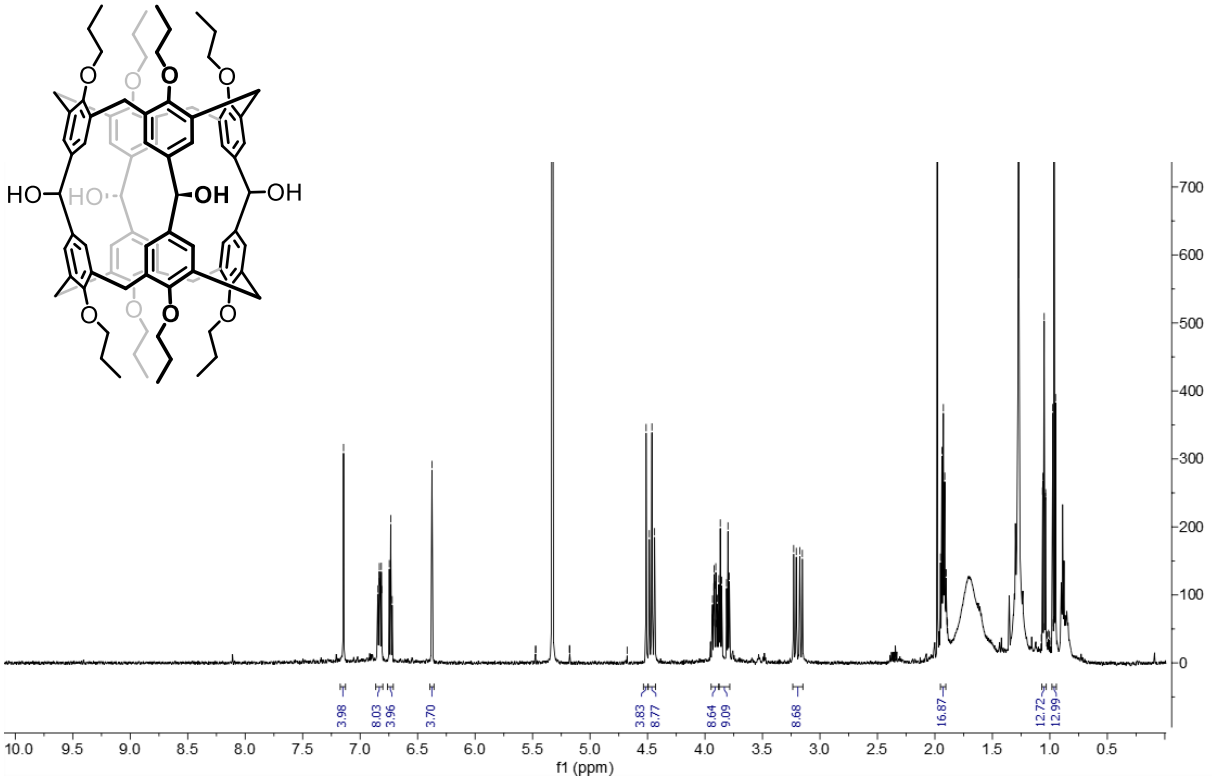

Figure 24. Measured ^{1}H-NMR of the isolated 2 mg from entry 5, showing possible **88** molecule. Following the strategy of isolating fractions without aldehydes, no signal is observed above shifts δ larger than 7.14 ppm. Measurement was conducted on a 600 MHz instrument in DCM-d_2 as solvent. Coupling constants are: δ 7.14 (s, 4H), 6.83 (ddd, J = 12.1, 7.5, 1.8 Hz, 8H), 6.73 (t, J = 7.5 Hz, 4H), 6.38 (s, 4H), 4.51 (s, 4H), 4.46 (t, J = 13.8 Hz, 8H), 3.95 – 3.88 (m, 8H), 3.83 (dt, J = 40.1, 7.2 Hz, 8H), 3.19 (dd, J = 31.6, 13.5 Hz, 8H), 1.92 (pd, J = 7.5, 4.5 Hz, 16H), 1.05 (td, J = 7.4, 1.2 Hz, 12H), 0.96 (t, J = 7.5 Hz, 12H) ppm.

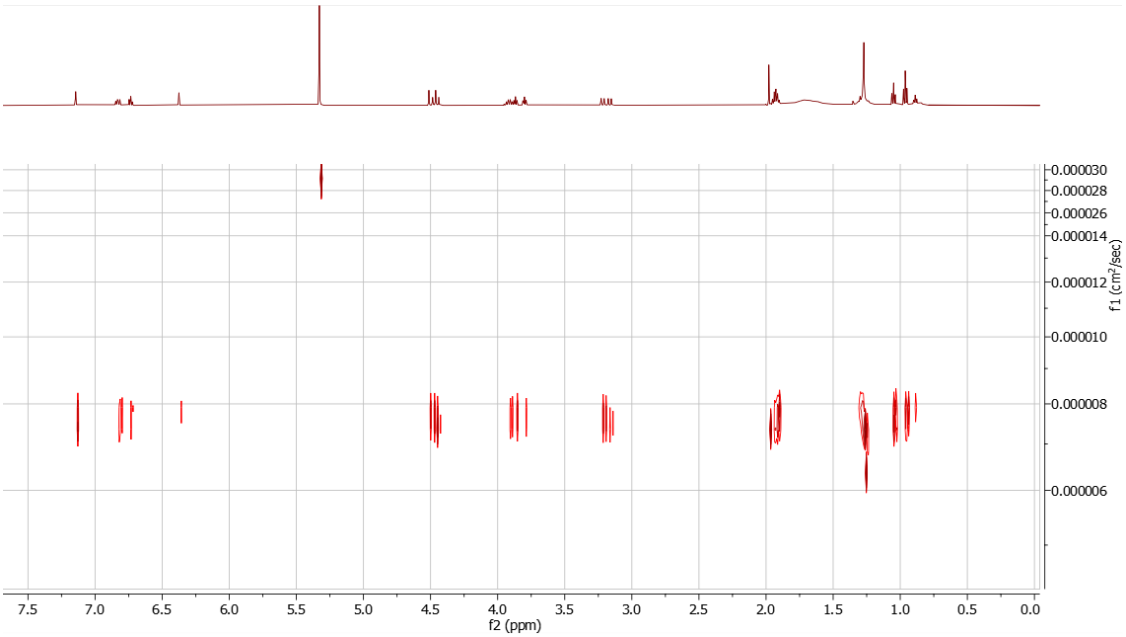

Figure 25. Measured DOSY spectrum of the isolated 2 mg from entry 5, showing possible **88** as single species.

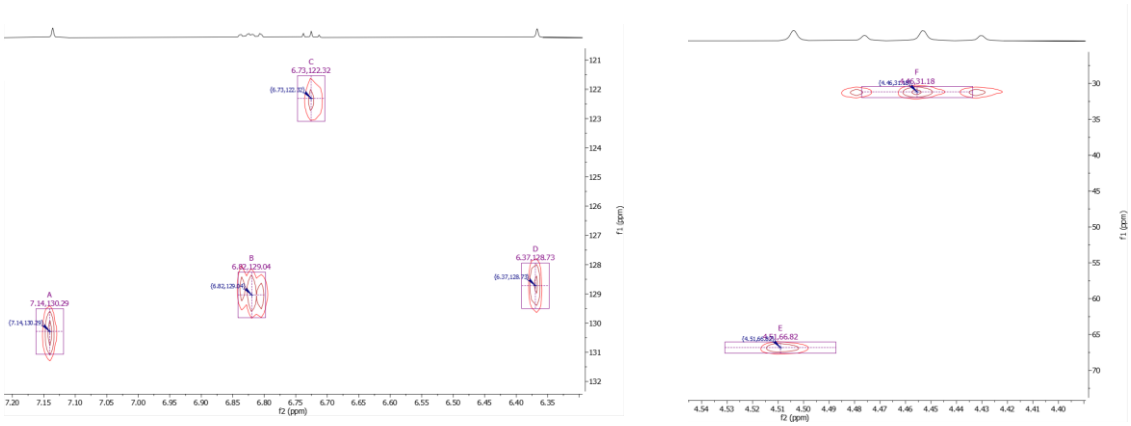

Figure 26. Aromatic region (left) and benzylic region (right) HSQC of possible **88**.

Another aldehyde free fraction was isolated when performing the reaction at a very high dilution of 3.5 mM (Table 2, entry 6) to gain 30 mg white crystals from 240 mg of **90**. Purification by chromatography techniques using normal phase first (eluents: cyclohexane: EtOAc 4:1, then cyclohexane: toluene: EtOAc 1:1:1) before reversed phase (eluent: acetonitrile) resulted in a reasonable ^{1}H-NMR spectrum (Figure 27) for **88** with similar integrals as seen for compound of entry 5 (Figure 24), but varying chemical shifts. However, the species does not remain in a stable form in solution, even after observing only one spot on the previously performed 2D TLC. No accurate *m/z* for target structure was found when measuring high resolution ESI. Nevertheless, since the sodium-adduct of **88** *m/z* 1319.68 Da was found (Figure 28) by UPLC-MS (ESI) measurements, we tried to reduce the *n*-propoxyl groups in assumption of having target structure **88** in hand.

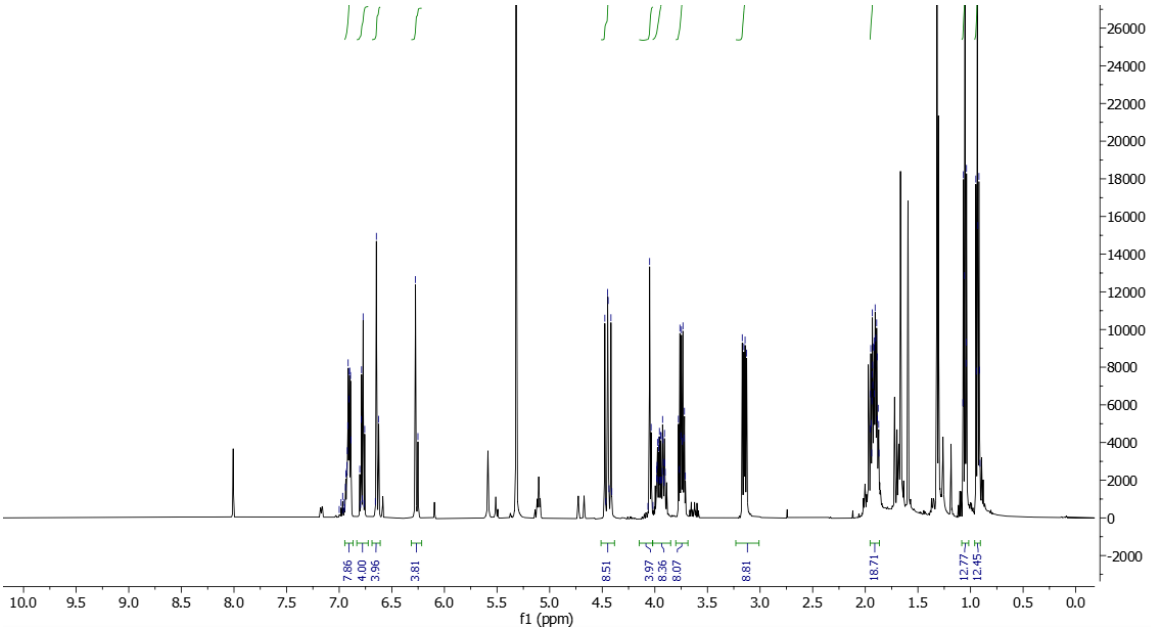

Figure 27. Measured ^{1}H-NMR spectrum of possible **88** (Table 2, entry 6), performed on a 500 MHz instrument in DCM-d_2. Non-integrated signals occur due to transformation in solution. Coupling constants are: δ 6.92 (dddd, J = 13.0, 7.5, 5.3, 1.8 Hz, 8H), 6.82 – 6.74 (m, 4H), 6.64 (d, J = 10.9 Hz, 4H), 6.26 (d, J = 11.7 Hz, 4H), 4.45 (dd, J = 15.8, 13.3 Hz, 8H), 4.04 (d, J = 7.2 Hz, 4H), 3.98 – 3.90 (m, 8H), 3.74 (dtd, J = 14.2, 7.0, 4.3 Hz, 8H), 3.15 (dd, J = 13.4, 7.5 Hz, 8H), 1.96 – 1.86 (m, 16H), 1.05 (td, J = 7.4, 2.0 Hz, 12H), 0.93 (td, J = 7.5, 2.2 Hz, 12H) ppm.

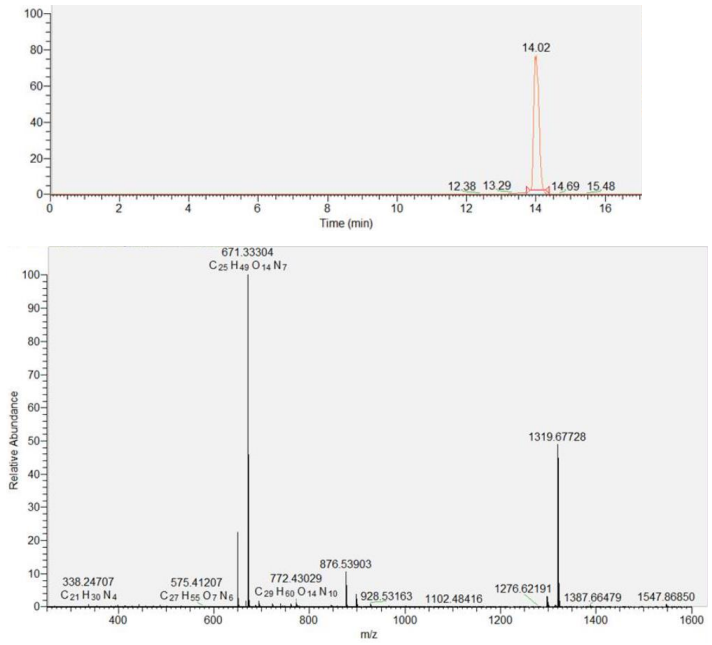

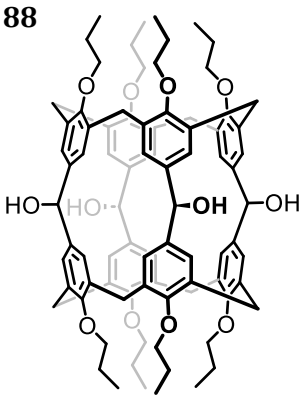

Exact Mass: 1296.69
Na-adduct: 1319.68

Figure 28. UPLC chromatogram (top) of possible **88** (Table 2, entry 6) including relative abundance vs. *m/z* in Da of signal appearing at 13.82-14.27 min. in the chromatogram. Sodium adduct *m/z* +Na of **88** fits accurately with the measured ESI mass.

The finding of *m/z* 1319.68 Da by UPLC-MS (ESI) but not by performing direct injection high resolution ESI might be correlated with the mode of measurement. As already seen for the previous discussed fraction (entry 5), direct mode injection for high resolution does not result in intense *m/z* signals (Figure 23).

The 30 mg white crystals of Table 2, entry 6 was divided into two equal portions to conduct reduction of *n*-propoxyl group adopting a procedure of A. Sergeev *et al.*[97] and benzylic alcohol reduction following a procedure of P. Gordon *et al.*[92] The latter procedure included dissolving 15 mg of white crystals (assumed as **88**) in AcOH prior to subsequently adding iodine and hypophosphorous acid as reducing agent mix and stirring at 60 °C for 1 h. Although starting material was fully converted and a less polar fraction was observed on TLC, conducted mass measurements and ^{1}H-NMR analysis did not suggest any alcohol reduction. Interesting results were found upon dealkoxygenation attempts to reduce aromatic C-O bonds, when starting material was heated up to 120 °C for 3 d in freshly distilled *m*-xylene and hydrogen gas atmosphere, whereby bis(1,5-cyclooctadiene)nickel(0) and sodium *tert*-butoxide as well as ligand 1,3-bis(2,6-diisopropylphenyl)imidazolium chloride was added. Full conversion of the starting material and less polar fractions as products were observed on TLC. Thereby, the isolated top fraction (eluent: cyclohexane: EtOAc 10:1) has led to *m/z* 769.77 Da, which is close (Δ*m/z* = 1.39 Da) to methylenespherophane **84** (*m/z* 768.38 Da) by using MALDI-spectrometry in the positive mode, including the correct isotope pattern (appendix, Figure 159). However, NMR spectra were inconclusive and did not allow the elucidation of the isolated compound.

Eventually, all dimerization attempts in this approach did not succeed in the synthesis and full characterization of **88**, which is the intended precursor for target structure **84**. Thus, the focus is shifted towards precursors for **84** which are more preorganized.

Second Approach: *Suzuki*-Type Reaction

Retro-Friedel-Crafts reaction conditions were applied for the conversion of commercially available **118** to **119** (Scheme 24). Unlike for calix[4]arenes, removal of *tert*-butyl groups proceeds in good yields without extended reaction times or excess of $AlCl_3$. The electron density of the aromatic C-O-bonds is expected to be removed to a high extent upon introduction of long perfluorooctanesulfonate chains, facilitating reduction of the phenolic carbon (C^{+I} to C^{-I}) atoms. This reduction has been performed successfully by L. Subramanian *et al*.[113] in good yields by simple Pd/C catalyst in MeOH under hydrogen atmosphere. To our regret, **120** was not synthesized from **119** and perfluorooctanesulfonyl fluoride even after extensive screening. Another option to remove phenol moieties is to substitute C-OH bonds first with phosphonate groups to then apply *Birch*-type reduction conditions as a second step[96]. **121** was synthesized electrochemically[114], but due to electrode deposition in low yields of 13%. Reduction of **121** to **93** in liquid ammonia and elemental potassium as electron donor (blue reaction solution) did not result in any formation of **93**.

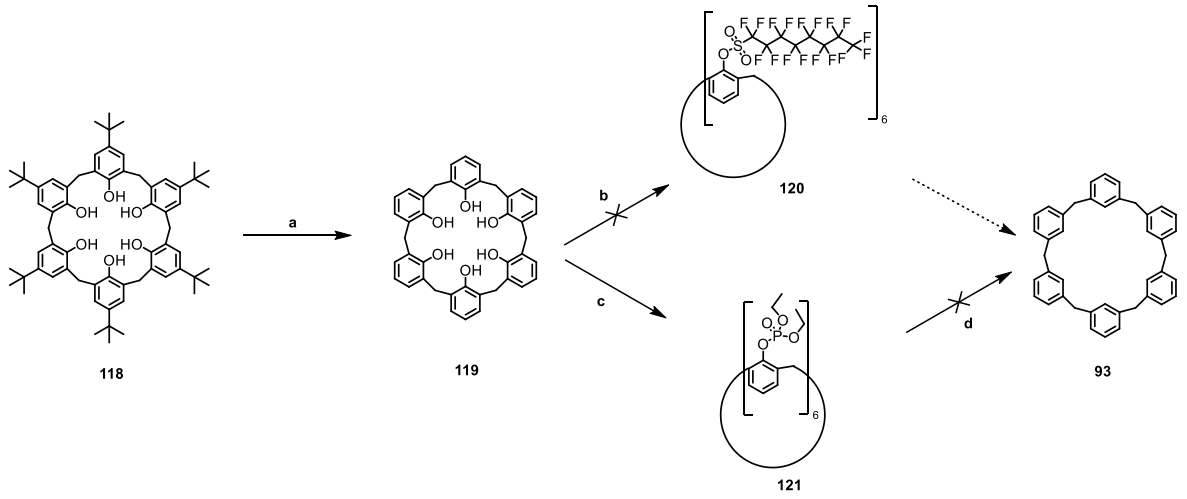

Scheme 24. Synthesis of calix[6]arene from commercially available **118**. Conditions: **a)** $AlCl_3$, toluene, rt, 3 h, 89% **b)** perfluorooctanesulfonyl fluoride, triethylamine, diethyl ether, 0 °C to rt, 16 h, none **c)** diethyl phosphonate, NaI, acetonitrile rt, 5 d, 20 mA, WE: Pt, CE: Pt, 13% **d)** 1.) K, NH_3, -78 °C to rt, none**.**

Ar-OH reduction to obtain fully reduced calix[6]arene **93** was not achieved from commercially available **118**. Hence, the desired calix[6]arene frame is aimed to be synthesized from monoaromatic building blocks.

Third Approach: *Vollhardt* Ring Closure

The idea behind this attempt to synthesize methylenespherophane **84** is to build up first the calix[6]arene rim by starting from small commercially available compounds. Since cross coupling reactions prefer substitution on the aromatic C-Br position, nucleophilic substitution S_N2 was the method of choice to introduce alkyne groups. First, 1,3-dibromo-5-(bromomethyl)benzene **122** was crystallized from acetone and then, by applying S_N2 reaction conditions, the benzyl bromide was expected to be replaced by either TMS-acetylene **123** or TIPS-acetylene **124**. By the chosen conditions (Scheme 25) benzylic bromo-chloro exchange was found instead of isolating **123**. Furthermore, hydrodehalogenation and *Wurtz*-type coupling was reported instead of **124**.

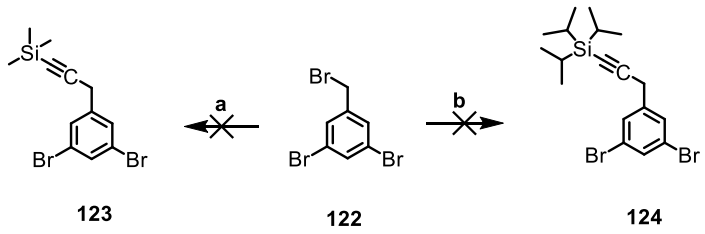

Scheme 25. Failed S_N2 reaction to introduce an acetylene moiety at a benzyl bromide position is shown. Conditions: **a)** iPrMgCl*LiCl, CuI, THF, 0 °C to 65 °C, 16 h, none **b)** *n*-BuLi, TIPS-acetylene, THF, -10 °C to 65 °C, 30 min., none**.**

We adapted the reaction path and started from the carboxylic acid **125** to form ethyl ester **126** and upon reduction with $LiAlH_4$, the alcohol **127**. This building block reacts further using *Dess-Martin* conditions to the respective aldehyde **128** and to introduce the acetylene **129**, *Seyferth-Gilbert* reaction using *Ohira-Bestmann* reagent was chosen. Purification of **128** has resulted in vast decomposition of the desired compound, due to instability in solution. Therefore, the crude of **128** was plugged over a short silica column before reacting further to **129**. Hence we circumvent any other unpleasant strategies to insert the acetylene. Drawback of this approach is the absence of a protecting group for the acetylene, which is usually introduced via BuLi-chemistry. But this step is not feasible for **129** in order to not lose Ar-Br groups. Experiments with 3-bromophenylacetylene have shown the feasibility to introduce an aromatic aldehyde by Br-Li exchange in presence of a free acetylene. We were optimistic to proceed with non-protected **129** in hand.

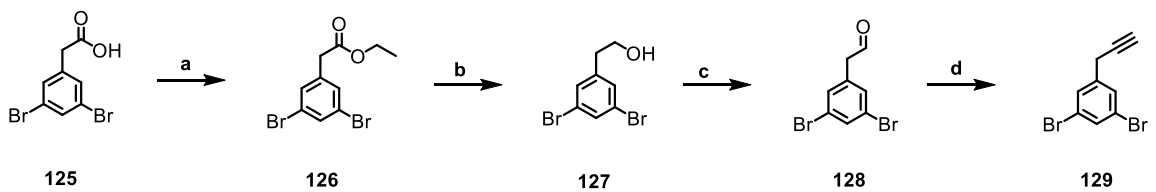

Scheme 26. Conversion of a benzylic carboxylic acid **125** to a benzylic acetylene **129** without breaking available aromatic C-Br bonds is shown. Conditions: **a)** EtOH, H_2SO_4, rt, 16 h, 99% **b)** $LiALH_4$, THF, 0 °C to 65 °C, 4 h, 80%**. c)** Dess-Martin periodinane, 0 °C to rt, 16 h, 82% **d)** dimethyl (1-diazo-2-oxo-propyl)phosphonate, MeOH, rt, 3 h, 65%**.**

The second building block **101** contains a benzylic acetylene on a isophthalaldehyde moiety. Similar to the attempts in Scheme 25, the experiments to introduce one acetylene to freshly crystallized **130** via *Turbo-Grignard* reaction conditions led to 1,3,5-tris(chloromethyl)benzene as product. Hence, TMS-acetylene was deprotonated at -78 °C before adding **130** in one portion, causing S_N2 mechanism. Even after exhaustive screening of temperatures and reaction times, the yield of 27% for **131** could not be exceeded (Scheme 27). A second drawback was the labile TMS-protecting group, which was cleaved upon column chromatography purification. As a consequence, TMS-acetylene was replaced by TIPS-acetylene leading to slightly higher yields of **132** in addition to a higher stable protective group for the acetylene. An alternative route to the so far commonly applied S_N2 introduction of the acetylene group was obtained when $[Pd(\mu\text{-}I)P(t\text{-}Bu)_3]_2$ palladium catalyst was used[115] to improve the yield to 40%. GC-MS (EI) measurements did show *m/z* of **132** only by loss of one isopropyl group. The oxidation of **132** to **101** (C^{-I} to C^{+I}) was accomplished in moderate yields of 51% by using 4-methylmorpholine N-oxide as oxidizing agent.

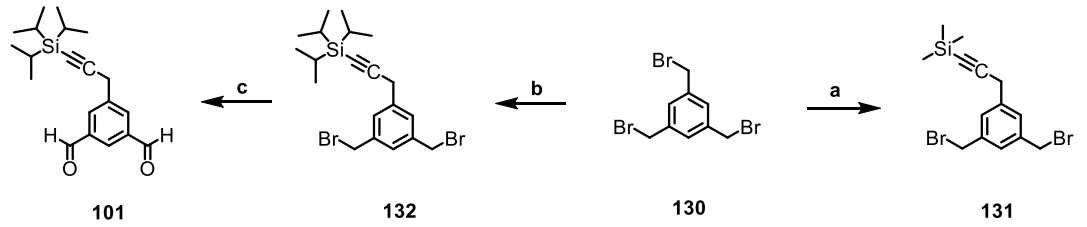

Scheme 27. Conversion of a trisbromobenzylic **130** to single introduced benzylic acetylenes **131** and **132**, followed by oxidation to the aldehyde **101** is shown. Conditions: **a)** *n*-BuLi, TMS-acetylene THF, -78 °C to rt °C, 16 h, 27% **b)** *n*-BuLi, TIPS-acetylene, THF, -10 °C to 65 °C, 30 min., 32%; alternative: $[Pd(\mu\text{-}I)P(t\text{-}Bu)_3]_2$ addition, rt, 2 h, 40% **c)** 4-methylmorpholine N-oxide, acetonitrile, rt to 80 °C, 2 h, 51%.

Since we have the two building blocks **129** and **101** in hand, synthesis towards the *zigzag*-like, semi cycle **133** was started. This precursor is only one dimerization step from calix[6]arene derivative target structures **94-95**. Conditions were kept on a facile extent, by applying *t*-BuLi-chemistry in THF. However, **133** was not synthesized but hydrodehalogenated product of **129** isolated mainly. Thus, the focus was laid on smaller target spherophanes.

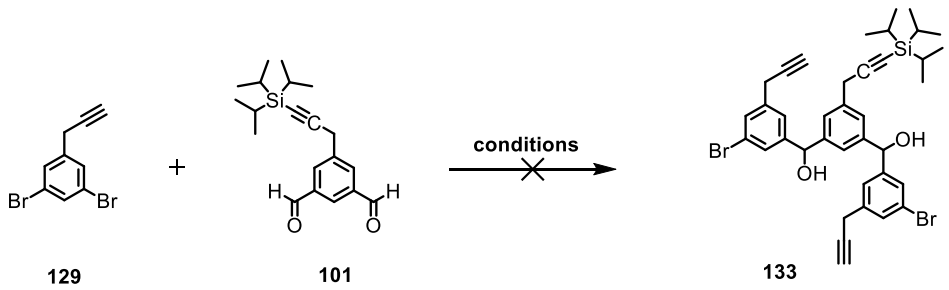

Scheme 28. Conversion of two equivalents of **129** and dialdehyde **101** to **133**. Conditions: *t*-BuLi, THF, -78 °C to rt °C, 16 h, none.

Conclusion and Future Perspectives

Dimerization of two hemispheres **90**, stabilized by *n*-propoxyl groups to form a cone-like structure has led to promising results towards hydroxylized and *n*-alkoxylized methylenespherophane **88**. The chosen *Turbo-Hauser-Grignard* approach to couple an Ar-H with a benzaldehyde moiety was chosen to have selective fourfold nucleophilic addition. The most promising results were found in experiments with only partial conversion of starting material (Table 2, entries 5 and 6) whereby one would assume an undesirable bottleneck-effect for all four nucleophilic attacks. But the analyzed species of interest did not show any residual aldehyde signals, which is possibly explained by enhanced reactivity upon the first formation of benzylic alcohol or the kinetic advances of intramolecular over intermolecular reactions. Temperature has influenced the outcome of the reaction substantially, to a much higher extent than other parameters as concentration or reaction duration. In principle, any reaction-type which results in an Ar-CH_2-Ar bond formation could be a possible candidate for the synthesis of a methylenespherophane derivative such as **88**. *Grignard*- and butyllithium chemistry was mainly discussed in this work, but also *Suzuki-Miyaura* cross-coupling reactions are well known to form Ar-CH_2-Ar. Drawback of this **first approach** is the high number of oligomeric side reactions when performing dimerization attempts with calix[4]arene-derivatives. Furthermore, final reduction of the electron rich *n*-alkoxyl groups, which is usually achieved only under harsh reaction conditions can be regarded as challenge.

***Suzuki*-type approach** was considered to be the most efficient due to a high degree of preorganization. However, required compound calix[6]arene **93** has not been synthesized from commercially available 4-*tert*-butylcalix[6]arene **118** by applying *retro-Friedel-Crafts* reaction conditions followed by complete reduction of any C-O bond contained in the molecule. Future attempts to synthesize **93** need to address this circumstance by avoiding phenol groups in the starting material. Instead, *Suzuki*-type cross-couplings[100] form the desired target structure (Scheme 29). One option is to start with 1-bromo-3-(methoxymethyl)benzene **134**, whereby the terminal protected methoxy group serves as endcap. The Ar-Br moiety is transformed to arylboronic derivatives **135** or **136**. By either adding excess of 3-bromobenzyl chloride or its borylated counterpart (3-borobenzyl chloride derivatives) under *Suzuki*-conditions, a stepwise elongation up to six aromatic units is aimed. Once we have **93** in hand, sixfold borylation to either compound **91** or **92** is favored to bind to the steric least hindered position. Electronic effects are for this particular formation negligible[116]. The obtained *zigzag* structure of the calix[6]-ring allows twofold Suzuki-type cross coupling with 1,3,5-tris(chloromethyl)benzene **166**, one from each side to generate spherical methylenespherophane **84**.[100] In addition, to support transitional *zigzag*-form, small Lewis acids could be supplied to the reaction mixture to keep on every side three boron atoms in plane.

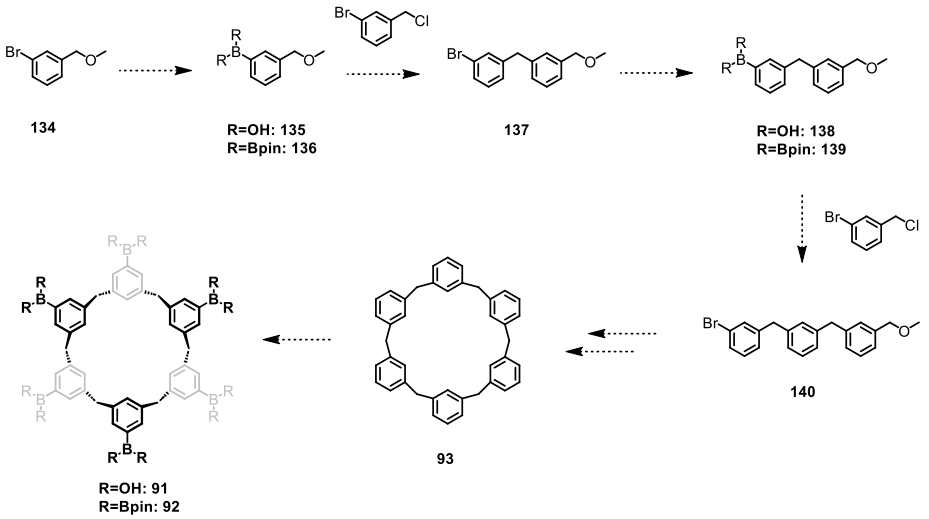

Scheme 29. Proposed reaction pathway for the synthesis of calix[6]arene **93** from small precursor 1-bromo-3-(methoxymethyl)benzene **134** reacting with 3-bromobenzyl chloride. As an alternative, Ar-Br moiety of 3-bromobenzyl chloride is transformed to an arylboronic derivative first.

The ***Vollhardt* ring closure** was the completely Ar-OH free approach to synthesize **84**. The idea resembles the *Suzuki*-type approach by having three acetylenes of deprotected **95** pointing upwards while the other three protrude on the other side. This form comprises all atoms for **84** in a well preorganized form. As seen in the previous described attempts, this is crucial not only because of the complexity to remove Ar-OH bonds, but also to avoid their potential of complexing small electrophilic species such as alkali metals, resulting in decreased analytical efficiency. Since this approach does not start from calix[4]arenes or calix[6]arenes, small building blocks **129** and **101** were synthesized in an elaborate reaction screening. The introduction of an acetylene required S_N2 reaction conditions, since more facile cross-coupling reactions were no option due to their preference to bind acetylene to aromatic positions. This strategy resulted in moderate yields. The necessity of keeping the silyl protecting groups for acetylenes over several reaction steps, as for example the synthesis of **101** from **130** caused product loss upon purification. Eventually, the desired *zigzag*-ring with 6 terminal protected acetylene groups **94-95** was not synthesized. Once in hand, reactions are performed to identify whether Co-mediated ring closure of the deprotected terminal alkynes takes place only on one or both sides of the *zigzag*-ring.

As methylenespherophane **84** was not successfully isolated in this work, the main challenges were found in its inherent cavity. It might be either filled up with small guests (mainly metal salts or small molecules, see introduction) or one of the eight aromatic units is pushed inside to form a bowl shape instead of a sphere (Scheme 30). This bowl form would distort NMR analytics and might even act as a host system itself.

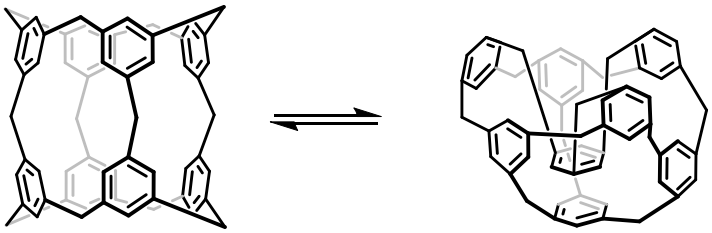

Scheme 30. Assumed equilibrium or persistent steric configuration of **84** which exhibits either a ball or a bowl shape.

To circumvent these issues, the molecular design was adapted to smaller molecules, consisting of only six aromatic units with smaller void and shorter reaction pathways to facilitate the screening.

3.2 Small Methylenespherophane **85**

As described in the introduction part, one of the most facile ways to synthesize cavitands is the $TiCl_4$ mediated coupling of benzyl bromide moieties with *ortho*-phenol positions[59]. In our example, oligomerization of starting molecules **141** and **146** is tried (Scheme 31). Even though the interlinking chain consists of only one -(CH_2)- group which causes strain and hence does not guarantee a successful spherical coupling product, this strategy is attempted, also for its direct reaction path. Synthesis for building block **145** was observed by LC-MS (ESI) and ^{1}H-NMR measurements. Due to a high polarity, neither normal nor reversed phase column chromatography resulted in pure product. Crystallization attempts could not remove all side products. Hence, **145** was reacted further upon a short reversed phase silica plug. Severe solubility issues did limit the scope of reactions for the synthesis of **146**, which was not formed under the chosen conditions.

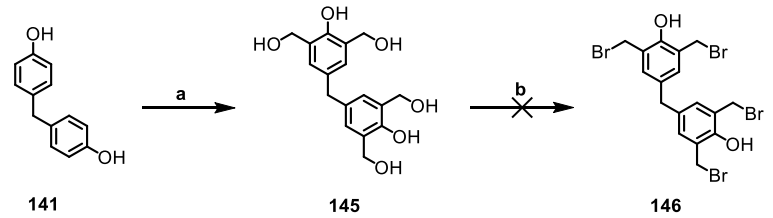

Scheme 31. Two step reaction pathway for **146** from 4,4′-methylenediphenol **141** is shown. Conditions: **a)** formaldehyde, NaOH, water, 40 °C, 16 h, not isolated **b)** HBr, AcOH, -10 °C to rt, 16 h; alternatively: triphenylphosphine, CBr_4, DMSO, 30 min.; no product seen with both methods.

In a new approach, other monomers were considered for trimerization experiments to form a sphere. As seen for methylenespherophane in previous chapter, compounds containing Ar-OH groups (attempts to **88**, see chapter 3.1) are not in favor for the molecular design, due to poor late stage reduction possibilities and their uncontrollable host-guest interaction potential.

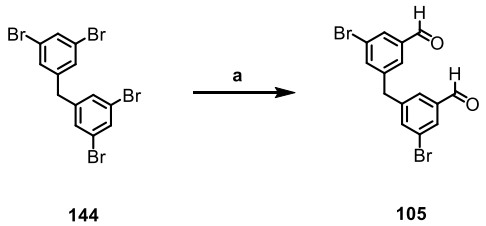

Scheme 32. Synthesis of **105** from **144**. Conditions: **a)** 1.) *t*-BuLi, THF, -78 °C, 1 h 2.) DMF, -78 to 0 °C, 2 h, 61%.

Starting material **144** was exposed to twofold bromine-lithium exchange and quenched with DMF at low temperatures to synthesize dialdehyde species **105**. Thereby we profit from single negative charge localization on each benzene core. **105** is expected to form spherical oligomers to a higher extent compared to monomer which binds two bromines on one benzene core and two aldehydes

on the other. In this case, more linear polymerization would be assumed due to competing intermolecular side reactions. A yield of 61% **105** was isolated only upon quenching the reaction mixture at 0°C after well controlled reaction time of 2 h (Scheme 32).

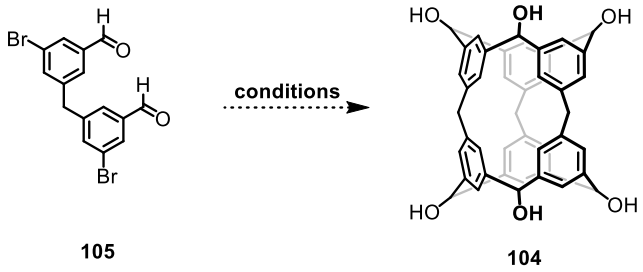

105 104

Scheme 33. Trimerization attempts for spherical **104** from **105** using butyllithium chemistry. Conditions: *t*-BuLi, THF, -78 to 0 °C (to rt), 2 h to 3 d.

Oligomerization with **105** was conducted in freshly distilled THF under highly diluted (2-4 mM) conditions to prevent competing linear polymerization reactions (Scheme 33). The reaction was kept at -78 °C for at least 1 h before warming up within 1 h gradient to 0 °C before stirring for 1 h at this temperature. HCl (1 M) was used as quenching agent before extracting with toluene. No significant difference in terms of newly observed TLC spots was reported between cold quench at 0 °C and the experiments quenched at room temperature. But in both cases, starting material was fully consumed. In principle, all isolated spherical oligomers are of great interest, whereby the trimer is assumed to be the most likely to isolate, considering conclusion of chapter 3.1 (Scheme 30).

m/z+1 of **104** (672.25 Da) with a value of 673 Da was detected from crude mixture by MALDI-TOF measurements using sinapinic acid as matrix (Figure 29). Furthermore, the *m/z*+1 of tetrameric oligomer (896 Da) was found as well. Supporting NMR analysis could not characterize target structure. All isolation attempts by chromatography techniques or size exclusion with Bio-Beads as filling material failed.

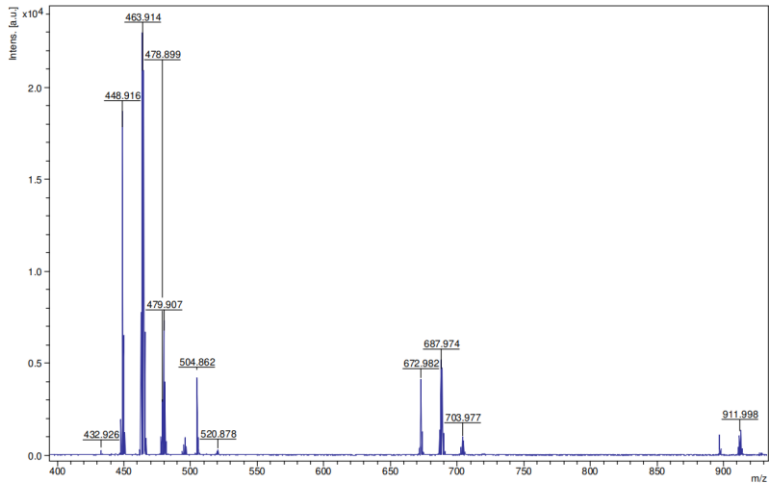

Figure 29. Measured MALDI on a Bruker microfleX device. *m/z* of possible **104** was measured in reflective mode, whereby also tetrameric product was detected.

Further reactions towards **85** were conducted, whereby **104** was assumed to be in the crude mixture. By performing reduction experiments to remove benzylic alcohol groups using known methods[93,92], no small methylenespherophane **85** was obtained.

An interesting result was obtained when the crude was completely deprotonated by an excess of NaH in freshly distilled THF prior to removing all side products on silica (eluent: EtOAc) and isolating a fraction at Rf: 0.7 when using MeOH as eluent. The residue was dissolved in THF and upon addition of a few drops of HCl 37%, white crystals precipitated in very low yields (1.2 mg on a 600 mg **105** batch reaction). Thereby, the solubility was absolutely limited to water and DMSO by using common solvents, which could indicate a 3D organic metal. ^{1}H-NMR in DMSO-*d* has shown signals in the aromatic region and MALDI measurements in the negative mode resulted in 671.24 Da, referring to *m/z*-1 of **104** (appendix, Figures 160 and 161). On the other hand, by measuring the sample in D_2O, vastly upfield shifted ^{1}H-NMR-signals between δ 4 and 3 ppm were reported, while MALDI measurements in the negative mode resulted in 666.26 Da (appendix, Figures 162 and 163). By titrating this sample with DMSO-d_6, the ^{1}H-NMR signals shifted downfield to the aromatic region. However, further NMR-measurements were inconclusive to verify **104**.

3.3 Hybrid Spherophane **86**

We started from commercially available 4,4'-methylenediphenol **141** which was crystallized from acetone before fourfold bromination in *ortho*-position to phenol was performed (Scheme 34). The isolated yield of **107** remained moderate compared to literature[117], even upon addition of a greater excess bromine and extended reaction times of 3 days. This is due to a high residual of threefold brominated compound, which is also not converted to **107** by the mentioned adapted reaction conditions. Furthermore, purification by chromatographic separation required increased column length to separate these two species with very close retention times. For the next step, Cu-catalyzed double sulfide arylation of aryl bromides was applied adopted from a literature procedure. While in the work of Chen *et al.*[103] these conditions result in a 90% isolated yield, we observe full conversion of **107** at 150 °C in PEG-400. However, the desired target structure **106** was not observed. No improvements were noticed upon pre-drying of fresh PEG-400 and replacement of Na_2S*9H_2O by anhydrous Na_2S.

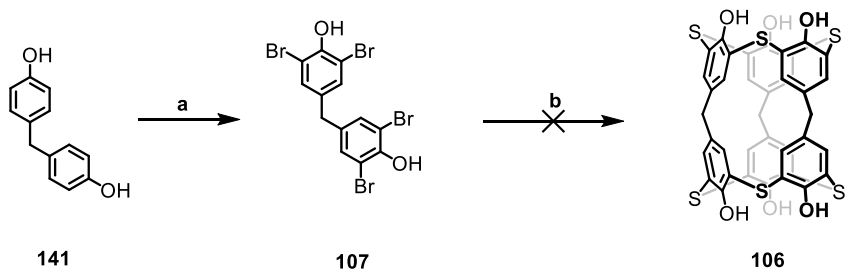

Scheme 34. Schematic representation of synthetic attempts for hybrid spherophane derivative **106** from **141**. Conditions: **a)** Br_2, AcOH, rt, 16 h, 27% **b)** Na_2S*9H_2O, CuI, K_3PO_4, PEG-400, 150 °C, days, no product seen; alternatively, dry Na_2S was used, no product seen.

The synthetic strategy was adapted and as a consequence of possible interfering guest inclusions by host compound **106**, all phenol groups were omitted to start from 4,4'-diaminodiphenylmethylene **142**. Fourfold bromination to **143** was conducted in good yields of 94% in MeOH: water deion. 1:1 by adding 5 eq of Br_2. High yields are the result of a very *ortho*-activating effect of aniline for the electrophilic substitution (Scheme 35). The removal of two amine groups occurred in a *Sandmeyer*-type reaction, whereby the formed diazonium salt was replaced by a proton under acidic conditions and reflux in EtOH to yield **144** moderately. For the one-pot synthesis experiments to **86** (Table 3), several oligomers were of interest and thus expected in the crude mixture of the reaction. Assumptions to mainly isolate the trimer arose from the work of Sergeev *et al.*[104] where cyclotris(m-phenylene sulfide) was isolated in 3.7% yield but no cyclo(tetra-1,3-phenylene sulfide), when dibromobenzene was reacted with Na_2S. Further aspects which justify the endeavors for the trimer is the reduced strain compared to the dimer and it is assumed to be less prone for host-guest chemistry or forming a bowl-shape in comparison with the tetramer. Screenings under argon atmosphere have been performed by either using Na_2S[104] or KSCN[118] as sulfur source.

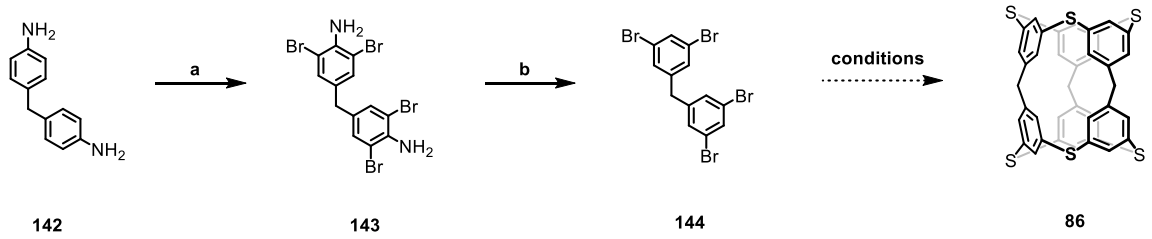

Scheme 35. Three step reaction sequence for synthesis of **86** from 4,4'-diaminodiphenylmethylene is shown. Conditions: **a)** Br_2, MeOH:DCM 1:1, rt, 3 h, 94% **b)** $NaNO_2$, H_2SO_4, EtOH, 78 °C, 16 h, 57% **conditions**) see Table 3.

Table 3. Reaction conditions for the trimerization approach of monomer **144** to target structure **86**.

#	m / mg	c / mM	conditions	conversion	*m/z* of 86	comment
1	200	25	Na_2S, NMP, 200 °C 16 h	full	yes	microwave
2	200	-	Na_2S, no solvent, 200 °C 16 h	partial	unclear	microwave
3	500	-	Na_2S, no solvent, 200 °C 16 h	combusted	no	combusted
4	200	41	KSCN, CuI, K_3PO_4, PEG-400, 150 °C, 16 h	full	no	microwave
5	250	3	KSCN, CuI, K_3PO_4, PEG-400, 150 °C, 20 h	partial	yes	-
6	1000	14	KSCN, CuI, K_3PO_4, PEG-400, 150 °C, 40 h	partial	yes	-
7	2000	14	KSCN, CuI, K_3PO_4, PEG-400, 170 °C, 40 h	partial	yes	-
8	1000	3	KSCN, CuI-excess, K_3PO_4, PEG-400, 150 °C, 20 h	partial	yes	-

Entry 1 of Table 3 has shown fraction of desired *m/z* 684.02 Da species by MALDI-TOF measurements. However, the target mass could not be isolated from the crude mixture. High amounts of NMP decomposition products hampered a facile purification. As no solvent was stated[104] in literature, neat reaction conditions (Table 3, entries 2-3) were attempted, resulting in only partial conversion to unwanted side-products or heat accumulation in upscale experiments.

Replacing the sulfur source by KSCN has resulted in successful detection of *m/z* 684.02 Da when the reaction was performed in a round bottom flask setup instead of a microwave (Table 3, entries 5-8). Even though only partial conversion of starting material **144** was observed, **86** might be formed. Incompletion of the reaction would give reason to consider six-fold diphenyl sulfide formation very unlikely, but increased reactivity upon first sulfide formation might occur. Nevertheless, a TLC-fraction very similar to **144** in polarity (Rf-value **144**: 0.55, Rf-value new spot: 0.61; eluent: cyclohexane) was isolated by chromatography on normal phase silica. This synthesized compound shows reasonable MALDI-TOF mass as well as NMR-measurements. The measured ^{1}H-NMR (Figure 30) indicates the exact number of protons and a severe downfield shift compared to starting material **144**. The singlet at δ 5.73 ppm represents the 6 benzylic protons, which is against all expectations, a vast downfield shift.

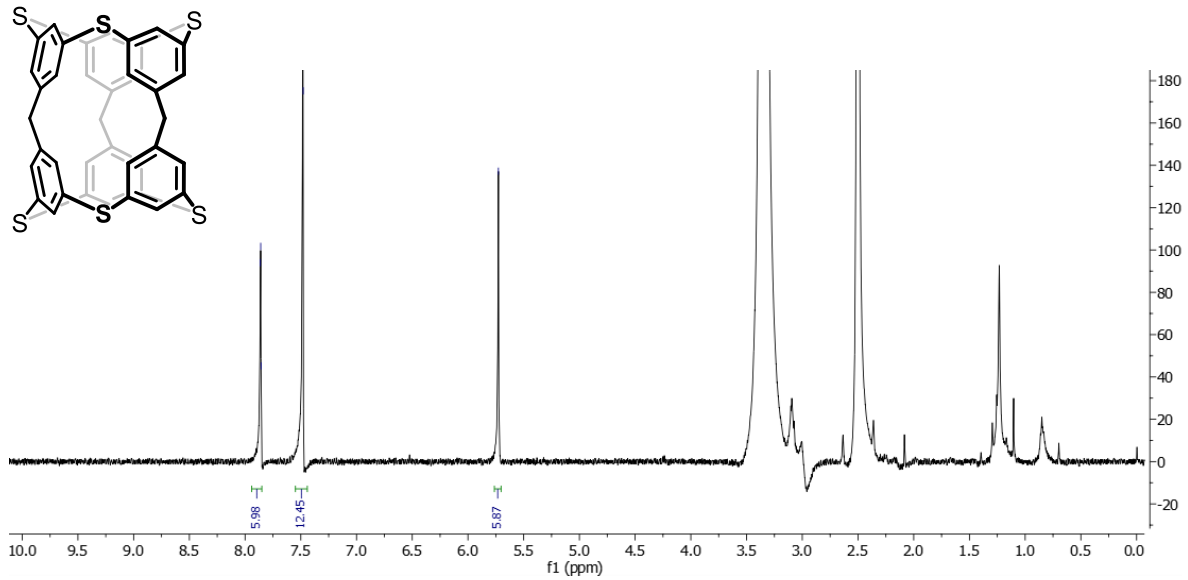

Figure 30. Measured ^{1}H-NMR of the newly formed spot from entries 5-8, showing possible **86** molecule. Signals below 3.5 ppm are attributed to solvent or H-grease. Measurement was conducted on a 500 MHz instrument in DMSO-d_6 as solvent. Coupling constants are: δ 7.86 (d, J = 1.8 Hz, 6H), 7.48 (d, J = 1.8 Hz, 12H), 5.73 (s, 6H) ppm.

Supportive for our target structure is the NOESY-data (Figure 31, left) which indicates an interaction between the 6 benzylic protons and the 12 aromatic protons in close proximity. COSY (Figure 31, right) indicates only a weak interaction between two aromatic proton shifts only, which is expected for **86**.

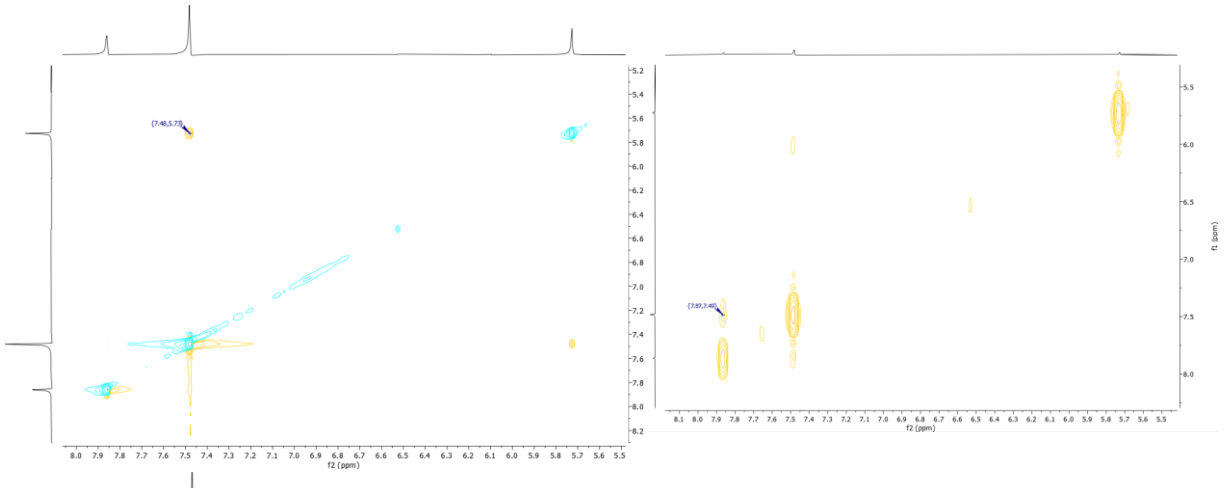

Figure 31. Measured NOESY (left) and COSY (right) in DMSO-d_6 of the newly formed fraction from entries 5-8, showing possible **86** molecule. Measurements were performed on a 500 MHz instrument.

Additional experiments were conducted in DCM-d_2. A slight upfield shift in ^{1}H-NMR spectrum (Figure 32) of δ 0.09 to 0.18 ppm compared to spectrum measured in DMSO-d_6 (Figure 30) is noticed in addition to a reasonable proton signal splitting. DOSY analysis (Figure 33) verified the isolated substrate as single species. HSQC studies (Figure 34) have resulted in 3 signals between δ 121 and 137 ppm and therefore no benzylic C-H bond, which disconfirms our target structure **86**. HMBC measurements (Figure 35) have shown two interactions of Ar-H at δ 7.39 ppm, one with its own ^{13}C-signal in *meta*-position of δ 132.7 ppm, which was extracted from HSQC. Furthermore, the other long range coupling of Ar-H at δ 7.39 ppm interacts with the Ar-H signal at δ 7.68 ppm, which would fit for the expected structure of **86**. However, Ar-H signal δ 7.68 ppm does only show unclear HMBC interaction with δ 7.39. Possible benzylic protons at δ 5.55 ppm show a HMBC interaction with a ^{13}C at δ 146.7 ppm, which in theory refers to the aromatic carbon atom next to the -CH_2- bridge.

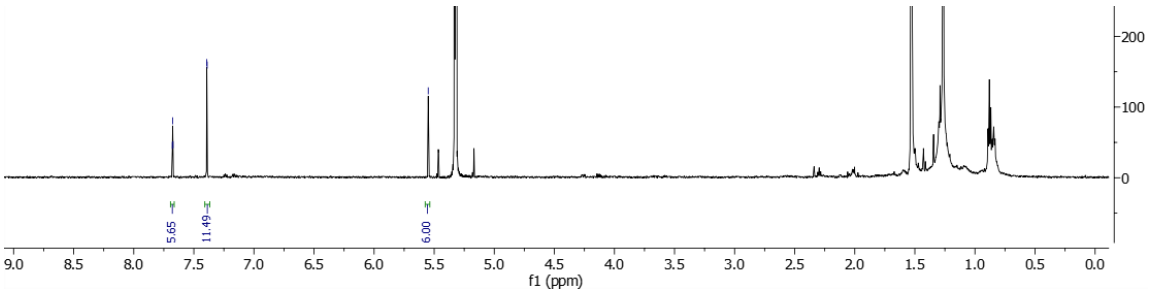

Figure 32. Measured ^{1}H-NMR showing possible **86** molecule. Solvent of sample (Figure 29) was changed to DCM-d_2 instead of DMSO-d_6. This results in a slight upfield shift. Measurement was conducted on a 600 MHz instrument. Coupling constants are: δ 7.68 (t, J = 1.8 Hz, 6H), 7.39 (d, J = 1.8 Hz, 12H), 5.55 (s, 6H) ppm.

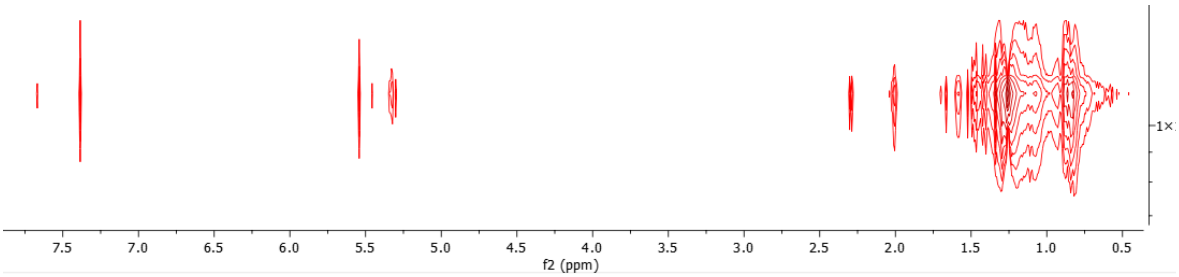

Figure 33. Measured DOSY of possible **86** molecule. Signals at δ 7.68, 7.39, 5.55 ppm do show same hydrodynamic behavior, as part of a single species.

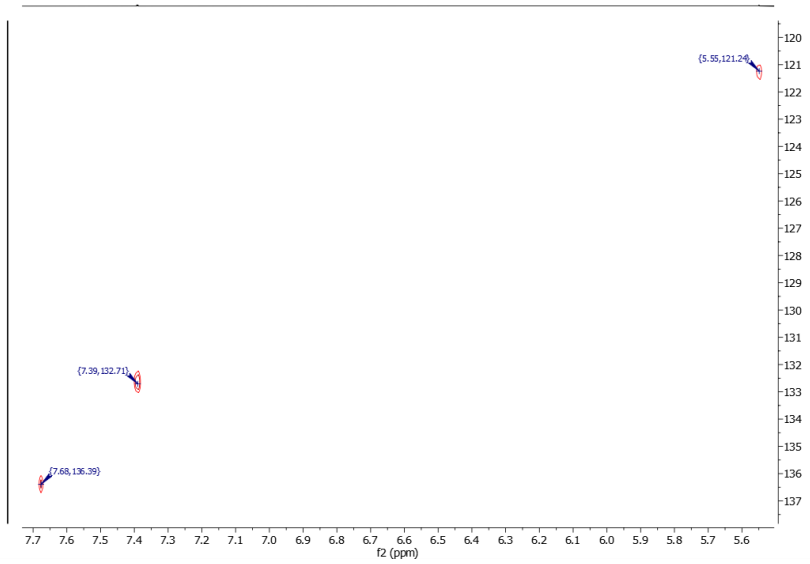

Figure 34. Measured HSQC in DCM-d_2 of the newly formed fraction from entries 5-8, measured on a 600 MHz instrument.

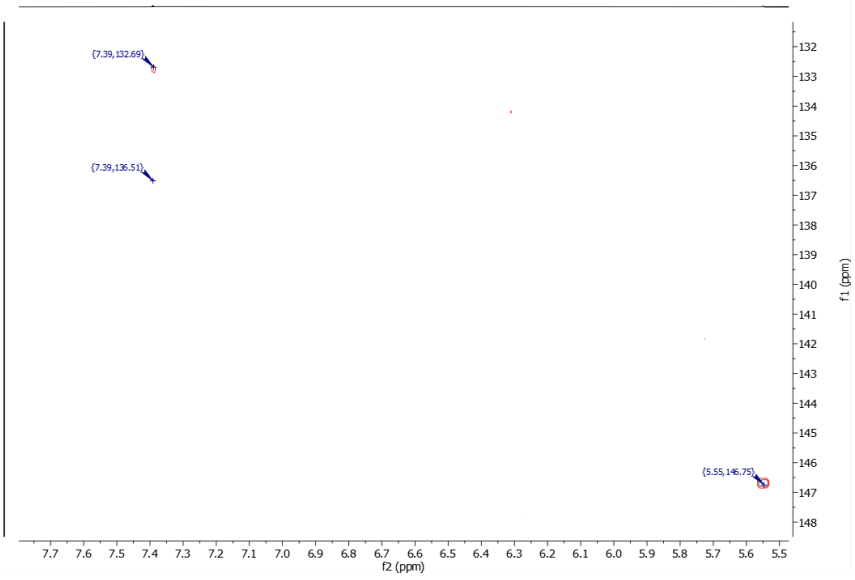

Figure 35. Measured HMBC in DCM-d_2 of the newly formed fraction from entries 5-8, measured on a 600 MHz instrument.

Due to low polarizability of target structure **86**, high resolution ESI was no option for accurate mass measurements. An alternative was found in high resolving MALDI devices. Exact *m/z* of 684.02 was not observed, *m/z*+1 seen instead by 685.09 Da (Figure 36). However, the slight deviance and the not precisely fitting isotope pattern of the isolated fraction (Table 3, entries 5-8) does not guarantee the accomplished synthesis of **86**. Masses for possibly higher order oligomers than the trimer product were not found by MALDI spectrometry.

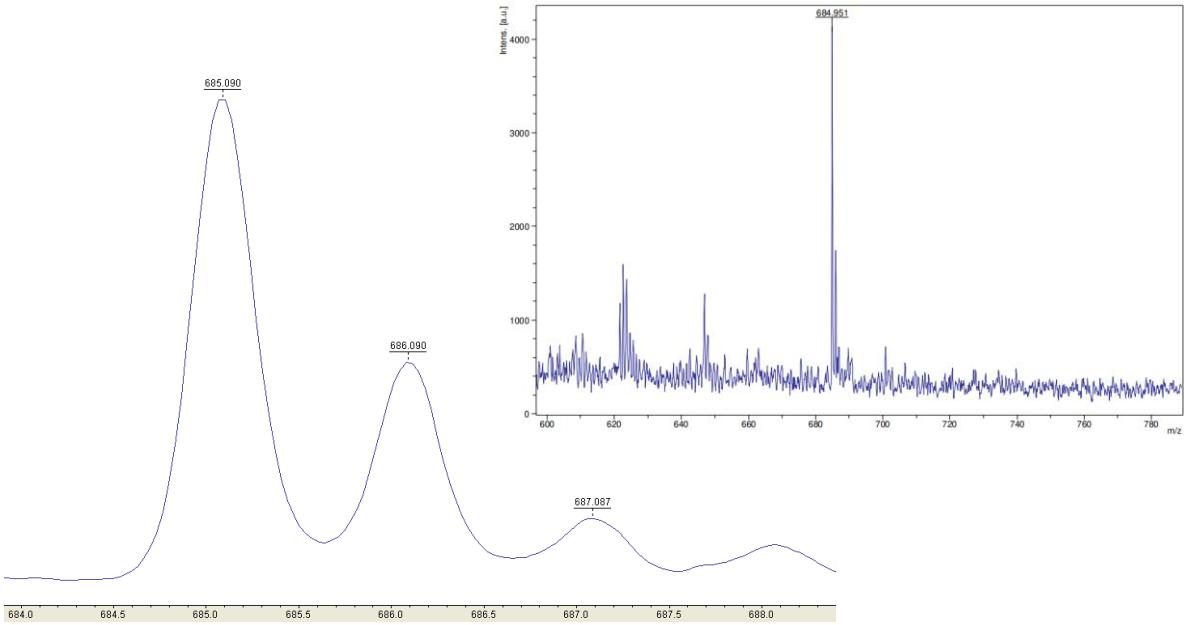

Figure 36. Measured MALDI on a high resolution Bruker rapifleX device. *m/z*+1 of possible **86** was measured in linear positive mode, whereby the isotope pattern for the third and fourth signal do not fit by intensity.

Upscale experiments (Table 3, entries 6-8) failed to increase the yield of the well investigated spot, whereby the mass of the isolated white crystals was in the order of 1 mg on a 2000 mg scale reaction. This refers to only 0.1% isolated yield for trimeric structure **86**. Investigations have shown necessity of basic workup to observe the signal of interest on TLC. CuI excess (Table 3, entry 8) has not shown improved conversion of starting material **144** to a higher extent than 90%, which excludes a stoichiometric function of the catalyst in the reaction mechanism.

Conclusion and Future Perspectives of **85** and **86**

Downscaling of original molecular design **88** to smaller spherical target compounds **85** and **86** was aimed. Even when the symmetry of these models is decreased from a cuboctahedron to a D_{3h} point group, the designed molecules relate to the novel class of spherical molecules which has not been published yet. Fast reaction screening was feasible since one pot reactions from accessible starting materials were performed. The coupling attempt of **141** with **146** was well described in literature by C. David Gutsche[58], but failed due to inaccessibility of **146**.

85's precursor **104** was attempted to synthesize in a one-pot reaction from **105** using butyllithium chemistry. *m/z* of **104** was found according to MALDI-TOF measurements in the crude mixture and an isolated fraction. However, all analytical techniques such as NMR-spectroscopy led to inconclusive results. For further experiments, we enlarge the screening methods by adding preorganizing species (e.g. cationic alkali metals, toluene as solvent; or covalently tether methylene-bridges) as reaction supplement to guarantee wrapping of the monomer **105** around this particular guest and therefore a spherical intermediate structure is formed.

In close analogy, hybrid spherophane **86**, containing 6 sulfur heteroatoms was attempted to synthesize. Even when numerous analytical techniques were indicative to have target compound isolated, HSQC-NMR analysis excluded its structure when measuring the most promising isolated fraction. Reliable reproducibility of the reaction was not achieved. Future bottom up approaches for **86** syntheses are depicted in Scheme 36, where a controlled intramolecular sphere formation possibly occurs over four *Buchwald-Hartwig*-type reaction steps and two thiol deprotections.

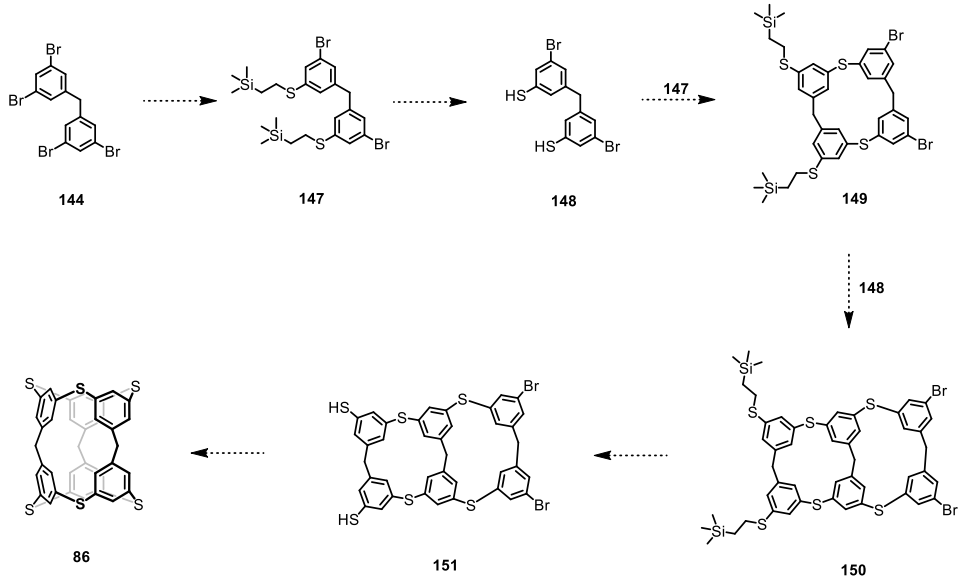

Scheme 36. Schematic six step reaction pathway for the synthesis of **86** from **144** by applying cross coupling reactions mainly.

4 Aim of This Work and Synthetic Strategy (Part B)

4.1 Aim of This Work

In this work, the focus is laid on the synthesis and isolation of a square pyramidal shaped cage molecule **108** composed of a calix[4]arene and a porphyrin subunit, interlinked via four phenylacetylene bridges (Figure 37). From a structural point of view, this target compound resembles the previous discussed spherophanes in regard of bearing 8 aromatic units with 4 methylene and 4 acetylene interlinkages. The major difference is the flat porphyrin moiety which equips the molecule not only with new characteristics but maintains a high C_{4v} symmetry. This design gives us the expectation of adsorbing the porphyrin on surfaces or interfaces[119], while the calix[4]arene points in a 90° angle towards the outside and might undergo derivatization to implement a variety of functional groups. For this reason, *n*-propoxyl-groups of the molecular design are not intended to be fully removed upon reduction. Regarding molecular architecture, resemblance of **108** with a Moon lander spacecraft is given.

108

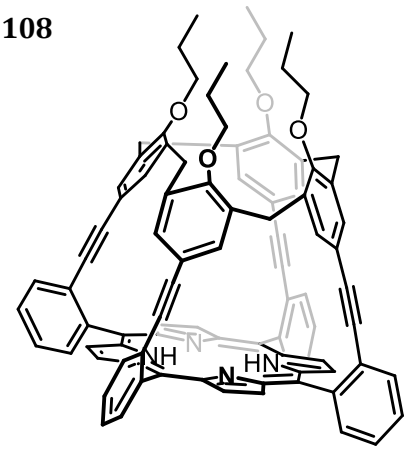

Figure 37. Target structure of square pyramidal shaped cage molecule **108**.

4.2 Retrosynthetic Analysis for Square Pyramidal Shaped Cage Molecule **108**

Target molecule **108** is synthesized from **109** by porphyrinogen oxidation to a porphyrin moiety (Scheme 37). In general, *Lindsey*-conditions[70] are applied for this 6 H^+ 6e^- loss step, but in combination with the calixarene-part and the steric hindrance and strain, alternative methods eventually need to be considered. **109** is necessarily oxidized to **108** to build its stable porphyrinoid form. This is due to the equilibrium with its precursor **110**, whereby four pyrrole units are condensed to a porphyrinogen. For this step, the pyrrole moieties are brought into close proximity. Thereby we profit from hydrophobic aggregation effects of the *n*-propoxyl tails of the calix[4]arene unit, which also explains why the calixarene is derivatized first and the porphyrin is introduced in a last step. Starting from the flat porphyrin, its planar symmetry is expected to be not in favor to overcome entropic hurdles for closure of calix[4]arene. Therefore, no synthetic efforts in such a reaction pathway were elaborated. **110** is readily synthesized in an eight step reaction sequence.

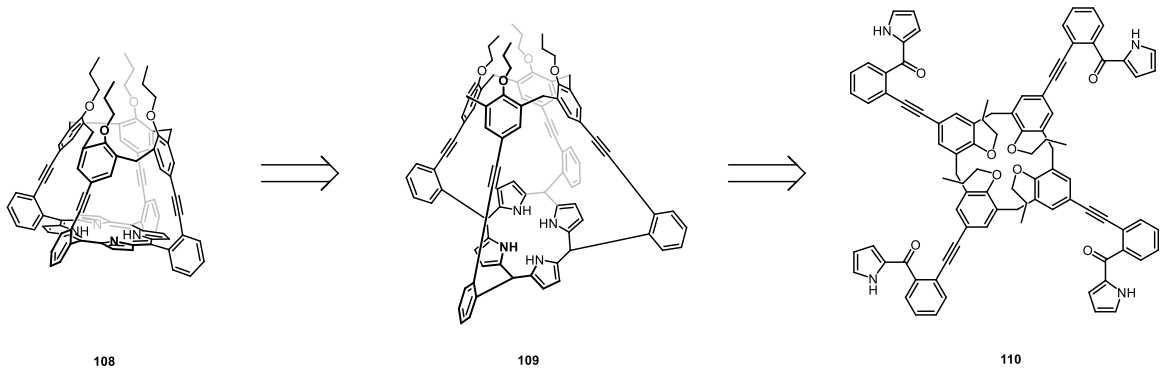

Scheme 37. Retrosynthesis for square pyramidal shaped cage molecule **108** containing a porphyrin subunit from its porphyrinogen precursor **109** and pyrrole building block **110**.

5 Results and Discussion

5.1 Electroorganic Synthesis in an Undivided Cell

Commercially purchased starting material **152** was distilled *in vacuo* (10 mbar) at 100 °C prior to use. Deprotonation of the α-carbonyl proton was achieved by adding LDA 2 M, before S_N2 reaction on *n*-alkyl bromide chain proceeded to products **153** and **156** in good yields (Scheme 38). Thereby, the α-substituent of the enolate was limited to carbanion stabilizing groups and steric hindrance. Deprotection of the methyl esters to corresponding carboxylic acids **154** and **157** was attained by LiOH addition without converting the nitrile groups to unintended side products. Final reaction steps of products **155** and **158** respectively were performed in an undivided electrochemical cell under current controlled conditions (8 mA) through a glassy carbon working electrode and a platinum gauze counter electrode. Initially, the carboxylic acid is deprotonated first before two consecutive single electron oxidation steps are performed whereby CO_2 is abstracted and the former α-carbon atom is converted to a carbenium ion in a *Hofer-Moest* reaction. Its stability strongly depends on the electronic effect of the α-carbon substituent. Hence, we are vastly limited in molecular screening since on one hand, promoting substituents for insertion of an alkyl chain under S_N2 conditions results in poor carbenium ion formation and *vice versa*. Intramolecular attack of the nitrile nitrogen electron lone pair to the now positively charged α-carbon followed by aqueous workup results in *Ritter*-reaction to form 5- or 6-membered ring lactams. The intended lactams were not isolated, however the overoxidized dihydropyridinone **158** from **157** was reported. In case of less favored six-ring formation product **155** from **154**, isolated yields were slightly decreased. A noteworthy side product is the nucleophilic attack of the solvent MeOH; replacement by hexafluoroisopropanol led to lower conductivity and poor to none conversion.

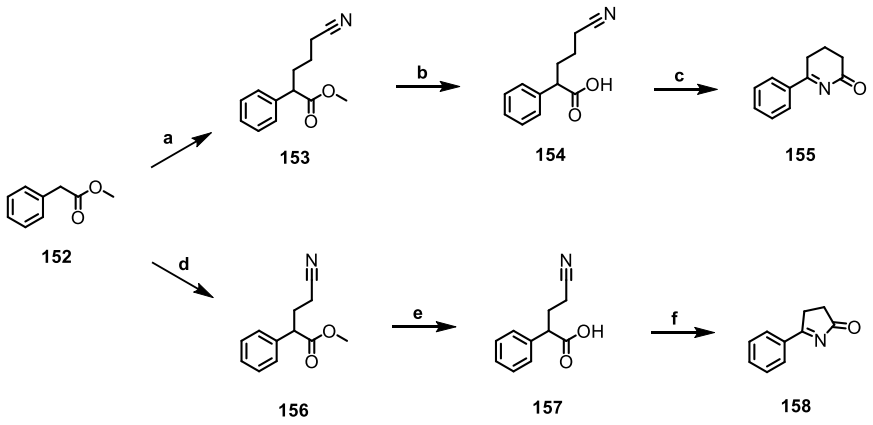

Scheme 38. Electroorganic synthesis of **155** and **158** from commercially available **152**. Conditions: **a)** LDA, 4-bromobutanenitrile, THF, -78 to rt °C, 16 h, 63% **b)** LiOH, THF: water 1:1, rt, 3 h, 80% **c)** K_2CO_3, MeOH, rt, 16 h, WE: glassy carbon RDE, CE: Pt-gauze, 8 mA, 14% **d)** LDA, 3-bromopropanenitrile, THF, -78 to rt °C, 16 h, 75% **e)** LiOH, THF: water 1:1, rt, 3 h, 83% **f)** K_2CO_3, MeOH, rt, 16 h, WE: Glassy carbon RDE, CE: Pt-gauze, 8 mA, 17%.

These results confirm the feasibility of electroorganic late stage modification for a so far non-reported reaction pathway to synthesize **155** and **158** in our undivided cell. This justifies the attempts to synthesize our target structure of a square pyramidal shaped cage molecule **108** also in electrochemical fashion. Concretely, a late stage modification of a porphyrinogen to a porphyrin is aimed (chapter 5.2).

5.2 Square Pyramidal Shaped Cage Molecule

Compounds **113** and **114** were already in hand from the methylenespherophane project. Fourfold aldehyde insertion on the upper calix[4]arene rim was performed best by exposing **114** to *t*-BuLi before cold quenching with DMF (Scheme 39). Yields of **159** dropped severely when *n*-BuLi was used instead of *t*-BuLi, as only twofold bromine-lithium exchange proceeded.

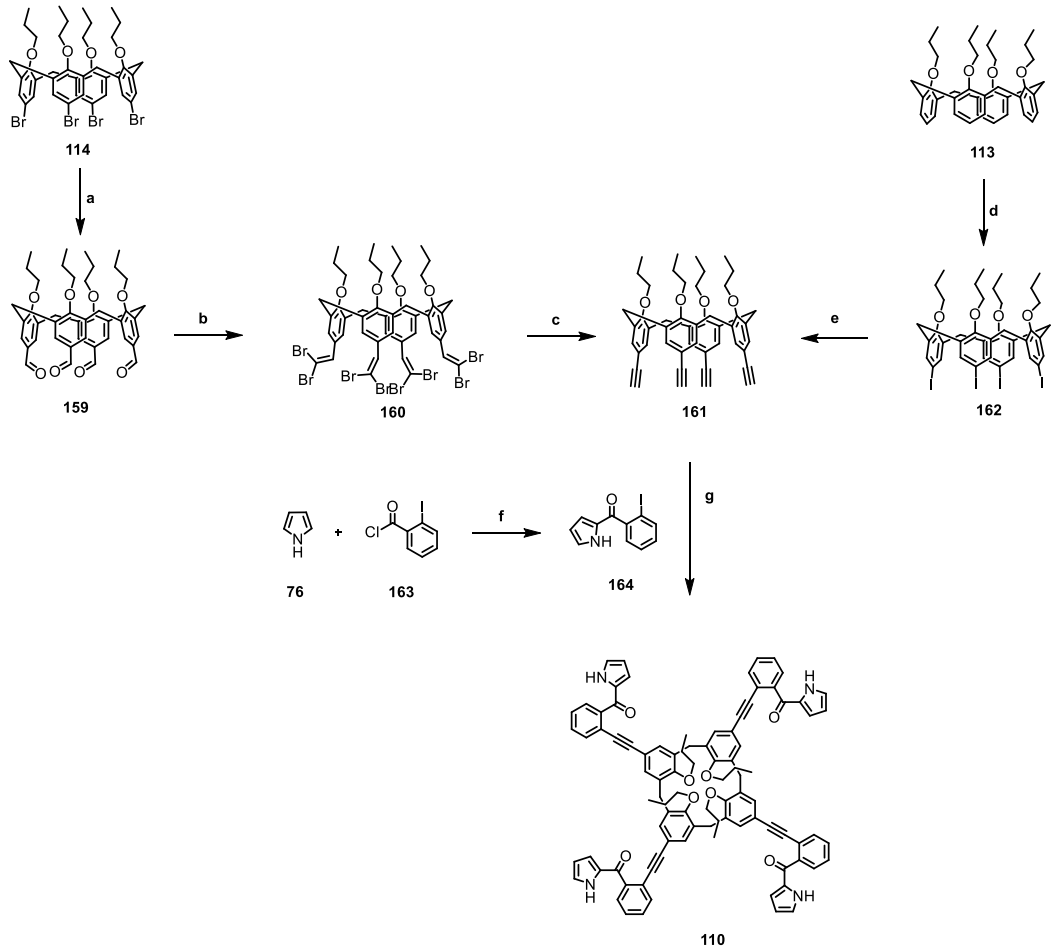

Scheme 39. Synthesis of pyrrole precursor **110** from **113** and **114**. Conditions: **a)** 1.) *t*-BuLi, THF, -78 °C, 30 min. 2.) DMF, -78 °C to rt, 3 h, 95% **b)** CBr_4, PPh_3, DCM, 0 °C to rt, 2 h, 64% **c)** *n*-BuLi, THF, -78 ° C to rt, 3 h, 60% **d)** I_2, $Na_2S_2O_8$, acetonitrile, 80 °C, 16 h, 76% **e)** 1.) TMS-acetylene, $PdCl_2(PPh_3)_2$, CuI, triethylamine, rt, 2 d, 82% of **170** 2.) TBAF, THF, rt, 1 h, 56% **f)** PhMgBr, toluene, 0 °C, 30 min., 50% **g) 164**, $PdCl_2(PPh_3)_2$, CuI, triethylamine, rt, 3 d, 34%

Next, two step *Corey-Fuchs* reaction resulted in **161**, which was isolated after cumbersome chromatography purification. Triphenylphosphine mediated reaction sequence to **160** from **159** was isolated in decent yields, while the second step to **161** required 2 equivalents of n-butyllithium to remove bromine and form lithium acetylides. Alternatively, **161** was synthesized from **113** in two steps. Iodination of **113** to **162** yielded 76% in acetonitrile, using I_2 as iodine source and adding $Na_2S_2O_8$ and phase transfer catalyst tetramethylammonium iodide. Next, *Sonogashira*-type cross coupling reaction with silyl protected acetylene was performed. Interestingly, yields were increased substantially when only triethylamine was used as solvent. Deprotection using TBAF resulted in **161**. Porphyrin precursor **164** was formed by pyrrole **76**, freshly filtered over Al_2O_3, reacting with *Grignard*-reagent PhMgBr and subsequent quenching with **163**.

The following product **110** was attained by fourfold cross-coupling reactions of **161** with **164** in moderate yields of 34%. As already seen for the alternative route to **161**, this *Sonogashira*-type cross coupling was performed best by only using triethylamine as solvent. Isolation of **110** showed to be challenging, due to significant product loss on column chromatography caused by smearing even upon elaborating a variety of eluents. Moreover, several crystallization attempts failed. Nevertheless, once in hand, all required moieties were present for following pyrrole ring closure experiments to porphyrinogen **109**. This is oxidized to porphyrin **108** subsequently.

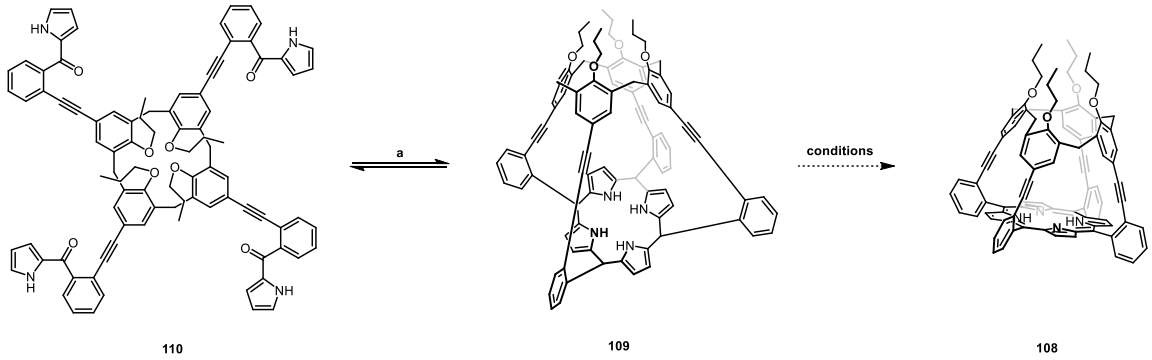

Scheme 40. Synthetic plan to condensate pyrroles **110** to porphyrinogen **109** and oxidation to porphyrin **108**. Conditions: **a)** BF_3-etherate/TFA, DCM, 40 °C, 2 h; alternatively: $NaBH_4$, THF: MeOH: iPrOH 3:1:15, 65 °C, 1 h; both not isolated, since unstable **conditions)** see Table 4.

n-Propoxyl-tails of the calix[4]arene moiety in **110** aggregate and hence, all of the four acetylenes point in the same direction. This is to our great advantage, since pyrroles are brought into close proximity to favor condensation to porphyrinogen **109**. This reaction is performed best by adding a Lewis-acid as BF_3-etherate or $NaBH_4$ in protic polar media. The stepwise loss of four oxygen atoms in **110** to **109** is monitored by MALDI-analysis (appendix, Figure 164). This reaction step is in equilibrium and thus, final oxidation to porphyrin facilitates isolation and characterization. Adding oxidizing agents[72] as the modified quinone molecule DDQ is sufficient to form porphyrin irreversibly. In case of **108**, this step did not succeed even after exhaustive screening. One possibility is the steric hindrance of the target compound, which blocks the oxidizing agent DDQ to

attach. Mechanistic studies have shown the necessity of forming a charge-transfer complex transition state[120] in order to oxidatively cleave *p*-methoxybenzyl groups to isolate alcohols. This supports the assumption of similar transitional state behavior for the conversion of porphyrinogens to porphyrins using quinone derivatives. Alternatively, this reaction step is performed electrochemically (Table 4), as the contact between electrode and atom might be sufficient to overcome kinetic hurdles without any need of steric demanding transition states. To our support, electrochemical oxidations of porphyrinogens to porphyrins have been conducted successfully[90] in the past.

Table 4. Reaction conditions for the oxidation of porphyrinogen **109** to porphyrin **108**.

#	e^- mediating agent	potential controlled vs. SCE	cycles	current controlled	*m/z* of **108**	comments
1	none	-0.5 to 1 V	100	-	no	-
2	chloranil	-0.5 to 1 V	100	-	traces	-
3	chloranil	-0.5 to 1 V	200	-	no	stirring
4	chloranil	-2 to 3 V	600	-	yes	Soret band
5	chloranil	-	-	1.5 h 10 mA	traces	-
6	chloranil	-	-	1.5 h 100 mA	yes	Soret band

Prior to all electrochemical experiments, crude mixture of **109** was plugged over a short silica column (eluent: cyclohexane: EtOAc 4:1) to remove solvents and Lewis acid. To not overoxidize target compound **108**, mild potential controlled reaction conditions between -0.5 and 1 V vs. SCE (CV in appendix, Figure 165) were applied in absence of oxidizing agent first (Table 4, entry 1). A glassy carbon rotating disc electrode (RDE) is chosen for mild oxidation processes, while a platinum gauze (enlarged surface) counter electrode catalyzes the reduction process to H_2. Solvent was MeOH: DCM 6.5:1.5 by adding a drop of H_2SO_2 96% as electrolyte replacement, H^+-supplier and protectant for overoxidation. Since no conversion to **108** was seen by MALDI measurements, chloranil as a mild electron mediator was added in equimolar amounts to porphyrinogen (Table 4, entries 2-6). *m/z* 1294.5 Da signal was detected by MALDI but porphyrinogen to a great extent available as well (entry 2). By increasing the number of cycles to 200 and rotation of the RDE, no **108** was found (entry 3). Thereby, our initial idea was the removal of possible formed **108** from the electrode surface. Hypothetically, the applied stirring might have resulted in disturbance of the diffusion regime close by the electrode and hampered the reaction. By driving the potential between -2 and 3 V vs. SCE (CV in appendix, Figure 166) and increasing the number of cycles to 600 (entry 4), to our delight **108** was detected by MALDI measurements as well as by high resolution ESI analysis (Figure 38) of the crude mixture.

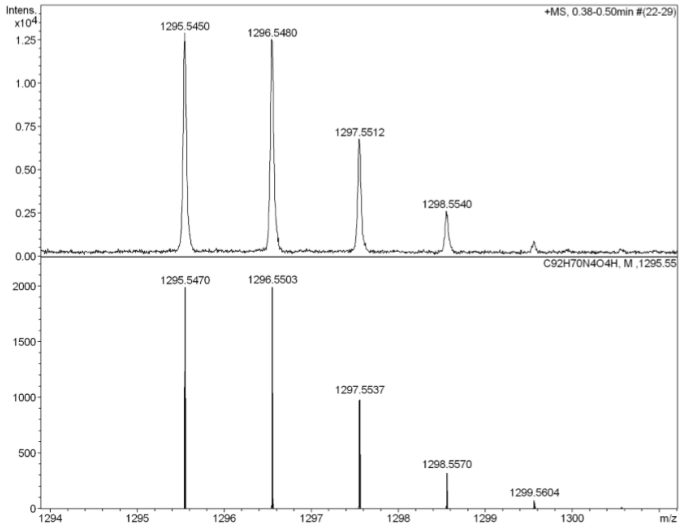

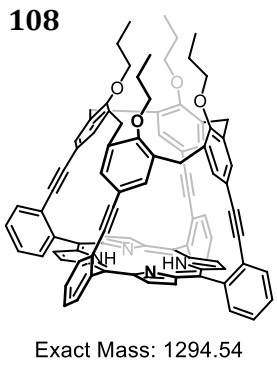

Figure 38. Intensity vs. *m/z* in Da is shown (Table 4, entry 4). *m/z* +1 calculation (bottom) as well as the expected isotope pattern fits for measured **108** sample (top). Measurements were performed by direct ESI on a high resolution instrument.

Furthermore, the characteristic Soret absorption band of a porphyrin at approximately 420 nm was observed by performing UV-VIS spectroscopy measurements (Figure 39, left). Inherent Q-bands possibly arise at 500 nm. The reaction mixture was colored in dark reddish, which is characteristic for porphyrin synthesis (Figure 39, right). However, ^{1}H-NMR spectroscopy could not identify the expected chemical upfield shift of the two porphyrin N-H atoms at around δ = -5 ppm.

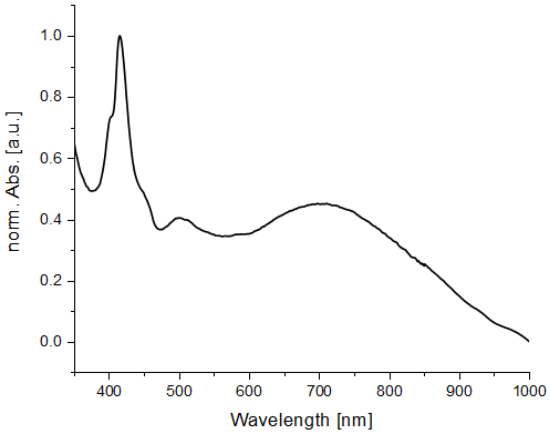

Figure 39. Left: UV-VIS spectroscopy of reaction mixture (Table 4, entry 4). Right: Electrochemical cell apparatus where the reaction was conducted and its characteristic dark reddish color.

Initial isolation trials of **108** by various chromatographic and size exclusion techniques as SX-columns and GPC were not successful, whereby the lability of the very strained design was assumed

to result in partial decomposition. To have a higher yield of **108**, which might facilitate its isolation, current controlled conditions were applied as an alternative to the so far potential controlled experiments. 10 mA current for 1.5 h (entry 5) did show only traces of **108** in MALDI (matrix: DCTB), while at 100 mA (entry 6) the mass was verified by MALDI and Soret absorption band detected. Isolation attempts of **108** by chromatography, size exclusion and GPC all failed. During GPC separation, only Soret band active species (420 nm as reference) were isolated. One of these fractions has given interesting ^{1}H-NMR signals with reasonable proton signals in the aromatic region for molecule **165**, which is the completely deoxygenized reduction product of **108** (Figure 40). The signals in the aromatic region correspond to expected ^{1}H-NMR shifts while signals between δ 3.80 and 1.80 ppm exclude the possibility of having isolated **165**. Additional HMBC and HSQC spectra could not resolve this fraction. The measured low resolution MALDI mass has given only *m/z*+4, 1066.5 Da (Figure 41), which disproves **165** as well.

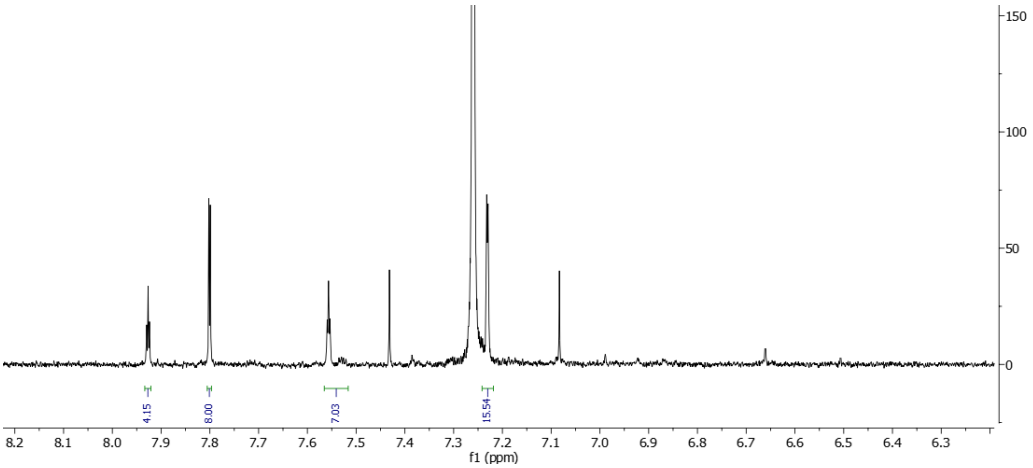

Figure 40. Measured ^{1}H-NMR of the GPC-isolated 420 nm active fraction, showing possible **165** molecule. Chloroform signal at δ 7.26 ppm and its satellites are not labelled. Measurement was conducted on a 600 MHz instrument in chloroform-*d* as solvent.

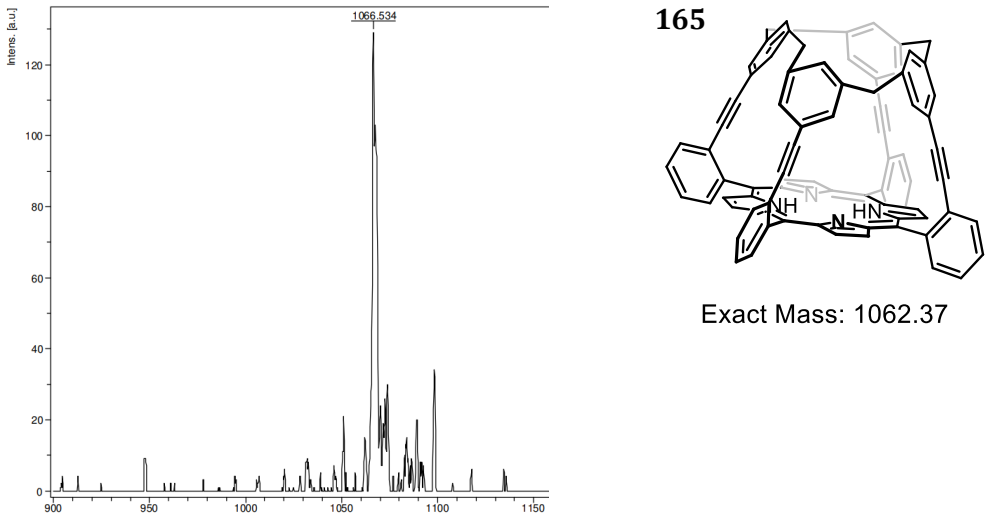

Figure 41. Intensity vs. *m/z* in Da is shown. *m/z* for measured **165** deviates by 4 Da. Measurements were performed by a low resolution MALDI-TOF instrument.

Conclusion and Future Perspectives

To proof the concept of performing electroorganic reactions with our setup in an undivided cell, we performed *Hofer-Moest*-reaction followed by intramolecular *Ritter*-reaction on two different previously synthesized substrates. Even though the *Ritter*-product lactam could not be detected by analytical methods, its overoxidized dihydropyridinones **155** and **158** were characterized for both products, showing the suitability of our electrochemical cell. By adjusting electrochemical parameters and varying the substituents in α-position of the carboxylic acid, the novelty of this work could extend the interest of this research upon a substantial amount of screenings, using this method.

Precursor **110** was successfully synthesized in an eight step reaction sequence whereby challenging purification steps were required especially for **161** and **110**. Alternative routes for **161** were elaborated as well to facilitate synthesis of **110**. **109** was successfully synthesized by condensation of four pyrrole unit to the poryphyrinogen which was monitored by MALDI-TOF analysis. However, due to instability of **109**, the intermediate was directly exposed to oxidizing conditions. Target molecule **108** was most likely synthesized under electrochemical conditions, which could be detected by high resolution ESI, MALDI-TOF and UV-VIS absorption spectroscopy. However, isolation attempts for this strained target molecule, which is possibly prone to decomposition in its pure state, failed upon a variety of separation methods.

Considering electroorganic reaction technique suitable for certain steps especially where conventional procedures fail is not often reported in literature. The more delightful that sophisticated target structure **108** is a possible example for a feasible electrochemical late stage modification. In the end, to successfully isolate such a structure which combines a calix[4]arene with a porphyrin subunit, one probably needs to adapt the molecular design. The phenylacetylene bridges need to be replaced with a less reactive moiety. In our outlook, the acetylene which gives much strain to **108** is reduced to an ethyl group (Figure 42). Thereby, the conjugated character of the design is lost but isolation trials of **167** from crude mixture might succeed with a higher probability.

167

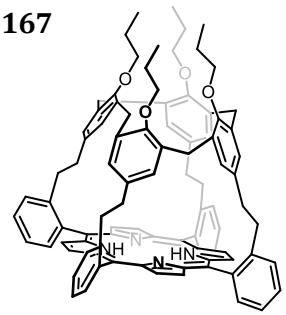

Figure 42. Alternative molecular design **167** for combining a calix[4]arene with a porphyrin.

6 Experimental

General Remarks

All reagents and solvents were purchased from Sigma-Aldrich, Acros, Alfa Aesar, Apollo Scientific, Combi-Blocks, Fluka, Fluorochem and TCI and applied without further purification unless stated otherwise. Solvents used in reactions were freshly distilled prior to use if necessary/required, otherwise solvents of reagent grade quality were used, which were stored over molecular sieves (4 Å).

Silica gel (40-63 µm) from SiliCycle Inc. was used for flash column chromatography and technical grade solvents from Biosolve were applied as eluents. TLC plates were purchased from Supelco as 60 F254 aluminum sheets. Glass-Backed, 2000 µm thick silica F254 with dimension 20 x 20 cm was used for preparative TLC.

^{1}H-NMR, ^{13}C-NMR, ^{19}F-NMR and ^{31}P-NMR and all 2D-NMR measurements were performed on Bruker Avance III or Avance III HD instruments equipped with either BBFO, BBI, or BBO probe heads, operating at 250, 400, 500 or 600 MHz proton frequencies. The spectra were recorded at 298 K and the proton shifts reported in ppm, referenced to the particular solvent shift. Coupling constants J are stated in Hz with an accuracy of ± 0.1 Hz.

MALDI-TOF measurements were performed on a Bruker microfleX and a Bruker rapifleX instrument by using different modes and matrices stated in the respective experiments.

GC-MS (EI) measurements were conducted on a Shimadzu GCMS-QP2010 SE gas chromatograph system containing a Zebron 5HT Inferno column (30 m x 0.25 mm x 0.25 mm) at a 1 mL/min. helium flow rate, coupled to a Shimadzu mass detector (EI 70 eV).

High resolution (ESI) mass spectrometry (HRMS) was measured on a Bruker maXis 4G instrument.

LC-MS (ESI): A Shimadzu LCMS-2020 for Electron-Spray Ionization was used.

UV-VIS-spectroscopy was measured in a Jasco V-770 instrument equipped with a cell holder (ETCR-762) to gauge temperature at 25 °C.

Electrochemical reactions were performed with a Metrohm AutoLab PGSTAT30 potentiostat-galvanostat controlled over NOVA 2.1 software in an undivided cell containing working and counter electrodes as stated in the protocol and silver chloride or calomel electrodes as reference.

25,26,27,28-Tetrahydroxycalix[4]arene (**112**)

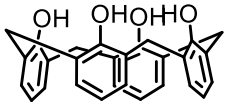

The synthetic procedure was adapted from Dai *et al.*[121]

To a 350 mL three round necked bottom flask under argon at room temperature was added 4-*tert*-butylcalix[4]arene **111** (4.31 g, 6.31 mmol, 1.00 equiv.) and phenol (3.63 g, 38.2 mmol, 6 equiv.), suspended in toluene (90 mL). Aluminium chloride (6.69 g, 49.2 mmol, 7.8 equiv.) was added in portions before heating the reaction mixture to 60 °C and stirred for 72 h at this temperature. Then, aq. HCl (3%, 90 ml) solution was added carefully before stirring for 30 minutes. The layers were separated and the aqueous layer was washed with 2x toluene (90 mL) before drying the combined organic layers over anhydrous Na_2SO_4. Solvent was concentrated under reduced pressure at 45 °C before adding ice cold MeOH (28 mL). The precipitate was filtered and washed with MeOH (5 mL). Yellow crystals (**112**, 2.22 g, 5.24 mmol, 83%) were obtained, no further purification was required.

^{1}H NMR (500 MHz, Chloroform-*d*): δ 10.21 (s, 4H), 7.07 (d, J = 7.6 Hz, 8H,), 6.74 (t, J = 7.6 Hz, 4H,), 4.28 (s, 4H), 3.52 (s, 4H) ppm.

^{13}C NMR (126 MHz, Chloroform-*d*): δ 148.92, 129.13, 128.39, 122.39, 31.85 ppm.

MS (MALDI-TOF, linear positive, TCNQ-matrix): *m/z* 424.2 $[M]^+$.

25,26,27,28-tetrapropyloxycalix[4]arene (**113**)

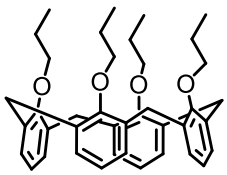

The synthetic procedure was adapted from Mastalerz *et al.*[122]

To a 50 mL three round bottom flask under argon was added **112** (500 mg, 1.18 mmol, 1.00 equiv.) dissolved in DMF (10 ml). The solution was cooled to 0 °C and sodium hydride dispersion on mineral oil (60%, 283 mg, 7.08 mmol, 6.00 equiv.) was added in portions. The reaction mixture was stirred for 20 min. at 0 °C before warming up to room temperature. 1-Bromopropane (1173 mg,

9.44 mmol, 8.00 equiv.) was added and the reaction mixture was continuously stirred for 2 h. A reaction control by TLC (cyclohexane:EtOAc 5:1) indicated full conversion. The reaction mixture was quenched with MeOH (1 mL) and the residue was extracted with 2x DCM (40 ml) and 2x aq. HCl (5%, 40 ml). The combined organic layers were dried over anhydrous Na_2SO_4, filtered and evaporated (45 °C). The dark yellow oil was mixed with MeOH (3 mL) and the precipitate filtered off and washed with 2x MeOH (1 mL) to obtain white crystals (**113**, 600 mg, 1.01 mmol, 86%).

^{1}H NMR (500 MHz, Chloroform-*d*): δ 6.63 (d, J = 6.5 Hz, 8H), 6.58 (dd, J = 8.6, 6.1 Hz, 4H), 4.47 (d, J = 13.3 Hz, 4H), 3.87 (dd, J = 8.0, 7.0 Hz, 8H), 3.17 (d, J = 13.4 Hz, 4H), 1.94 (h, J = 7.4 Hz, 8H), 1.01 (t, J = 7.5 Hz, 12H) ppm.

^{13}C NMR (126 MHz, Chloroform-*d*): δ 156.73, 135.28, 128.24, 122.00, 76.82, 31.13, 23.39, 10.48 ppm.

MS (MALDI-TOF, reflective positive, TCNQ-matrix): *m/z* 615.2 $[M+Na]^+$.

5,11,17,23-tetrabromo-25,26,27,28-tetrapropyloxycalix[4]arene (**114**)

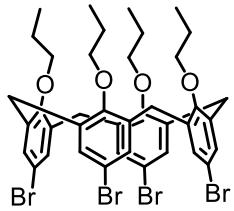

The synthetic procedure was adapted from Mastalerz *et al.*[122]

To a 500 mL round bottom flask under argon atmosphere was added **113** (8.00 g, 13.5 mmol, 1.00 equiv.) and dissolved in freshly distilled 2-butanone (120 mL). NBS (14.6 g, 81.0 mmol, 6.00 equiv.) added and the reaction solution was stirred for 2 h at room temperature. Reaction control by TLC (cyclohexane:EtOAc 5:1) indicated that the reaction had run to completion. Reaction mixture was quenched with aq. sodium bisulfite solution (40%, 40 mL) and extracted with 2x DCM (250 mL) and aq. HCl (5%, 20 mL). The combined organic layers were dried over anhydrous Na_2SO_4 and concentrated under reduced pressure (45 °C). The residue was mixed with MeOH (40 mL) and the white precipitate filtered and washed with 2x EtOH (20 mL). White crystals (**114**, 10.1 g, 11.1 mmol, 82%) were obtained.

^{1}H NMR (500 MHz, Chloroform-*d*): δ 6.80 (s, 8H), 4.35 (d, J = 13.4 Hz, 4H), 3.84 – 3.77 (m, 8H), 3.08 (d, J = 13.5 Hz, 4H), 1.87 (h, J = 7.5 Hz, 8H), 0.97 (t, J = 7.4 Hz, 12H) ppm.

^{13}C NMR (126 MHz, Chloroform-*d*): δ 155.71, 136.59, 131.15, 115.31, 77.40, 30.88, 23.22, 10.35 ppm.

MS (MALDI-TOF, reflective positive, DCTB-matrix): *m/z* 903.9 $[M]^+$.

5,11,17,23-tetraiodo-25,26,27,28-tetrapropyloxycalix[4]arene (**162**)

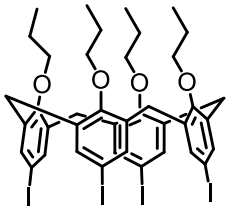

The synthetic procedure was adapted from Barton *et al.*[123]

To a 250 mL two round necked bottom flask under argon was added a combined mixture of **113** (500 mg, 0.843 mmol, 1.00 equiv.), I_2 (1072 mg, 4.22 mmol, 5.00 equiv.), $Na_2S_2O_8$ (1004 mg, 4.22 mmol, 5.00 equiv.) and tetramethylammonium iodide (136 mg, 0.675 mmol, 0.8 equiv.) and dissolved in distilled acetonitrile (80 mL). The mixture was heated to 80 °C for 16 h before TLC (cyclohexane) did show full conversion. Reaction mixture was cooled to room temperature and subsequently poured into H_2O (50 mL) containing aq. sodium bisulfite solution (40%, 2.4 mL, 12 mmol). The mixture was extracted with 2x EtOAc (30 mL) and the organic layer was washed with water deion. and dried over anhydrous Na_2SO_4, filtered and evaporated at 45 °C. Residue was triturated with MeOH (15 mL), filtered and washed to gain (**162**, 700 mg, 0.461 mmol, 76%) as white crystals.

^{1}H NMR (500 MHz, Chloroform-*d*): δ 7.00 (s, 8H), 4.29 (d, J = 13.4 Hz, 4H), 3.84 – 3.77 (m, 8H), 3.05 (d, J = 13.4 Hz, 4H), 1.86 (h, J = 7.5 Hz, 8H), 0.96 (t, J = 7.4 Hz, 12H) ppm.

^{13}C NMR (126 MHz, Chloroform-*d*): δ 156.38, 137.10, 136.82, 86.09, 77.04, 30.37, 23.07, 10.20 ppm.

MS (MALDI-TOF, reflective positive, TCNQ-matrix): *m/z* 1119.2 $[M+Na]^+$.

5,17-dibromo-11,23-diformyl-25,26,27,28-tetrapropyloxycalix[4]arene (**89**)

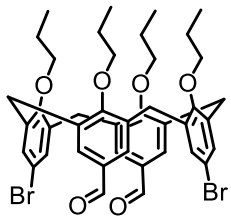

The synthetic procedure was adapted from Wong *et al.*[124]

To a 50 mL two round bottom flask under argon was **114** (200 mg, 0.22 mmol, 1.00 equiv.) dissolved in THF (10 mL) and cooled to -78 °C. *n*-BuLi 2.5 M (0.19 ml, 0.46 mmol, 2.10 equiv.) was added to the reaction mixture within 5 min. and the solution was stirred for 30 min., before quenching with DMF (0.12 ml, 1.54 mmol, 7.00 equiv.). The reaction mixture was warmed up to room and stirred for 1.5 h until reaction control by TLC (hexanes: EtOAc 5:1) indicated complete conversion of the starting material. Saturated aqueous ammonium chloride (10 mL) was used to quench the reaction before THF was removed by vacuum and the residue extracted with 2x DCM (20 mL) and aq. HCl (5%, 8 mL). The organic layer was dried over anhydrous Na_2SO_4, filtered and evaporated on the rotavap (45 °C). The residue was triturated and sonicated for 15 min. with MeOH (2 mL), filtered and washed with 2x EtOH (1 mL) to obtain (**89**, 120 mg, 0.150 mmol, 68%) in form of white crystals.

^{1}H NMR (500 MHz, Chloroform-*d*): δ 9.61 (s, 2H), 7.15 (s, 4H), 6.82 (s, 4H), 4.43 (d, *J* = 13.7 Hz, 4H), 3.92 (t, *J* = 8.0, 7.5 Hz, 4H), 3.82 (t, 4H), 3.22 (d, *J* = 13.7 Hz, 4H), 1.88 (ddt, *J* = 15.0, 12.5, 7.5 Hz, 8H), 0.99 (td, *J* = 7.4, 5.2 Hz, 12H) ppm.

^{13}C NMR (126 MHz, Chloroform-*d*): δ 191.61, 162.10, 155.68, 136.60, 135.71, 131.50, 131.38, 130.25, 115.50, 77.36, 77.28, 77.23, 30.97, 23.41, 23.25, 10.35 ppm.

MS (MALDI-TOF, linear negative, DCTB-matrix): *m/z* 803.0 $[M-H]^-$.

5,17-dibromo-25,26,27,28-tetrapropyloxycalix[4]arene (**115**)

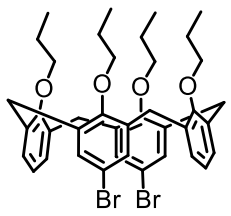

The synthetic procedure was adapted from Sameni *et al.*[125]

To a 100 mL three round bottom flask under argon was added **114** (5.00 g, 5.50 mmol, 1.00 equiv.), dissolved in freshly distilled THF (50 mL). The reaction mixture was cooled to -78 °C. *n*-BuLi 2.5 M (4.44 ml, 11.1 mmol, 2.02 equiv.) was added within 10 min. to the reaction mixture and stirred for 30 min. before quenching with MeOH (1.56 ml, 38.5 mmol, 7.00 equiv.) and warmed up to room temperature. After 1.5 h, the reaction was quenched with saturated aqueous ammonium chloride (20 mL) and THF was removed under reduced pressure. The residue was extracted with 2x DCM (80 mL) and washed with aq. HCl (5%, 80 mL). The organic layer was dried over anhydrous Na_2SO_4, filtered and evaporated (45 °C). The obtained foam was purified by column chromatography (SiO_2, petroleum ether) to yield white crystals (**115**, 3.65 g, 4.84 mmol, 88%).

^{1}H NMR (500 MHz, Chloroform-*d*): δ 6.78 (s, 4H), 6.68 – 6.60 (m, 6H), 4.41 (d, J = 13.4 Hz, 4H), 3.88 – 3.76 (m, 8H), 3.12 (d, J = 13.4 Hz, 4H), 1.97 – 1.84 (m, 8H), 0.99 (td, J = 7.4, 6.2 Hz, 12H) ppm.

^{13}C NMR (126 MHz, Chloroform-*d*): δ 156.50, 155.83, 137.35, 134.50, 130.89, 128.54, 122.61, 114.83, 77.04, 76.93, 30.98, 23.32, 10.44, 10.40 ppm.

MS (MALDI-TOF, reflective positive, DCTB-matrix): *m/z* 771.2 $[M+Na]^+$.

5,17-diformyl-25,26,27,28-tetrapropyloxycalix[4]arene (**90**)

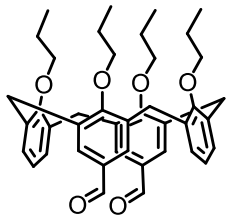

To a 100 mL three round bottom flask under argon **115** (2700 mg, 3.60 mmol, 1.00 equiv.) was dissolved in freshly distilled THF (45 ml) and cooled to -78 °C. Within 15 minutes *t*-BuLi 1.6 M (9.90 ml, 15.8 mmol, 4.40 equiv.) was added to the reaction mixture and stirred for 30 min. The reaction mixture quenched with DMF (1.96 ml, 25.2 mmol, 7.00 equiv.) and warmed up to room temperature. The solution was stirred for 2 h before quenching, using saturated aqueous ammonium chloride (10 mL). The solvent was removed by vacuum (45 °C) and residue extracted with 2x DCM (80 mL) and washed with water deion. (80 mL). The combined organic layers were dried over anhydrous Na_2SO_4, filtered and evaporated (45 °C). The crude was purified by chromatography (SiO_2, petrol ether: TBME 9:1) to obtain white crystals (**90**, 1.78 g, 2.74 mmol, 76%).

^{1}H NMR (500 MHz, Chloroform-*d*): δ 9.47 (s, 2H), 7.00 (s, 4H), 6.77 – 6.67 (m, 6H), 4.47 (d, J = 13.6 Hz, 4H), 3.88 (q, J = 7.1 Hz, 8H), 3.23 (d, J = 13.6 Hz, 4H), 1.97 – 1.85 (m, 8H), 1.00 (dt, J = 29.8, 7.5 Hz, 12H) ppm.

^{13}C NMR (126 MHz, Chloroform-*d*): δ 191.83, 162.09, 156.71 136.09, 134.92, 131.17, 129.99, 128.92, 122.80, 77.14, 76.93, 31.08, 23.52, 23.30, 10.52, 10.31 ppm.

MS (MALDI-TOF, reflective positive, DCTB-matrix): *m/z* 671.4 $[M+Na]^+$.

5,11,17,23-tetraformyl-25,26,27,28-tetrapropyloxycalix[4]arene (**159**)

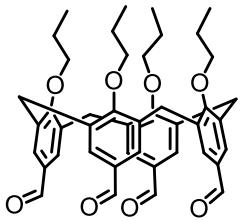

The synthetic procedure was adapted from Wong *et al.*[124]
In a 100 mL two round bottom flask under argon was added **114** (2000 mg, 2.20 mmol, 1.00 equiv.), dissolved in THF (30 mL) and cooled to -78 °C. *t*-BuLi 1.6 M (12.4 ml, 19.8 mmol, 9.00 equiv.) added within 15 min. to the reaction mixture and stirred for 30 min at this temperature. The reaction mixture was then quenched with DMF (1.71 ml, 22.0 mmol, 10.0 equiv.), warmed up to room temperature and stirred for 16 h. The reaction mixture poured onto saturated aqueous ammonium chloride (20 mL) and THF concentrated under reduced pressure (45 °C). The residue was extracted with 2x DCM (40 mL) and washed with water deion. (40 mL). The combined organic layers were dried over anhydrous Na_2SO_4, filtered and evaporated on the rotavap (45 °C). Residue was sonicated with MeOH (10 mL) for 10 min., filtered and washed with 2x MeOH (5 mL) before drying under high vacuum to yield white crystals (**159**, 1.47 g, 2.09 mmol, 95 %).

^{1}H NMR (500 MHz, Chloroform-*d*): δ 9.58 (s, 4H), 7.15 (s, 8H), 4.51 (d, J = 13.9 Hz, 4H), 3.97 – 3.90 (m, 8H), 3.35 (d, J = 13.9 Hz, 4H), 1.91 (h, J = 7.4 Hz, 8H), 1.01 (t, J = 7.4 Hz, 12H) ppm.

^{13}C NMR (126 MHz, Chloroform-*d*): δ 191.44, 162.04, 135.73, 131.56, 130.38, 77.37, 31.07, 23.45, 10.36 ppm.

MS (MALDI-TOF, reflective positive, TCNQ-matrix): *m/z* 703.5 $[M-H]^+$.

5,11,17,23-tetraethynyl-25,26,27,28-tetrapropyloxycalix[4]arene (**161**)

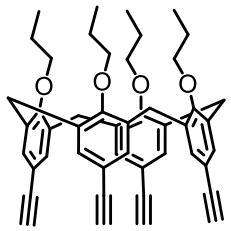

The synthetic procedure was adapted from Dyker *et al.*[126]
To a 250 mL two round bottom flask under argon was added **160** (3.75 g, 2.82 mmol, 1.00 equiv.) and dissolved in THF (60 mL) and cooled to -78 °C. *n*-BuLi 2.5 M (9.25 ml, 23.1 mmol, 8.20 equiv.) was added within 15 min. before stirring another 15 min. Warmed up to room temperature and after 1 h quenched with saturated aqueous ammonium chloride (25 mL) and stirred for 30 min. The solvent was removed under reduce pressure and residue was extracted with 2x DCM (100 mL). The combined organic layers were washed with water deion. (100 mL) and dried over anhydrous Na_2SO_4, filtered and evaporated (45 °C). The residue was purified by column chromatography (SiO_2, cyclohexane:EtOAc 79:1) to yield white crystals (**161**, 1.03 g, 1.49 mmol, 53%).

Alternative route:

To a 100 mL two round bottom flask under argon was added **162** (700 mg, 0.638 mmol, 1.00 equiv.) and TMS-acetylene (0.37 mL, 2.62 mmol, 4.10 equiv.), dissolved in triethylamine (60 mL). The reaction mixture was degassed with argon for 15 min. CuI (6.1 mg, 0.03 mmol, 0.05 equiv.) and $PdCl_2(PPh_3)_2$ (13 mg, 0.02 mmol, 0.03 equiv.) was added subsequently before stirring for 5 d at room temperature. The reaction was extracted with DCM (150 mL) and water deion. (150 mL). The organic layer was dried over anhydrous Na_2SO_4, filtered and evaporated (40 °C). Residue was purified by chromatography (SiO_2, cyclohexane: EtOAc 4:1) before redissolving the obtained white crystals in MeOH (30 mL). Solution was transferred to a two round bottom flask and K_2CO_3 (530 mg, 3.828 mmol, 6.00 equiv.) was added, before stirring for 2 h at room temperature. The solvent was removed under reduced pressure and residue purified by column chromatography (SiO_2, cyclohexane: EtOAc 79:1) to yield white crystals (**161**, 245 mg, 0.357 mmol, 56%).

^{1}H NMR (500 MHz, Chloroform-*d*): δ 6.83 (s, 8H), 4.37 (d, J = 13.4 Hz, 4H), 3.87 – 3.80 (m, 8H), 3.10 (d, J = 13.4 Hz, 4H), 2.89 (s, 4H), 1.88 (h, J = 7.4 Hz, 8H), 0.97 (t, J = 7.4 Hz, 12H) ppm.

^{13}C NMR (126 MHz, Chloroform-*d*): δ 157.30, 134.87, 132.41, 116.07, 84.11, 77.10, 75.98, 30.80, 23.31, 10.39 ppm.

MS (MALDI-TOF, reflective positive, DCTB-matrix): *m/z* 688.4 $[M]^+$.

(2-iodophenyl)(1H-pyrrol-2-yl)methanone (**164**)

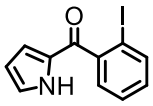

To a 500 mL two round necked bottom flask under argon was added Al_2O_3 filtered pyrrole (1.55 ml, 22.4 mmol, 1.00 equiv.) and dissolved in freshly distilled toluene (150 mL) before cooling it to 0 °C. At this temperature, phenylmagnesium bromide 3 M (7.47 ml, 22.4 mmol, 1.00 equiv.) was added dropwise and reaction mixture stirred for 15 min. 2-Iodobenzoyl chloride (5.97 g, 22.4 mmol, 1.00 equiv.) was added and stirred for 1 h at 0 °C. Reaction mixture quenched with saturated aqueous ammonium chloride (100 mL) and organic layer washed with water deion. (100 mL). The organic layer was dried over anhydrous Na_2SO_4 and solvent removed under reduced pressure. Purified using chromatography (SiO_2, cyclohexane: EtOAc 4:1) followed by recrystallization (DCM: cyclohexane 1:1) to obtain light green crystals (**164**, 3.33 g, 11.2 mmol, 50%).

^{1}H NMR (500 MHz, Chloroform-*d*): δ 10.61 (s, 1H), 7.85 (dd, J = 8.1, 1.1 Hz, 1H), 7.41 – 7.30 (m, 2H), 7.20 – 7.15 (m, 1H), 7.08 (ddd, J = 7.9, 7.2, 1.9 Hz, 1H), 6.50 (ddd, J = 3.8, 2.4, 1.4 Hz, 1H), 6.21 (dt, J = 3.8, 2.4 Hz, 1H) ppm.

^{13}C NMR (126 MHz, Chloroform-*d*): δ 186.14, 143.70, 140.05, 131.23, 130.93, 128.90, 127.61, 127.60, 121.77, 111.38, 93.04 ppm.

GC-MS (EI): *m/z* (%) = 93.9, (100) ; 296.7, (80) [M] ; 169.9, (59) ; 114.9, (41) ; 66.0, (29) ; 75.9, (22) ; 142.0, (15) ; 77.0, (14) ; 50.0, (12) ; 297.7, (11).

Pyrrole precursor for the spherical shaped cage molecule (**110**)

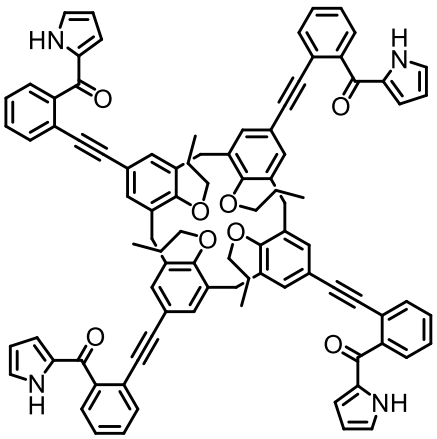

In a 50 mL two necked round bottom flask under argon **161** (400 mg, 0.581 mmol, 1.00 equiv.) and **164** (725 mg, 2.44 mmol, 4.20 equiv.) was dissolved in triethylamine (20 mL). This solution was purged with argon for 15 min. before adding $PdCl_2(PPh_3)_2$ (40.8 mg, 0.058 mmol, 0.1 equiv.) and CuI (5.5 mg, 0.029 mmol, 0.05 equiv.). The reaction mixture was stirred for 72 h at room temperature. Upon full completion, the reaction mixture was extracted with EtOAc (100 mL) and the organic layer washed with 2x water deion. (60 mL). The organic layer was dried over Na_2SO_4 and solvent removed under reduced pressure (40 °C) before purifying residue by column chromatography and preparative TLC (SiO_2, cyclohexane:EtOAc 2:1) to obtain red crystals (**110**, 270 mg, 0.198 mmol, 34 %).

^{1}H NMR (500 MHz, Chloroform-*d*): δ 11.20 (s, 4H), 7.55 – 7.47 (m, 8H), 7.35 – 7.27 (m, 8H), 7.22 (ddd, J = 3.0, 2.4, 1.4 Hz, 4H), 6.72 (ddd, J = 3.8, 2.4, 1.4 Hz, 4H), 6.60 (s, 8H) 6.25 (dt, J = 3.9, 2.4 Hz, 4H), 4.31 (d, J = 13.1 Hz, 4H), 3.84 – 3.77 (m, 8H), 3.02 (d, J = 13.2 Hz, 4H), 1.88 (h, J = 7.5 Hz, 8H), 0.95 (t, J = 7.5 Hz, 12H) ppm.

^{13}C NMR (126 MHz, Chloroform-*d*): δ 185.45, 156.99, 141.40, 134.57, 132.79, 131.97, 131.82, 129.98, 128.55, 127.43, 127.04, 122.24, 121.76, 116.94, 111.12, 94.95, 86.81, 77.16, 30.93, 23.24, 10.36 ppm.

HRMS (ESI): calculated for $C_{92}H_{76}N_4O_8$ $[M+Na]^+$ 1387.5555, found 1387.5564.

5,11,17,23-tetrakis(trimethylsilylethynyl)-25,26,27,28-tetrapropyloxycalix[4]arene (**170**)

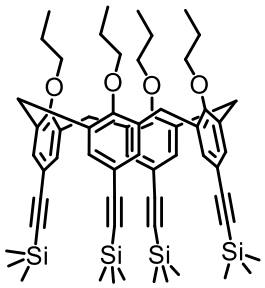

To a 100 mL two round necked bottom flask under argon **162** (700 mg, 0.638 mmol, 1.00 equiv.) was dissolved in dry triethylamine (40 mL) before degassing the solution for 15 min. with argon. $PdCl_2(PPh_3)_2$ (13.4 mg, 0.019 mmol, 0.03 equiv.) and CuI (6.1 mg, 0.032 mmol, 0.05 equiv.) was added and the reaction mixture stirred at room temperature for 5 d. The reaction mixture was diluted with DCM (100 mL) and the organic layer washed with water deion. (100 mL), dried over anhydrous Na_2SO_4, filtered and evaporated at 45 °C. The residue was triturated with MeOH (15 mL) to obtain a brown powder. Purification by chromatography (SiO_2, cyclohexane: EtOAc 10:1) resulted in the target compound (**170**, 510 mg, 0.523 mmol, 82%).

^{1}H NMR (500 MHz, Chloroform-*d*): δ 6.94 (s, 8H), 4.35 (d, J = 12.9 Hz, 4H), 3.86 – 3.80 (m, 8H), 3.10 (d, J = 13.0 Hz, 4H), 1.96 – 1.85 (m, 8H), 0.96 (t, J = 7.4 Hz, 12H), 0.24 (s, 36H) ppm.

^{13}C NMR (126 MHz, Chloroform-*d*): δ 156.95, 134.38, 132.57, 117.08, 105.64, 92.84, 77.16, 30.90, 23.22, 10.37, 0.30 ppm.

MS (MALDI-TOF, reflective positive, TCNQ-matrix): *m/z* 977.6 $[M]^+$.

5,11,17,23-tetra(2,2-dibromovinyl)-25,26,27,28-tetrapropyloxycalix[4]arene (**160**)

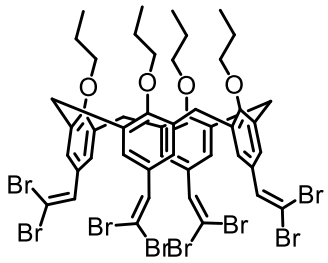

The synthetic procedure was adapted from Dyker *et al.*[126]

In a 100 mL two round necked bottom flask under argon freshly activated Zn dust (1.64 g, 25.1 mmol, 12.0 equiv.) was suspended in dry DCM (25 mL). Triphenylphosphine (6.64 g, 25.1 mmol, 12.0 equiv.) was added before cooling the reaction mixture to 0 °C and adding carbon tetrabromide (4.24 g, 12.5 mmol, 6.00 equiv.) dissolved in DCM (6 mL) dropwise over 10 min. After stirring for 10 min. at this temperature, **159** (1.47 g, 2.09 mmol, 1.00 equiv.) dissolved in DCM (10 ml) was added dropwise to the reaction mixture before warming up to room temperature. After 3 h the reaction mixture was diluted with water deion. (30 mL) and extracted with 2x DCM (50 mL). The organic layer was washed with aqueous H_2O_2 (10%, 25 mL) and aqueous $NaHSO_3$ (10%, 25 mL). The combined organic layers were dried over anhydrous Na_2SO_4 and evaporated at 45 °C. Residue purified by column chromatography (SiO_2, cyclohexane: TBME 9:1) to yield 2.27 g white crystals (**160**, 2.27 g, 1.71 mmol, 82%).

^{1}H NMR (500 MHz, Chloroform-*d*): δ 7.18 (s, 4H), 6.89 (s, 8H), 4.43 (d, J = 13.2 Hz, 4H), 3.86 (t, J = 7.5 Hz, 8H), 3.16 (d, J = 13.3 Hz, 4H), 1.92 (h, J = 7.5 Hz, 8H), 1.00 (t, J = 7.5 Hz, 12H) ppm.

^{13}C NMR (126 MHz, Chloroform-*d*): δ 156.82, 136.58, 134.85, 129.33, 128.84, 87.59, 77.06, 31.09, 23.41, 10.42 ppm.

MS (MALDI-TOF, linear positive, DCTB-matrix): *m/z* 1320.7 $[M+H]^+$.

ethyl 2-(3,5-dibromophenyl)acetate (**126**)

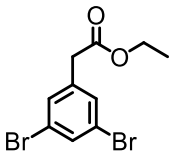

To a 500 mL round bottom flask 2-(3,5-dibromophenyl)acetic acid (25.0 g, 85.1 mmol, 1.00 equiv.) was dissolved in EtOH (200 mL) and H_2SO_4 (96%, 0.86 mL, 8.51 mmol, 0.1 equiv.) added. Heated to reflux and stirred for 16 h, before cooling to room temperature and removing solvent under reduced pressure. The residue was extracted with TBME (300 mL) and organic layer washed with 2x water deion. (150 mL). Purification by distillation (5 mbar, 110 °C) yielded in a colorless oil (**126**, 26.3 g, 81.7 mmol, 96%).

^{1}H NMR (500 MHz, Chloroform-*d*): δ 7.58 (t, J = 1.8 Hz, 1H), 7.42 – 7.36 (m, 2H), 4.17 (q, J = 7.1 Hz, 2H), 3.55 (d, J = 0.6 Hz, 2H), 1.27 (t, J = 7.1 Hz, 3H) ppm.

^{13}C NMR (126 MHz, Chloroform-*d*): δ 170.43, 137.84, 132.99, 131.34, 123.04, 61.46, 40.60, 14.28 ppm.

GC-MS (EI): *m/z* (%) = 248.6, (100) ; 88.9, (58) ; 246.6, (54) ; 250.6, (48) ; 321.6, (37) ; 63.0, (26) ; 249.6, (20) ; 168.8, (19) ; 319.6, (19) [M] ; 323.6, (19).

2-(3,5-dibromophenyl)ethan-1-ol (**127**)

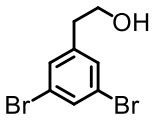

To a 100 mL two round bottom flask under argon was added **126** (3.00 g, 9.32 mmol, 1.00 equiv.), dissolved in THF (50 mL) and cooled to 0 °C. $LiAlH_4$ (0.37 g, 9.32 mmol, 1.00 equiv.) was added subsequently and the reaction mixture was slowly warmed up to reflux temperature for 4 h. Cooled to 0 °C and quenched with MeOH (5 mL) before diluting with EtOAc (50 mL). The organic layer was washed with water deion. (50 mL) and dried over anhydrous Na_2SO_4, filtered and evaporated (45 °C). The residue was purified by column chromatography (SiO_2, cyclohexane: EtOAc 4:1) to yield white crystals (**127**, 2.09 g, 7.46 mmol, 80%).

^{1}H NMR (500 MHz, Chloroform-*d*): δ 7.54 (t, J = 1.8 Hz, 1H), 7.33 (d, J = 1.8 Hz, 2H), 3.85 (t, J = 6.4 Hz, 2H), 2.81 (t, J = 6.4 Hz, 2H), 1.48 (s, 1H) ppm.

^{13}C NMR (126 MHz, Chloroform-*d*): δ 142.78, 132.16, 130.89, 122.96, 62.97, 38.40 ppm.

GC-MS (EI): *m/z* (%) = 168.9, (100) ; 170.8, (95) ; 249.7, (91) ; 88.9, (77) ; 279.7, (76) ; 247.7, (47) ; 251.7, (43) ; 248.7, (41) ; 277.7, (39) [M] ; 62.9, (39) ; 281.7, (37) ; 90.0, (27) ; 169.9, (26) ; 250.7, (25) ; 91.0, (24) ; 101.9, (20) ; 167.9, (20) ; 246.7, (20) ; 61.9, (15) ; 235.7, (14) ; 74.9, (11).

2-(3,5-dibromophenyl)acetaldehyde (**128**)

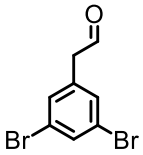

The synthetic procedure was adapted from Le Bihan *et al.*[127]

To a 100 mL two round bottom flask under argon was added **127** (1.07 g, 3.82 mmol, 1.00 equiv.), dissolved in THF (45 mL) and cooled to 0 °C. Dess-Martin periodinane (1.78 g, 4.20 mmol, 1.10 equiv.) was added carefully and slowly warmed up to room temperature. After 16 h, the reaction was quenched with aqueous $NaHSO_3$ (10%, 15 mL) before extracting with EtOAc (50 mL). Organic layer was washed with water deion. (50 mL) and dried over anhydrous Na_2SO_4, filtered and evaporated (35 °C). The residue was purified by column chromatography (SiO_2, cyclohexane: EtOAc 4:1) to yield white crystals (**128**, 870 mg, 3.13 mmol, 82%).

GC-MS (EI): *m/z* (%) = 89.0, (100) ; 168.9, (74) ; 170.9, (69) ; 63.0, (60) ; 248.8, (49) ; 90.0, (46) ; 249.8, (39) ; 277.8, (34) ; 169.9, (28) ; 62.0, (27) ; 247.8, (26) ; 250.7, (26) ; 246.8, (25) ; 167.9, (24) ; 251.8, (18) ; 275.8, (17) [M] ; 279.8, (16) ; 49.9, (14) ; 88.0, (12) ; 74.0, (11).

1,3-dibromo-5-(prop-2-yn-1-yl)benzene (**129**)

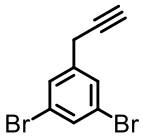

The synthetic procedure was adapted from Müller *et al.*[128]

To a 100 mL two round bottom flask under argon **128** (1.00 g, 3.60 mmol, 1.00 equiv.) was added and dissolved in dry MeOH (60 mL). Dimethyl (1-diazo-2-oxo-propyl) phosphonate (0.83 g, 4.32 mmol, 1.20 equiv.) added and stirred at room temperature for 3 h. Afterwards, the reaction was cooled to 5 °C and quenched with $NaHSO_3$ (10%, 20 mL) before extracting with EtOAc (80 mL). The organic layer was washed with water deion. (50 mL) and dried over anhydrous Na_2SO_4, filtered and evaporated (35 °C). The residue was purified by chromatography (SiO_2, cyclohexane: TBME 30:1) to yield volatile colorless oil (**129**, 640 mg, 2.34 mmol, 65%).

^{1}H NMR (400 MHz, Chloroform-*d*): δ 7.47 (q, J = 1.2 Hz, 1H), 7.35 (d, J = 1.8 Hz, 2H), 6.03 (t, J = 6.8 Hz, 1H), 5.23 (d, J = 6.8 Hz, 2H) ppm.

^{13}C NMR (126 MHz, DCM-*d*): δ 210.47, 138.61, 132.46, 128.65, 123.40, 92.34, 80.13 ppm.

GC-MS (EI): *m/z* (%) = 114.0, (100) ; 192.9, (61) ; 194.9, (58) ; 273.8, (57) ; 113.0, (38) ; 63.0, (29) ; 271.8, (29) [M] ; 275.8, (28) ; 88.0, (20) ; 87.0, (20) ; 61.9, (17) ; 74.0, (16) ; 86.0, (13) ; 75.0, (12) ; 57.0, (12) ; 96.4, (11) ; 115.0, (10) ; 97.4, (10).

(3-(3,5-bis(bromomethyl)phenyl)prop-1-yn-1-yl)triisopropylsilane (**132**)

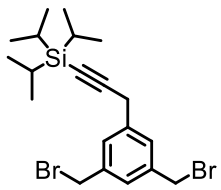

To a 100 mL two round bottom flask under argon was added (triisopropylsilyl)acetylene (0.66 mL, 2.94 mmol, 1.05 equiv.) in THF (50 mL) and the solution was cooled to -78 °C. *n*-BuLi 2.5 M in hexane (1.18 mL, 2.94 mmol, 1.05 equiv.) was added within 8 min. and stirred at -78 °C for 30 min. 1,3,5-Tris(bromomethyl)benzene (1.00 g, 2.80 mmol, 1.00 equiv.) was added subsequently and the reaction was stirred for 10 min. before warming up to room temperature. $[Pd(\mu\text{-}I)P(t\text{-}Bu)_3]_2$ (20 mg, 0.04 mmol, 0.01 equiv.) added and stirred for 16 h at room temperature before cooling to 5 °C and quenched with HCl 1 M (15 mL). Extracted with 2x EtOAc (50 mL). The combined organic layer washed with water deion. (50 mL) and dried over anhydrous Na_2SO_4, filtered and evaporated (40 °C). The residue was purified by column chromatography (SiO_2, cyclohexane: TBME 10:1) to yield colorless oil (**132**, 512 mg, 1.12 mmol, 40%).

^{1}H NMR (500 MHz, DCM-*d*): δ 7.40 (dd, J = 1.8, 0.9 Hz, 2H), 7.31 (t, J = 1.8 Hz, 1H), 4.49 (s, 4H), 3.70 (q, J = 0.8 Hz, 2H), 1.14 – 1.10 (m, 21H) ppm.

^{13}C NMR (126 MHz, DCM-*d*): δ 139.16, 138.73, 129.09, 128.12, 105.37, 84.11, 33.27, 26.21, 18.89, 11.76 ppm.

GC-MS (EI): *m/z* (%) = 143.0, (100) ; 330.7, (51) ; 142.0, (42) ; 140.9, (40) ; 138.9, (37) ; 250.8, (32) ; 119.0, (29) ; 332.7, (29) ; 248.8, (29) ; 139.9, (28) ; 182.9, (26) ; 372.7, (26) ; 328.7, (25) ; 168.9, (24) ; 414.7, (22) ; 416.7, (12) ; 412.7, (12) ; 455.8, (0.6) [M] ; 457.8, (1.2) ; 459.8, (0.6).

5-(3-(triisopropylsilyl)prop-2-yn-1-yl)isophthalaldehyde (**101**)

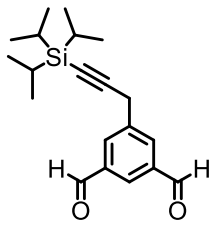

The synthetic procedure was adapted from Tabata *et al.*[129]

To a 50 mL three round bottom flask under argon was added **132** (300 mg, 0.66 mmol, 1.00 equiv.) and 4-methylmorpholine 4-oxide (633 mg, 5.24 mmol, 8.00 equiv.) in acetonitrile (20 mL) to heat up to reflux for 2 h. The reaction mixture was cooled to room temperature, diluted with water deion. (20 mL) and extracted with 2x TBME (50 mL). The combined organic layer was washed with brine (30 mL) and dried over anhydrous Na_2SO_4, filtered and evaporated (40 °C). The residue was purified by chromatography (SiO_2, cyclohexane: TBME 4:1) to yield white crystals (**101**, 110 mg, 0.34 mmol, 51%).

^{1}H NMR (500 MHz, DCM-*d*): δ 10.09 (s, 2H), 8.24 (tq, J = 1.4, 0.8 Hz, 1H), 8.19 (dt, J = 1.6, 0.8 Hz, 2H), 3.88 (q, J = 0.8 Hz, 2H), 1.11 (d, J = 2.2 Hz, 21H) ppm.

^{13}C NMR (126 MHz, DCM-*d*): δ 191.34, 139.95, 137.76, 134.31, 129.33, 104.34, 85.18, 26.17, 18.81, 11.70 ppm.

GC-MS (EI): *m/z* (%) = 285.0, (100) ; 228.9, (67) ; 240.9, (38) ; 214.9, (35) ; 256.9, (26) ; 114.0, (25) ; 286.0, (24) ; 184.9, (24) ; 242.9, (20) ; 127.0, (13) ; 229.9, (13) ; 128.0, (11) ; 114.9, (10) ; 328.0, (1.1) [M] ; 329.0, (0.3).

1,3-bis(bromomethyl)-5-(prop-2-yn-1-yl)benzene (**131 deprotected**)

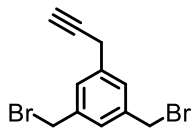

To a 50 mL two round bottom flask under argon was added trimethylsilylacetylene (0.42 mL, 2.94 mmol, 1.05 equiv.) in THF (25 mL) and cooled to -78 °C. *n*-BuLi 2.5 M in hexane (1.18 mL, 2.94

mmol, 1.05 equiv.) was added within 5 min. and the reaction mixture was stirred at -78 °C for 30 min. 1,3,5-Tris(bromomethyl)benzene (1.00 g, 2.80 mmol, 1.00 equiv.) was added subsequently and stirred for 10 min. before warming up to room temperature. After 16 h, cooled to 5 °C and quenched with HCl 1 M (10 mL) and extracted with 2x EtOAc (50 mL). The combined organic layer washed with water deion. (50 mL) and dried over anhydrous Na_2SO_4, filtered and evaporated (40 °C). The residue (trimethylsilyl-protected) was purified by chromatography (SiO_2, cyclohexane: TBME 49:1) to yield volatile colorless oil (**131 deprotected**, 134 mg, 0.45 mmol, 16%).

^{1}H NMR (500 MHz, Chloroform-*d*): δ 7.25 (d, J = 1.6 Hz, 1H), 7.24 (d, J = 1.6 Hz, 2H), 6.14 (t, J = 6.8 Hz, 1H), 5.19 (dd, J = 6.9, 0.7 Hz, 2H), 4.45 (s, 4H) ppm.

1,3,5-tris(chloromethyl)benzene (**166**)

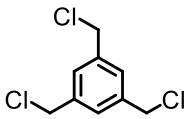

The synthetic procedure was adapted from Hermes *et al.*[130]

To a 50 mL two round bottom flask under argon was added 1,3,5-tris(bromomethyl)benzene (1.00 g, 2.80 mmol, 1.00 equiv.) and dissolved in DMF (20 mL). The reaction mixture was cooled to 0 °C and then LiCl (1.78 g, 42.0 mmol, 15.00 equiv.) added in portions before stirring at this temperature for 30 min. Then the reaction mixture was warmed up to room temperature and stirred for 16 h. TBME (50 mL) added and then the organic layer was washed with 2x water deion. (30 mL). Organic layer dried over anhydrous Na_2SO_4, filtered and evaporated (45 °C). The residue was purified by column chromatography (SiO_2, cyclohexane) to yield white crystals (**166**, 590 mg, 2.63 mmol, 94%).

^{1}H NMR (500 MHz, DCM-*d*): δ 7.41 (s, 3H), 4.61 (s, 6H) ppm.

^{13}C NMR (126 MHz, DCM-*d*): δ 139.24, 129.08, 45.91. ppm.

GC-MS (EI): *m/z* (%) = 186.9, (100) ; 188.9, (64) ; 115.0, (38) ; 221.8, (18) [M] ; 223.8, (18) ; 152.0, (16) ; 116.0, (14) ; 117.0, (12) ; 187.9, (11) ; 190.9, (10) ; 57.1, (10).

Hexahydroxycalix[6]arene (**119**)

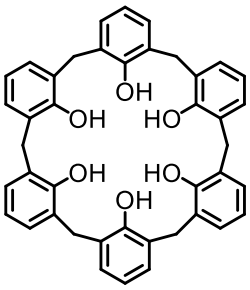

The synthetic procedure was adapted from Gutsche *et al.*[131]

A 350 mL three round necked bottom flask under argon was charged with 4-*tert*-butyl-calix[6]arene (10.0 g, 10.3 mmol, 1.00 equiv.) and phenol (5.98 g, 62.9 mmol, 6.11 equiv.), which were suspended in toluene (110 mL). Aluminium chloride (11.4 g, 83.9 mmol, 8.15 equiv.) was added in portions before stirring the reaction mixture at room temperature for 3 h. The reaction mixture was quenched by pouring into ice water (75 mL) before adding toluene (50 ml) and stirred for 2 h. The layers were separated and the aqueous layer was extracted with toluene (100 mL). The combined organic layers were washed with brine (150 mL), dried over anhydrous Na_2SO_4 and solvent concentrated under reduced pressure at 45 °C before adding ice cold MeOH (40 mL) to form precipitate. Suspension was filtered and washed with MeOH (5 mL). Yellow crystals were purified by chromatography (SiO_2, cyclohexane: EtOAc 10:1) to yield white crystals (**119**, 5.81 g, 9.16 mmol, 89%).

^{1}H NMR (500 MHz, DCM-*d*): δ 10.28 (s, 6H), 7.17 (d, J = 7.6 Hz, 12H), 6.85 (t, J = 7.5 Hz, 6H), 3.92 (s, 12H) ppm.

^{13}C NMR (126 MHz, DCM-*d*): δ 150.05, 129.77, 127.93, 122.19, 32.34 ppm.

MS (MALDI-TOF, reflective positive, TCNQ-matrix): *m/z* 635.3 $[M-H]^+$.

Hexakis(diethyl phenyl phosphate)calix[6]arene (**121**)

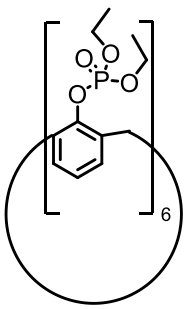

The synthetic procedure was adapted from Zhong *et al.*[132]

In an undivided electrochemical cell under air, **119** (500 mg, 0.79 mmol, 1.00 equiv.) was suspended in acetonitrile (30 ml) before adding diethyl phosphite (664 mg, 4.71 mmol, 6.00 equiv.) and sodium iodide (141 mg, 0.92 mmol, 1.20 equiv.). The reaction mixture was stirred (3000 rpm) and current (20 mA) was applied for 5 d, using a Pt gauze as WE and CE (a slight yellow color after 20 sec. reaction time indicted catalytic iodine formation, turning after 10 min. into a deep yellow suspension). The reaction mixture was extracted with EtOAc (50 mL) and washed with $NaHSO_3$ (10%, 20 mL) and water deion. (50 mL). Organic layer dried over anhydrous Na_2SO_4, filtered and evaporated (45 °C). The residue was purified by chromatography (SiO_2, cyclohexane: EtOAc 4:1) to yield white crystals (**121**, 150 mg, 0.10 mmol, 13%).

^{1}H NMR (500 MHz, DCM-*d*): δ 7.28 (d, J = 7.4 Hz, 2H), 7.18 (dd, J = 7.6, 1.7 Hz, 2H), 7.14 (dd, J = 7.5, 1.7 Hz, 2H), 7.12 – 7.03 (m, 6H), 6.87 (t, J = 7.5 Hz, 2H), 6.84 (d, J = 7.4 Hz, 2H), 6.77 (t, J = 7.5 Hz, 2H), 4.66 – 4.54 (m, 3H), 4.46 (d, J = 16.8 Hz, 3H), 4.06 – 3.99 (m, 2H), 3.98 – 3.93 (m, 4H), 3.64 (ddd, J = 51.1, 21.1, 13.8 Hz, 6H), 2.34 – 2.27 (m, 4H), 1.66 – 1.60 (m, 4H), 1.38 – 1.32 (m, 4H), 1.32 – 1.27 (m, 14H), 1.26 (s, 16H), 0.91 – 0.88 (m, 12H) ppm.

^{31}P NMR (162 MHz, chloroform-*d*): δ -10.70 ppm.

HRMS (ESI): calculated for $C_{66}H_{90}O_{24}P_6$ $[M+Na]^+$ 1475.4140, found 1475.4653.

MS (MALDI-TOF (rapifleX), reflective positive, TCNQ-matrix): *m/z* 1474.41 $[M-H+Na]^+$.

methyl 5-cyano-2-phenylpentanoate (**153**)

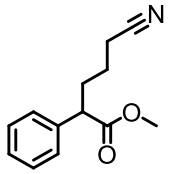

To a 250 mL two round bottom flask under argon freshly distilled (10 mbar, 100 °C) methyl 2-phenylacetate (1.68 ml, 11.9 mmol, 1.00 equiv.) was dissolved in THF (100 mL) and the reaction mixture cooled to -78 °C. LDA 2 M (6.55 ml, 13.1 mmol, 1.10 equiv.) added within 10 min. and stirred at -78 °C for 1 h. 4-Bromobutyronitrile (1.84 mL, 17.9 mmol, 1.50 equiv.) added dropwise before warming up to room temperature. The reaction mixture was quenched after 16 h using saturated aqueous ammonium chloride (30 mL). The aqueous layer was extracted with EtOAc (100 mL), washed the organic layer with brine (50 mL) before drying the organic layer over anhydrous Na_2SO_4, filtered and evaporated (40 °C). Residue was purified by column chromatography (SiO_2, cyclohexane: EtOAc 20:3) to yield colorless oil (**153**, 1.64 g, 7.50 mmol, 63%).

^{1}H NMR (400 MHz, DCM-*d*): δ 7.38 – 7.25 (m, 5H), 3.64 (s, 3H), 3.57 (t, J = 7.7 Hz, 1H), 2.33 (t, J = 7.2 Hz, 2H), 2.18 (dddd, J = 13.2, 10.7, 7.6, 5.4 Hz, 1H), 1.91 (dddd, J = 13.4, 10.5, 7.7, 5.5 Hz, 1H), 1.71 – 1.47 (m, 2H) ppm.

^{13}C NMR (101 MHz, DCM-*d*): δ 174.01, 138.88, 129.15, 128.24, 127.86, 119.76, 52.37, 51.15, 32.69, 23.88, 17.37 ppm.

GC-MS (EI): *m/z* (%) = 117.0, (100) ; 158.0, (94) ; 91.0, (59) ; 184.9, (26) ; 115.0, (18) ; 118.0, (13) ; 149.9, (13) ; 103.9, (12) ; 159.0, (11) ; 216.9, (11) [M] ; 77.0, (10) ; 102.9, (10).

methyl 4-cyano-2-phenylbutanoate (**156**)

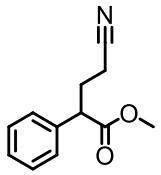

To a 250 mL two round bottom flask under argon freshly distilled (10 mbar, 100 °C) methyl 2-phenylacetate (3.38 ml, 24.0 mmol, 1.00 equiv.) was dissolved in THF (100 mL) and the reaction mixture cooled to -78 °C. LDA 2 M (13.2 ml, 26.4 mmol, 1.10 equiv.) added within 15 min. and

stirred at -78 °C for 1 h. 3-Bromopropionitrile (2.40 mL, 28.8 mmol, 1.20 equiv.) was added dropwise before warming up to room temperature. The reaction mixture was quenched after 16 h using saturated aqueous ammonium chloride (45 mL). The aqueous layer was extracted with EtOAc (150 mL) and the organic layer washed with brine (100 mL) before drying over anhydrous Na_2SO_4, then filtered and evaporated (40 °C). Residue was purified by chromatography (SiO_2, cyclohexane: EtOAc 10:1) to yield colorless oil (**156**, 3.66 g, 18.0 mmol, 75%).

^{1}H NMR (400 MHz, DCM-*d*): δ 7.41 – 7.24 (m, 5H), 3.73 – 3.68 (t, J = 7.4 Hz, 1H), 3.66 (s, 3H), 2.45 – 2.30 (m, 2H), 2.30 – 2.17 (m, 1H), 2.17 – 2.04 (m, 1H) ppm.

^{13}C NMR (101 MHz, DCM-*d*): δ 173.35, 137.70, 129.39, 128.29, 128.27, 119.33, 52.61, 50.27, 29.23, 15.57 ppm.

GC-MS (EI): *m/z* (%) = 144.0, (100) ; 91.0, (33) ; 117.0, (26) ; 104.0, (26) ; 55.0, (24) ; 118.0, (19) ; 202.9, (14) [M] ; 103.0, (13) ; 77.0, (12) ; 115.0, (12) ; 78.0, (11) ; 145.0, (11).

5-cyano-2-phenylpentanoic acid (**154**)

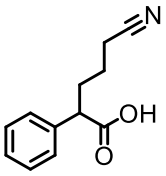

To a 100 mL two round bottom flask under argon was added **153** (1.00 g, 4.60 mmol, 1.00 equiv.) and dissolved in THF (20 mL). A solution of LiOH (0.33 g, 13.8 mmol, 3.00 equiv.) dissolved in water deion. (10 mL) was added within 2 min. and stirred at room temperature for 1 h before heating up to 60 °C. The reaction mixture was quenched after 16 h using HCl 1 M (30 mL) and extracted with TBME (100 mL) and washed organic layer with brine (40 mL) before drying over anhydrous Na_2SO_4, then filtered and evaporated (40 °C). The residue was purified by column chromatography (SiO_2, cyclohexane: EtOAc 2:1) to yield white crystals (**154**, 750 mg, 3.68 mmol, 80%).

^{1}H NMR (500 MHz, DCM-*d*): δ 10.49 – 9.09 (s, 1H) 7.40 – 7.28 (m, 5H), 3.61 (td, J = 7.7, 1.2 Hz, 1H), 2.33 (t, J = 7.1 Hz, 2H), 2.20 (dddd, J = 13.1, 10.7, 7.5, 5.3 Hz, 1H), 1.94 (dddd, J = 13.4, 10.8, 7.9, 5.3 Hz, 1H), 1.72 – 1.50 (m, 2H) ppm.

^{13}C NMR (126 MHz, DCM-*d*): δ 179.58, 138.10, 129.21, 128.34, 128.13, 119.69, 51.09, 32.11, 23.71, 17.30 ppm.

HRMS (ESI, negative mode): calculated for $C_{12}H_{12}NO_2$ $[M]^-$ 202.0874, found 202.0878.

4-cyano-2-phenylbutanoic acid (**157**)

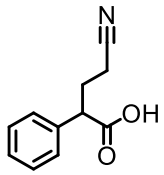

To a 100 mL two round bottom flask under argon was added **156** (1.21 g, 5.95 mmol, 1.00 equiv.) and dissolved in THF (20 mL). A solution of LiOH (0.43 g, 17.9 mmol, 3.00 equiv.) dissolved in water deion. (10 mL) added within 2 min. and heated up to 60 °C. The reaction mixture was quenched after 16 h using HCl 1 M (30 mL) and extracted with TBME (100 mL) and washed organic layer with water deion. (50 mL) before drying over anhydrous Na_2SO_4, then filtered and evaporated (40 °C). Residue was purified by column chromatography (SiO_2, cyclohexane: EtOAc 2:1) to yield white crystals (**157**, 930 mg, 4.94 mmol, 83%).

^{1}H NMR (500 MHz, DCM-*d*): δ 9.98 - 8.90 (s, 1H) 7.42 – 7.28 (m, 5H), 3.79 – 3.71 (m, 1H), 2.45 – 2.33 (m, 2H), 2.30 – 2.21 (m, 1H), 2.17 – 2.10 (m, 1H) ppm.

^{13}C NMR (126 MHz, DCM-*d*): δ 178.58, 136.89, 129.45, 128.53, 128.39, 119.20, 50.17, 28.62, 15.44 ppm.

HRMS (ESI, negative mode): calculated for $C_{11}H_{10}NO_2$ $[M]^-$ 188.0717, found 188.0719.

6-phenyl-4,5-dihydropyridin-2(3H)-one (**155**)

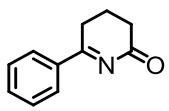

In an undivided electrochemical cell under air, **154** (100 mg, 0.49 mmol, 1.00 equiv.) and K_2CO_3 (14 mg, 0.10 mmol, 0.20 equiv.) was dissolved in MeOH (10 ml). Reaction mixture was stirred (2000 rpm) and current (11 mA) applied for 16 h, using glassy carbon RDE as WE and Pt gauze as

CE. Reaction mixture was extracted with TBME (30 mL) and washed with brine (15 mL). Organic layer dried over anhydrous Na_2SO_4, filtered and evaporated (45 °C). The residue was purified by column chromatography (SiO_2, cyclohexane: TBME 5:1) to yield white crystals (**155**, 12 mg, 0.07 mmol, 14%).

^{1}H NMR (500 MHz, DCM-*d*): δ 7.98 – 7.95 (m, 2H), 7.63 – 7.56 (m, 1H), 7.53 – 7.46 (m, 2H), 3.16 (t, J = 6.9 Hz, 2H), 2.51 (t, J = 7.1 Hz, 2H), 2.09 (p, J = 7.0 Hz, 2H) ppm.

^{13}C NMR (126 MHz, DCM-*d*): 198.09, 136.71, 133.24, 128.68, 127.81, 119.57, 36.49, 19.79, 16.54 ppm. Data extracted from HMBC.

HRMS (ESI): calculated for $C_{11}H_{11}NO$ $[M+Na]^+$ 196.0733, found 196.0730.

5-phenyl-3,4-dihydro-2H-pyrrol-2-one (**158**)

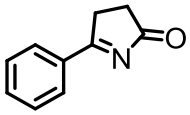

In an undivided cell under air, **157** (100 mg, 0.53 mmol, 1.00 equiv.) and K_2CO_3 (15 mg, 0.11 mmol, 0.20 equiv.) was dissolved in MeOH (10 ml). Reaction mixture was stirred (2000 rpm) and current (11 mA) applied for 16 h, using glassy carbon RDE as WE and Pt gauze as CE. Reaction mixture was extracted with TBME (30 mL) and washed with brine (15 mL). Organic layer dried over anhydrous Na_2SO_4, filtered and evaporated (45 °C). The residue was purified by column chromatography (SiO_2, cyclohexane: TBME 4:1) to yield colorless oil (**158**, 14 mg, 0.09 mmol, 17%).

^{1}H NMR (500 MHz, DCM-*d*): δ 8.03 – 7.93 (m, 2H), 7.68 – 7.59 (m, 1H), 7.55 – 7.47 (m, 2H), 3.38 (t, J = 7.0 Hz, 2H), 2.75 (t, J = 7.0 Hz, 2H) ppm.

^{13}C NMR (126 MHz, DCM-*d*): 195.49, 135.84, 133.67, 128.90, 127.81, 119.35, 34.33, 11.77 ppm. Data extracted from HMBC.

HRMS (ESI): calculated for $C_{10}H_9NO$ $[M+Na]^+$ 182.0576, found 182.0573.

(methylenebis(2-hydroxybenzene-5,1,3-triyl))tetramethanol (**145**)

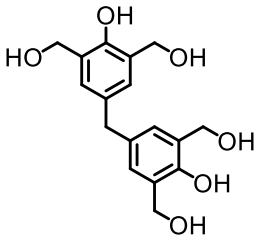

The synthetic procedure was adapted from Okada *et al.*[133]

To a 50 mL two round bottom flask was added NaOH (0.80 g, 20.0 mmol, 4.00 equiv.), dissolved in water deion. (15 mL). 4,4'-Methylenediphenol (1.00 g, 5.00 mmol, 1.00 equiv.) and paraformaldehyde (1.80 g, 20.0 mmol, 4.00 equiv.) was added to the flask and the reaction mixture was warmed up to 40 °C before stirring for 18 h at this temperature. Cooled to room temperature and adjusted the pH to 3 before extracting with 2x DCM (50 mL) and 2x with toluene (50 mL). Combined organic layers dried over anhydrous Na_2SO_4, filtered and evaporated (45 °C) to obtained dark red oil residue. Plugged over reversed phase SiO_2 (eluent: acetonitrile) before removing the solvent. **145** was used as crude without further purification.

^{1}H NMR (400 MHz, MeOD): δ 6.97 (s, 4H), 4.65 (d, J = 4.5 Hz, 8H), 3.78 (s, 2H) ppm.

LC-MS (ESI, negative): *m/z* (%) 319.10 (100), 320.05 (22), 321.10 (3).

4,4'-methylenebis(2,6-dibromophenol) (**107**)

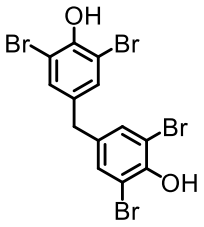

The synthetic procedure was adapted from Lü *et al.*[134]

To a 250 mL three round bottom flask, 4,4'-methylenediphenol (5.00 g, 25.0 mmol, 1.00 equiv.) was dissolved in AcOH (80 mL). Br_2 (5.76 ml, 113 mmol, 4.50 equiv.) was added dropwise within 15 min. After 16 h reaction time at room temperature, the formed precipitate was filtered and washed with AcOH (30 mL) and 2x ice cold EtOH (10 mL). The obtained crystals were dried in the

oven at 60 °C for 20 h before purifying by chromatography (SiO_2, pentane: TBME 10:1) to yield (**107**, 3.49 g, 6.78 mmol, 27%) as white crystals.

^{1}H NMR (400 MHz, DCM-*d*): δ 7.26 (s, 4H), 5.86 (s, 2H), 3.77 (s, 2H) ppm.

^{13}C NMR (126 MHz, DCM-*d*): δ 148.56, 135.30, 132.69, 110.26, 39.12 ppm.

HRMS (ESI, negative mode): calculated for $C_{13}H_7Br_4O_2$ $[M]^-$ 510.7185, found 510.7192.

4,4'-methylenebis(2,6-dibromoaniline) (**143**)

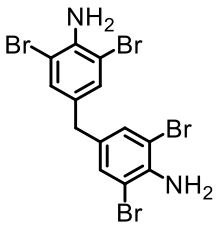

The synthetic procedure was adapted from Tour *et al.*[135]

In a 2000 mL two round bottom flask under argon was added 4,4'-diaminodiphenylmethylene (30.0 g, 147 mmol, 1.00 equiv.) in MeOH:DCM (1:1) (1300 mL). Br_2 (37.8 ml, 735 mmol, 5.00 equiv.) was added dropwise within 45 min. The slightly exothermic reaction mixture was kept at 0 °C, before warming up to room temperature and stirring for 3 h. Fully converted reaction was poured over aqueous NaOH 1 N (1000 mL) and ice (500 g). The mixture was filtered and washed with 4x water deion. (150 mL). The residue dried at 60 °C for 16 h to give titled compound (**143**, 61 g, 119 mmol, 81%).

^{1}H NMR (500 MHz, DMSO-*d*): δ 7.32 (s, 4H), 5.18 (s, 4H), 3.62 (s, 2H) ppm.

HRMS (ESI, positive mode): calculated for $C_{13}H_{10}Br_4N_2$ $[M+H]^+$ 510.7650, found 510.7640.

bis(3,5-dibromophenyl)methane (**144**)

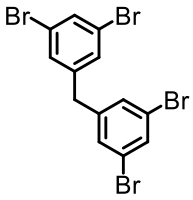

To a 2000 mL two round bottom flask was added **143** (15.5 g, 30.2 mmol, 1.00 equiv.), dissolved in EtOH (900 mL) and the solution was heated to 50 °C. H_2SO_4 (96%, 59 mL, 1057 mmol, 35.0 equiv.) was added dropwise within 20 min. before the temperature was raised to 70 °C. $NaNO_2$ (11.6 g, 166 mmol, 5.50 equiv.) added in 10 portions over the course of 2 h to the reaction mixture. After the addition was completed the temperature was raised to 80°C and stirred at this temperature for 4 d. The mixture was then poured over ice (1000 g) and extracted with toluene (1500 mL). The organic layer was washed with 2x brine (200 mL) and dried over anhydrous Na_2SO_4, filtered and evaporated under reduced pressure (45 °C). The residue was recrystallized from EtOAc and then purified by column chromatography (SiO_2, cyclohexane) to obtain white crystals (**144**, 8.3 g, 17.2 mmol, 57%).

^{1}H NMR (500 MHz, Chloroform-*d*): δ 7.56 (t, J = 1.7 Hz, 2H), 7.23 (d, J = 1.7 Hz, 4H), 3.84 (s, 2H) ppm.

^{13}C NMR (126 MHz, Chloroform-*d*): δ 143.26, 132.70, 130.84, 123.41, 40.53 ppm

GC-MS (EI): *m/z* (%) = 242.9, (100) ; 244.9, (94) ; 483.5, (81) ; 162.9, (61) ; 481.6, (58) ; 485.5, (52) ; 81.5, (51) ; 164.0, (46) ; 121.4, (45) ; 122.4, (42); 402.7, (40) ; 404.7, (39) ; 89.0, (23) ; 161.9, (20) ; 75.0, (18) ; 63.0, (18) ; 243.9, (17) ; 479.5, (15) [M] ; 400.7, (14) ; 245.9, (13) ; 187.5, (13) ; 406.7, (13) ; 484.5, (12).

5,5'-methylenebis(3-bromobenzaldehyde) (**105**)

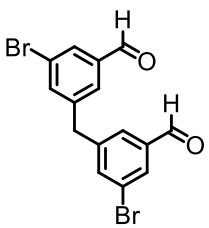

In a 250 mL two round bottom flask under argon was added **144** (1.25 g, 2.58 mmol, 1.00 equiv.) and dissolved in THF (80 mL) and cooled to -78 °C. *t*-BuLi 1.7 M in hexane (6.23 mL, 10.6 mmol, 4.10 equiv.) added dropwise within 15 min. before stirring the reaction mixture for 30 min. at this temperature. DMF (0.80 mL, 10.3 mmol, 4.00 equiv.) was added before warming up to 0 °C within 1 h. After 2 h at this temperature, quenched with HCl 1 M (60 mL) and extracted with 2x EtOAc (100 mL). Combined organic layers washed with water deion. (100 mL) and dried over anhydrous Na_2SO_4, filtered and concentrated under reduced pressure (40 °C). Suspension filtered and washed with EtOAc (5 mL) and TBME (5 mL). White crystals were dried in the oven (45 °C) for 4 h to isolate (**105**, 600 mg, 1.57 mmol, 61%).

^{1}H NMR (400 MHz, Chloroform-*d*): δ 9.93 (s, 2H), 7.90 (t, J = 1.6 Hz, 2H), 7.60 (dt, J = 15.5, 1.7 Hz, 4H), 4.08 (s, 2H) ppm.

^{13}C NMR (126 MHz, DCM-*d*): δ 190.91, 143.29, 138.81, 137.90, 131.19, 128.77, 123.92, 40.82 ppm.

HRMS (ESI, negative mode): calculated for $C_{15}H_9Br_2O_2$ $[M]^-$ 378.8975, found 378.8977.

7 References

1. Pedersen, C. J. Cyclic Polyethers and Their Complexes with Metal Salts. *J Am Chem Soc* **89**, 7017–7036 (1967).
2. Cram, D. J. Host-Guest Chemistry. *Science* **183**, 803–809 (1974).
3. Dietrich, B., Lehn, J. M. & Sauvage, J. P. Les CRYPTATES. *Tetrahedron Lett.* **34**, 2889–2892 (1969).
4. Geue, R., Jacobson, S. H. & Pizer, R. Cryptand Conformational Analysis and Its Mechanistic Implications. Molecular Mechanics Calculations on Cryptands [111] and [222]. *J Am Chem Soc* **108**, 1150–1155 (1986).
5. Metz, B., Moras, D. & Weiss, R. Coordination des Cations Alcalino-Terreux dans leurs Complexes avec des Molécules Macrobicycliques. I. Structure Cristalline et Moléculaire du Cryptate de Calcium $C_{18}H_{36}N_20_6$ x $CaBr_2$ x $3H_20$. *Acta Cryst* **B29**, 1377–1381 (1973).
6. Cram, D. J. The Design of Molecular Hosts, Guests, and Their Complexes (Nobel Lecture). *Angew. Chem. Int. Ed. Engl.* **27**, 1009–1020 (1988).
7. Cram, D. J., Kaneda, T., Helgeson, R. C. & Lein, G. M. Spherands—Ligands Whose Binding of Cations Relieves Enforced Electron-Electron Repulsions. *J Am Chem Soc* **101**, 6752–6754 (1979).
8. Cram, D. J., Kaneda, T., Lein, G. M. & Helgeson, R. C. A spherand containing an enforced cavity that selectively binds lithium and sodium ions. *J. Chem. Soc. Chem. Commun.* **21**, 948b-950 (1979).
9. Gutsche, C. D. & muthukrisnan, R. Calixarenes. 1. Analysis of the Product Mixtures Produced by the Base-Catalyzed Condensation of Formaldehyde with Para-Substituted Phenols. *J Org Chem* **43**, 4905–4906 (1978).
10. Zinke, A., Kretz, R., Leggewie, E. & Hössinger, K. Zur Kenntnis des Härtungsprozesses von Phenol-Formaldehyd-Harzen. *K Monatsh Chem* **83**, 1213–1227 (1952).

11. Hayes, B. T. & Hunter, R. F. Phenol-formaldehyde and allied resins VI: Rational synthesis of a 'cyclic' tetranuclear p-cresol novolak. *J. Appl. Chem.* **8**, 743–748 (2007).
12. Kämmerer, H., Happel, G. & Caesar, F. Die spektroskopische untersuchung einer cyclischen, tetrameren verbindung aus p-kresol und formaldehyd. *Makromol. Chem.* **162**, 179–197 (1972).
13. Gutsche, C. D., Dhawan, B., Hyun No, K. & Muthukrishnan, R. Calixarenes. 4. The Synthesis, Characterization, and Properties of the Calixarenes from p-terf-Butylphenol. *J Am Chem Soc* **103**, 3782–3792 (1981).
14. Moran, J. R., Karbach, S. & Cram, D. J. Cavitands: Synthetic Molecular Vessels. *J Am Chem Soc* **104**, 5826–5828 (1982).
15. Cram, D. J. Shell Closure of Two Cavitands Forms Carcerand Complexes with Components of the Medium as Permanent Guests. *J Am Chem Soc* **107**, 2575–2576 (1985).
16. Sun, W. *et al.* Self-Assembled Carcerand-like Cage with a Thermoregulated Selective Binding Preference for Purification of High-Purity C_{60} and C_{70}. *J. Org. Chem.* **83**, 14667–14675 (2018).
17. Zhou, W. *et al.* A Superphane-based carcerand for arsenic detoxification via imprisoning arsenate. *Cell Rep. Phys. Sci.* **4**, 101295 (2023).
18. Meissner, R. S., Rebek, J. & de Mendoza, J. Autoencapsulation Through Intermolecular Forces: A Synthetic Self-Assembling Spherical Complex. *Science* **270**, 1485–1488 (1995).
19. Rebek, J. *Hydrogen-bonded capsules: molecular behavior in small spaces*. (World Scientific, 2016).
20. Zhang, Q. & Tiefenbacher, K. Hexameric Resorcinarene Capsule is a Brønsted Acid: Investigation and Application to Synthesis and Catalysis. *J. Am. Chem. Soc.* **135**, 16213–16219 (2013).
21. Némethová, I., Schmid, D. & Tiefenbacher, K. Supramolecular Capsule Catalysis Enables the Exploration of Terpenoid Chemical Space Untapped by Nature. *Angew. Chem. Int. Ed.* **62**, (2023).
22. Kroto, H. W. C_{60}: Buckminsterfullerene. *Nature* **318**, 162–163 (1985).

23. Krätschmer, W., Lamb, L. D., Fostiropoulos, K. & Huffman, D. R. Solid C_{60}: a new form of carbon. *Nature* **347**, 354–358 (1990).

24. Scott, L. T. *et al.* A Rational Chemical Synthesis of C_{60}. *Science* **295**, 1500–1503 (2002).

25. Herrmann, A., Diederich, F., Thilgen, C., Meer, H.-U. T. & Müller, W. H. Chemistry of the Higher Fullerenes: Preparative isolation of C_{76} by HPLC and synthesis, separation, and characterization of *Diels - Alder* monoadducts of C_{70} and C_{76}. *Helv. Chim. Acta* **77**, 1689–1706 (1994).

26. Hawkins, J. M., Meyer, A. & Solow, M. A. Osmylation of C_{70}: reactivity versus local curvature of the fullerene spheroid. *J. Am. Chem. Soc.* **115**, 7499–7500 (1993).

27. Chai, Y., Alford, J. M. & Smalley, R. E. Fullerenes with Metals Inside. *J Phys Chem* **95**, 7564–7568 (1991).

28. Saunders, M., Jiménez-Vázquez, H. A., Cross, R. J. & Poreda, R. J. Stable Compounds of Helium and Neon: He@C_{60} and Ne@C_{60}. *Science* **259**, 1428–1430 (1993).

29. Hummelen, J. C., Prato, M. & Wudl, F. There Is a Hole in My Bucky. *J. Am. Chem. Soc.* **117**, 7003–7004 (1995).

30. Ruoff, R. S., Tse, D. S., Malhotra, R. & Lorents, D. C. Solubility of fullerene (C_{60}) in a variety of solvents. *J. Phys. Chem.* **97**, 3379–3383 (1993).

31. Prato, M., Li, Q. C., Wudl, F. & Lucchini, V. Addition of azides to fullerene C_{60}: synthesis of azafulleroids. *J. Am. Chem. Soc.* **115**, 1148–1150 (1993).

32. Komatsu, K., Murata, M. & Murata, Y. Encapsulation of Molecular Hydrogen in Fullerene C_{60} by Organic Synthesis. *Science* **307**, 238–240 (2005).

33. Murata, Y., Murata, M. & Komatsu, K. 100% Encapsulation of a Hydrogen Molecule into an Open-Cage Fullerene Derivative and Gas-Phase Generation of H_2@C_{60}. *J. Am. Chem. Soc.* **125**, 7152–7153 (2003).

34. Bloodworth, S. *et al.* First Synthesis and Characterization of CH_4@C_{60}. *Angew. Chem. Int. Ed.* **58**, 5038–5043 (2019).

35. Haddon, R. C. *et al.* Conducting films of C_{60} and C_{70} by alkali-metal doping. *Nature* **350**, 320–322 (1991).

36. Hebard, A. F. *et al.* Superconductivity at 18 K in potassium-doped C_{60}. *Nature* **350**, 600–601 (1991).

37. Sparn, G. *et al.* Pressure Dependence of Superconductivity in Single-Phase K_3C_{60}. *Science* **252**, 1829–1831 (1991).

38. Margadonna, S. & Prassides, K. Recent Advances in Fullerene Superconductivity. *J. Solid State Chem.* **168**, 639–652 (2002).

39. Foroutan-Nejad, C., Straka, M., Fernández, I. & Frenking, G. Buckyball Difluoride $F_2^-@C_{60}^+$ — A Single-Molecule Crystal. *Angew. Chem. Int. Ed.* **57**, 13931–13934 (2018).

40. Allemand, P.-M. *et al.* Organic Molecular Soft Ferromagnetism in a Fullerene C $_{60}$. *Science* **253**, 301–302 (1991).

41. Marrocchi, A., Tomasi, I. & Vaccaro, L. Organic Small Molecules for Photonics and Electronics from the [2.2]Paracyclophane Scaffold. *Isr. J. Chem.* **52**, 41–52 (2012).

42. Reznikova, K. *et al.* Substitution Pattern Controlled Quantum Interference in [2.2]Paracyclophane-Based Single-Molecule Junctions. *J. Am. Chem. Soc.* **143**, 13944–13951 (2021).

43. Brown, C. J. & Farthing, A. C. Preparation and Structure of Di-p-Xylylene. *Nature* **164**, 915–916 (1949).

44. Cram, D. J. & Steinberg, H. Macro rings. I. Preparation and spectra of the paracyclophanes. *J Am Chem Soc* **73**, 5691–5704 (1951).

45. Kane, V. V., Wolf, A. D. & Jones, M. [6]Paracyclophane. *J. Am. Chem. Soc.* **96**, 2643–2644 (1974).

46. Mannancherry, R., Devereux, M., Häussinger, D. & Mayor, M. Molecular Ansa-Basket: Synthesis of Inherently Chiral All-Carbon [12](1,6)Pyrenophane. *J. Org. Chem.* **84**, 5271–5276 (2019).

47. Schirch, P. F. T. & Boekelheide, V. [2.2.2.2.2](1,2,3,4,5)Cyclophane. *J. Am. Chem. Soc.* **101**, 3125–3126 (1979).

48. Jabłoński, M. Endo- and exohedral complexes of superphane with cations. *J. Comput. Chem.* **43**, 1120–1133 (2022).

49. Cram, D. J. Cavitands: Organic Hosts with Enforced Cavities. *Science* **219**, 1177–1183 (1983).

50. Gabard, J. & Collet, A. Synthesis of a (D_3)-bis(cyclotriveratrylenyl) macrocage by stereospecific replication of a (C_3)-subunit. *J. Chem. Soc. Chem. Commun.* **21**, 1137-1139 (1981).
51. Ross, R. S., Pincus, P. & Wudl, F. Polarizabilities of Hollow Spherical Organic Molecules with Encapsulated Cations. *J. Phys. Chem.* **96**, (1992).
52. Saal, A., Daul, C. A., Jarrosson, T. & Ouamerali, O. Theoretical study of the geometrical and electronic structures and thermochemistry of spherophanes. *J. Mol. Model.* **15**, 1067–1078 (2009).
53. Saal, A., Jarrosson, T., Ouamerali, O. & Daul, C. A. Molecular hydrogen encapsulation in spherophanes. *Chem. Phys. Lett.* **480**, 225–230 (2009).
54. Goel, A., Howard, J. B. & Vander Sande, J. B. Size analysis of single fullerene molecules by electron microscopy. *Carbon* **42**, 1907–1915 (2004).
55. West, A. P., Van Engen, D. & Pascal, R. A. Short synthesis and structure of a large molecular bowl. *J. Am. Chem. Soc.* **111**, 6846–6847 (1989).
56. Delarue Bizzini, L. Polycyclic- and sulfurcontaining-compounds: from polycyclic hydrocarbons to thiaspherophane. (2019) UNIBAS-007177103.
57. Gantenbein, M. Small organic molecules : building blocks of functional materials. (2015) UNIBAS-006436289.
58. Gutsche, C. D. & Gutsche, C. D. *Calixarenes: an introduction*. (RSC Pub, 2008).
59. Böhmer, V., Goldmann, H., Vogt, W., Vicens, J. & Asfari, Z. The synthesis of double-calixarenes. *Tetrahedron Lett.* **30**, 1391–1394 (1989).
60. Rose, K. N. Self-assembly of carcerand-like dimers of calix[4]resorcinarene facilitated by hydrogen bonded solvent bridges. *Chem. Commun.* **3**, 407–408 (1998).
61. Zhang, G., Presly, O., White, F., Oppel, I. M. & Mastalerz, M. A Permanent Mesoporous Organic Cage with an Exceptionally High Surface Area. *Angew. Chem. Int. Ed.* **53**, 1516–1520 (2014).
62. Lauer, J. C., Zhang, W.-S., Rominger, F., Schröder, R. R. & Mastalerz, M. Shape-Persistent [4+4] Imine Cages with a Truncated Tetrahedral Geometry. *Chem. - Eur. J.* **24**, 1816–1820 (2018).
63. Tahoun, M., Gee, C. T., McCoy, V. E., Sander, P. M. & Müller, C. E. Chemistry of porphyrins in fossil plants and animals. *RSC Adv.* **11**, 7552–7563 (2021).

64. Auwärter, W., Écija, D., Klappenberger, F. & Barth, J. V. Porphyrins at interfaces. *Nat. Chem.* **7**, 105–120 (2015).

65. *Tetrapyrroles: birth, life, and death*. (Landes Bioscience ; Springer Science & Business Media, 2009).

66. Soret, jacques-L. Analyse spectrale: Sur le spectre d'absorption du sang dans la partie violette et ultra-violette. *Comptes Rendus Académie Sci.* **97**, 1269–1270 (1883).

67. Rothemund, P. FORMATION OF PORPHYRINS FROM PYRROLE AND ALDEHYDES. *J Am Chem Soc* **57**, 2010–2011 (1935).

68. Rothemund, P. A New Porphyrin Synthesis. The Synthesis of Porphin [1]. *J. Am. Chem. Soc.* **58**, 625–627 (1936).

69. Adler, A. D. *et al.* A simplified synthesis for meso-tetraphenylporphine. *J. Org. Chem.* **32**, 476–476 (1967).

70. Linsdey, J. S. SYNTHESIS OF TETRAPHRNYLPORPRYRINS UNDER VERY MILD CONDITIONS. *Tetrahedron Lett.* **27**, 4969–4970 (1986).

71. Lindsey, J. S. Rothemund and Adler-Longo Reactions Revisited: Synthesis of Tetraphenylporphyrins under Equilibrium Conditions. *J. Org. Chem.* **52**, 827–836 (1987).

72. Lindsey, J. S. One-Flask Synthesis of Meso-Substituted Dipyrromethanes and Their Application in the Synthesis of Trans-Substituted Porphyrin Building Blocks. *Tetrahedron Lett.* **50**, 11427–11440 (1994).

73. Leary, E. *et al.* Bias-Driven Conductance Increase with Length in Porphyrin Tapes. *J. Am. Chem. Soc.* **140**, 12877–12883 (2018).

74. El Abbassi, M. *et al.* Unravelling the conductance path through single-porphyrin junctions. *Chem. Sci.* **10**, 8299–8305 (2019).

75. Zwick, P. *et al.* Mechanical Fixation by Porphyrin Connection: Synthesis and Transport Studies of a Bicyclic Dimer. *J. Org. Chem.* **85**, 118–128 (2020).

76. Schosser, W. M. *et al.* Mechanical conductance tunability of a porphyrin–cyclophane single-molecule junction. *Nanoscale* **14**, 984–992 (2022).

77. Jung, T. A., Schlittler, R. R. & Gimzewski, J. K. Conformational identification of individual adsorbed molecules with the STM. *Nature* **386**, 696–698 (1997).

78. Yokoyama, T., Yokoyama, S., Kamikado, T. & Mashiko, S. Nonplanar adsorption and orientational ordering of porphyrin molecules on Au(111). *J. Chem. Phys.* **115**, 3814–3818 (2001).

79. Kuck, S. *et al.* "Naked" Iron-5,10,15-triphenylcorrole on Cu(111): Observation of Chirality on a Surface and Manipulation of Multiple Conformational States by STM. *J. Am. Chem. Soc.* **130**, 14072–14073 (2008).

80. XVII. On the electricity excited by the mere contact of conducting substances of different kinds. In a letter from Mr. Alexander Volta, F. R. S. Professor of Natural Philosophy in the University of Pavia, to the Rt. Hon. Sir Joseph Banks, Bart. K.B. P. R. S. *Philos. Trans. R. Soc. Lond.* **90**, 403–431 (1800).

81. Faraday, M. Siebente Reihe von Experimental-Untersuchungen über Elektricität. *Ann. Phys. Chem.* **109**, 481–520 (1834).

82. Waldvogel, S. R., Lips, S., Selt, M., Riehl, B. & Kampf, C. J. Electrochemical Arylation Reaction. *Chem. Rev.* **118**, 6706–6765 (2018).

83. Yoshida, J., Kataoka, K., Horcajada, R. & Nagaki, A. Modern Strategies in Electroorganic Synthesis. *Chem. Rev.* **108**, 2265–2299 (2008).

84. Pollok, D. & Waldvogel, S. R. Electro-organic synthesis – a 21st century technique. *Chem. Sci.* **11**, 12386–12400 (2020).

85. Seidler, J., Strugatchi, J., Gärtner, T. & Waldvogel, S. R. Does electrifying organic synthesis pay off? The energy efficiency of electro-organic conversions. *MRS Energy Sustain.* **7**, 42 (2020).

86. Lin, Y. & Malins, L. R. Total synthesis of biseokeaniamides A–C and late-stage electrochemically-enabled peptide analogue synthesis. *Chem. Sci.* **11**, 10752–10758 (2020).

87. Kolbe, H. Unt,ersuchungen iiber die Elektrolyse organischer Verbindungen. *Ann. Chem. Pharm.* **69**, 257–294 (1849).

88. Hofer, H. & Moest, M. Ueber die Bildung von Alkoholen bei der Elektrolyse fettsaurer Salze. *Justus Liebigs Ann. Chem.* **323**, 284–323 (1902).

89. Xiang, J. *et al.* Hindered dialkyl ether synthesis with electrogenerated carbocations. *Nature* **573**, 398–402 (2019).

90. Bondon, A. *et al.* Tetraarylporphyrin synthesis by electrochemical oxidation of porphyrinogens. *Electrochimica Acta* **46**, 1899–1903 (2001).

91. Olah, G. A., Wu, A. H. & Farooq, O. Synthetic methods and reactions. 157. Reductive alkylation and reduction of tertiary, secondary, and benzylic alcohols with trimethyl-(triethyl-, and triisopropyl)boron/trifluoromethanesulfonic (triflic) acid. *J. Org. Chem.* **56**, 2759–2761 (1991).

92. Gordon, P. E. & Fry, A. J. Hypophosphorous acid–iodine: a novel reducing system. Part 2: Reduction of benzhydrols to diarylmethylene derivatives. *Tetrahedron Lett.* **42**, 831–833 (2001).

93. Mirza-Aghayan, M., Boukherroub, R. & Rahimifard, M. A simple and efficient hydrogenation of benzyl alcohols to methylene compounds using triethylsilane and a palladium catalyst. *Tetrahedron Lett.* **50**, 5930–5932 (2009).

94. Okano, T., Tsukiyama, K., Konishi, H. & Kiji, J. VERSATILE POLYMER-BOUND RHODIUM CATALYSTS. FACILE HYDROGENATION OF AROMATIC COMPOUNDS IN THE LIQUID PHASE. *Chem. Lett.* **11**, 603–606 (1982).

95. Sankaranarayanan, T. M. *et al.* Hydrodeoxygenation of anisole as bio-oil model compound over supported Ni and Co catalysts: Effect of metal and support properties. *Catal. Today* **243**, 163–172 (2015).

96. Goren, Z. & Biali, S. E. Multiple reductive cleavage of calixarene diethyl phosphate esters: a route to [1 n]metacyclophanes. *J. Chem. Soc. Perkin 1* **5**, 1484-1487 (1990).

97. Sergeev, A. G. & Hartwig, J. F. Selective, Nickel-Catalyzed Hydrogenolysis of Aryl Ethers. *Science* **332**, 439–443 (2011).

98. Guan, Z. *et al.* A highly efficient catalyst for Suzuki–Miyaura coupling reaction of benzyl chloride under mild conditions. *RSC Adv* **4**, 36437–36443 (2014).

99. Crockett, M. P., Tyrol, C. C., Wong, A. S., Li, B. & Byers, J. A. Iron-Catalyzed Suzuki–Miyaura Cross-Coupling Reactions between Alkyl Halides and Unactivated Arylboronic Esters. *Org. Lett.* **20**, 5233–5237 (2018).

100. Sun, Y.-Y. *et al.* Cu-Catalyzed Suzuki–Miyaura reactions of primary and secondary benzyl halides with arylboronates. *Chem Commun* **50**, 11060–11062 (2014).

101. Yamamoto, T. *et al.* C–H Activation-Based Transformation of Naphthalenes to 3-Iodo-2-naphthylboronic Acid Derivatives for Use in Iterative Coupling Synthesis of Helical Oligo(naphthalene-2,3-diyl)s. *Bull. Chem. Soc. Jpn.* **90**, 604–606 (2017).

102. Vollhardt, K. P. C. Cobalt-vermittelte [2+2+2]-Cycloadditionen: eine ausgereifte Synthesestrategie. *Angew. Chem.* **96**, 525–541 (1984).

103. Chen, J., Zhang, Y., Liu, L., Yuan, T. & Yi, F. Efficient Copper-Catalyzed Double S-Arylation of Aryl Halides with Sodium Sulfide in PEG-400. *Phosphorus Sulfur Silicon Relat. Elem.* **187**, 1284–1290 (2012).

104. Sergeev, V. A. SYNTHESIS AND CRYSTAL STRUCTURE OF CYCLOTRIS(m-PHENYLENESULFIDE). 1440–1444 (1989).

105. Gutsche, C. D. & Alam, I. Calixarenes. 23. the complexation and catalytic properties of water soluble calixarenes. *Tetrahedron* **44**, 4689–4694 (1988).

106. Strobel, M. *et al.* Self-Assembly of Amphiphilic Calix[4]arenes in Aqueous Solution. *Adv. Funct. Mater.* **16**, 252–259 (2006).

107. Mastalerz, M. *et al.* Oligophenylcalix[4]arenes as Potential Precursors for Funnelenes and Calix[4]triphenylenes: Syntheses and Preliminary Cyclodehydration Studies. *Eur. J. Org. Chem.* **2006**, 4951–4962 (2006).

108. Larsen, M. & Jørgensen, M. Selective Halogen−Lithium Exchange Reaction of Bromine-Substituted 25,26,27,28-Tetrapropoxycalix[4]arene. *J. Org. Chem.* **61**, 6651–6655 (1996).

109. García-Álvarez, P. *et al.* Unmasking Representative Structures of TMP-Active Hauser and Turbo-Hauser Bases. *Angew. Chem.* **120**, 8199–8201 (2008).

110. Krasovskiy, A., Krasovskaya, V. & Knochel, P. Mixed Mg/Li Amides of the Type $R_2NMgCl \cdot LiCl$ as Highly Efficient Bases for the Regioselective Generation of Functionalized Aryl and Heteroaryl Magnesium Compounds. *Angew. Chem. Int. Ed.* **45**, 2958–2961 (2006).

111. Petrier, C. & Luche, J. L. Allylzinc reagents additions in aqueous media. *J. Org. Chem.* **50**, 910–912 (1985).

112. Okude, Y., Hirano, S., Hiyama, T. & Nozaki, H. Grignard-type carbonyl addition of allyl halides by means of chromous salt. A chemospecific synthesis of homoallyl alcohols. *J. Am. Chem. Soc.* **99**, 3179–3181 (1977).

113. Subramanian, L. R., Martinez, A. G., Fernandez, A. H. & Alvarez, R. M. Hydrierende Spaltung phenolischer und enolischer Perfluoroalkansulfonate. *Synthesis* **1984**, 481–485 (1984).

114. Zhong, Z., Xu, P. & Zhou, A. Electrochemical phosphorylation of arenols and anilines leading to organophosphates and phosphoramidates. *Org. Biomol. Chem.* **19**, 5342–5347 (2021).

115. Mondal, A., Visser, P., Doze, A. M., Buter, J. & Feringa, B. L. Pd-catalyzed sp–sp^3 cross-coupling of benzyl bromides using lithium acetylides. *Chem. Commun.* **57**, 7529–7532 (2021).

116. Mkhalid, I. A. I., Barnard, J. H., Marder, T. B., Murphy, J. M. & Hartwig, J. F. C–H Activation for the Construction of C–B Bonds. *Chem. Rev.* **110**, 890–931 (2010).

117. Lü, J., Han, L.-W., Lin, J.-X. & Cao, R. Supramolecular Organic Frameworks of Brominated Bisphenol Derivatives with Organoamines. *Cryst. Growth Des.* **11**, 3551–3557 (2011).

118. Li, X., Yuan, T. & Chen, J. Efficient Copper(I)-Catalyzed S-Arylation of KSCN with Aryl Halides in PEG-400. *Chin. J. Chem.* **30**, 651–655 (2012).

119. Auwärter, W., Écija, D., Klappenberger, F. & Barth, J. V. Porphyrins at interfaces. *Nat. Chem.* **7**, 105–120 (2015).

120. SK. p-Methoxybenzyl (PMB) Protective Group. *Chem-Station Int. Ed.* (2014).

121. Dai, X. *et al.* A nanodrug to combat cisplatin-resistance by protecting cisplatin with *p*-sulfonatocalix[4]arene and regulating glutathione *S* -transferases with loaded 5-fluorouracil. *Chem. Commun.* **55**, 7199–7202 (2019).

122. Mastalerz, M. *et al.* Oligophenylcalix[4]arenes as Potential Precursors for Funnelenes and Calix[4]triphenylenes: Syntheses and Preliminary Cyclodehydration Studies. *Eur. J. Org. Chem.* **2006**, 4951–4962 (2006).

123. Barton, O. & Mattay, J. Iodination of Activated Aromatic Compounds Using Sodium Peroxodisulfate and Iodine: An Efficient Way to Iodinate Alkylated Calix[4]arenes. *Synthesis* **2008**, 110–114 (2008).

124. Wong, M. S., Li, Z. H. & Kwok, C. C. Highly extended styrylstyrylcalix[4]arene assemblies: synthesis and optical properties. *Tetrahedron Lett.* **41**, 5719–5723 (2000).

125. Sameni, S., Lejeune, M., Jeunesse, C., Matt, D. & Welter, R. Calixarene-monophosphines as supramolecular chelators. *Dalton Trans.* **38**, 7912-7923 (2009).

126. Dyker, G., Mastalerz, M. & Müller, I. M. Electron-Rich Cavitands via Fourfold Sonogashira Cross-Coupling Reaction of Calix[4]arenes and Bromopyridines - Effect of the Nitrogen Position on Complexation Abilities. *Eur. J. Org. Chem.* **2005**, 3801–3812 (2005).

127. Le Bihan, Y.-V. *et al.* C_8-substituted pyrido[3,4-d]pyrimidin-4(3H)-ones: Studies towards the identification of potent, cell penetrant Jumonji C domain containing histone lysine demethylase 4 subfamily (KDM4) inhibitors, compound profiling in cell-based target engagement assays. *Eur. J. Med. Chem.* **177**, 316–337 (2019).

128. Müller, S., Liepold, B., Roth, G. J. & Bestmann, H. J. An Improved One-pot Procedure for the Synthesis of Alkynes from Aldehydes. *Synlett* **1996**, 521–522 (1996).

129. Tabata, M., Moriyama, K. & Togo, H. One-Pot Transformation of Methylarenes into Aromatic Aldehydes under Metal-Free Conditions: Metal-Free One-Pot Oxidation of Methylarenes. *Eur. J. Org. Chem.* **2014**, 3402–3410 (2014).

130. Hermes, J. P. *et al.* Gold Nanoparticles Stabilized by Thioether Dendrimers. *Chem. - Eur. J.* **17**, 13473–13481 (2011).

131. Gutsche, C. D. & Lin, L.-G. Calixarenes 12. *Tetrahedron* **42**, 1633–1640 (1986).

132. Zhong, Z., Xu, P. & Zhou, A. Electrochemical phosphorylation of arenols and anilines leading to organophosphates and phosphoramidates. *Org. Biomol. Chem.* **19**, 5342–5347 (2021).

133. Okada, Y., Ishii, F., Kasai, Y. & Nishimura, J. Stereoselective synthesis of meta- and three-bridged cyclophanes with intramolecular [2 + 2] photocycloaddition by using the steric effect of methoxyl group. *Tetrahedron* **50**, 12159–12184 (1994).

134. Lü, J., Han, L.-W., Lin, J.-X. & Cao, R. Supramolecular Organic Frameworks of Brominated Bisphenol Derivatives with Organoamines. *Cryst. Growth Des.* **11**, 3551–3557 (2011).

135. Tour, J. M. *et al.* Synthesis and Preliminary Testing of Molecular Wires and Devices. *Chem. - Eur. J.* **7**, 5118–5134 (2001).

8 Appendix

List of Abbreviations

Å	Ångström
ACN	Acetonitrile
AcOH	Acetic acid
aq.	Aqueous
Ar	Aryl
Bn	Benzyl
CE	Counter electrode
COSY	Correlation spectroscopy
CV	Cyclic voltammetry
δ	Chemical shift
d	Doublet
D	Dimension
DART	Direct analysis in real time
DBA	Dibenzylidenacetone
DCM	Dichloromethane
DCTB	Trans-2-[3-(4-*tert*-butylphenyl)-2-methyl-2-propenylidene]malono-nitrile
DDQ	2,3-Dichloro-5,6-dicyano-p-benzoquinone
DMA	N,N-Dimethyl acetamide
DMF	N,N-Dimethyl formamide
DMI	1,3-Dimethyl-2-imidazolidinone
DMSO	Dimethyl sulfoxide
DOSY	Diffusion ordered spectroscopy
EI	Electron ionization
Eq/ Equiv.	Equivalent
ESI	Electrospray ionization

EtOAc	Ethyl acetate
EtOH	Ethanol
GCMS	Gas chromatography
H	Hour
HMBC	Heteronuclear multiple-bond correlation spectroscopy
HPLC	High performance liquid chromatography
HSQC	Heteronuclear single-quantum correlation spectroscopy
K	Kelvin
LC	Liquid chromatography
LUMO	Lowest unoccupied molecular orbital
m	Multiplett
M	Molar
min.	Minute
m/z	Mass-to-charge ratio
MALDI	Matrix assisted laser desorption/ionization
MeOH	Methanol
MS	Mass spectrometry
NBS	N-Bromosuccinimide
nm	Nanometer
NMP	N-Methyl-2-pyrrolidone
NMR	Nuclear magnetic resonance
NOESY	Nuclear Overhauser effect spectroscopy
PEG	Polyethylene glycol
Ph	Phenyl
ppm	Parts per million
quant.	quantitative
Rf	Retention factor
RT	Room temperature
SCE	Saturated calomel electrode

S_N	Nucleophilic substitution
STM	Scanning tunneling microscopy
t	Triplet
T	Temperature
TBAF	Tetrabutyl ammonium fluoride
TBME	*tert*-butyl methyl ether
TCNQ	Tetracyanoquinodimethane
TFA	Trifluoroacetic acid
THF	Tetrahydrofuran
TIPS	Triisopropylsilyl
TLC	Thin layer chromatography
TMS	Trimethylsilyl
TOF	Time of flight
UPLC	Ultra performance liquid chromatography
UV-Vis	Ultraviolet–visible
Xantphos	4,5-Bis(diphenylphosphino)-9,9-dimethylxanthene
V	Volt
WE	Working electrode

Analytical Data

25,26,27,28-Tetrahydroxycalix[4]arene (**112**)

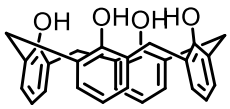

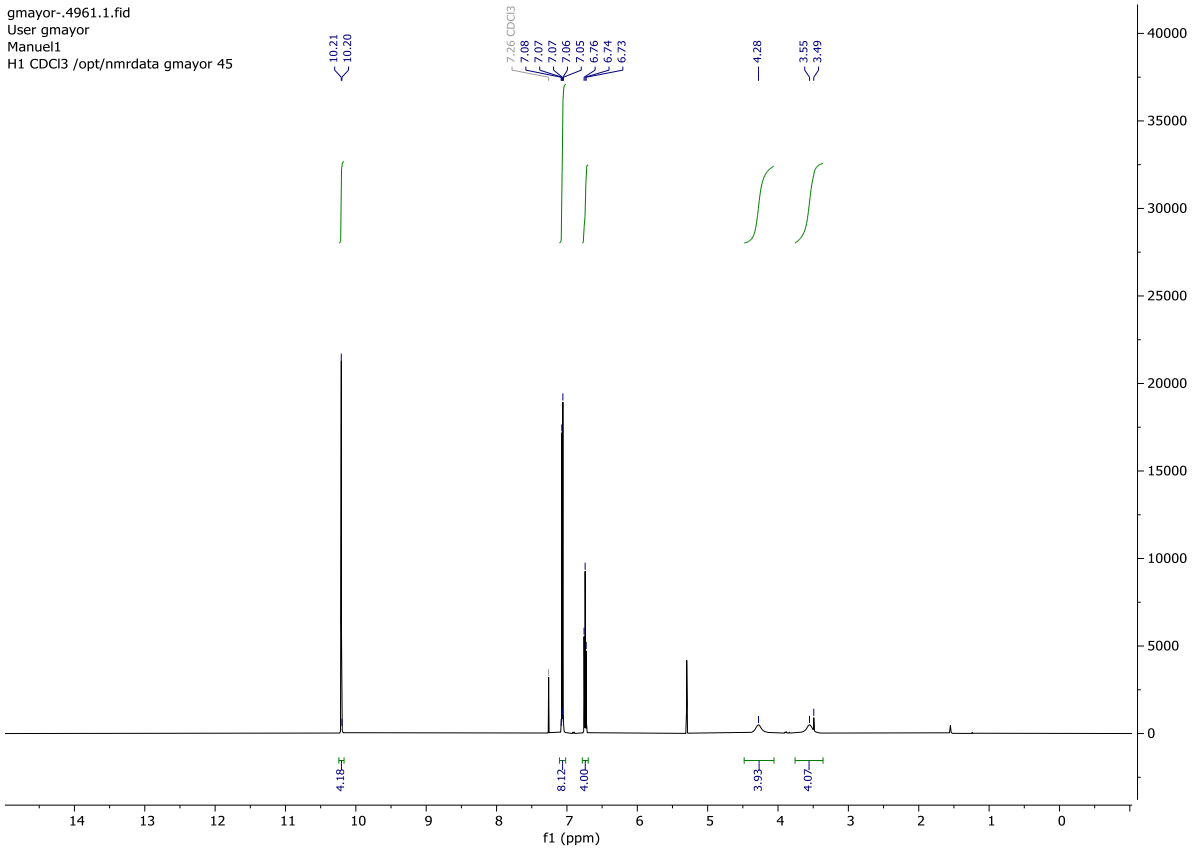

Figure 43. ^{1}H NMR spectrum of **112**

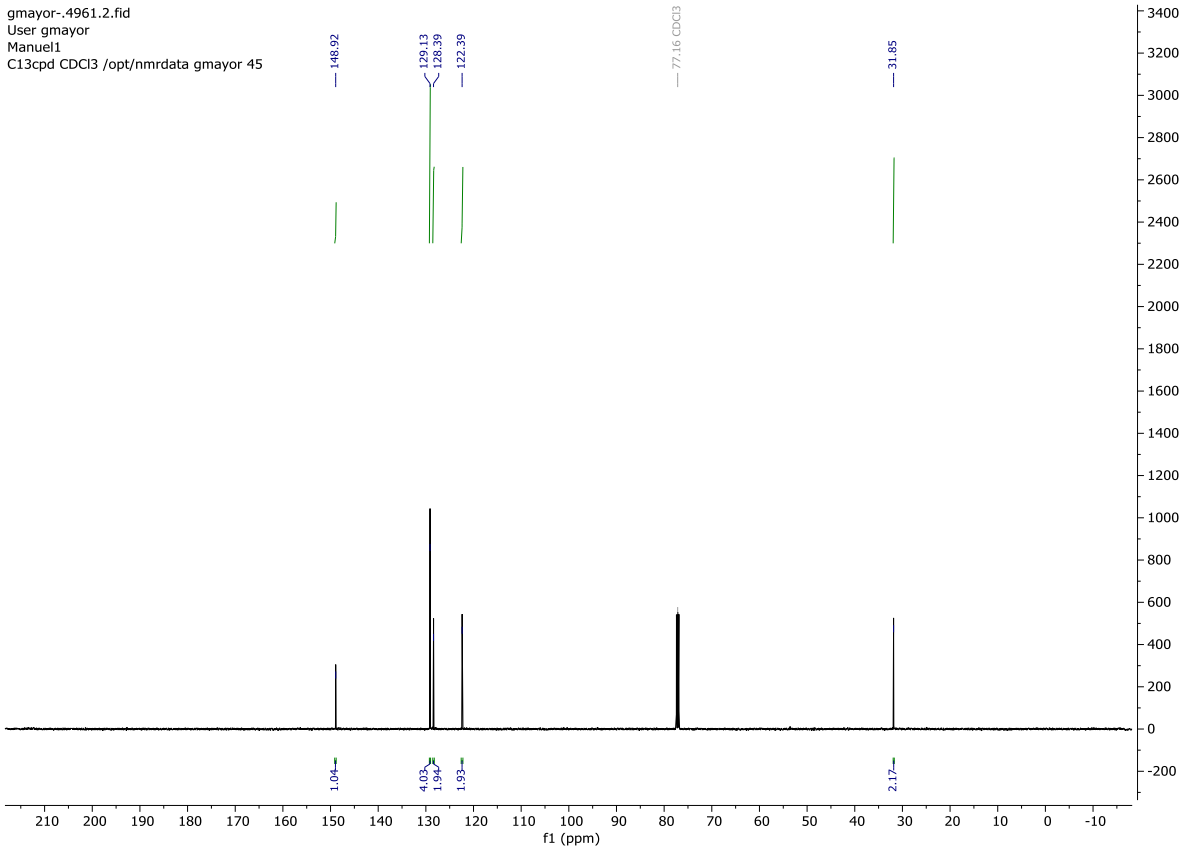

Figure 44. ^{13}C NMR spectrum of **112**

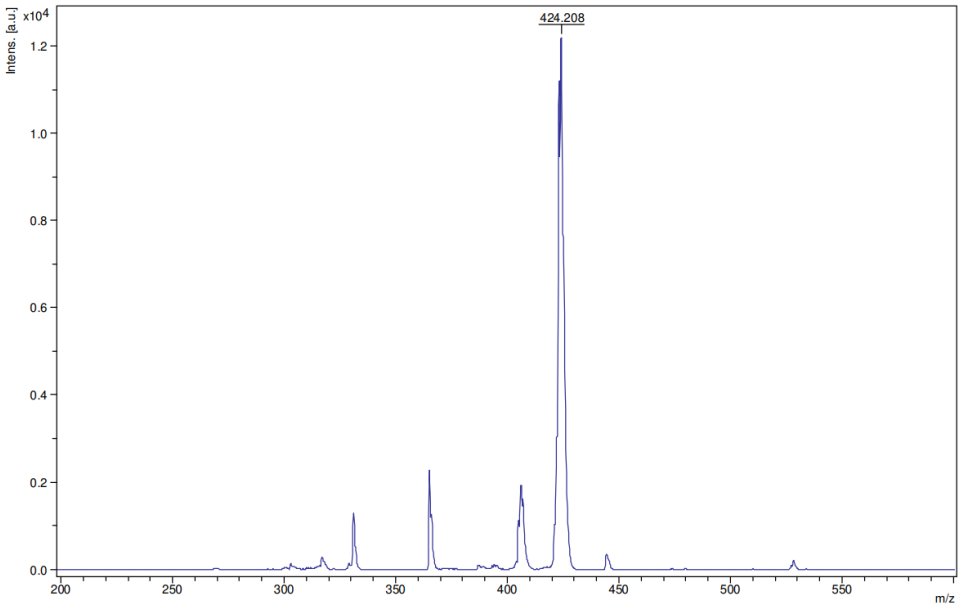

Figure 45. MALDI-TOF spectrum of **112**

25,26,27,28-tetrapropyloxycalix[4]arene (**113**)

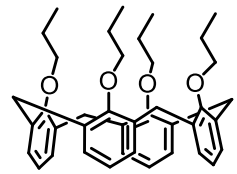

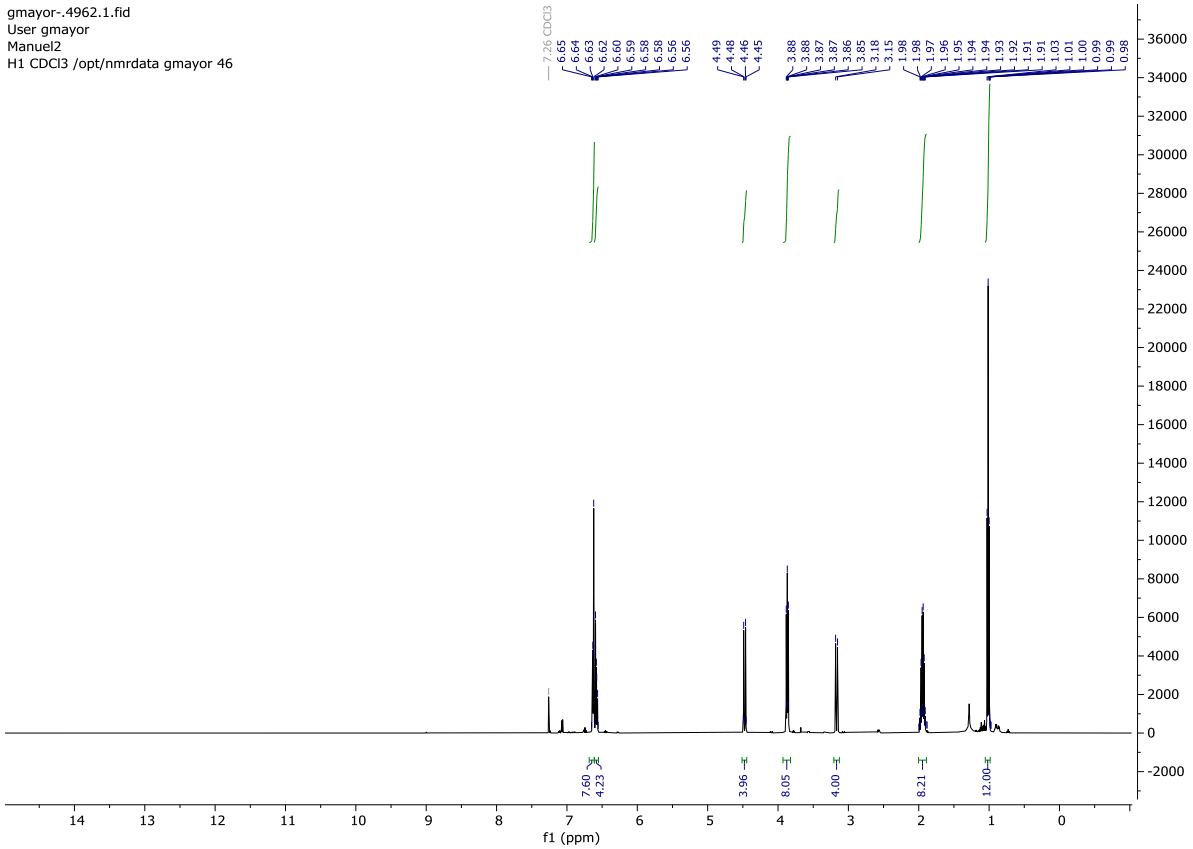

Figure 46. ^{1}H NMR spectrum of **113**

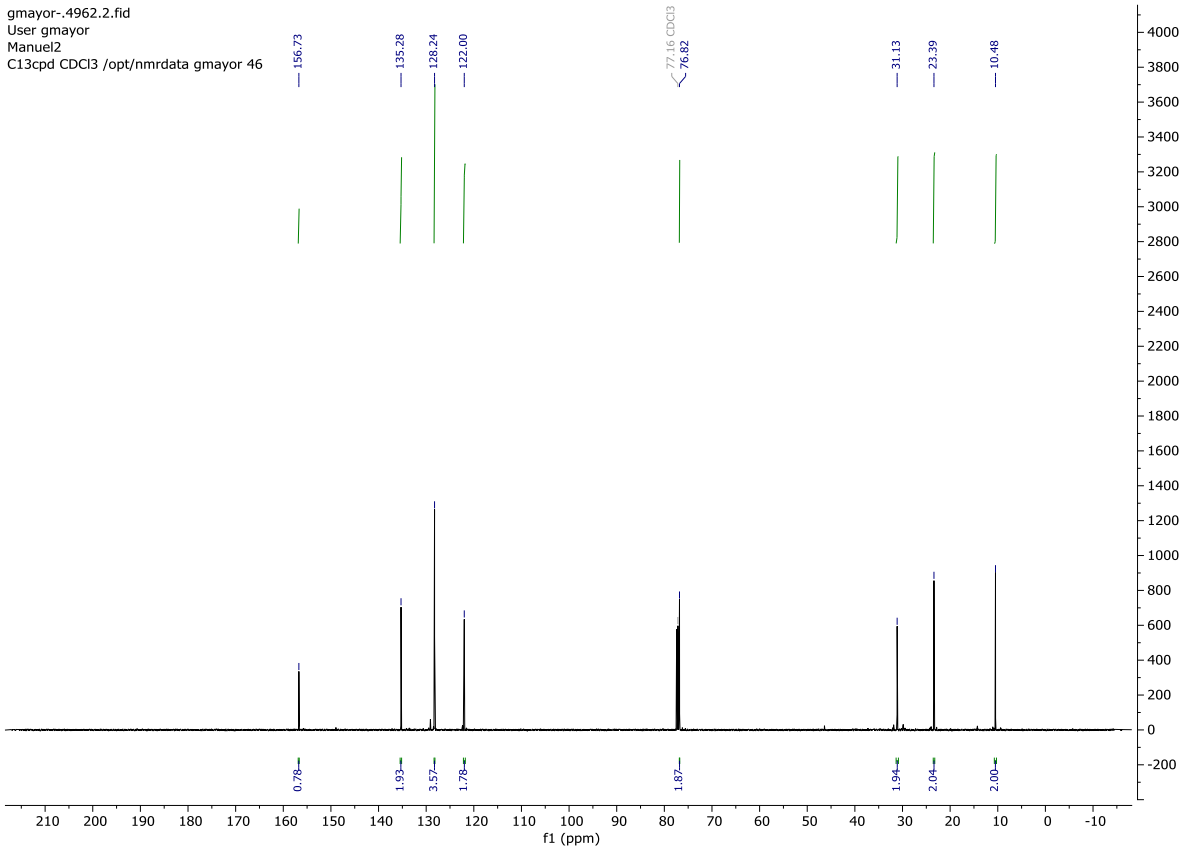

Figure 47. ^{13}C NMR spectrum of **113**

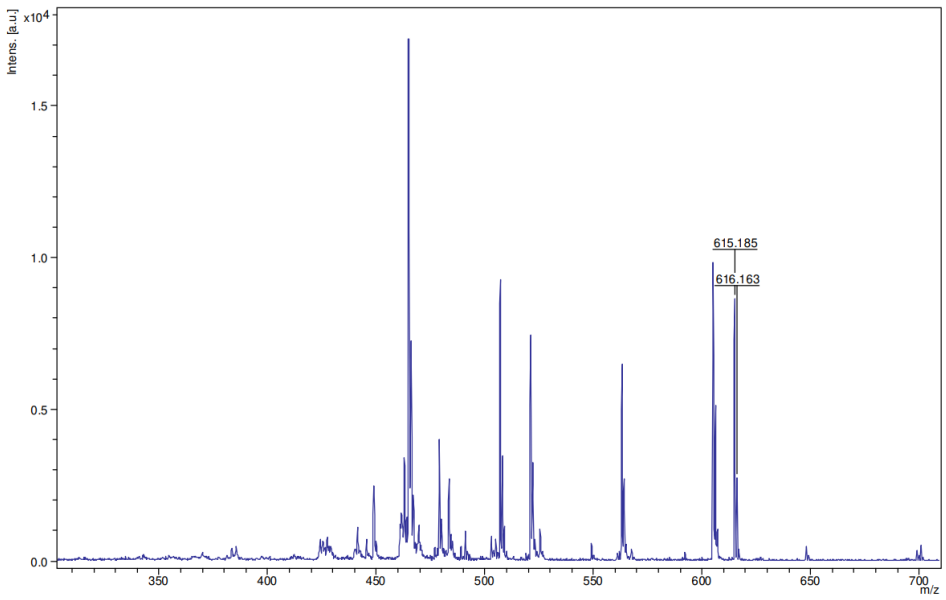

Figure 48. MALDI-TOF spectrum of **113**

5,11,17,23-tetrabromo-25,26,27,28-tetrapropyloxycalix[4]arene (**114**)

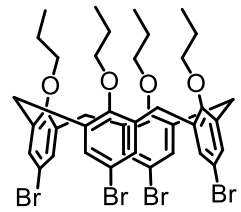

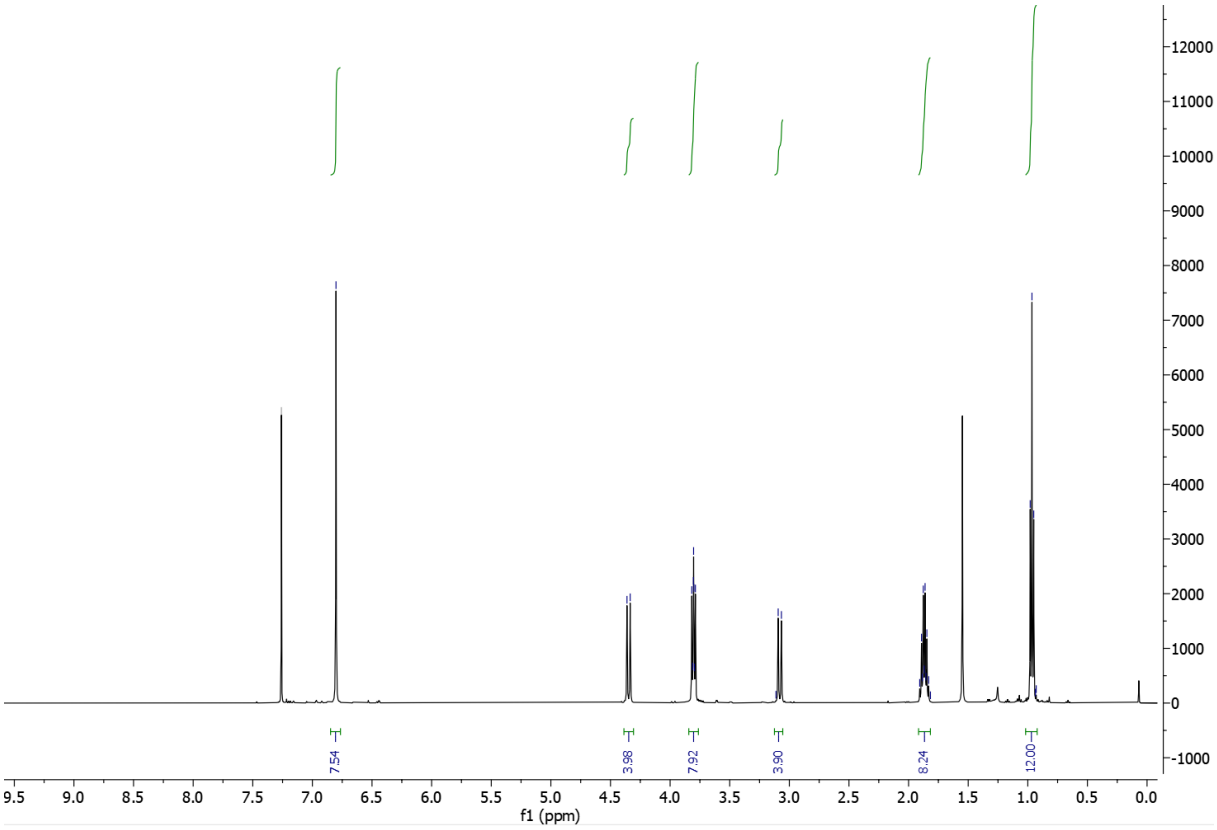

Figure 49. ^{1}H NMR spectrum of **114**

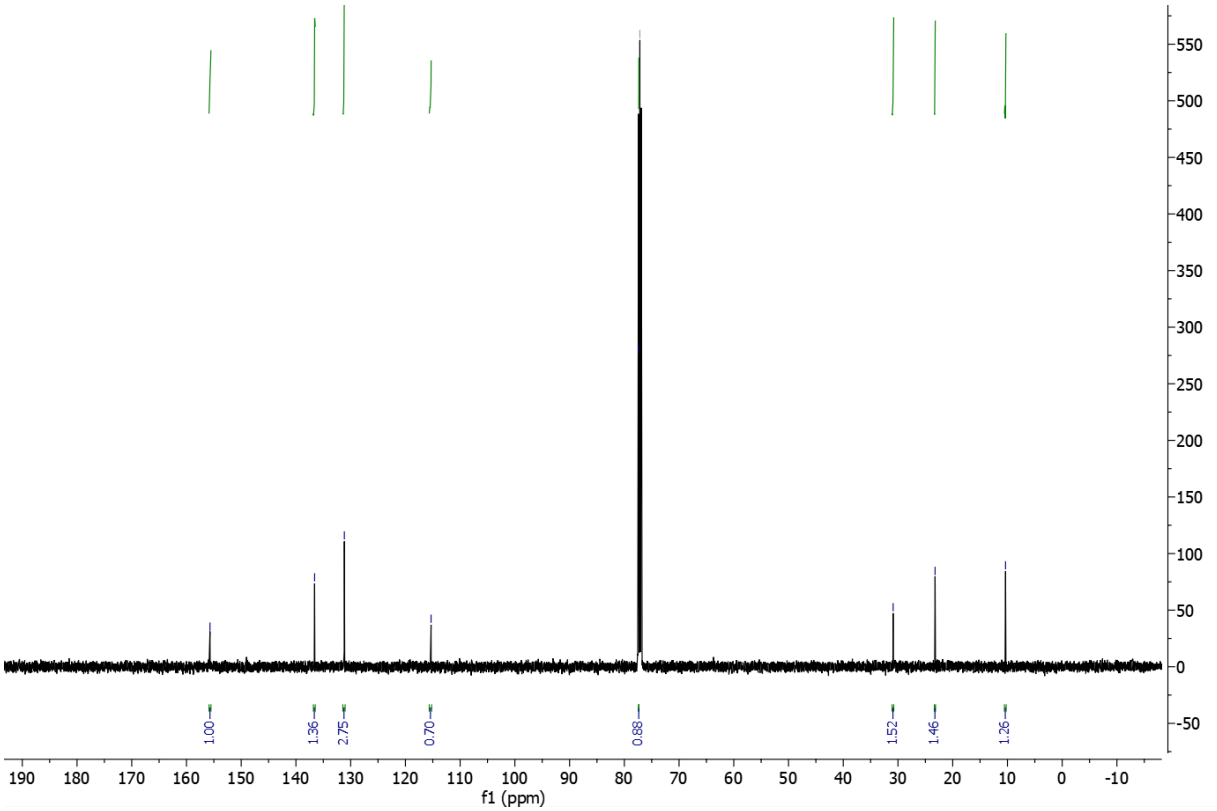

Figure 50. ^{13}C NMR spectrum of **114**

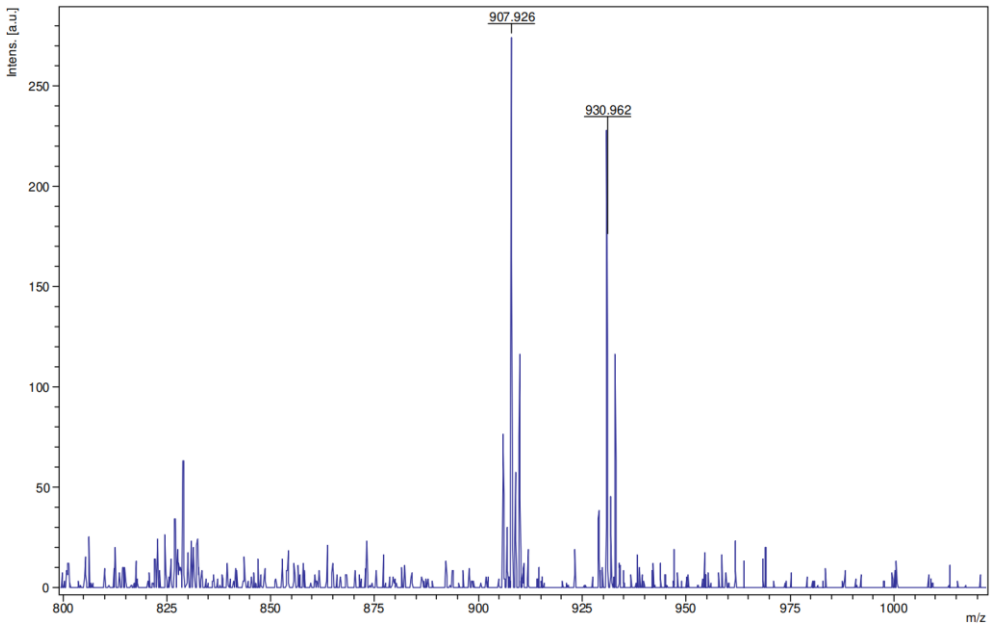

Figure 51. MALDI-TOF spectrum of **114**

5,11,17,23-tetraiodo-25,26,27,28-tetrapropyloxycalix[4]arene (**162**)

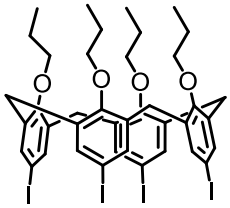

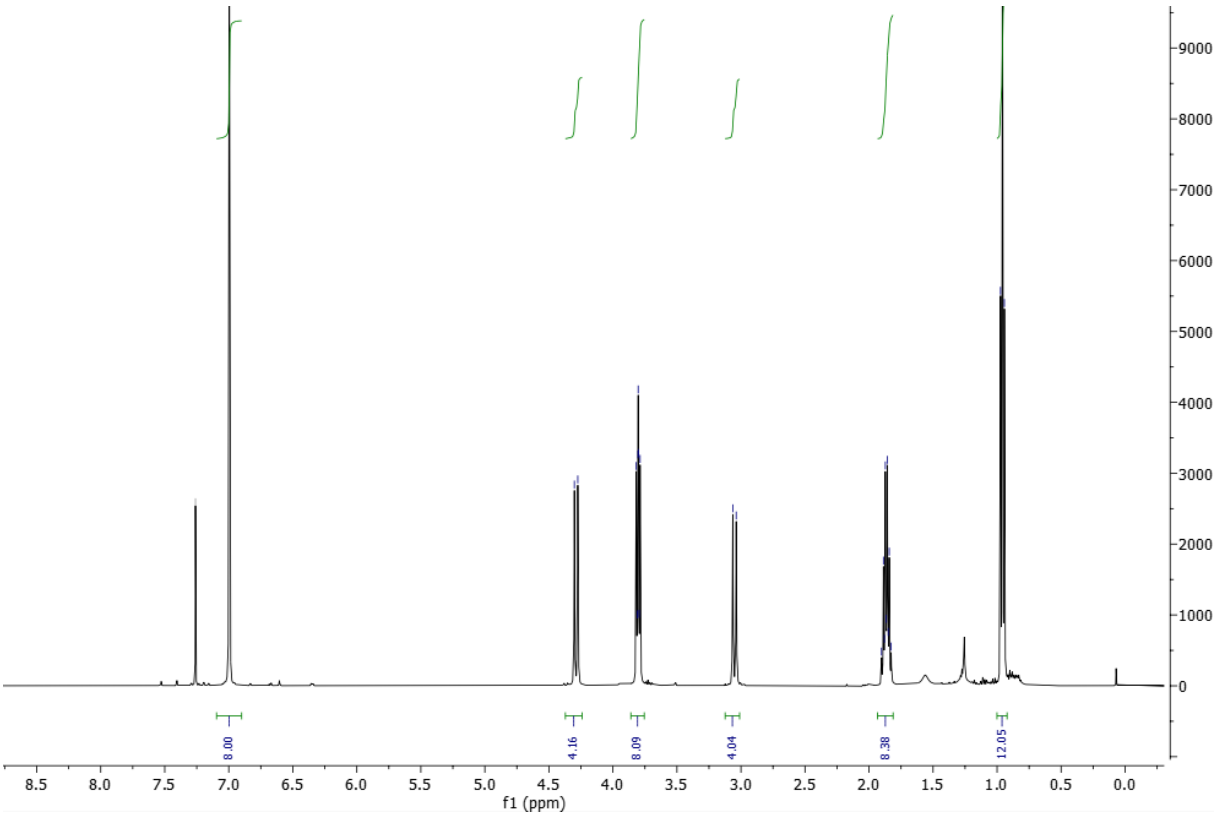

Figure 52. ^{1}H NMR spectrum of **162**

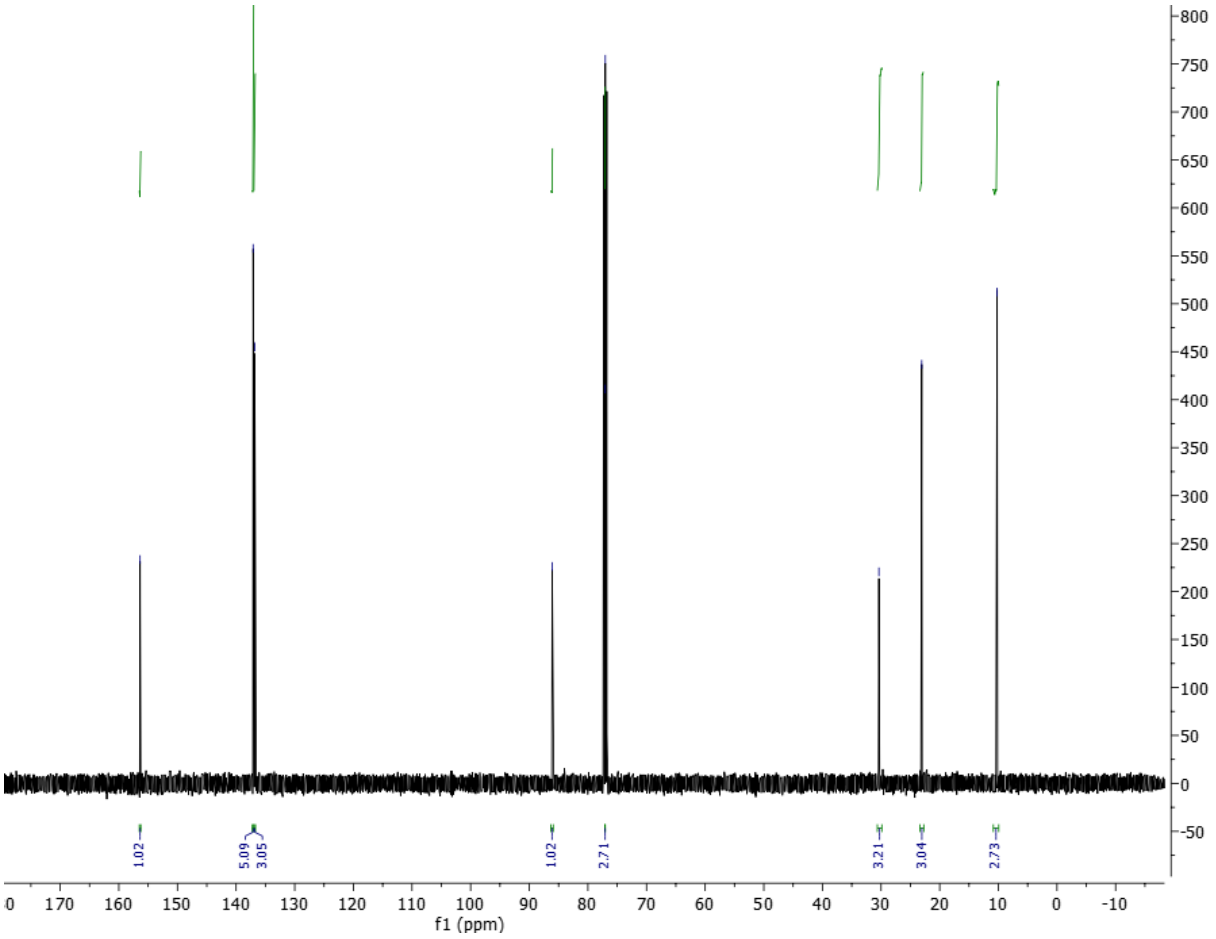

Figure 53. ^{13}C NMR spectrum of **162**

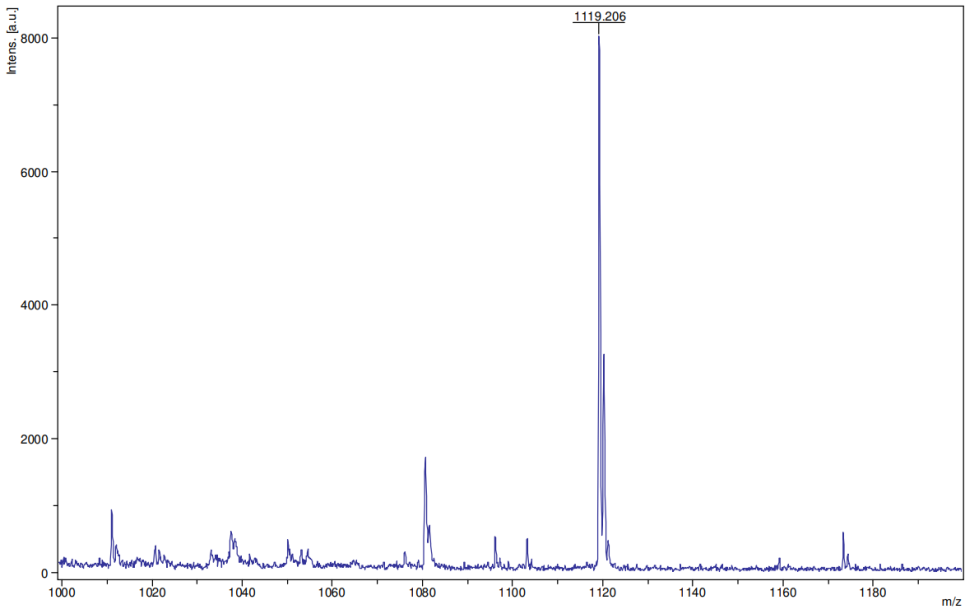

Figure 54. MALDI-TOF spectrum of **162**

5,17-dibromo-11,23-diformyl-25,26,27,28-tetrapropyloxycalix[4]arene (**89**)

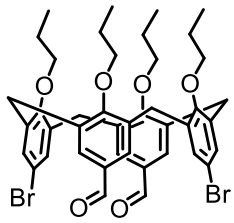

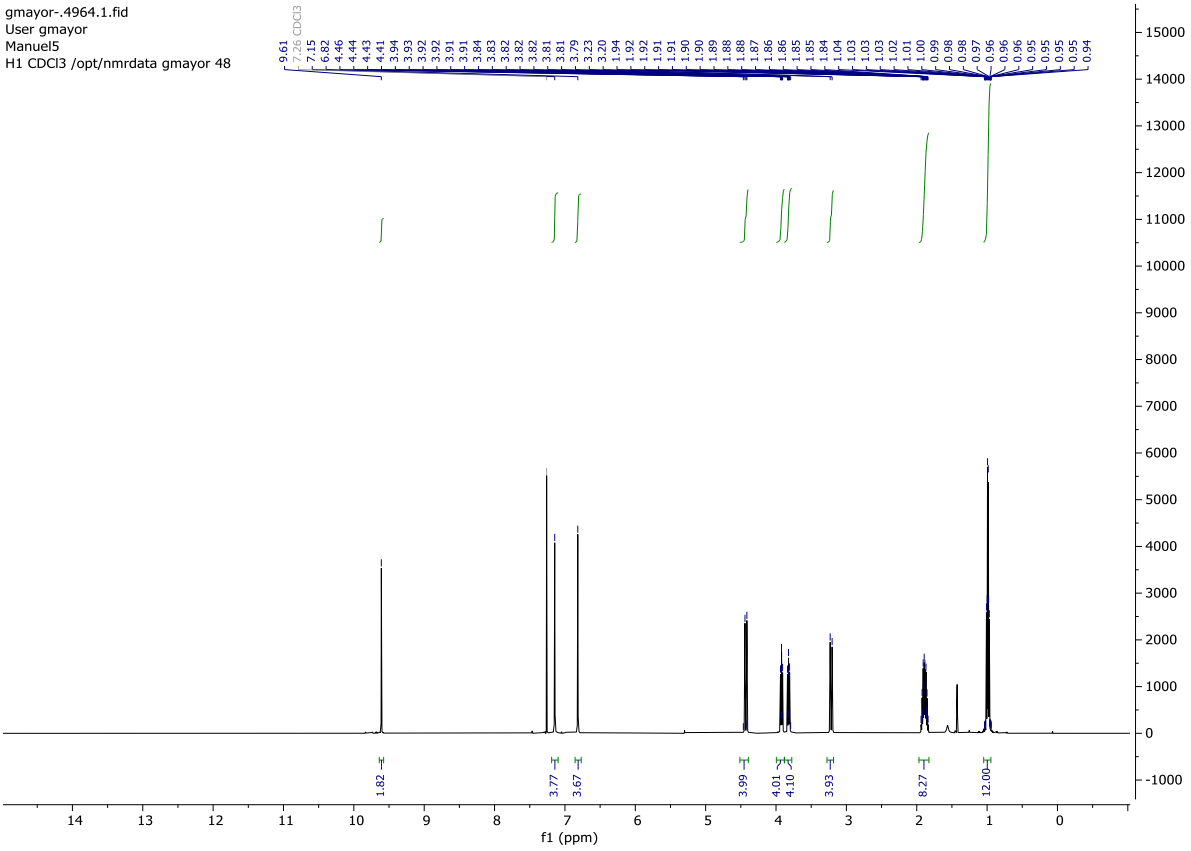

Figure 55. ^{1}H NMR spectrum of **89**

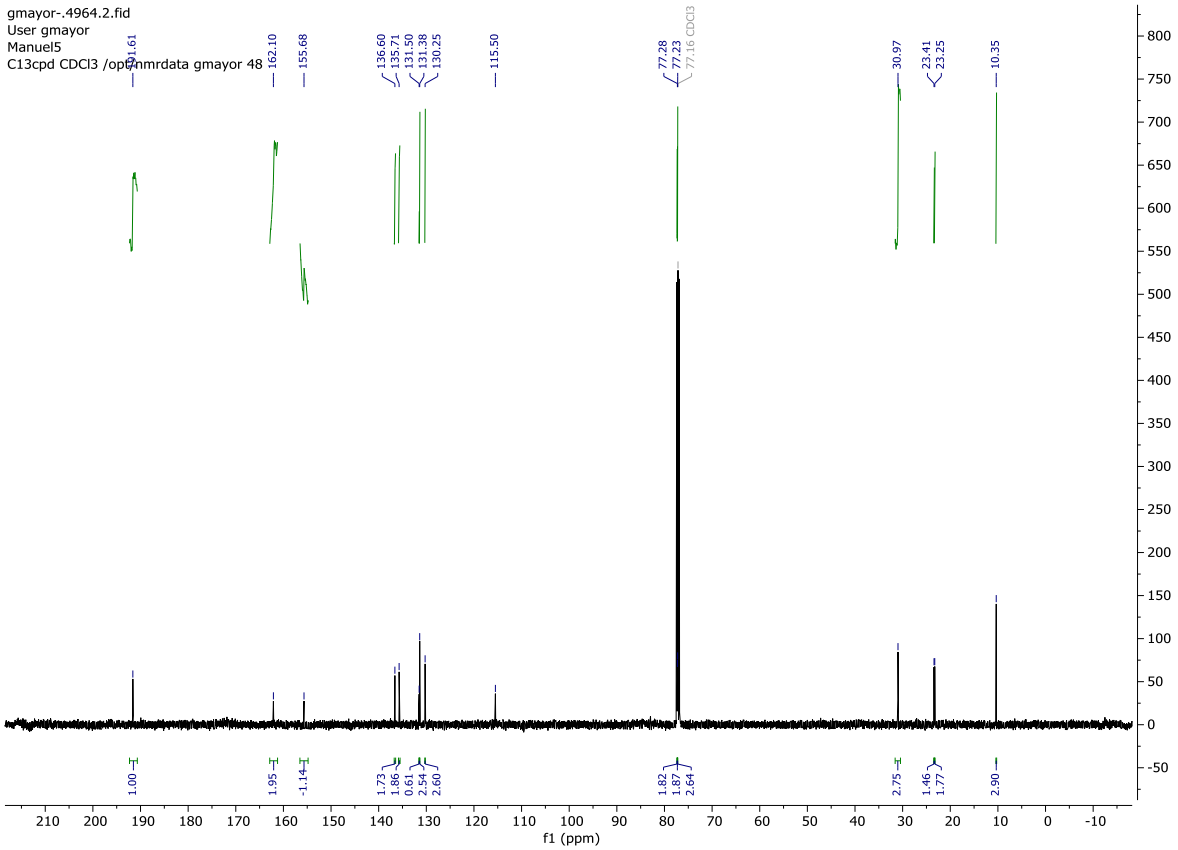

Figure 56. ^{13}C NMR spectrum of **89**

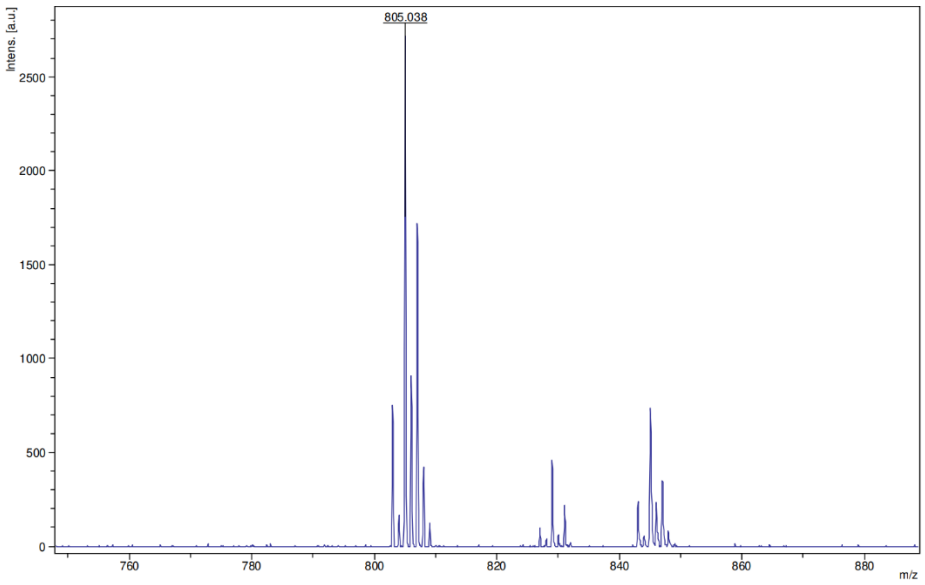

Figure 57. MALDI-TOF spectrum of **89**

5,17-dibromo-25,26,27,28-tetrapropyloxycalix[4]arene (**115**)

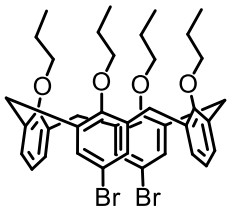

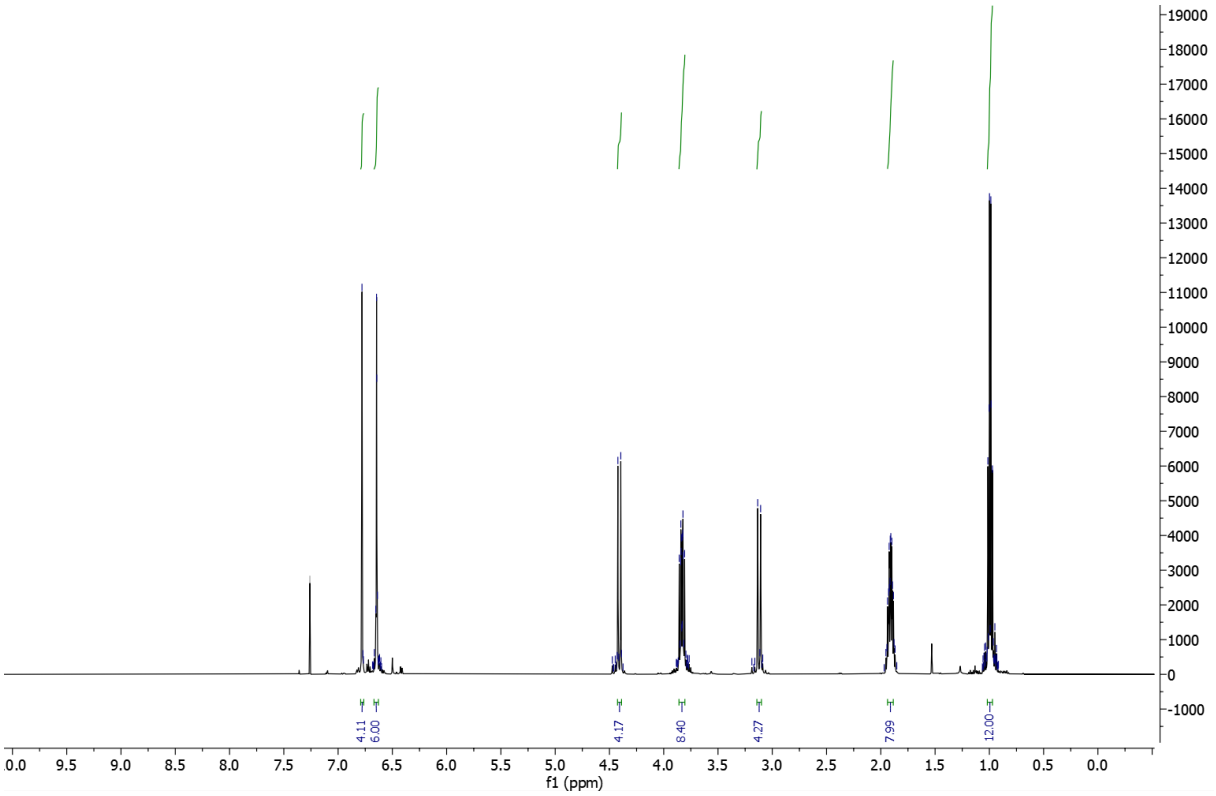

Figure 58. ^{1}H NMR spectrum of **115**

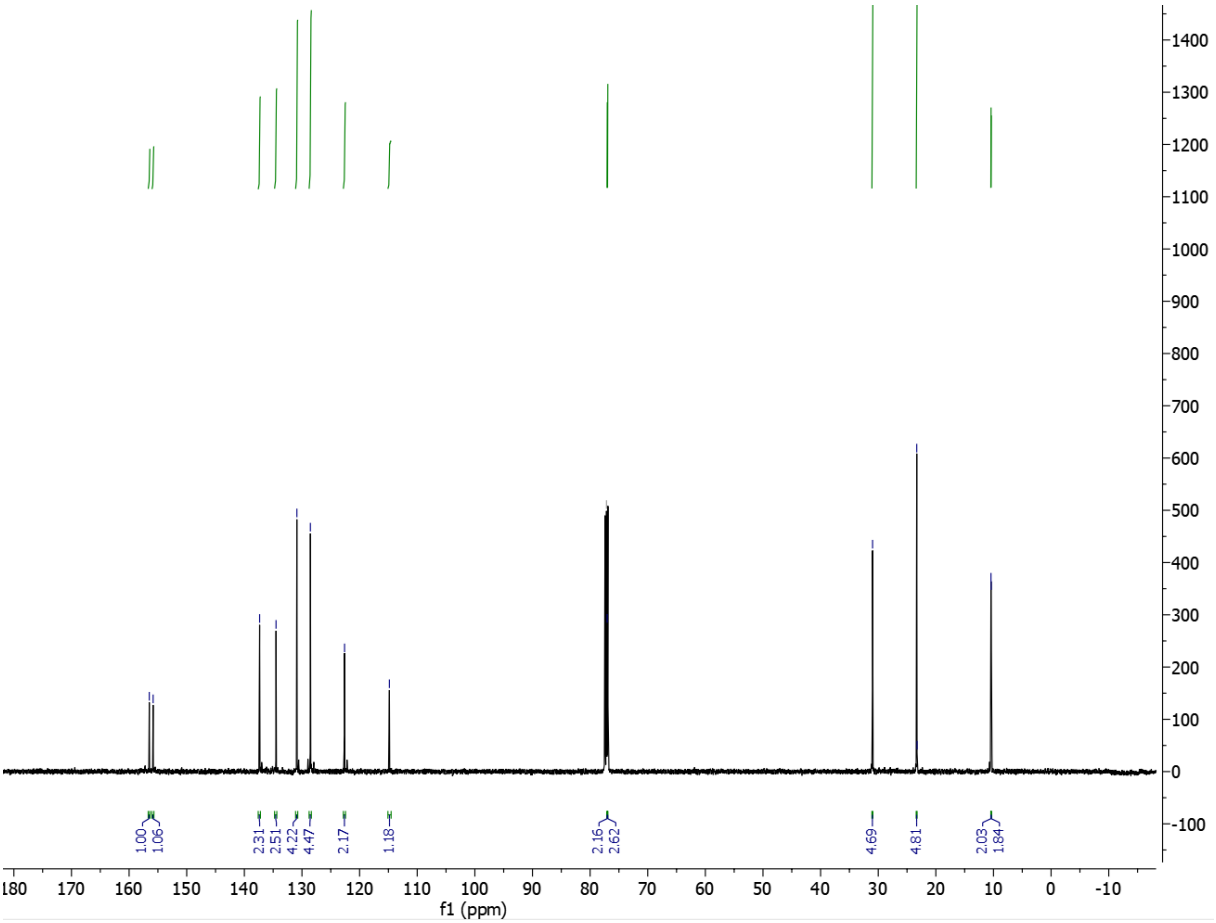

Figure 59. ^{13}C NMR spectrum of **115**

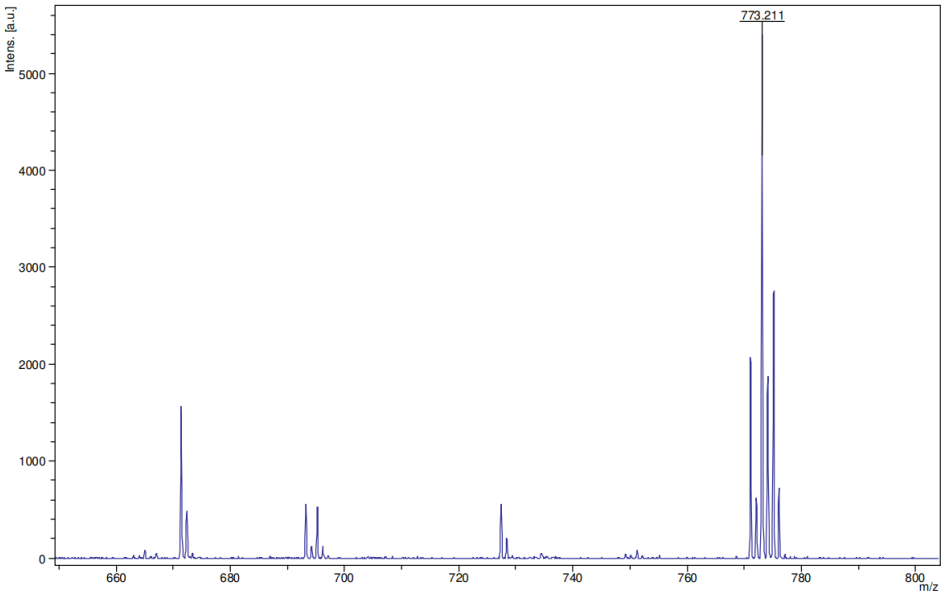

Figure 60. MALDI-TOF spectrum of **115**

5,17-diformyl-25,26,27,28-tetrapropyloxycalix[4]arene (**90**)

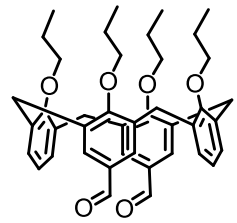

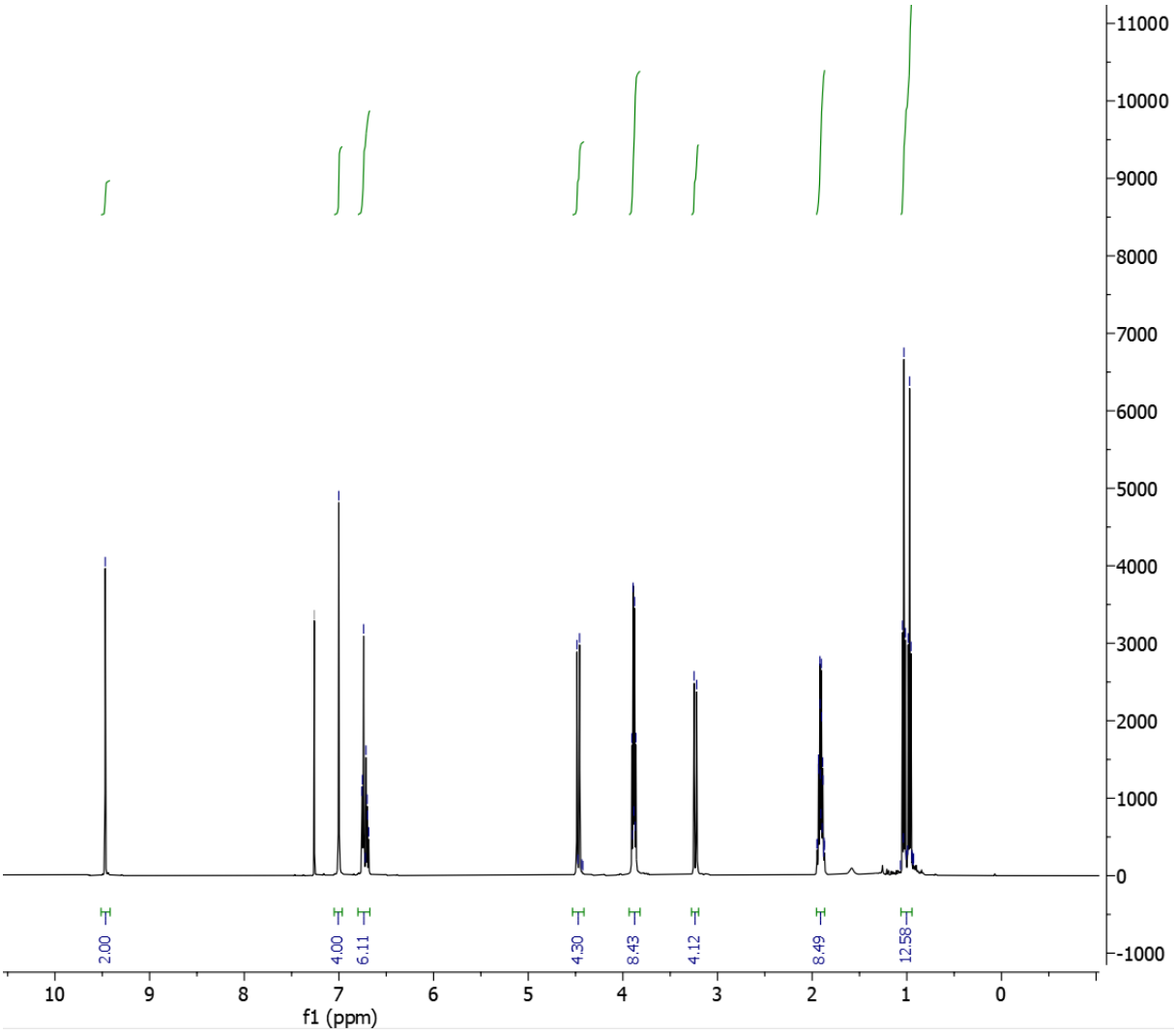

Figure 61. ^{1}H NMR spectrum of **90**

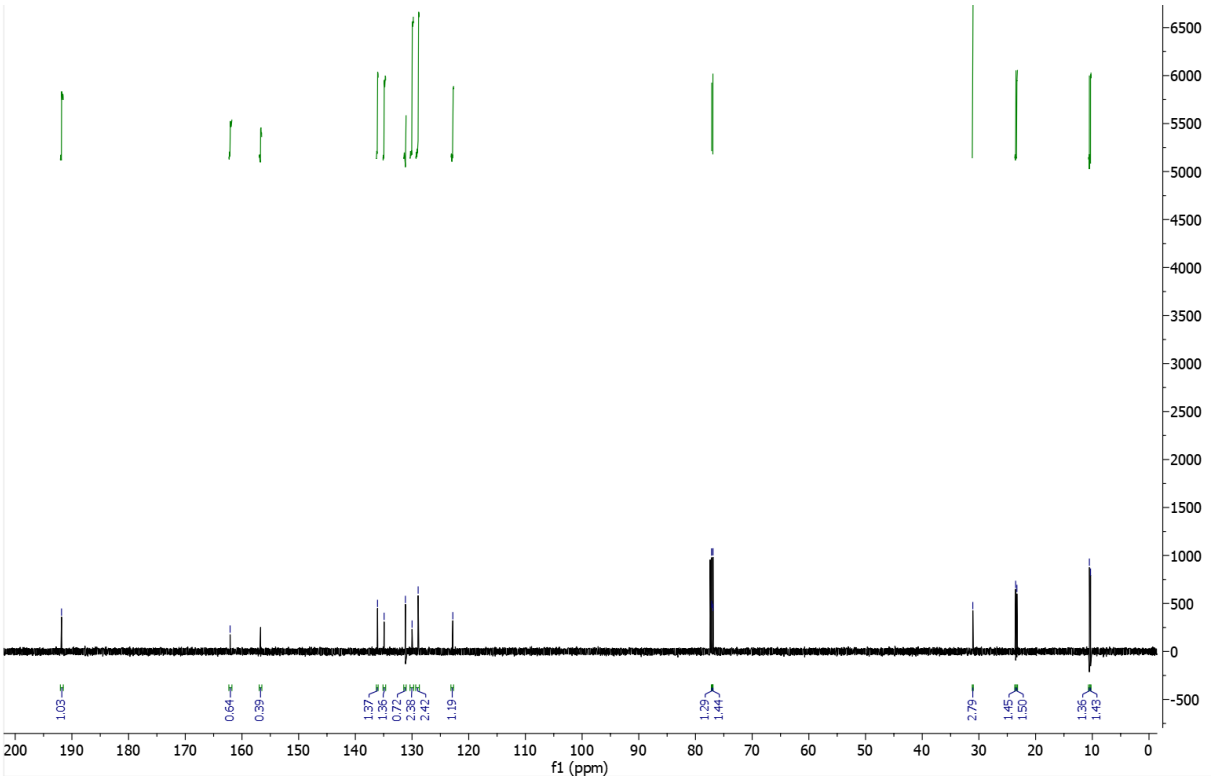

Figure 62. ^{13}C NMR spectrum of **90**

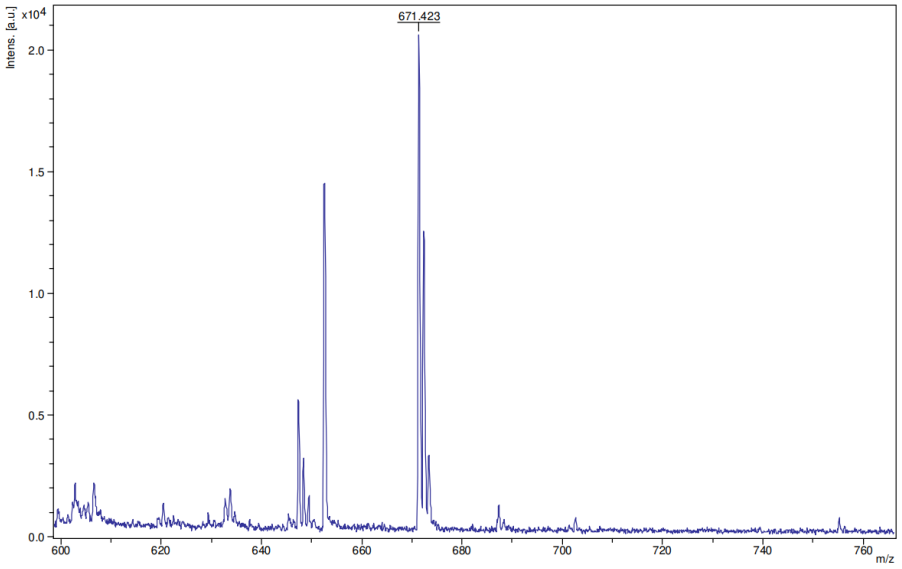

Figure 63. MALDI-TOF spectrum of **90**

5,11,17,23-tetraformyl-25,26,27,28-tetrapropyloxycalix[4]arene (**159**)

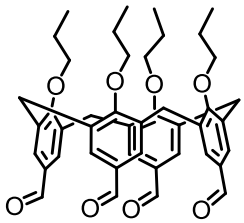

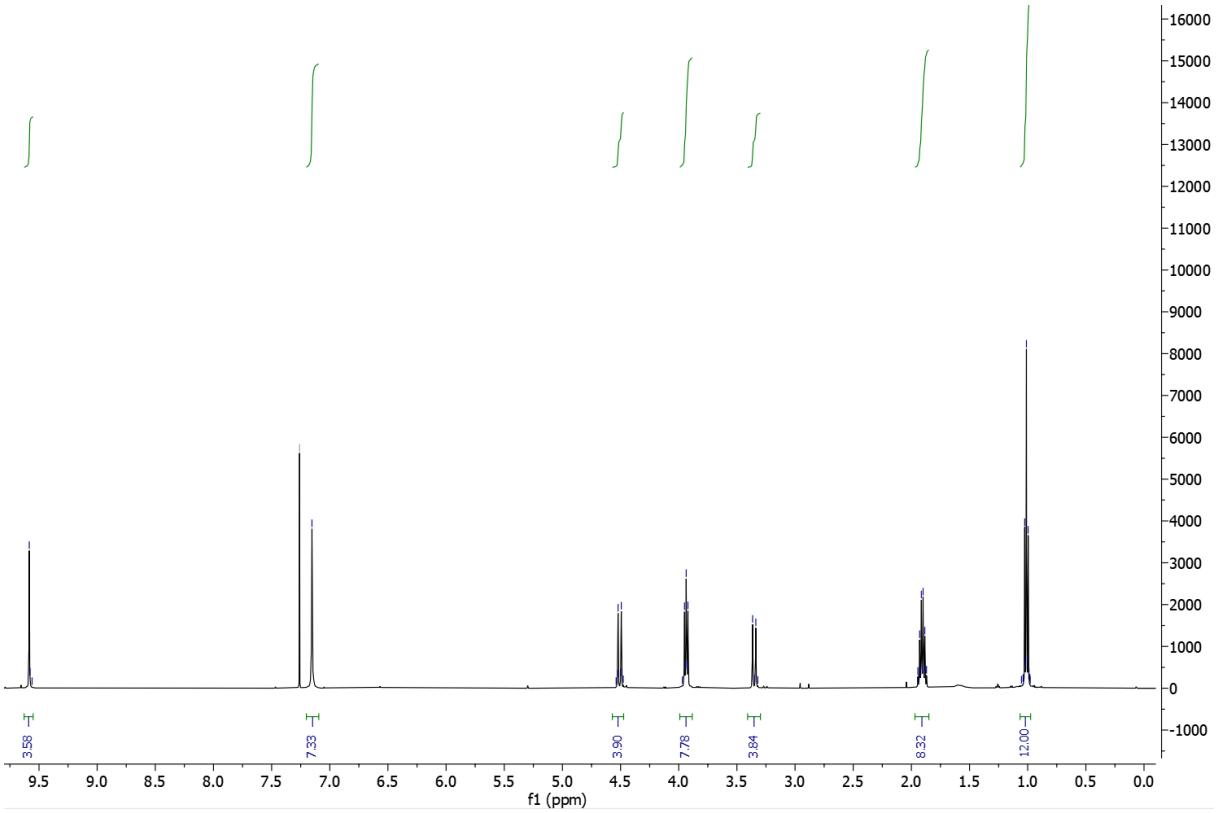

Figure 64. ^{1}H NMR spectrum of **159**

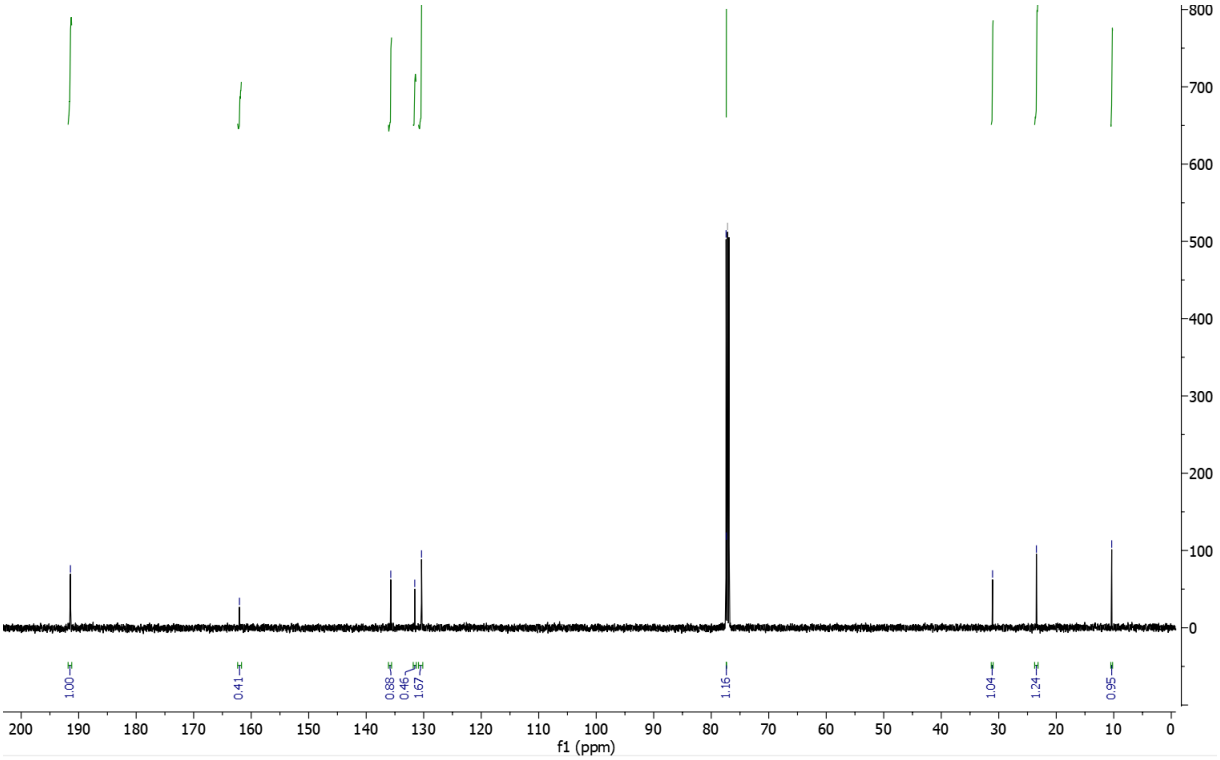

Figure 65. ^{13}C NMR spectrum of **159**

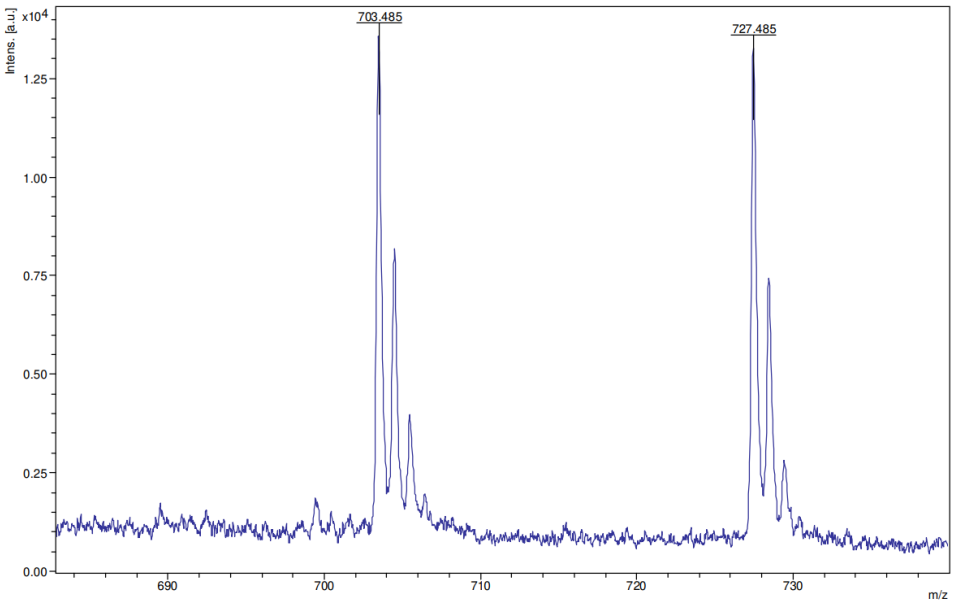

Figure 66. MALDI-TOF spectrum of **159**

5,11,17,23-tetraethynyl-25,26,27,28-tetrapropyloxycalix[4]arene (**161**)

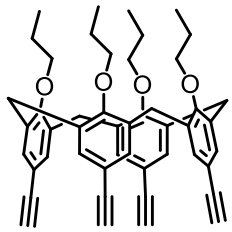

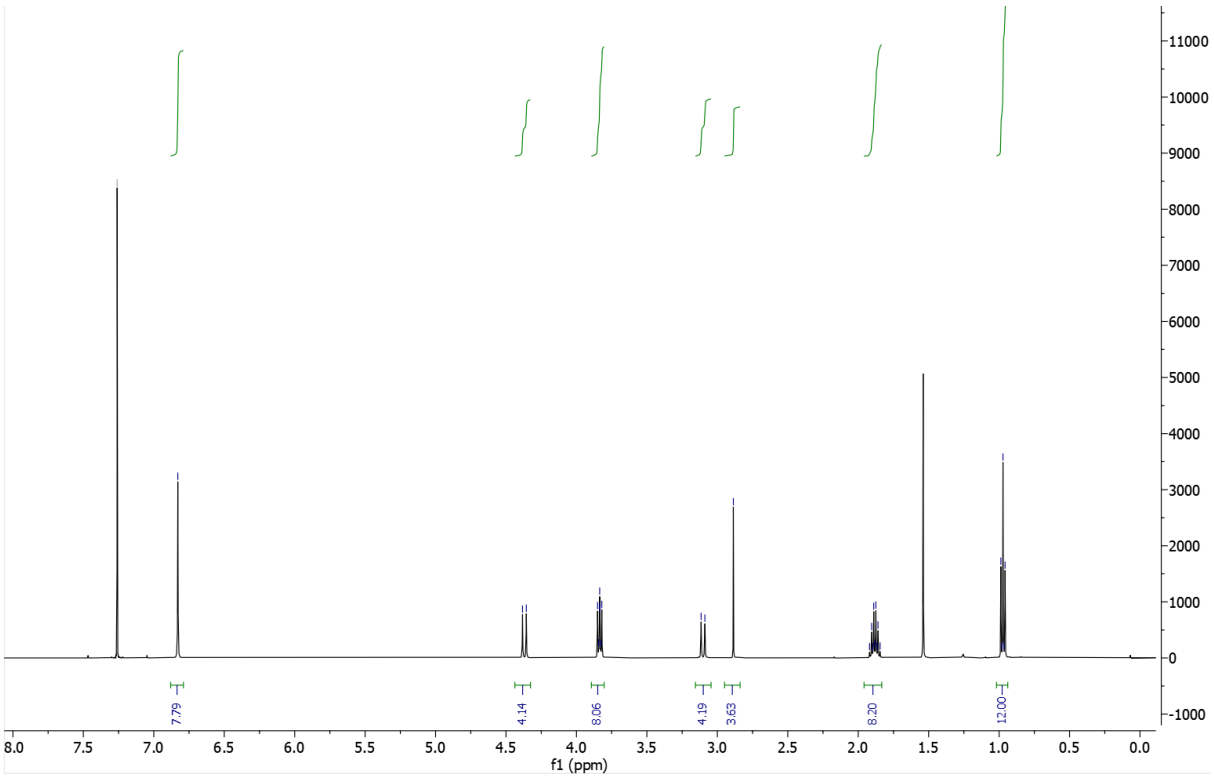

Figure 67. ^{1}H NMR spectrum of **161**

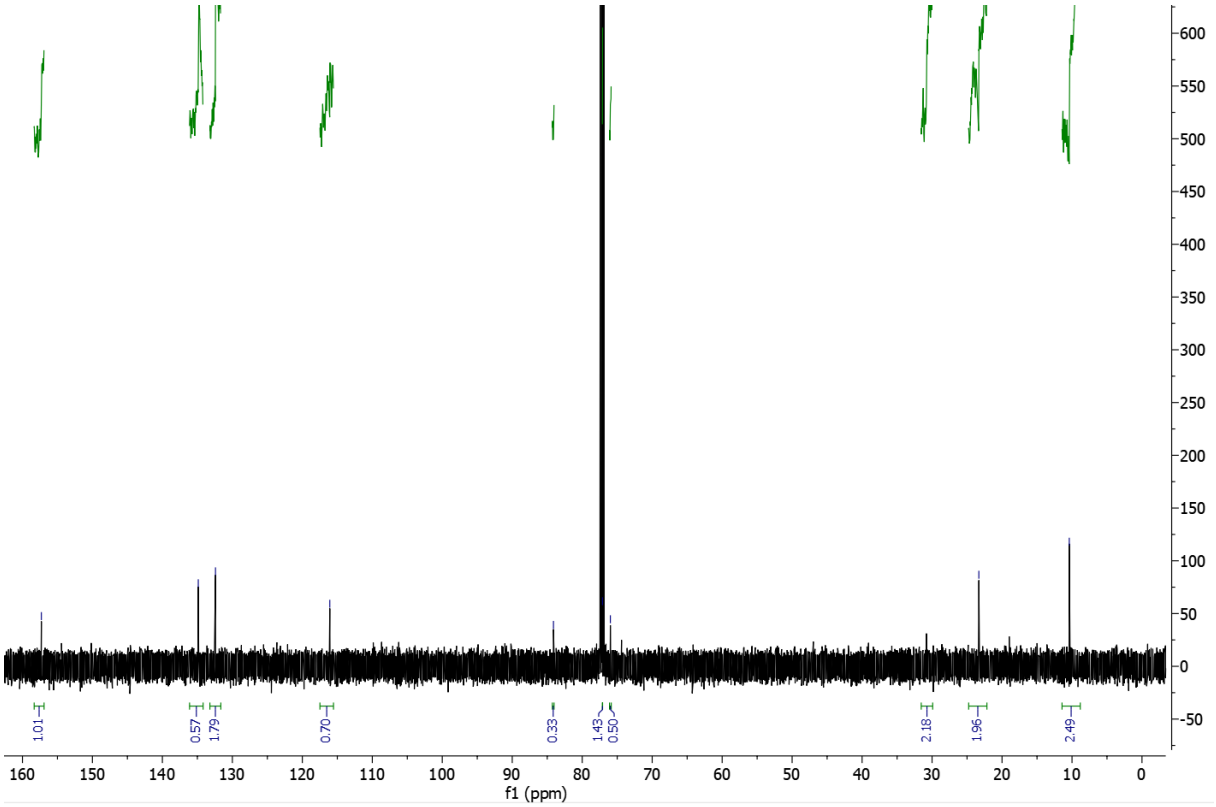

Figure 68. ^{13}C NMR spectrum of **161**

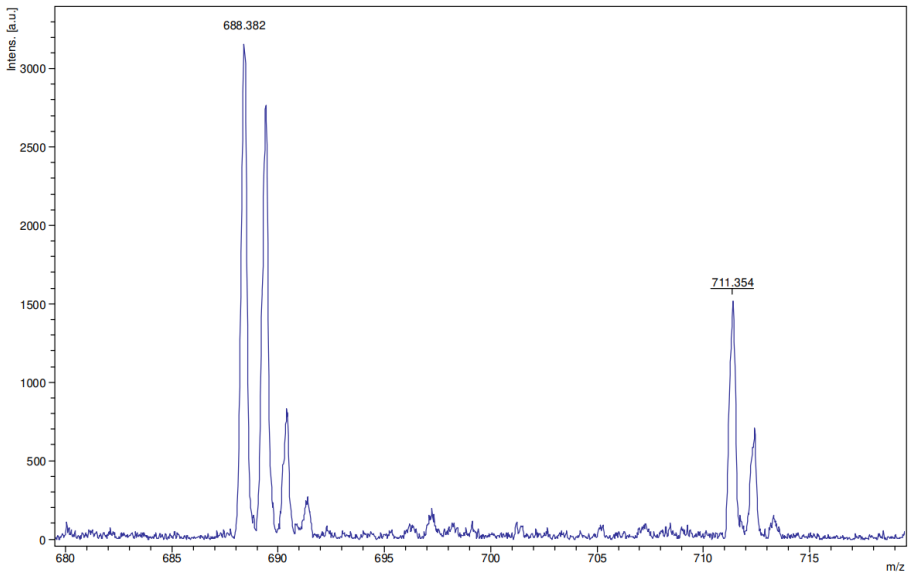

Figure 69. MALDI-TOF spectrum of **161**

(2-iodophenyl)(1H-pyrrol-2-yl)methanone (**164**)

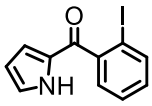

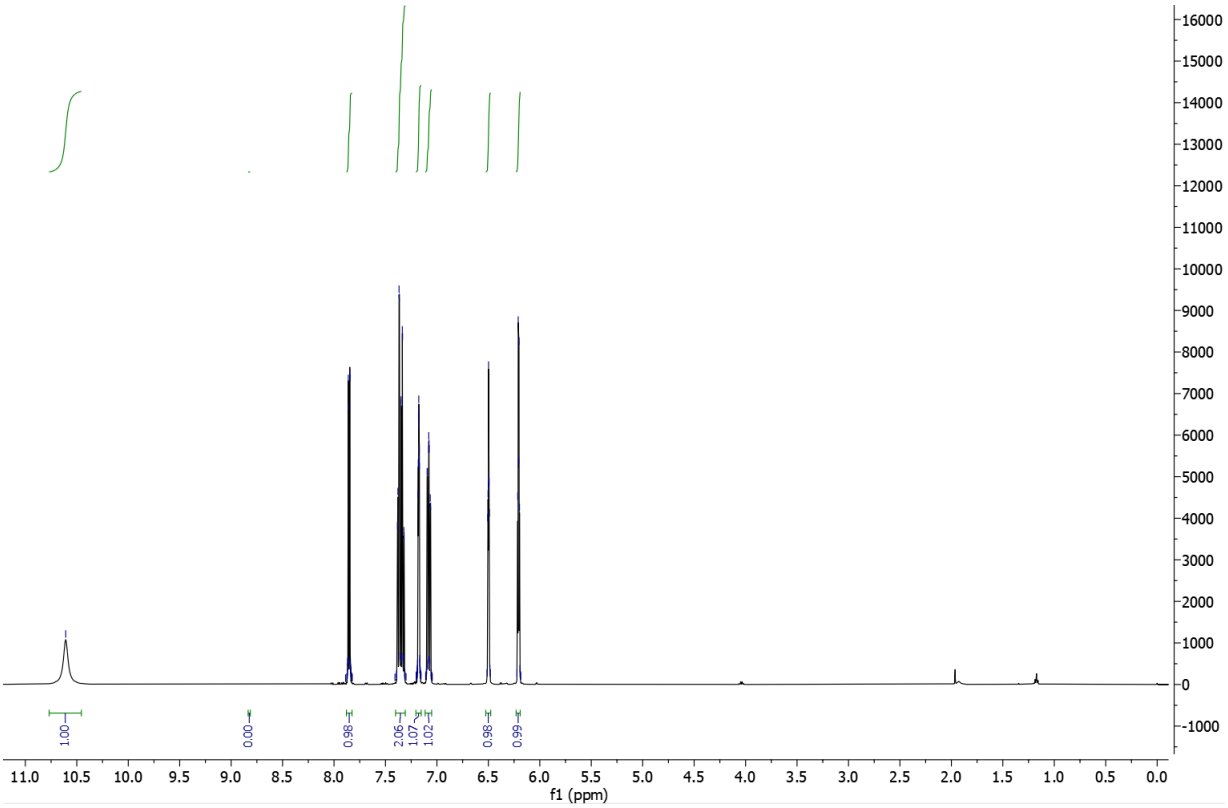

Figure 70. ^{1}H NMR spectrum of **164**

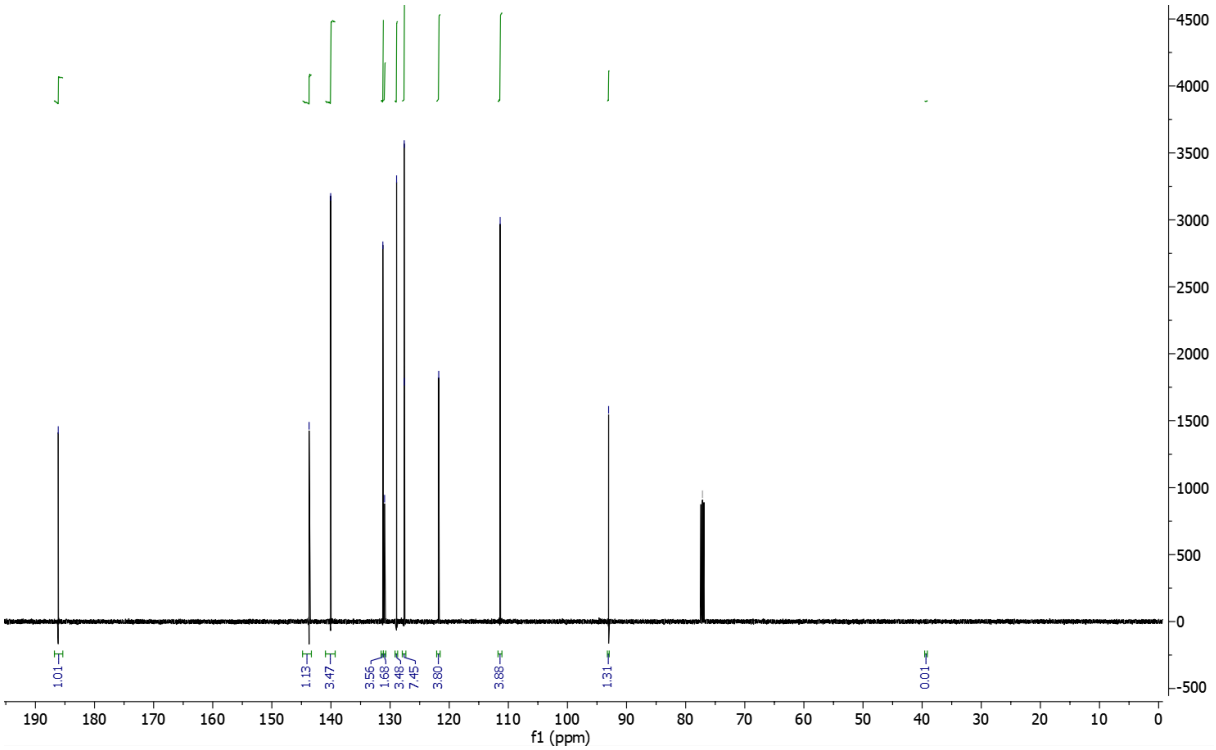

Figure 71. ^{13}C NMR spectrum of **164**

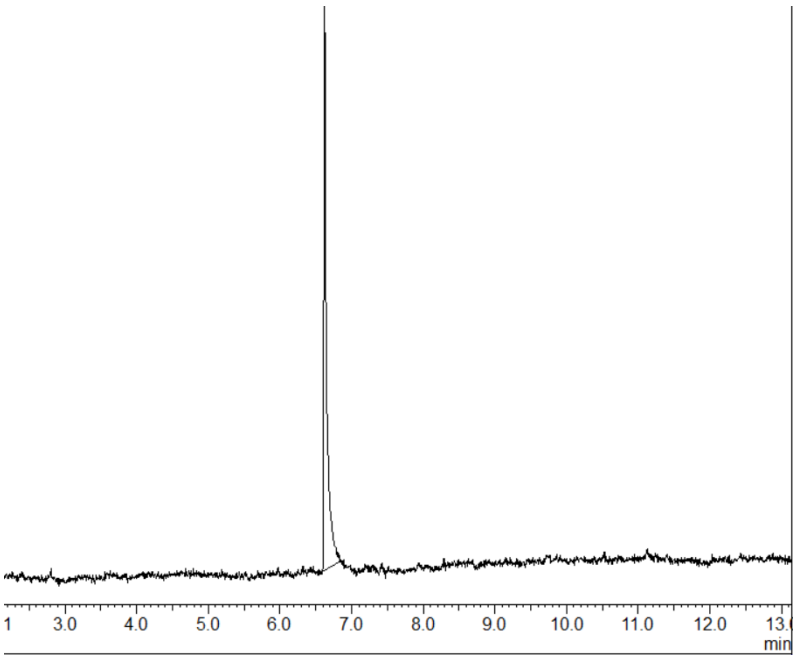

Figure 72. GC chromatogram of **164**

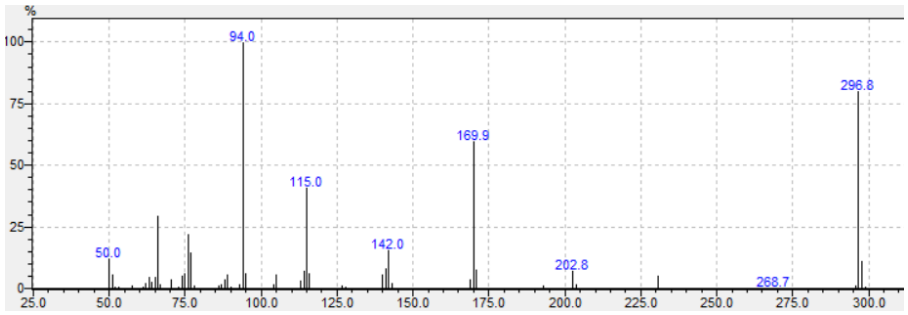

Figure 73. EI spectrum of **164**

Pyrrole precursor for the spherical shaped cage molecule (**110**)

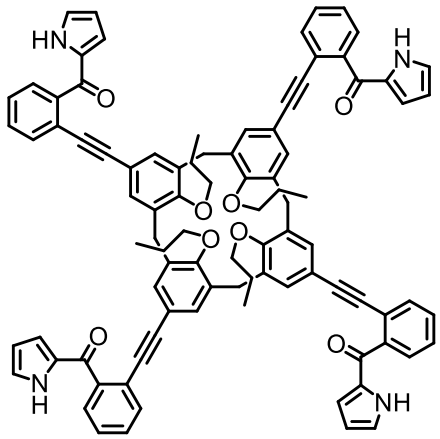

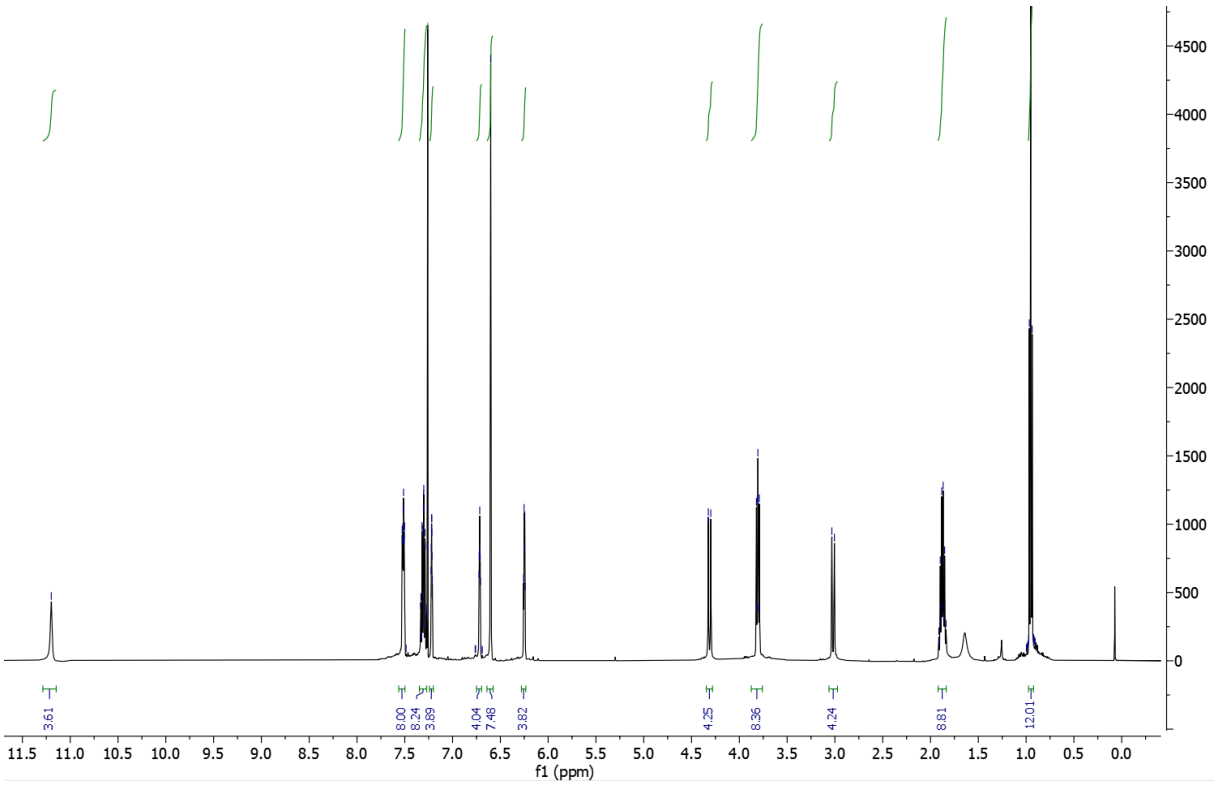

Figure 74. ^{1}H NMR spectrum of **110**

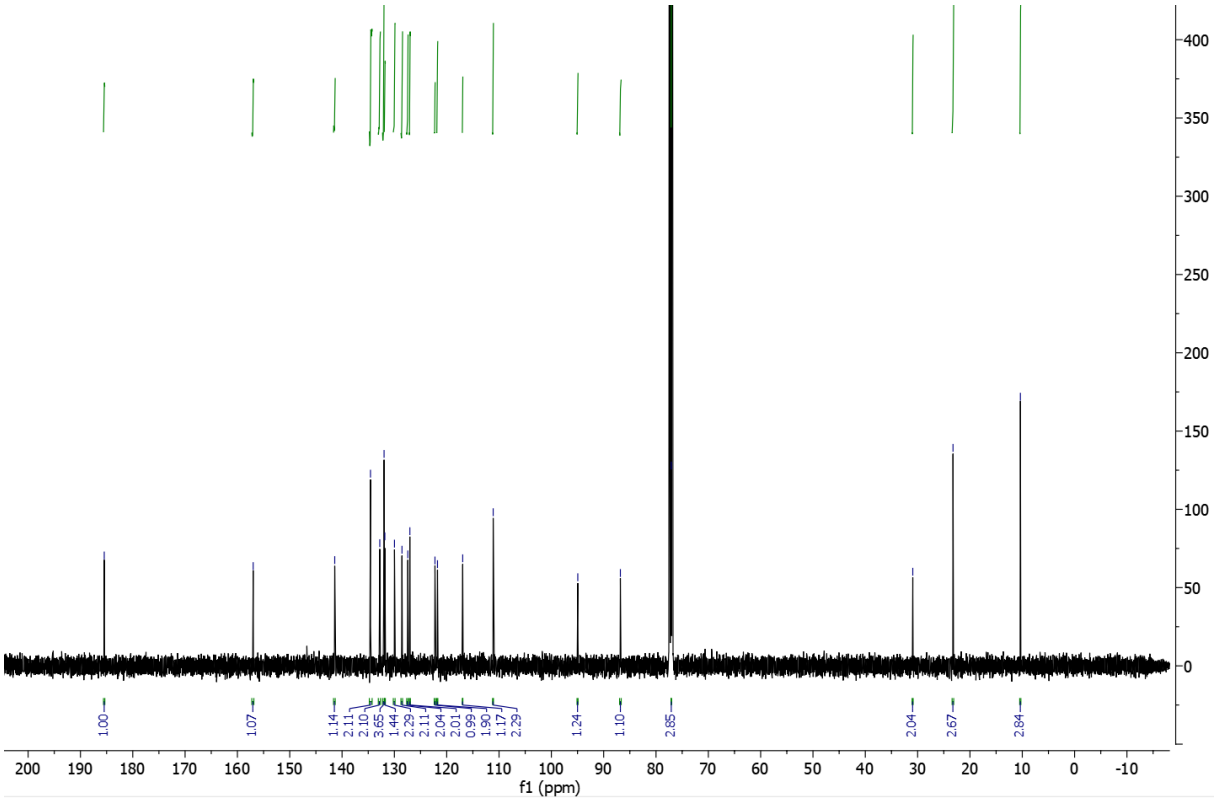

Figure 75. ^{13}C NMR spectrum of **110**

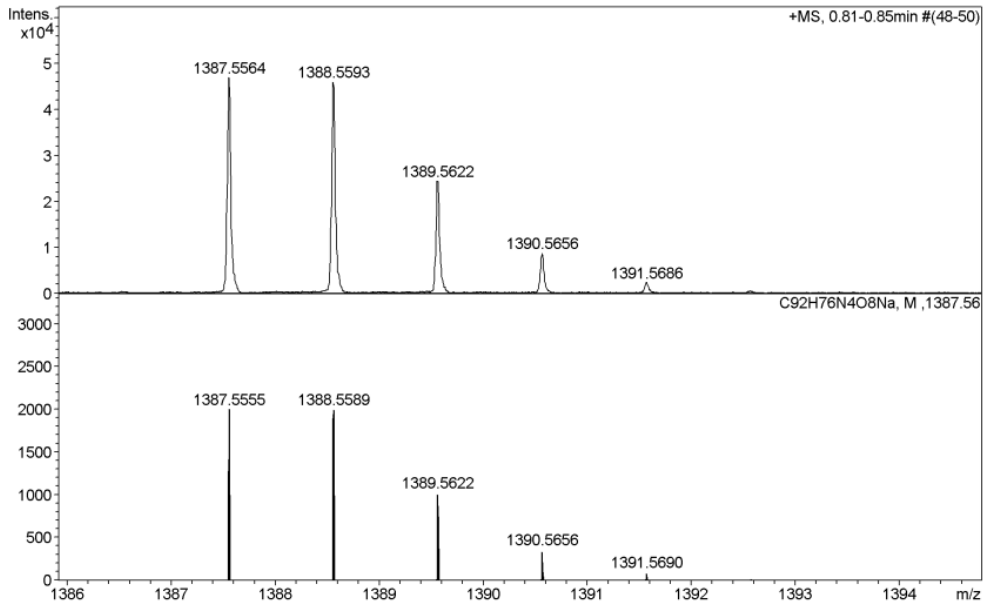

Figure 76. High resolution ESI spectrum of **110**

5,11,17,23-tetrakis(trimethylsilylethynyl)-25,26,27,28-tetrapropyloxycalix[4]arene (**170**)

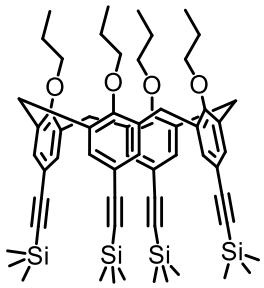

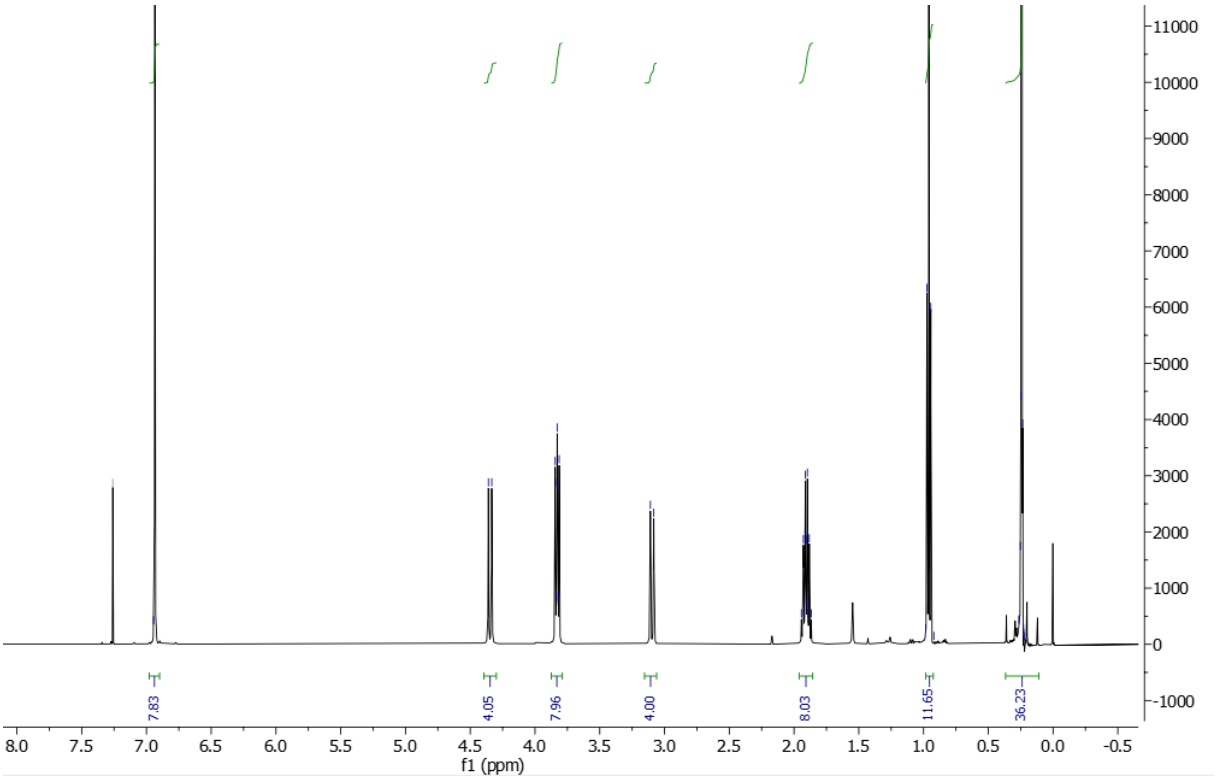

Figure 77. ^{1}H NMR spectrum of **170**

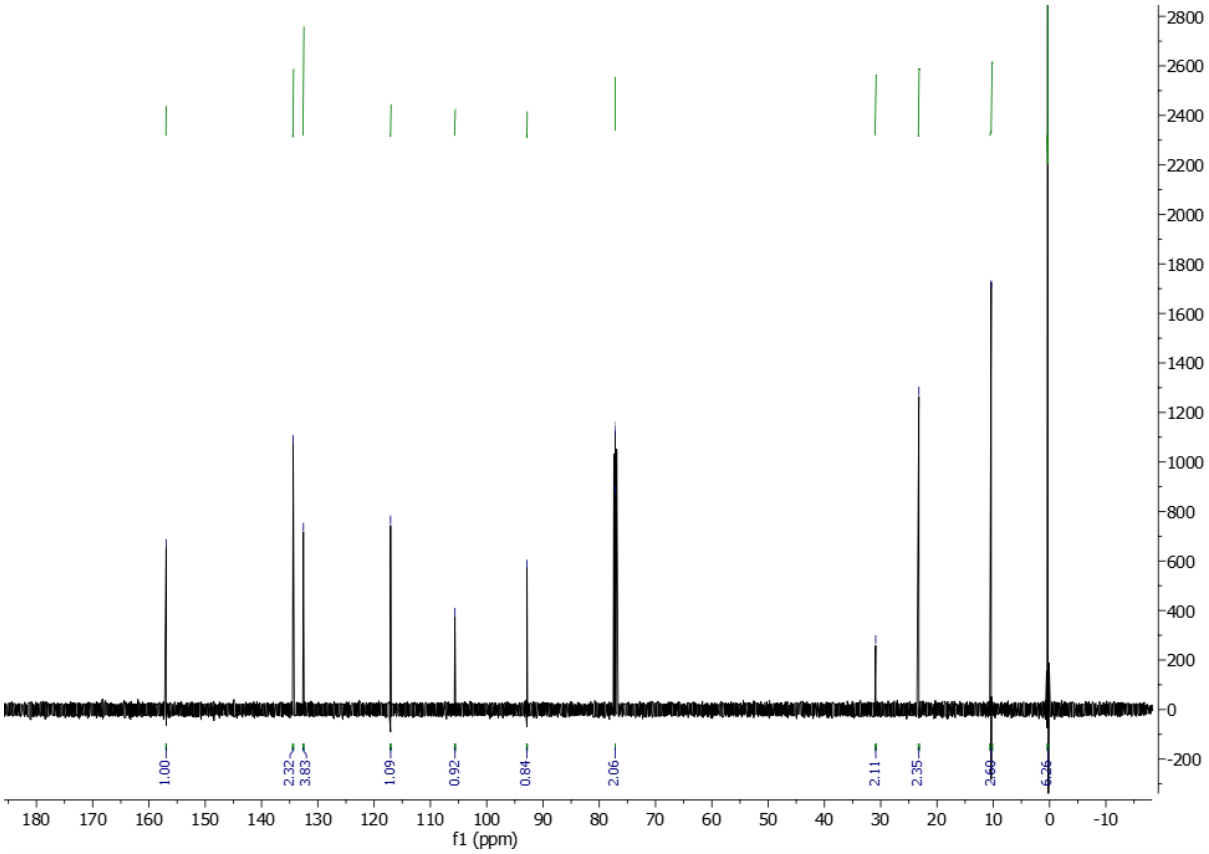

Figure 78. ^{13}C NMR spectrum of **170**

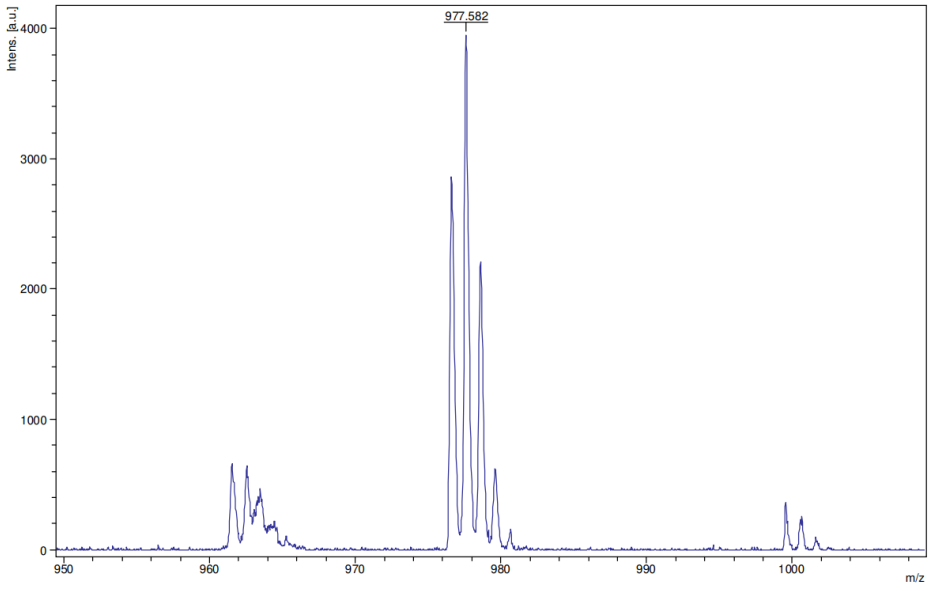

Figure 79. MALDI-TOF spectrum of **170**

5,11,17,23-tetra(2,2-dibromovinyl)-25,26,27,28-tetrapropyloxycalix[4]arene (**160**)

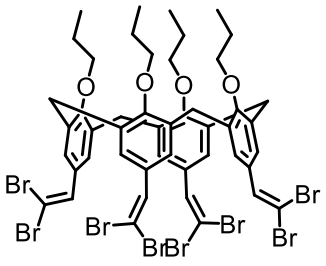

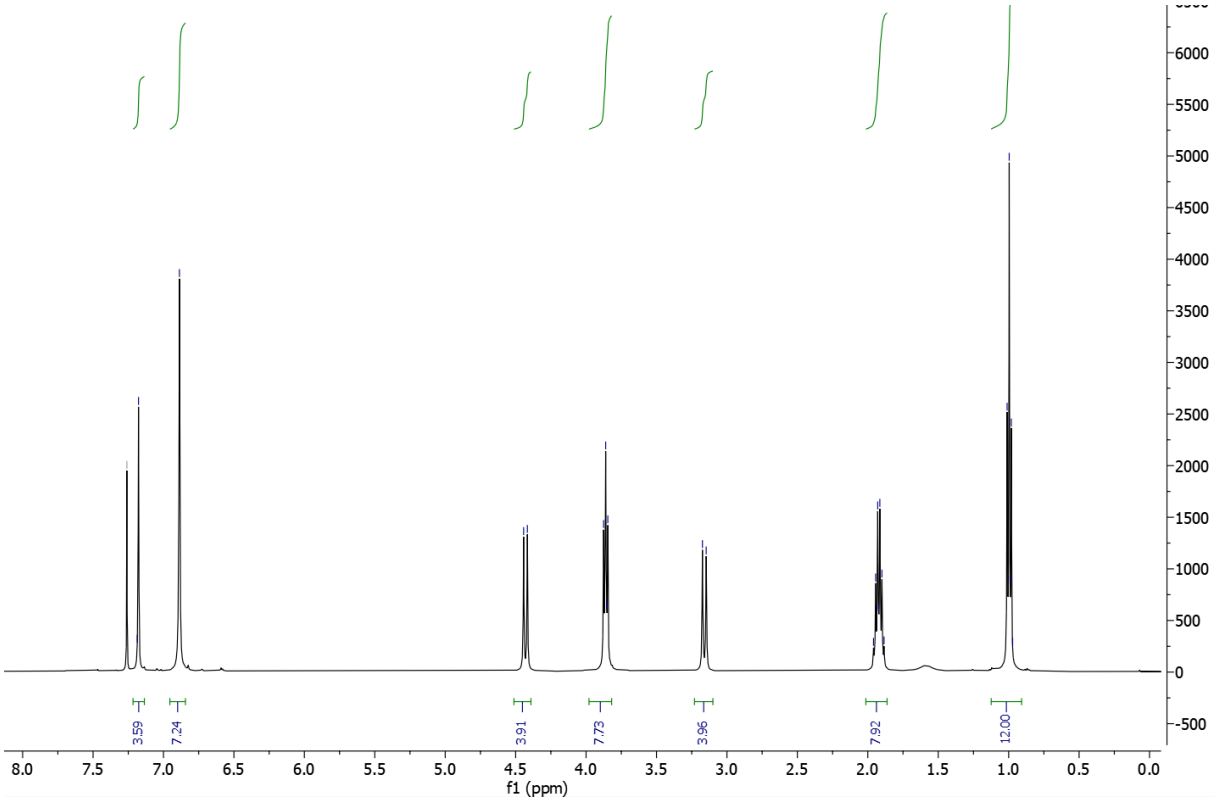

Figure 80. ^{1}H NMR spectrum of **160**

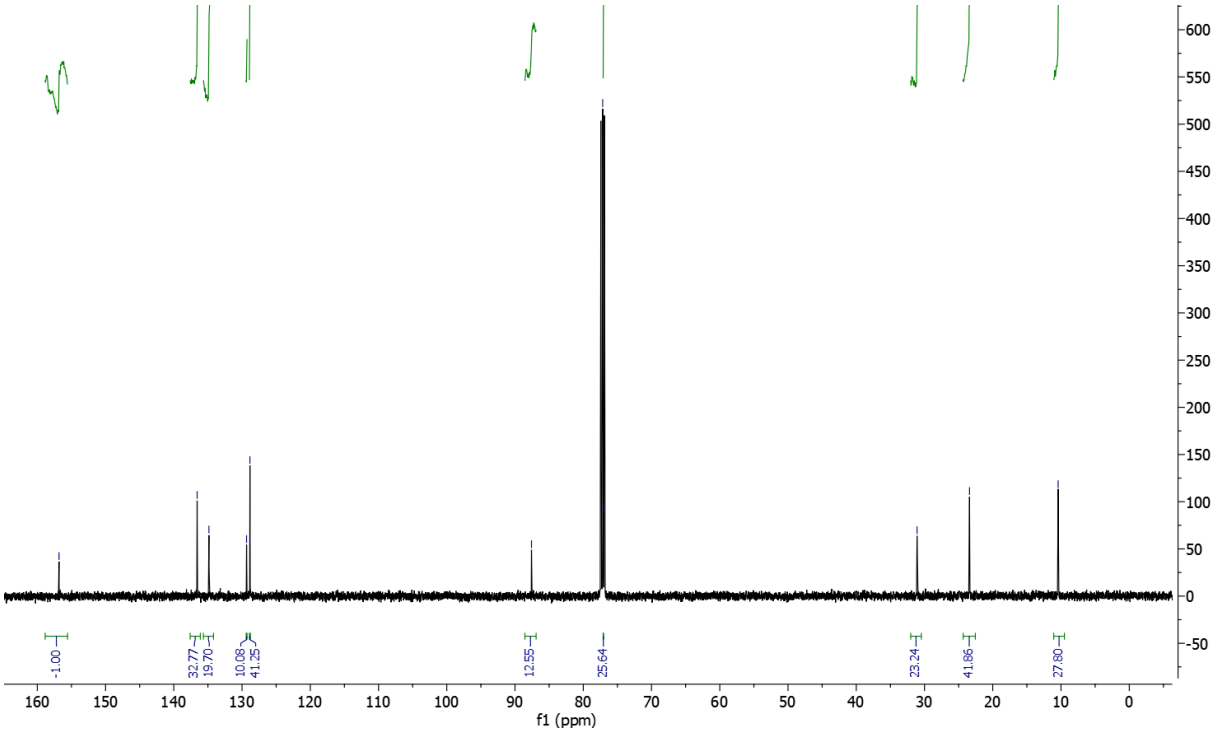

Figure 81. ^{13}C NMR spectrum of **160**

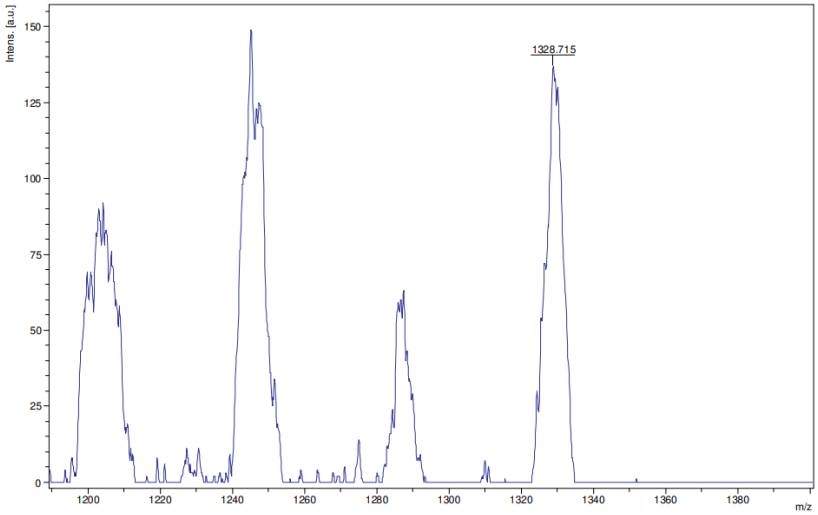

Figure 82. MALDI-TOF spectrum of **160**

ethyl 2-(3,5-dibromophenyl)acetate (**126**)

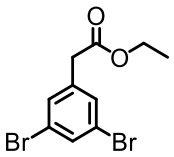

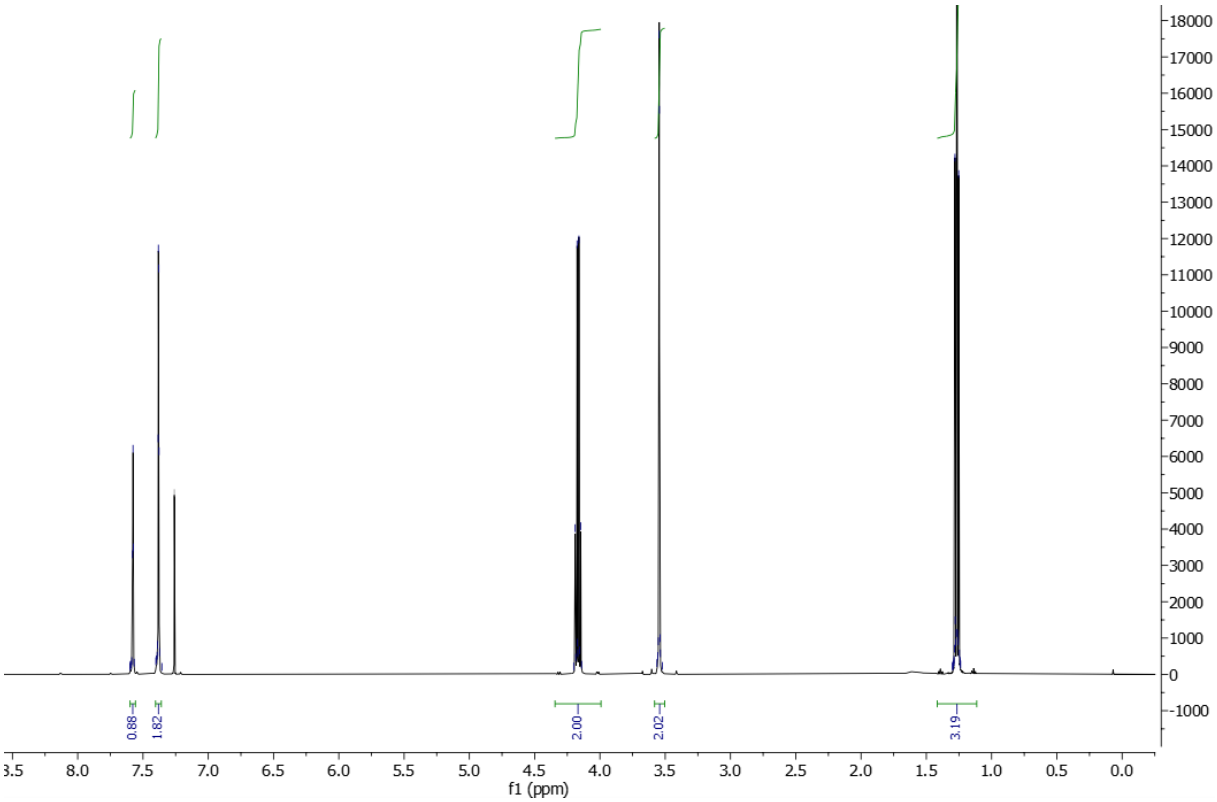

Figure 83. ^{1}H NMR spectrum of **126**

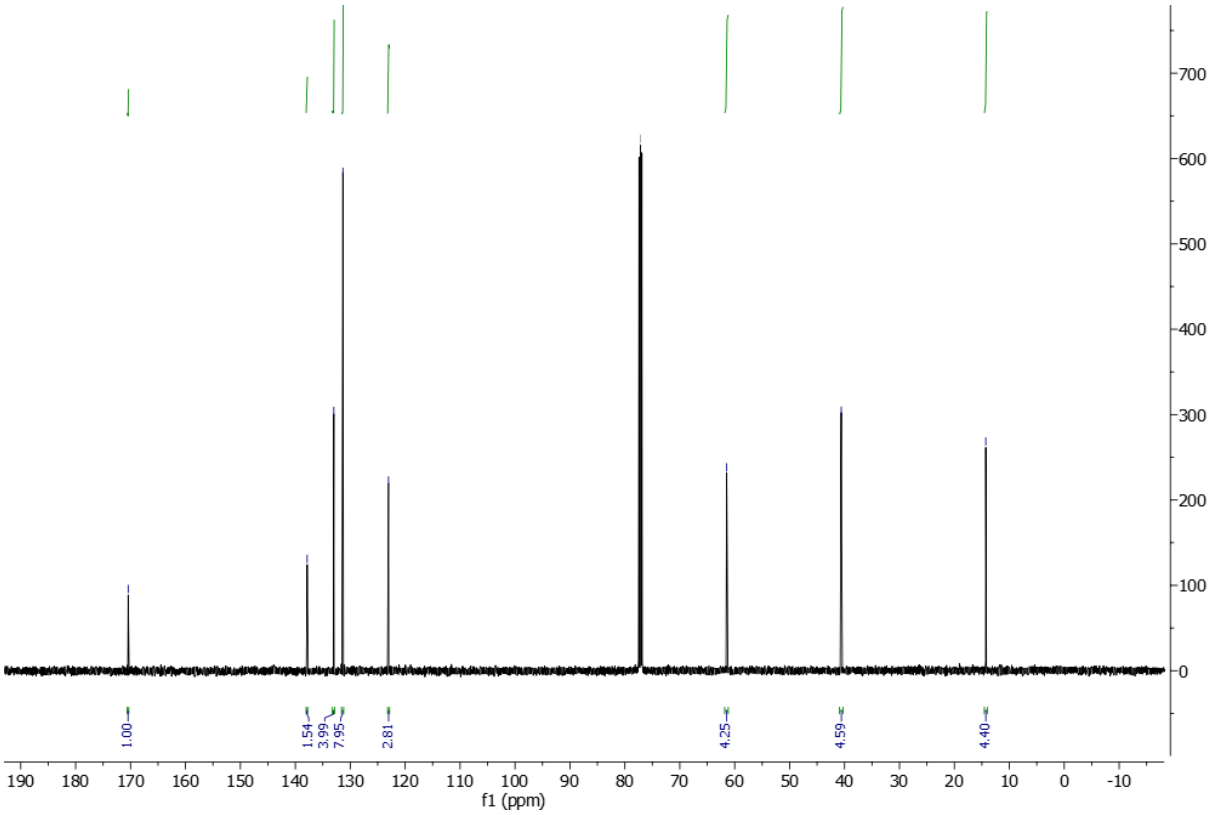

Figure 84. ^{13}C NMR spectrum of **126**

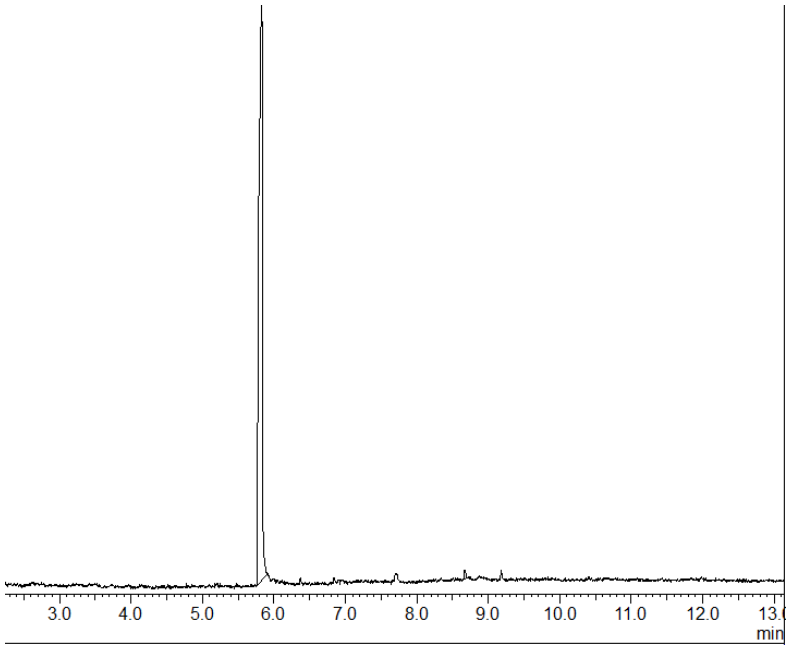

Figure 85. GC chromatogram of **126**

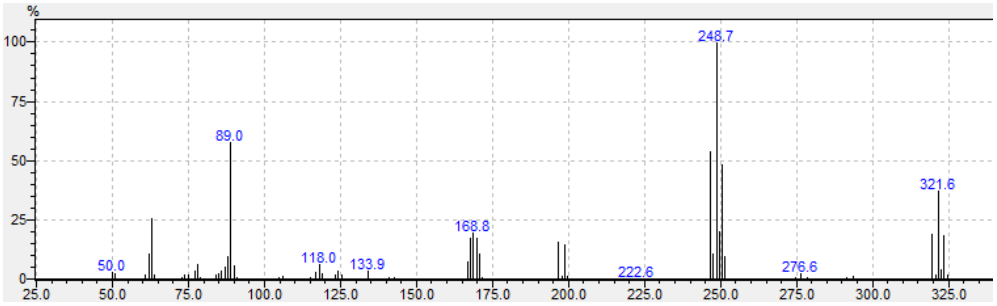

Figure 86. EI spectrum of **126**

2-(3,5-dibromophenyl)ethan-1-ol (**127**)

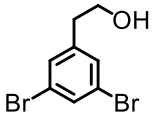

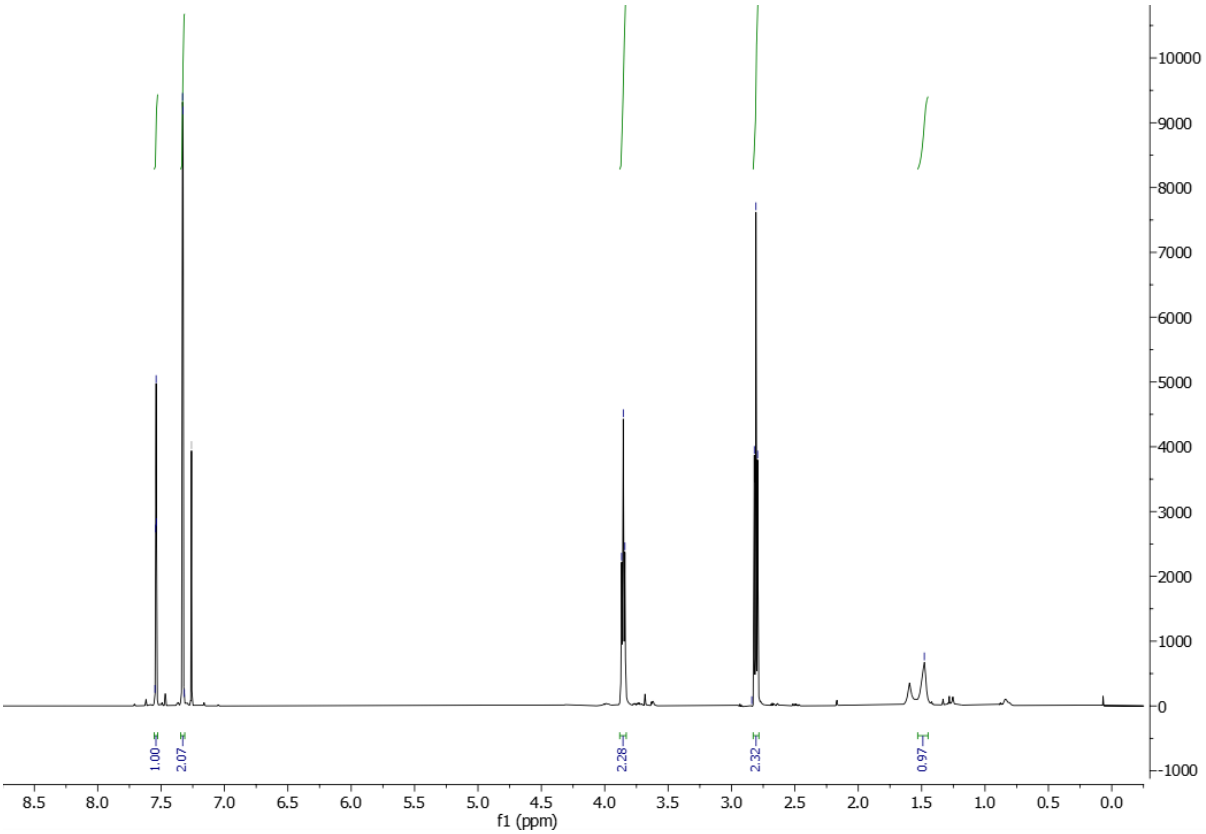

Figure 87. ^{1}H NMR spectrum of **127**

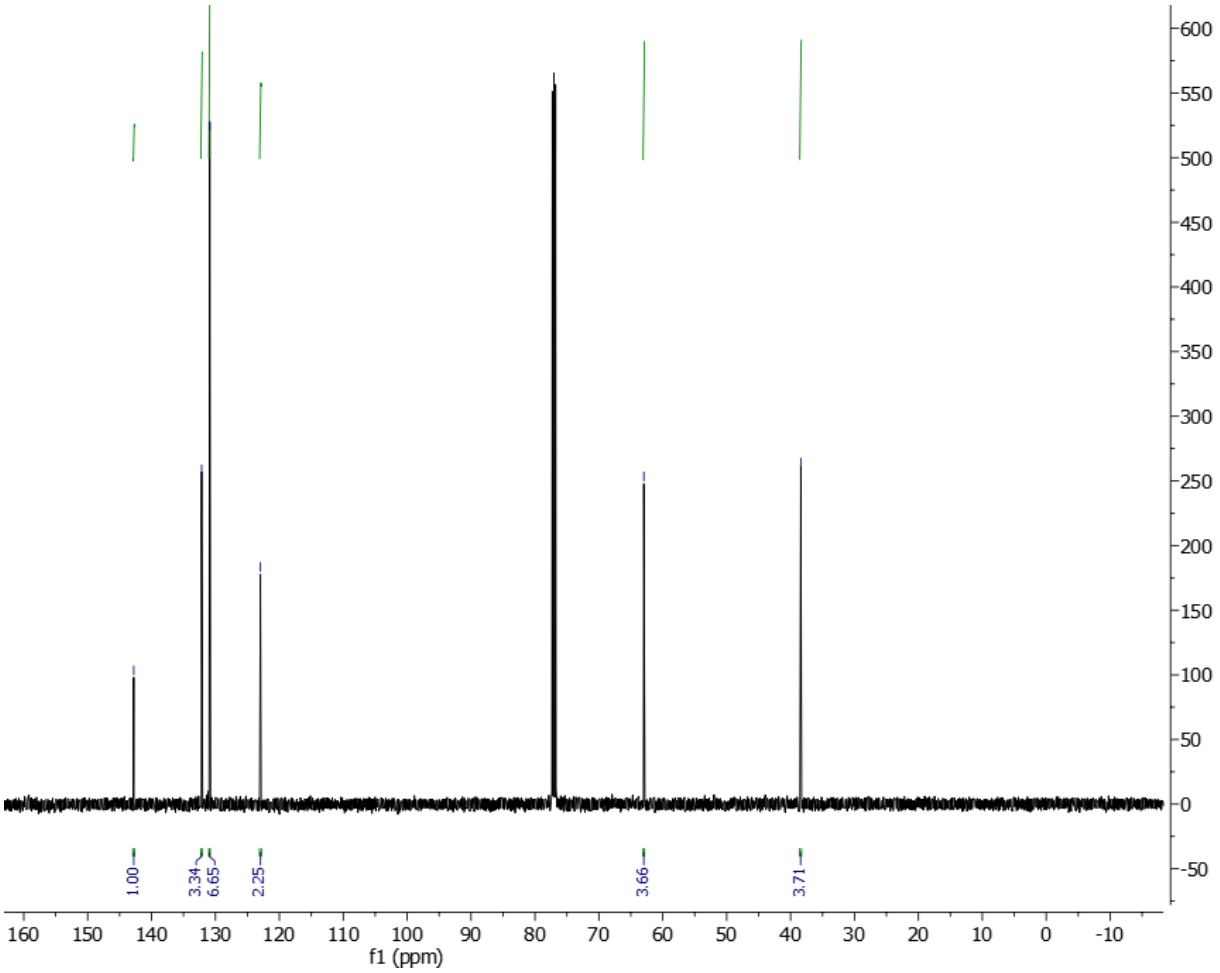

Figure 88. ^{13}C NMR spectrum of **127**

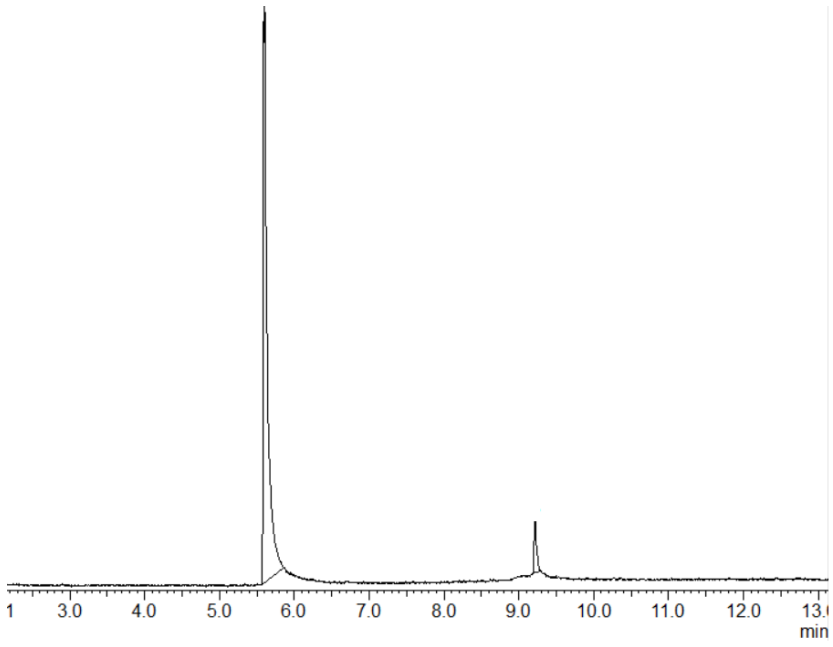

Figure 89. GC chromatogram of **127**

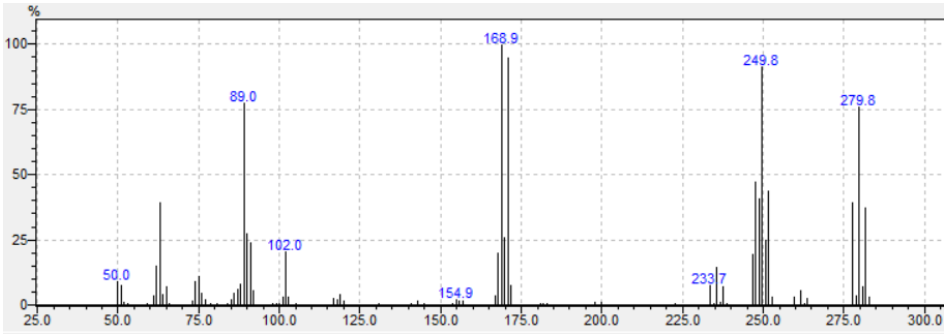

Figure 90. EI spectrum of **127**

2-(3,5-dibromophenyl)acetaldehyde (**128**)

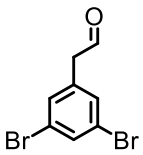

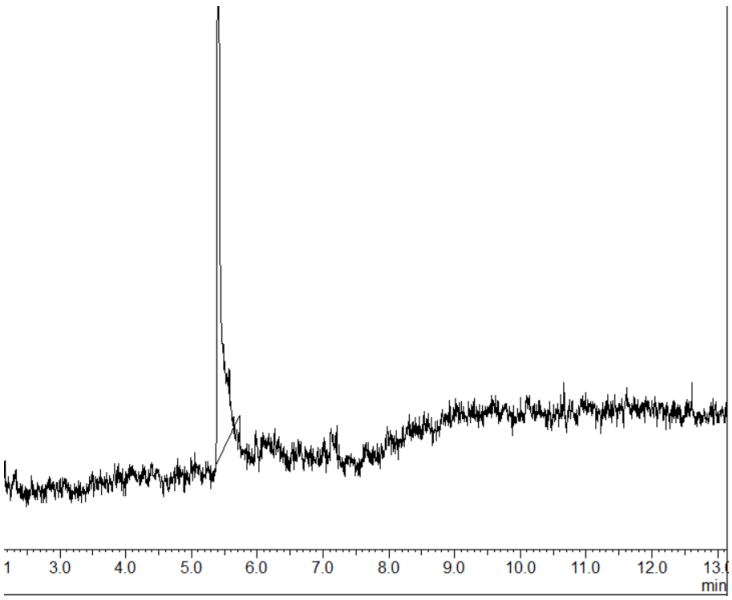

Figure 91. GC chromatogram of **128**

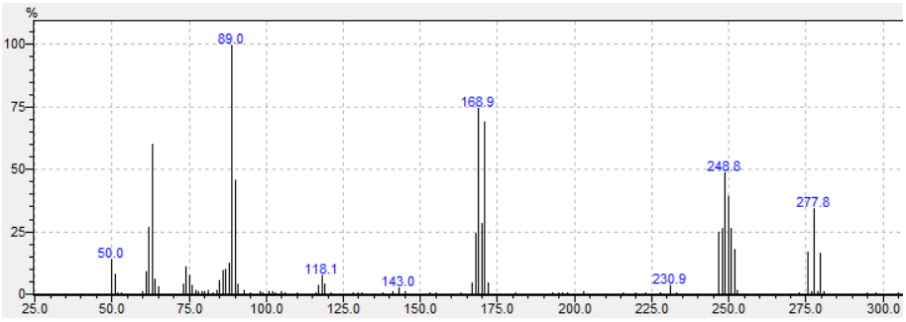

Figure 92. EI spectrum of **128**

1,3-dibromo-5-(prop-2-yn-1-yl)benzene (**129**)

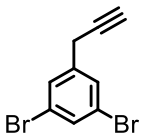

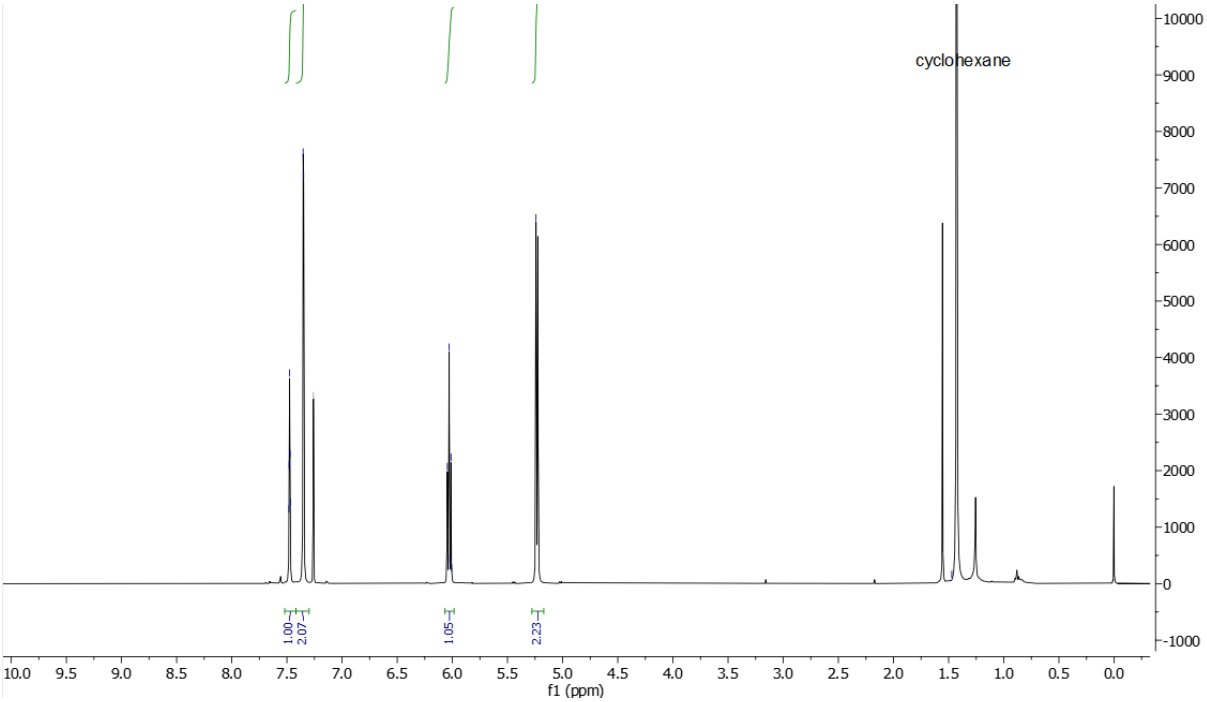

Figure 93. ^{1}H NMR spectrum of **129**

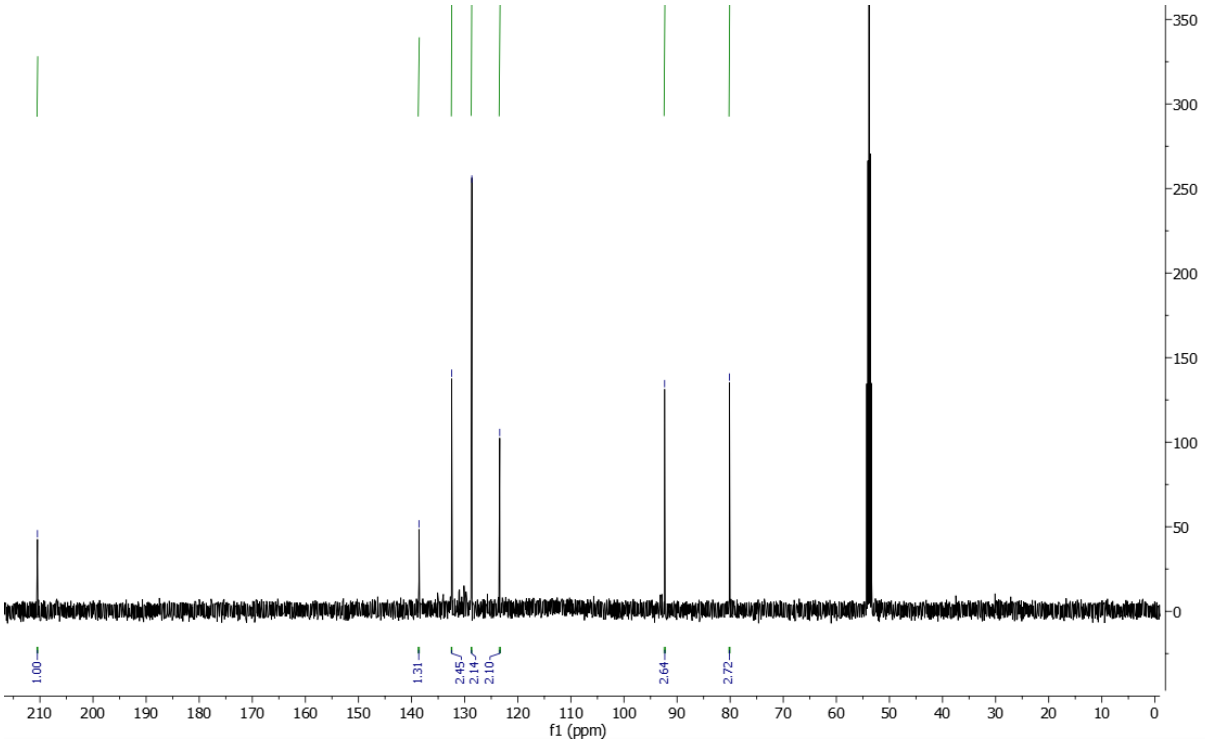

Figure 94. ^{13}C NMR spectrum of **129**

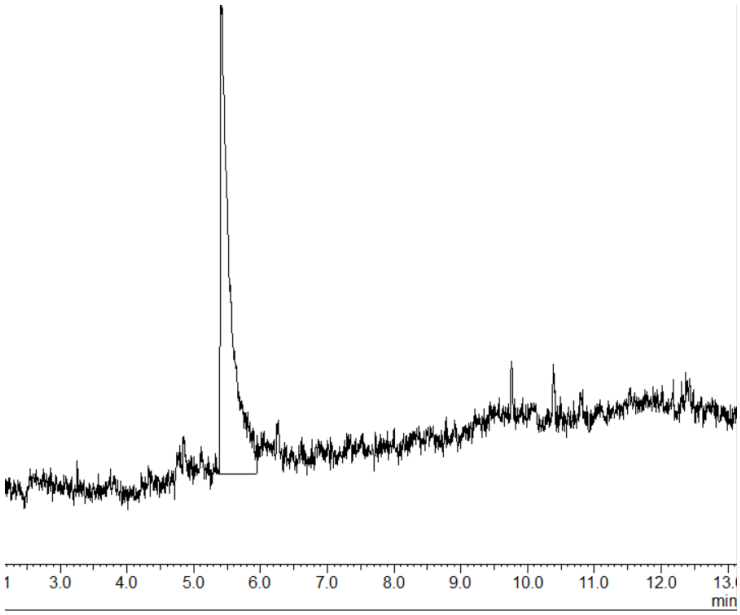

Figure 95. GC chromatogram of **129**

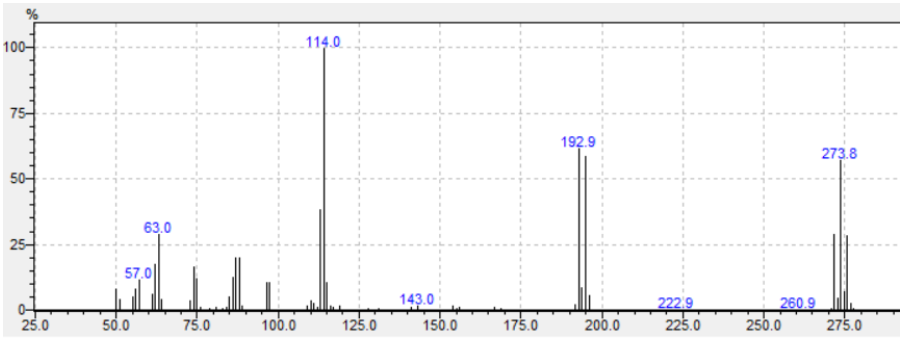

Figure 96. EI spectrum of **129**

(3-(3,5-bis(bromomethyl)phenyl)prop-1-yn-1-yl)triisopropylsilane (**132**)

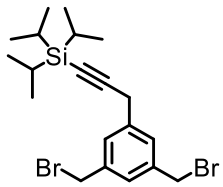

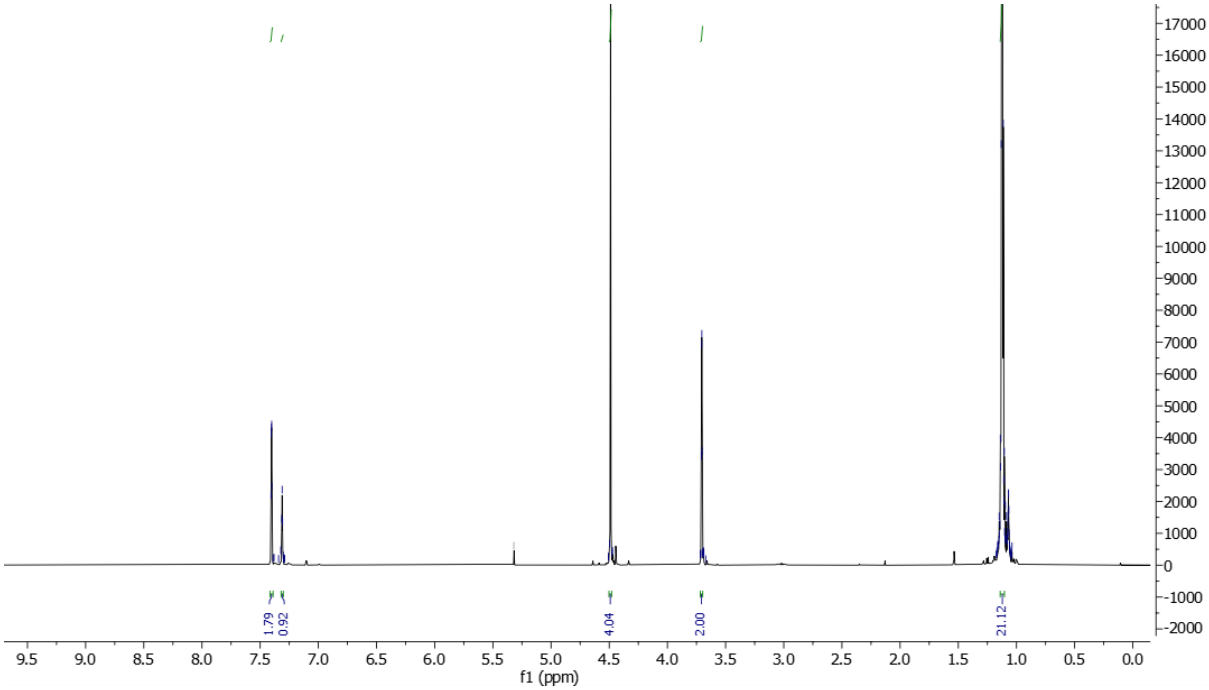

Figure 97. ^{1}H NMR spectrum of **132**

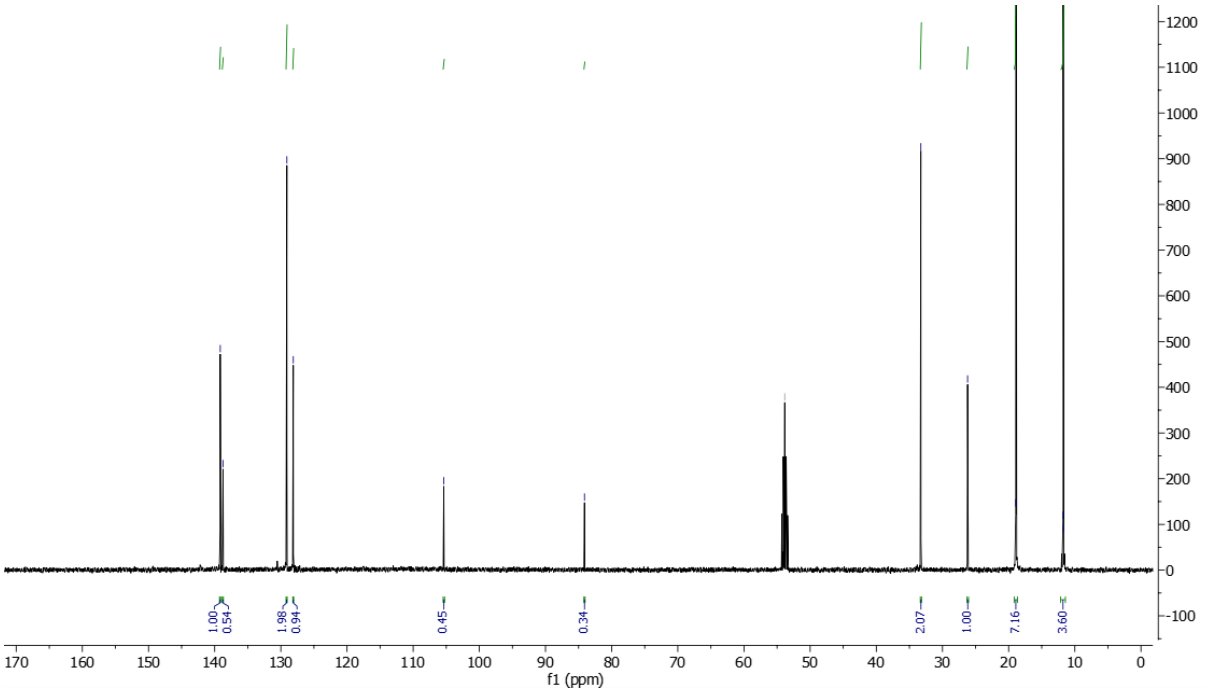

Figure 98. ^{13}C NMR spectrum of **132**

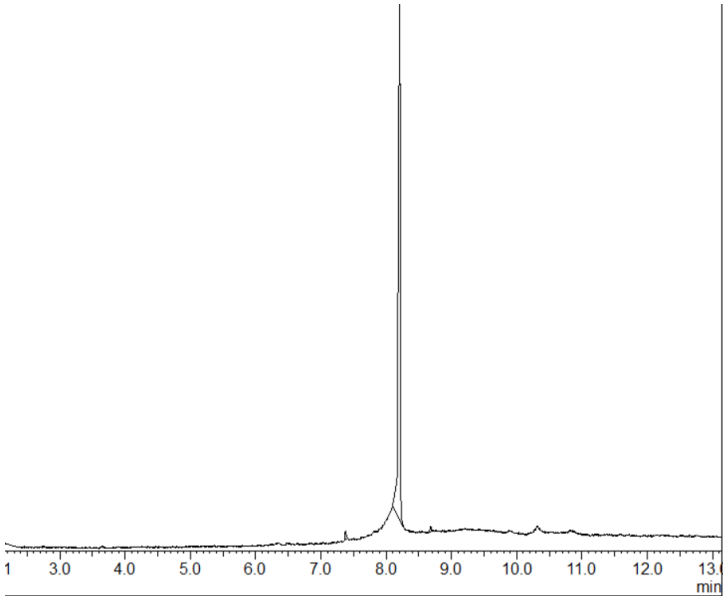

Figure 99. GC chromatogram of **132**

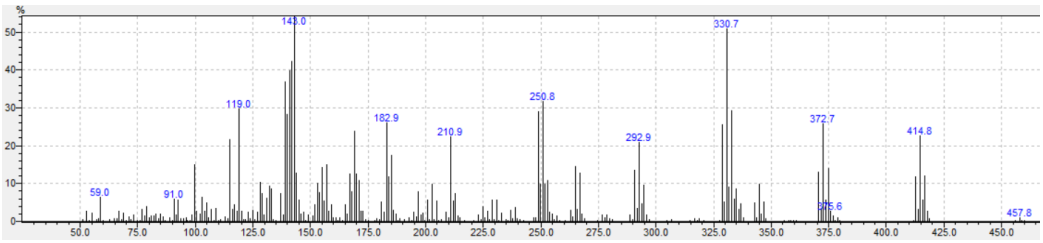

Figure 100. EI spectrum of **132**

5-(3-(triisopropylsilyl)prop-2-yn-1-yl)isophthalaldehyde (**101**)

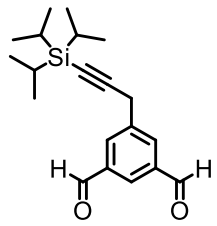

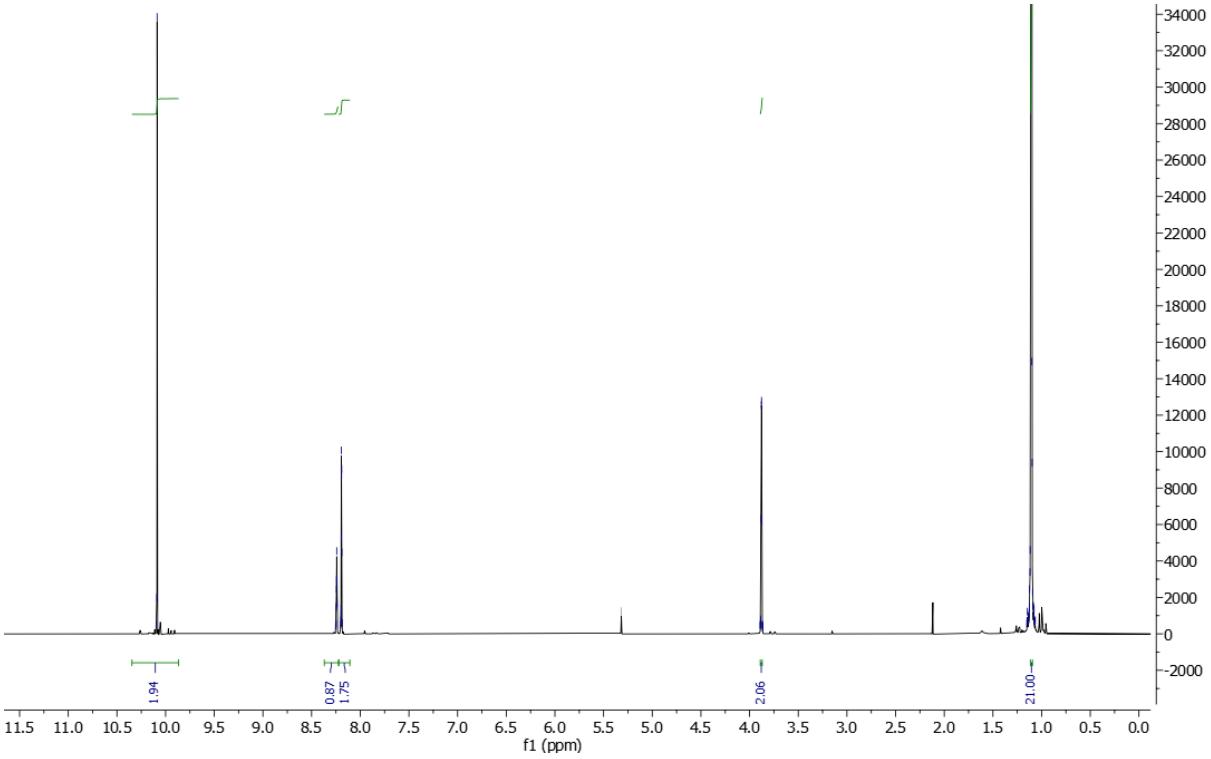

Figure 101. ^{1}H NMR spectrum of **101**

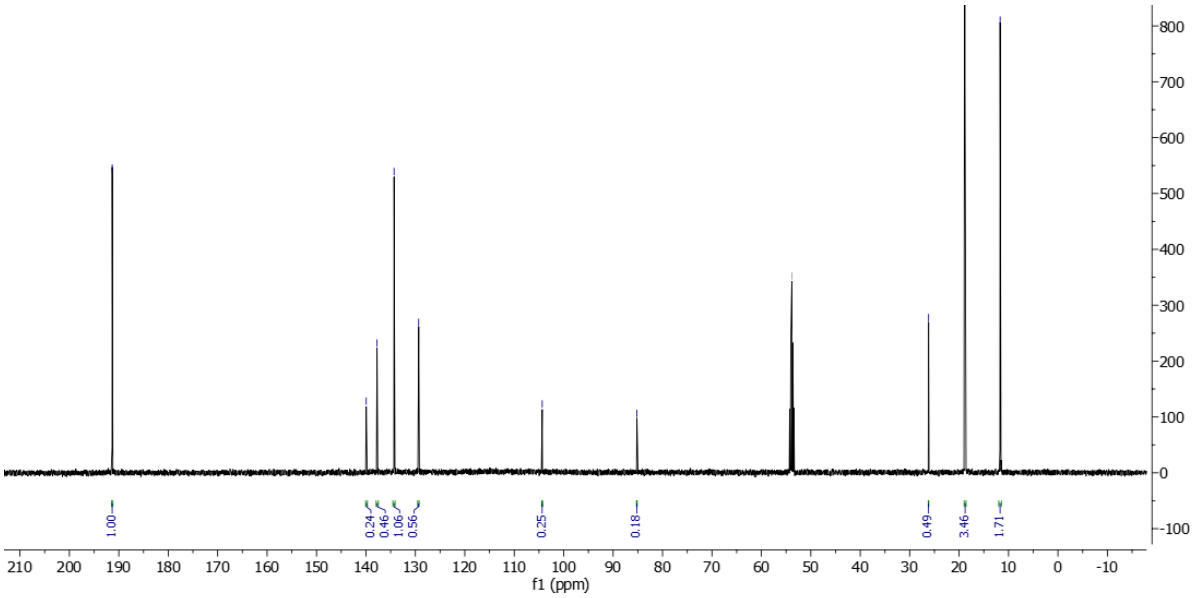

Figure 102. ^{13}C NMR spectrum of **101**

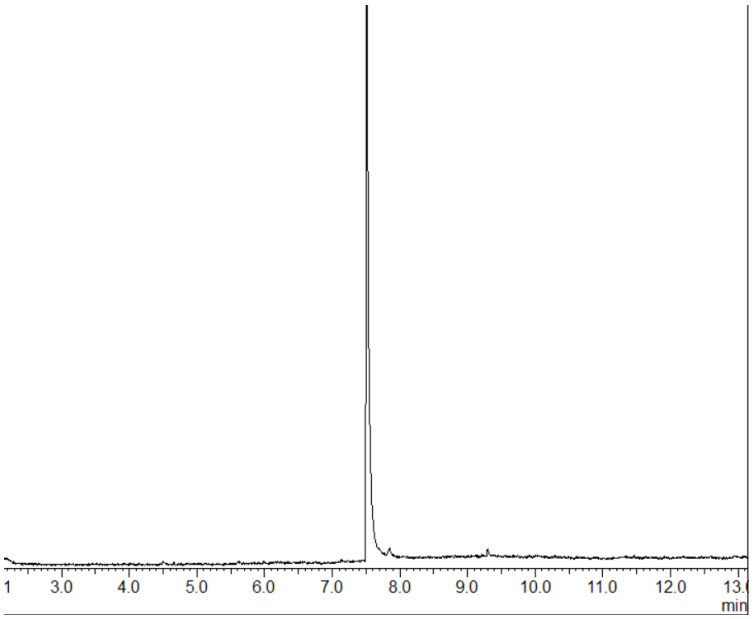

Figure 103. GC chromatogram of **101**

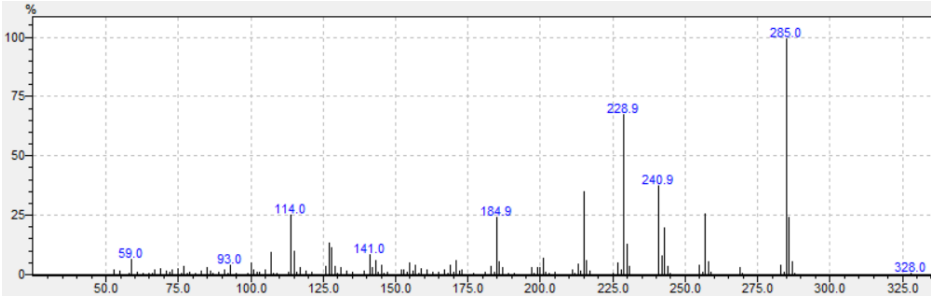

Figure 104. EI spectrum of **101**

1,3-bis(bromomethyl)-5-(prop-2-yn-1-yl)benzene (**131 deprotected**)

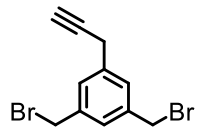

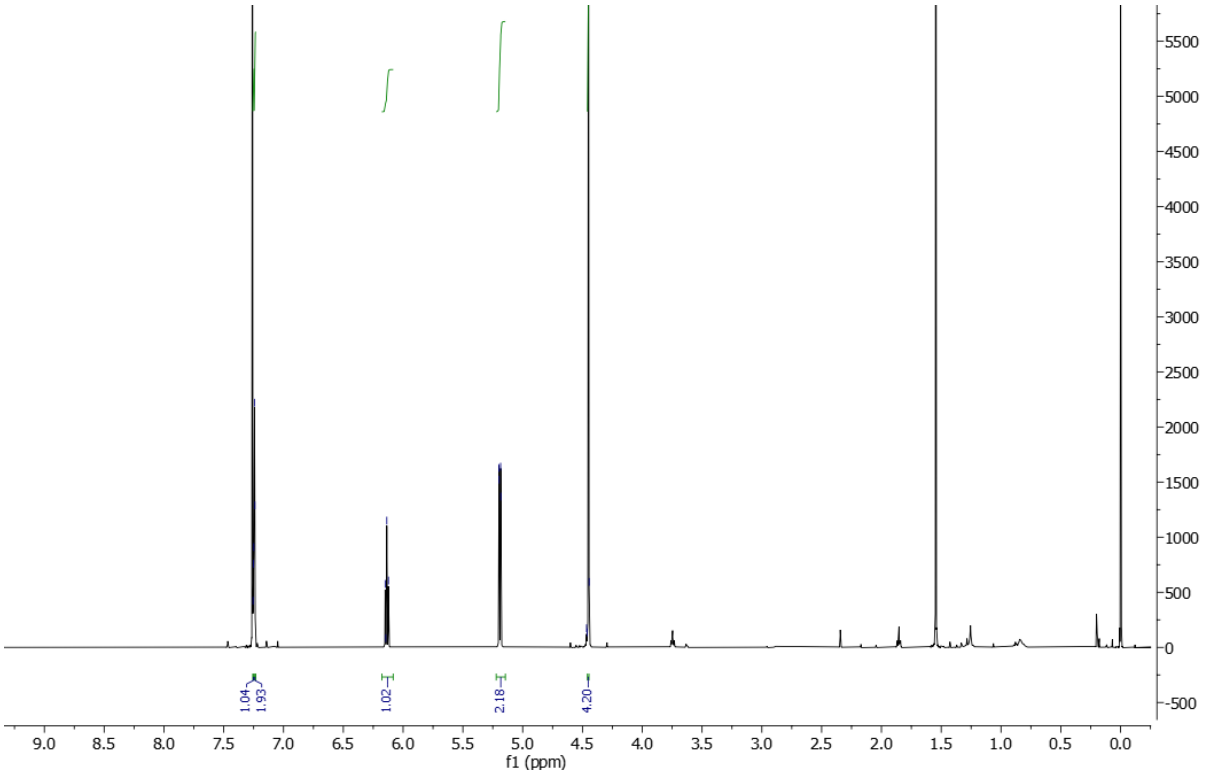

Figure 105. ^{1}H NMR spectrum of **131 deprotected**

1,3,5-tris(chloromethyl)benzene (**166**)

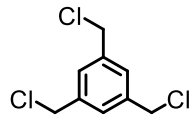

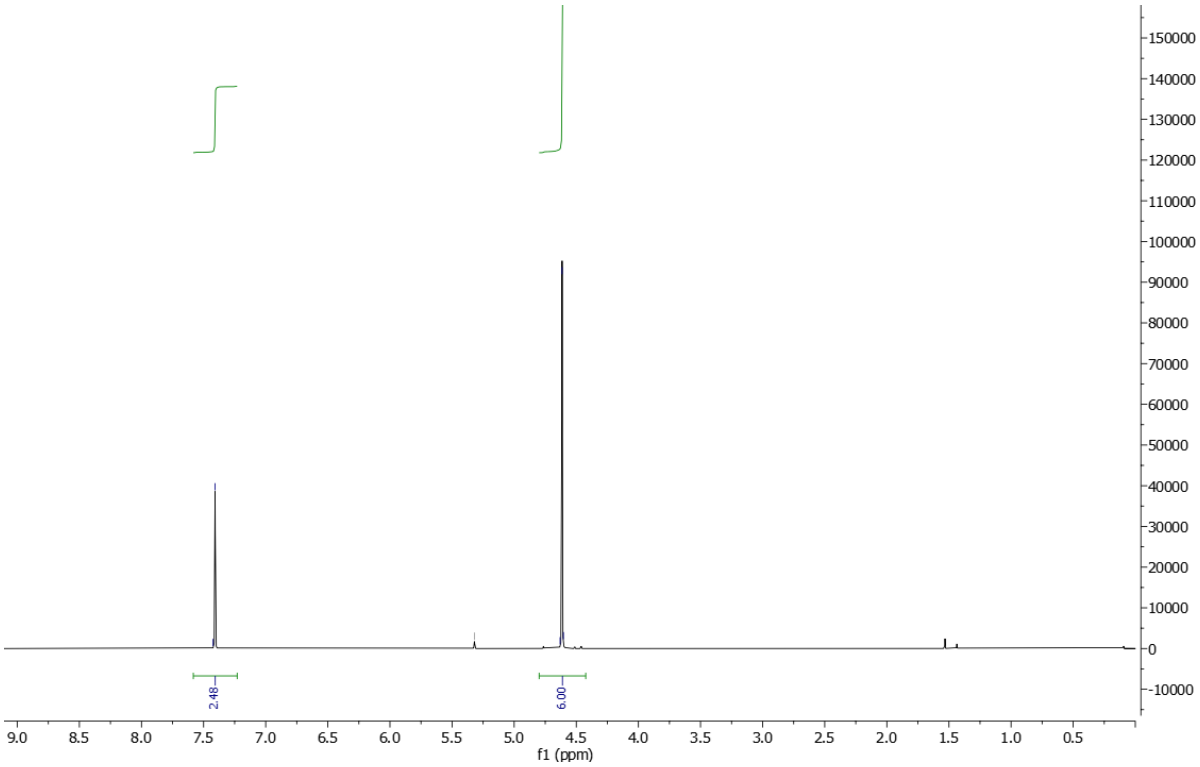

Figure 106. ^{1}H NMR spectrum of **166**

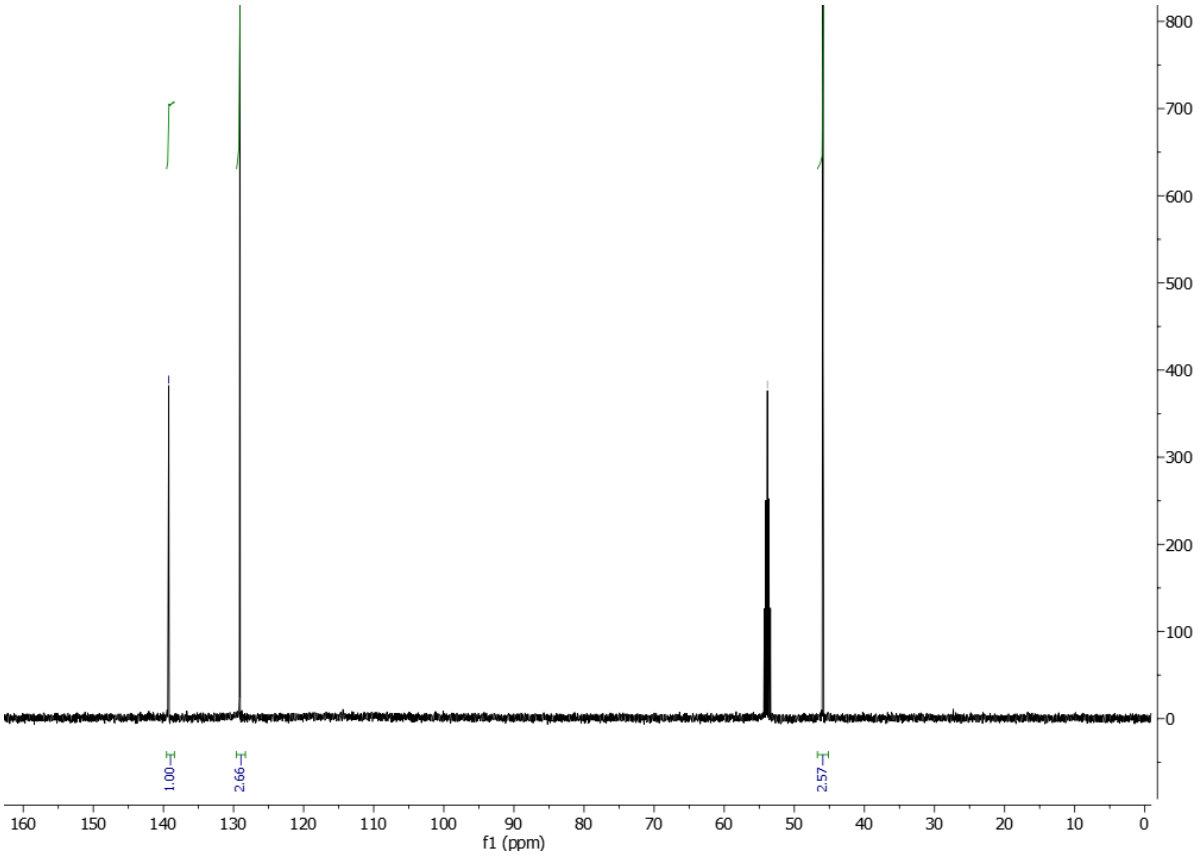

Figure 107. ^{13}C NMR spectrum of **166**

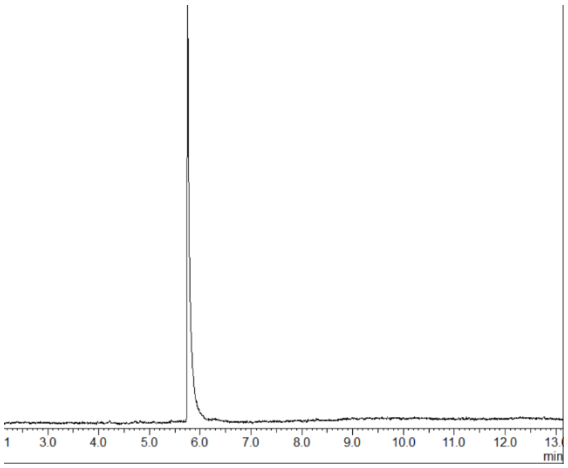

Figure 108. GC chromatogram of **166**

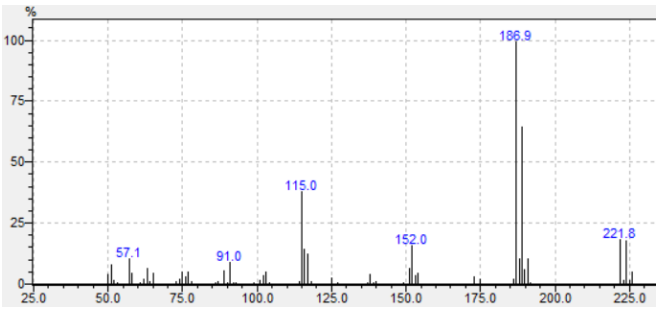

Figure 109. EI spectrum of **166**

Hexahydroxycalix[6]arene (**119**)

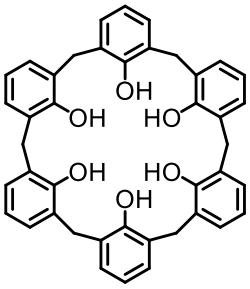

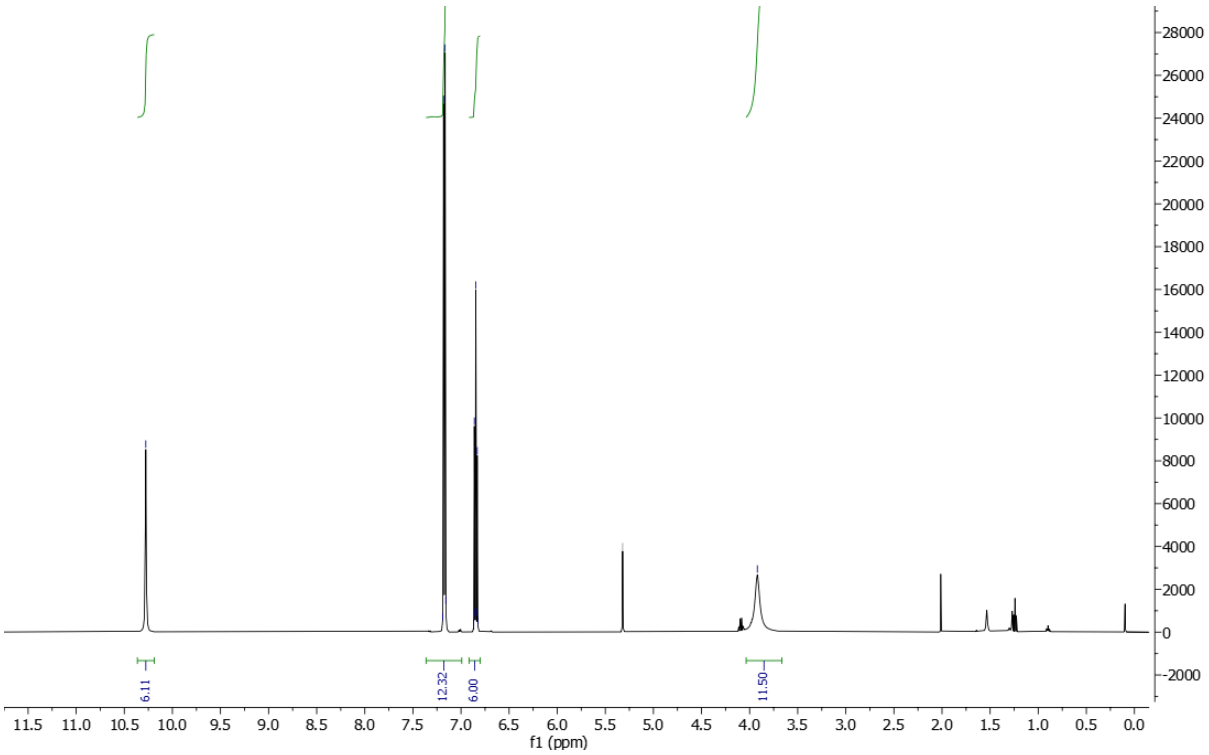

Figure 110. ^{1}H NMR spectrum of **119**

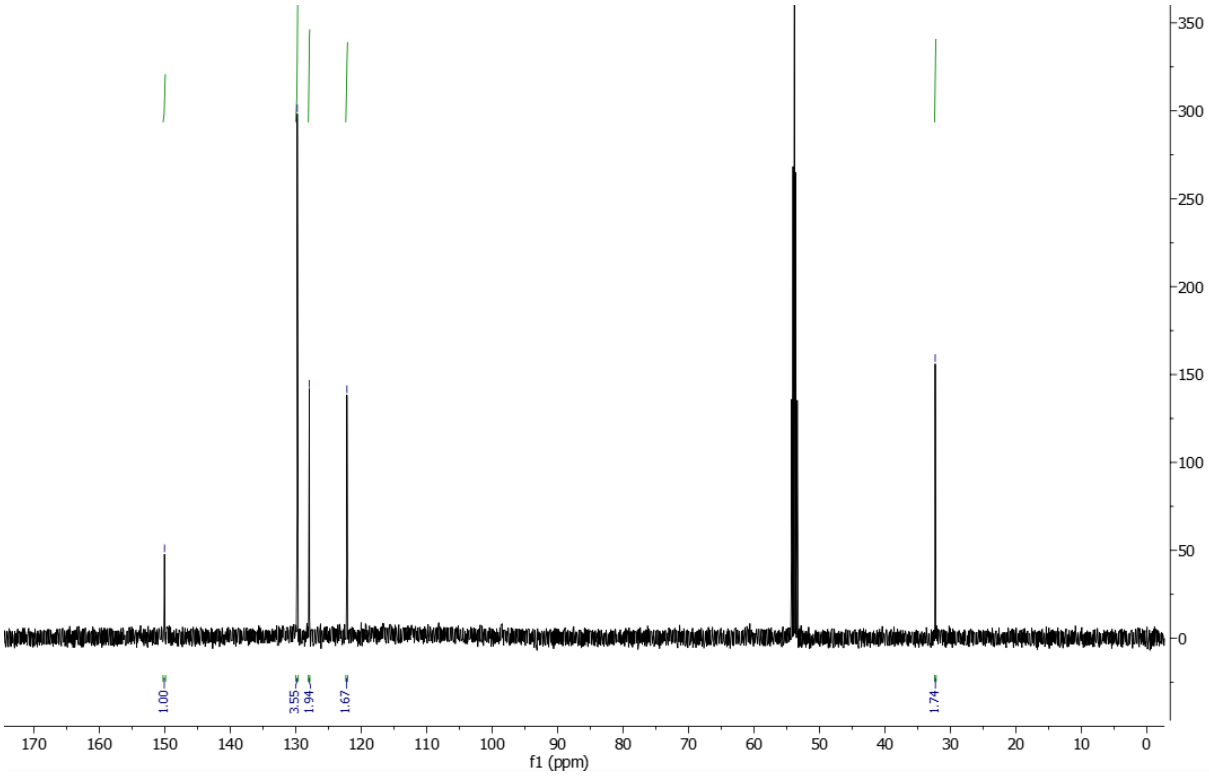

Figure 111. ^{13}C NMR spectrum of **119**

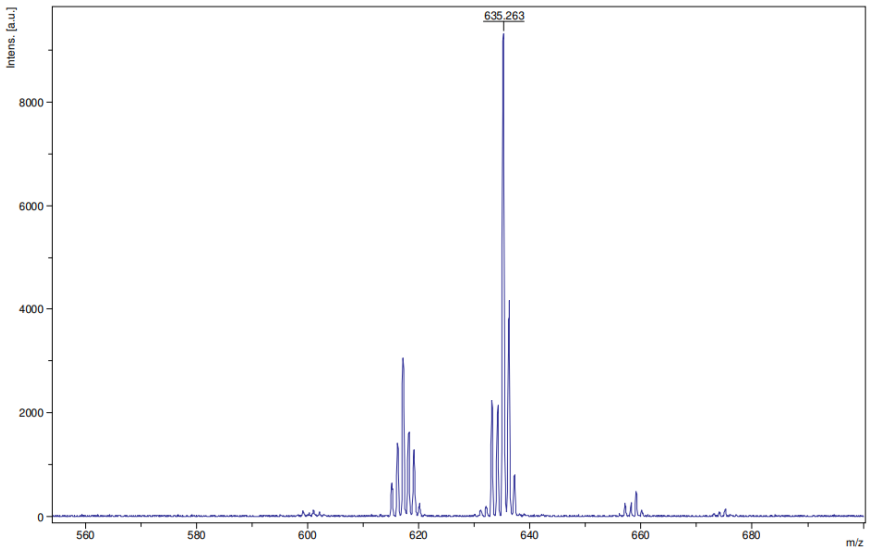

Figure 112 MALDI-TOF spectrum of **119**

Hexakis(diethyl phenyl phosphate)calix[6]arene (**121**)

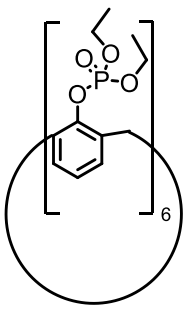

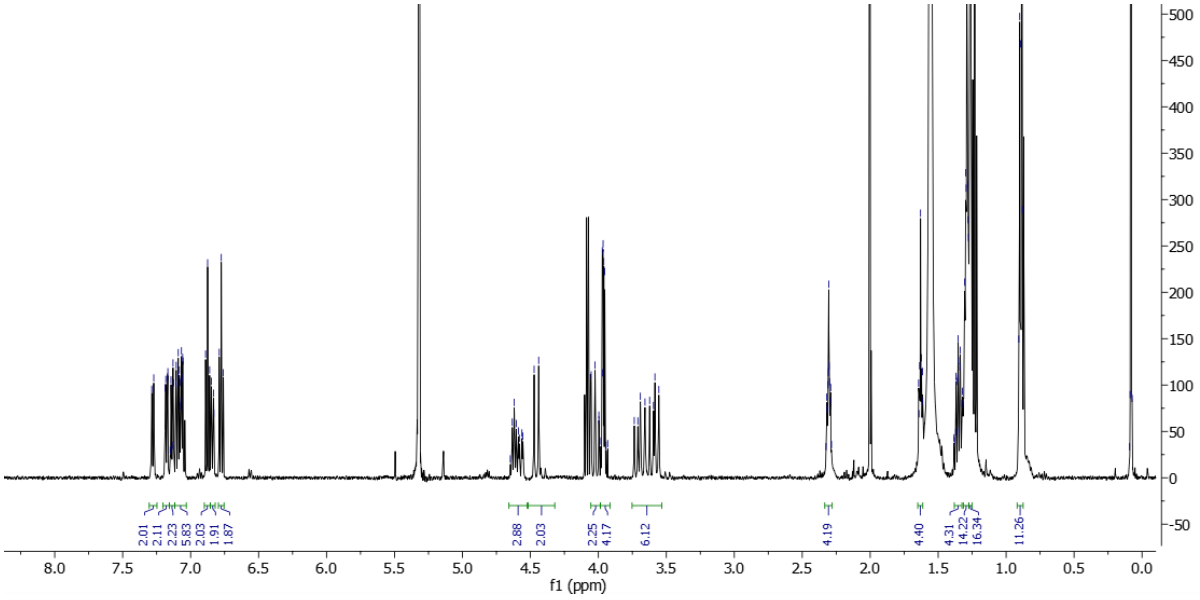

Figure 113. ^{1}H NMR spectrum of **121**

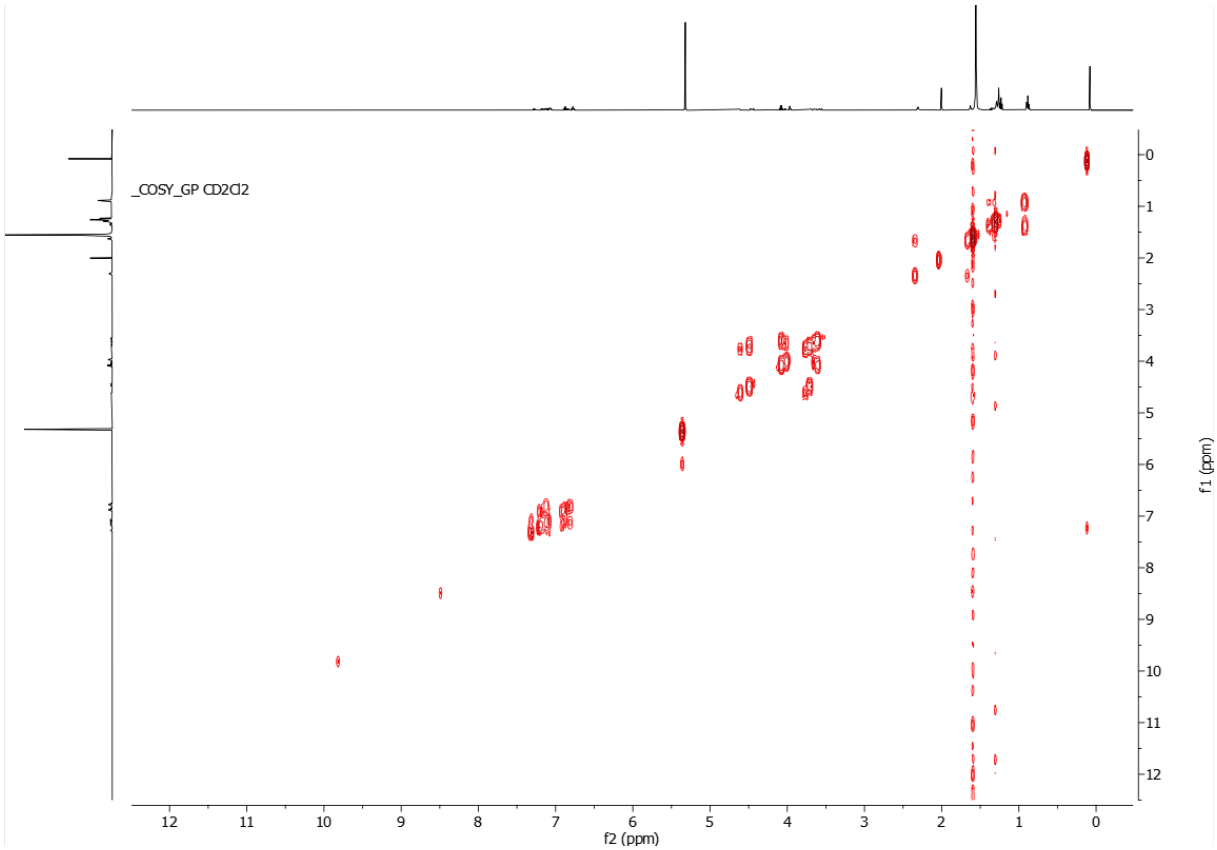

Figure 114. COSY NMR spectrum of **121**

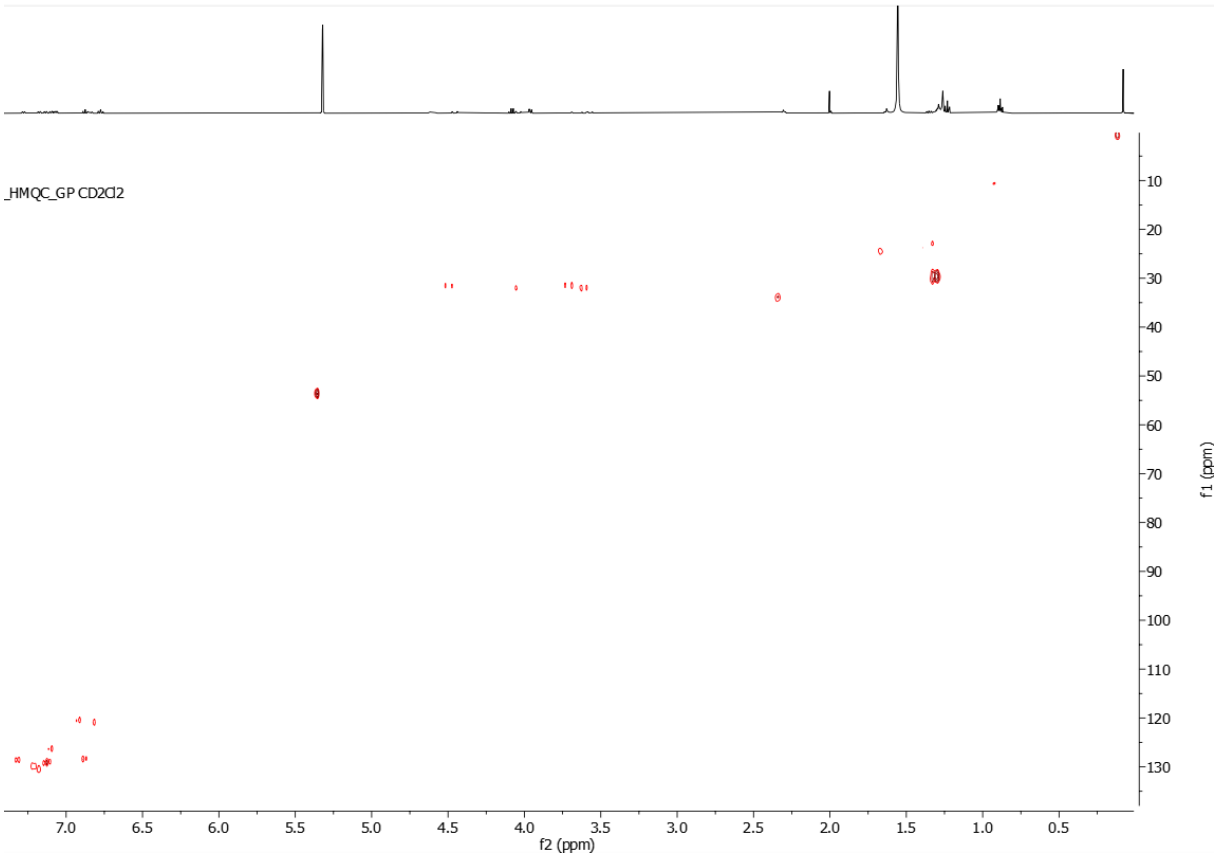

Figure 115. HMQC NMR spectrum of **121**

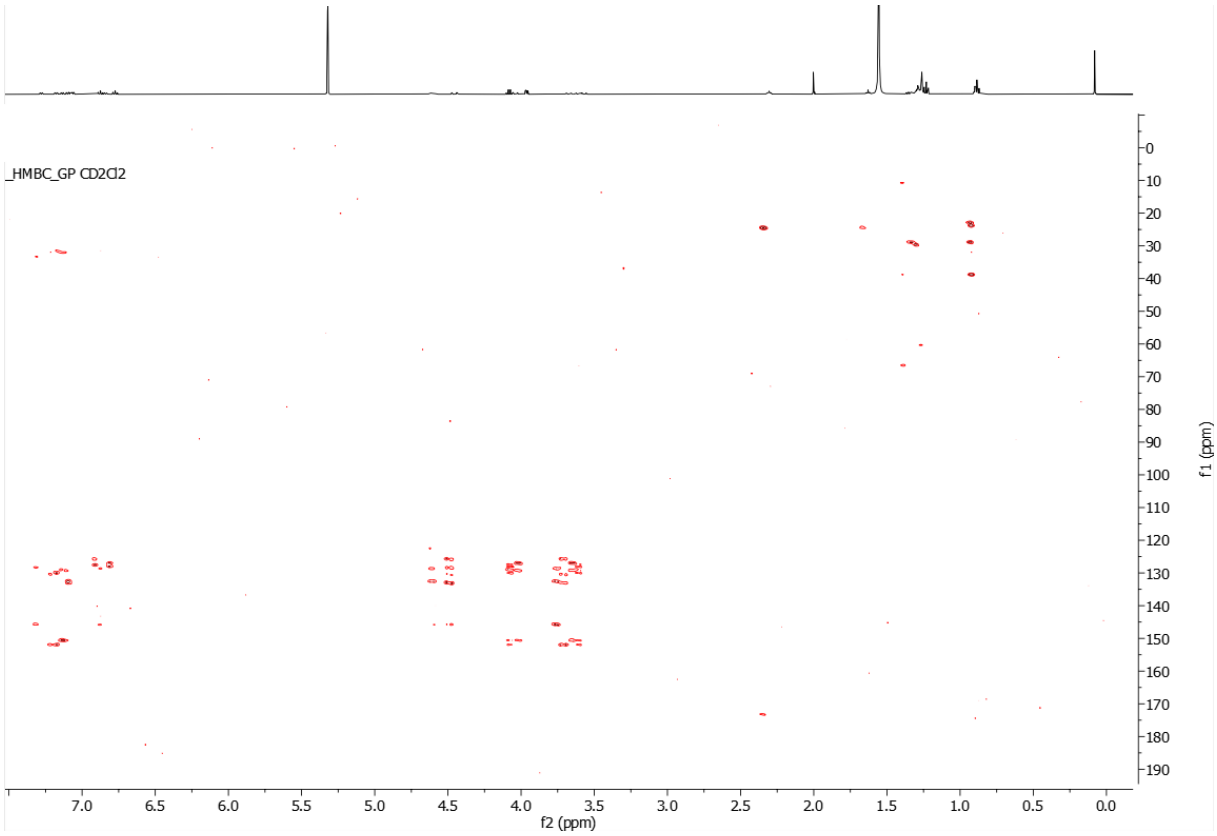

Figure 116. HMBC NMR spectrum of **121**

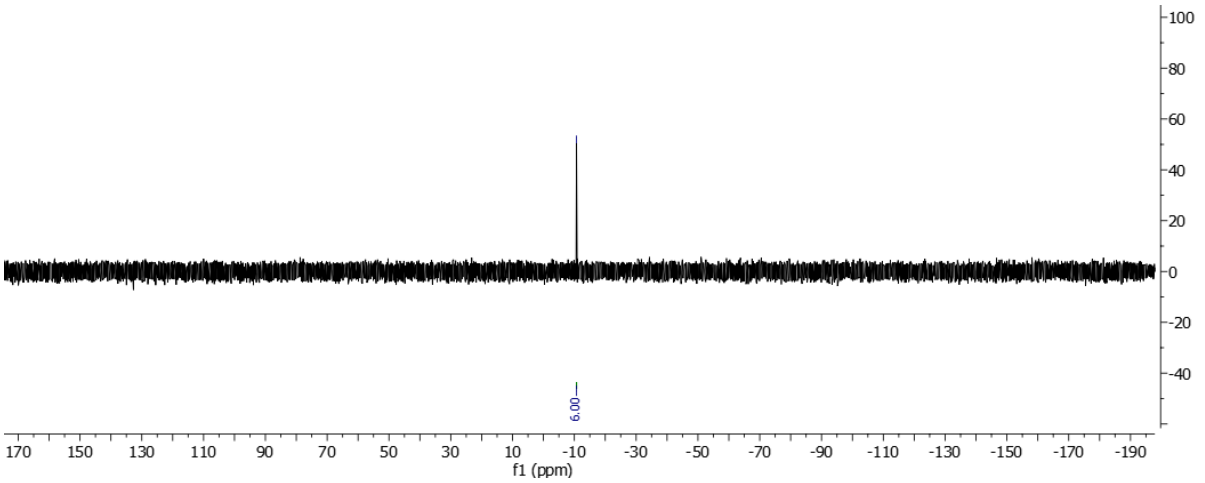

Figure 117. ^{31}P NMR spectrum of **121**

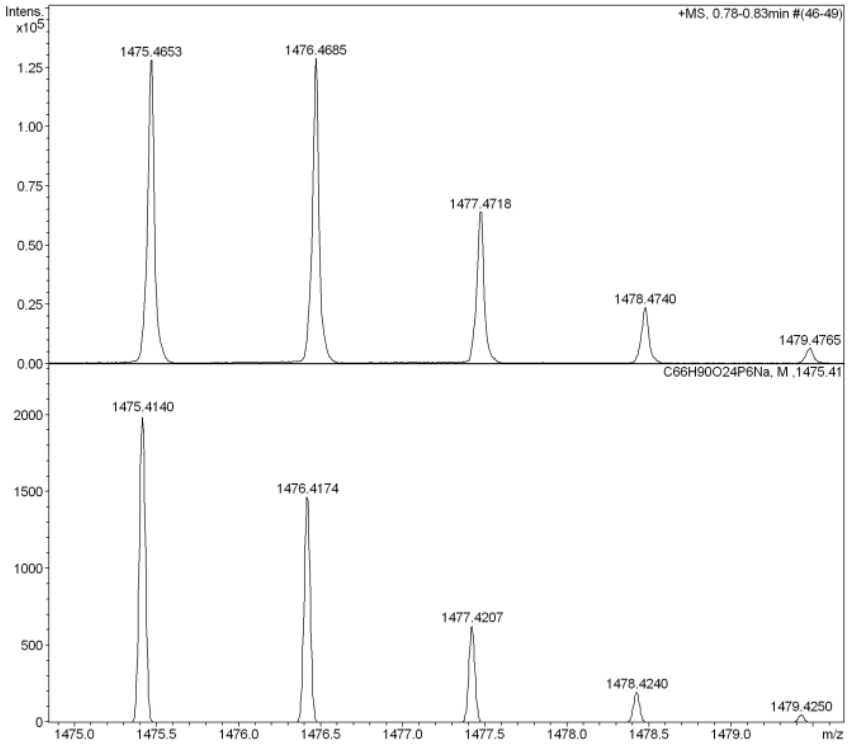

Figure 118. High resolution ESI spectrum of **121**

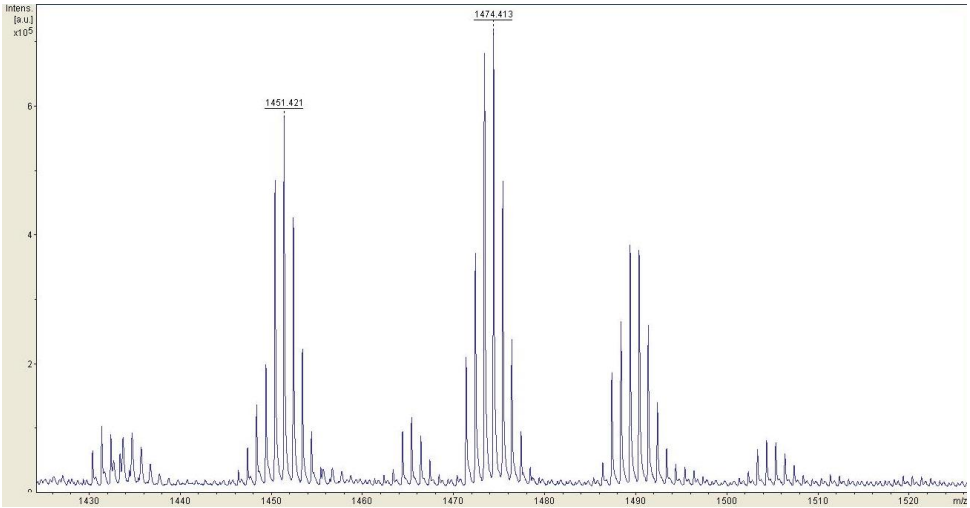

Figure 119 MALDI-TOF spectrum of **121**

methyl 5-cyano-2-phenylpentanoate (**153**)

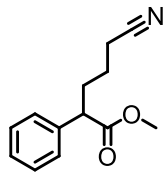

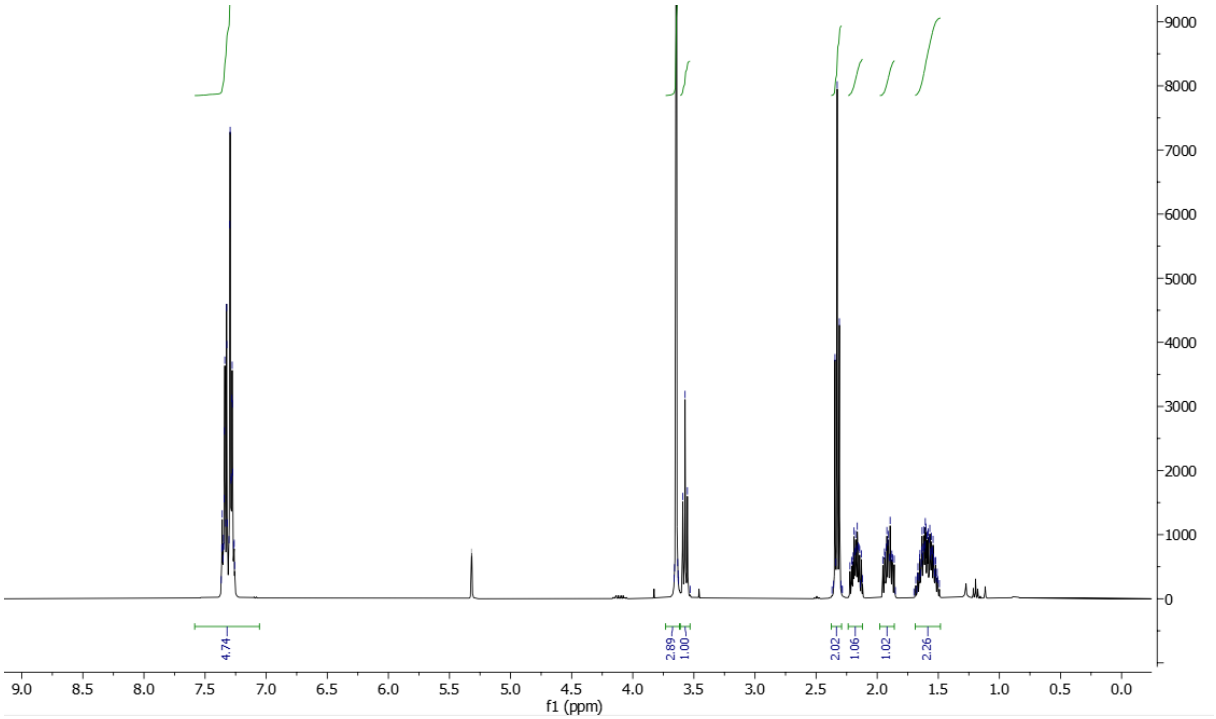

Figure 120. ^{1}H NMR spectrum of **153**

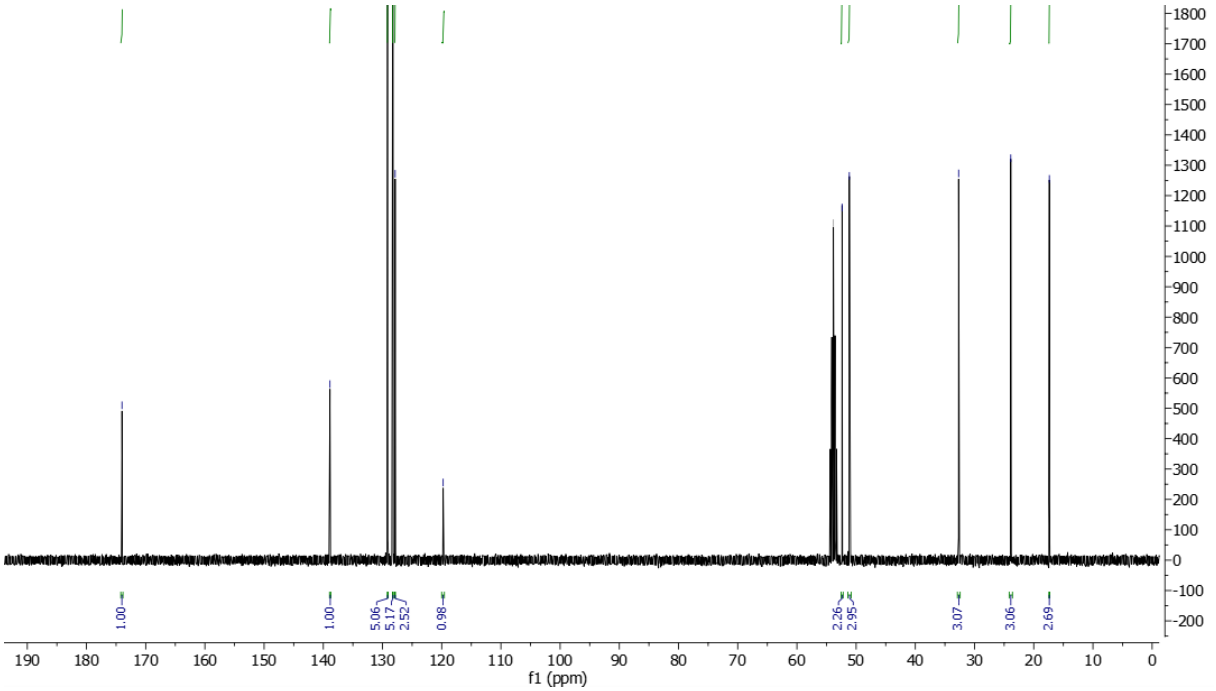

Figure 121. ^{13}C NMR spectrum of **153**

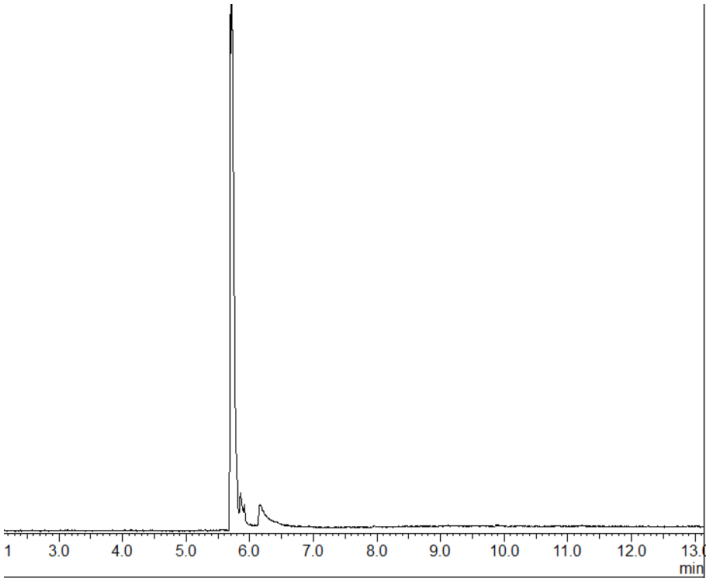

Figure 122. GC chromatogram of **153**

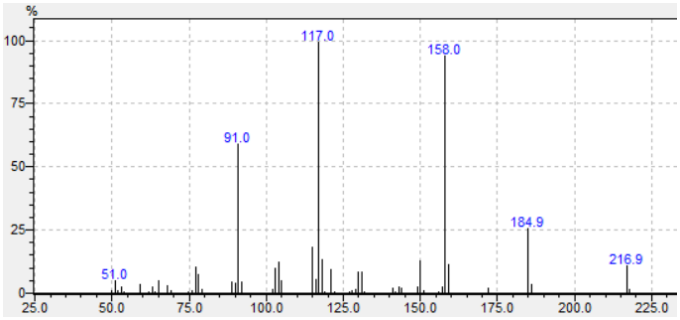

Figure 123. EI spectrum of **153**

methyl 4-cyano-2-phenylbutanoate (**156**)

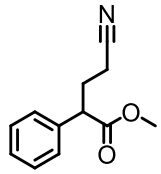

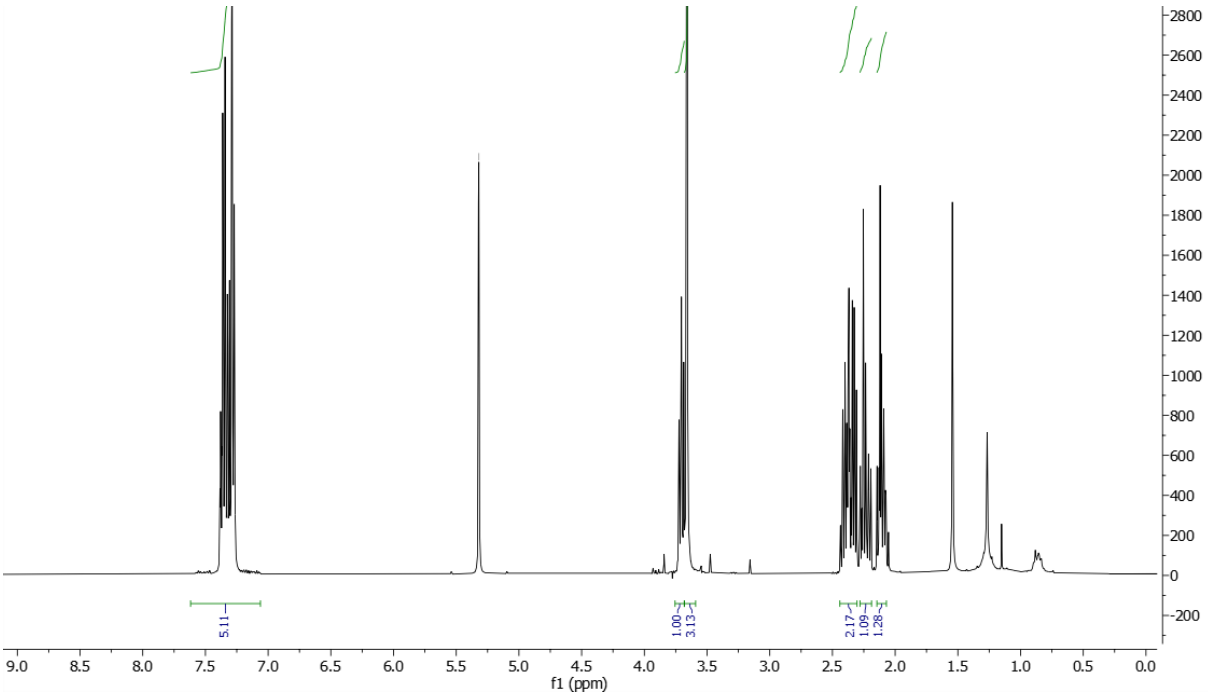

Figure 124. ^{1}H NMR spectrum of **156**

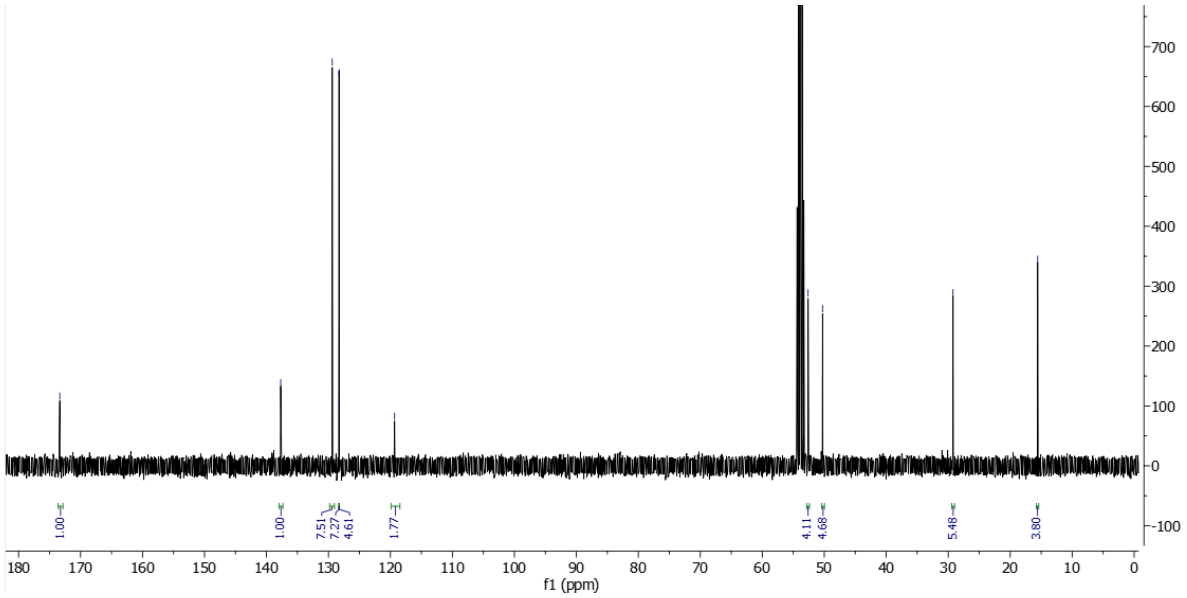

Figure 125. ^{13}C NMR spectrum of **156**

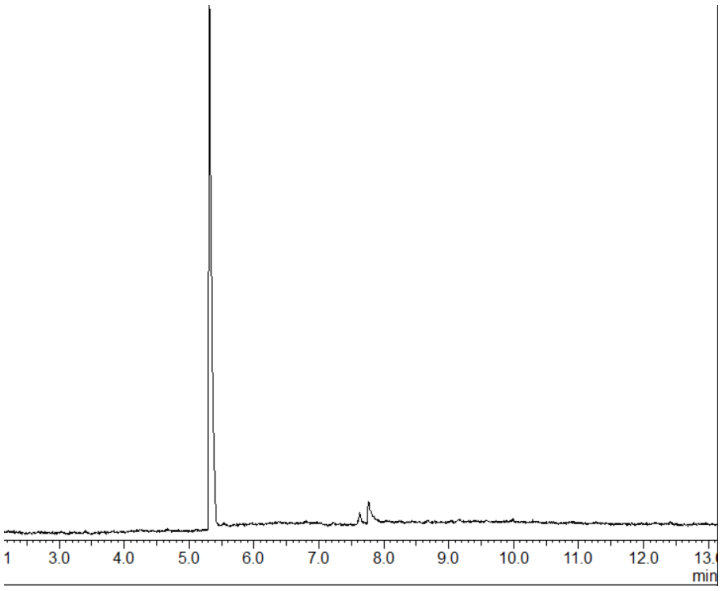

Figure 126. GC chromatogram of **156**

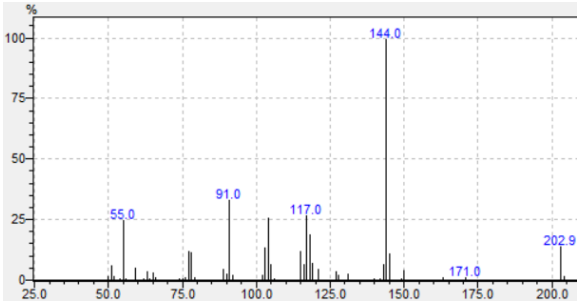

Figure 127. EI spectrum of **156**

5-cyano-2-phenylpentanoic acid (**154**)

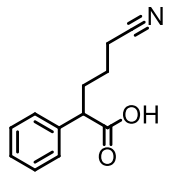

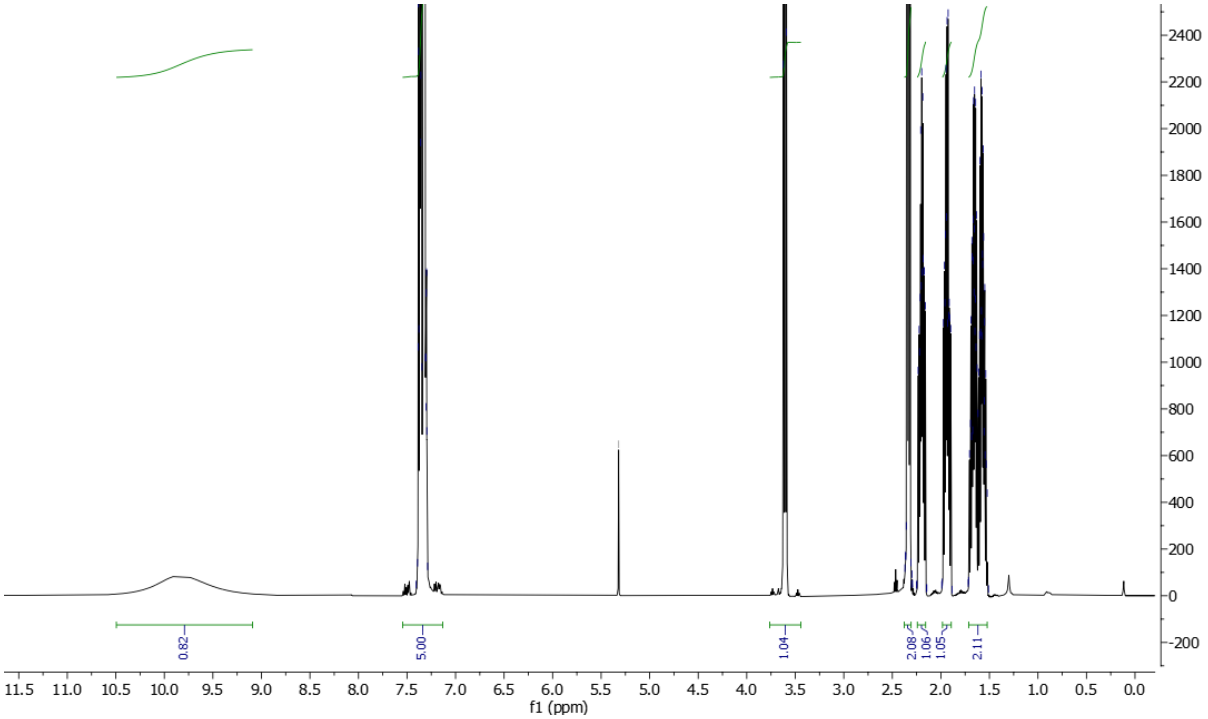

Figure 128. ^{1}H NMR spectrum of **154**

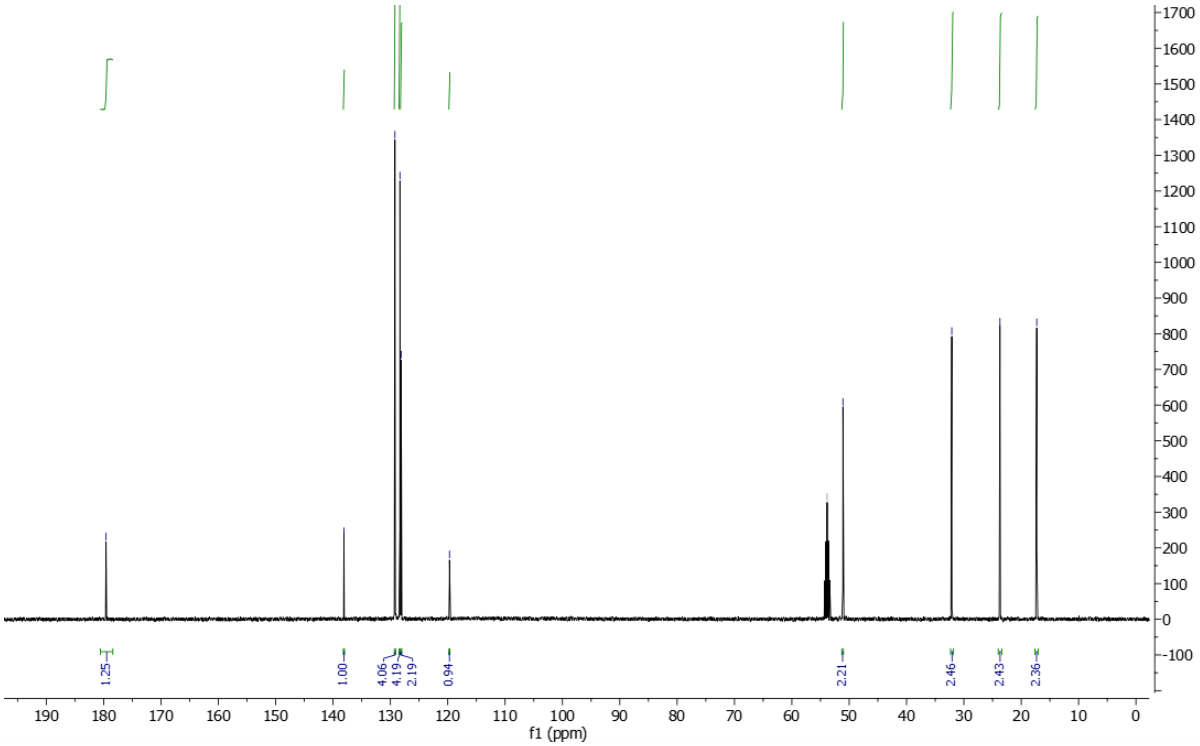

Figure 129. ^{13}C NMR spectrum of **154**

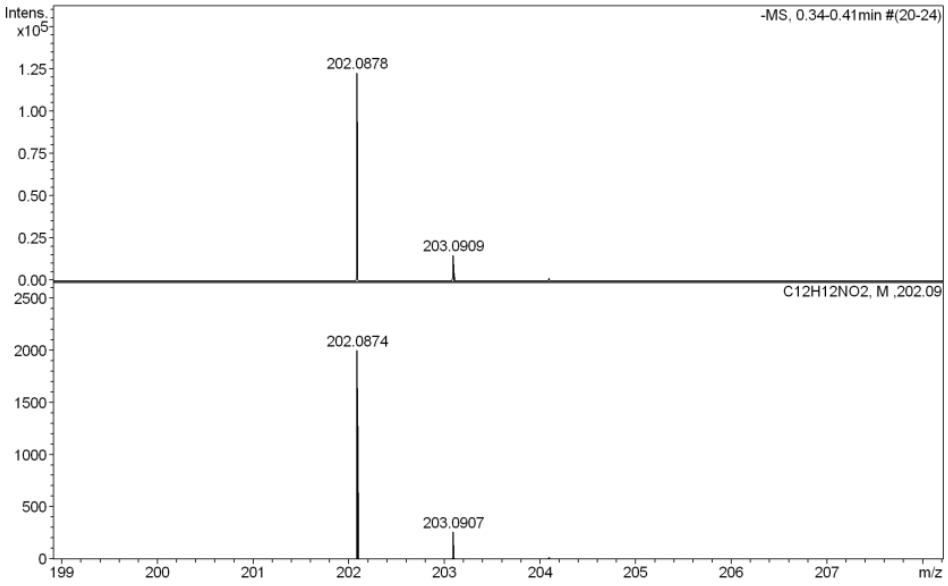

Figure 130. High resolution ESI spectrum of **154**

4-cyano-2-phenylbutanoic acid (**157**)

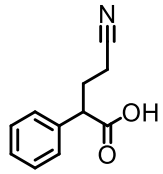

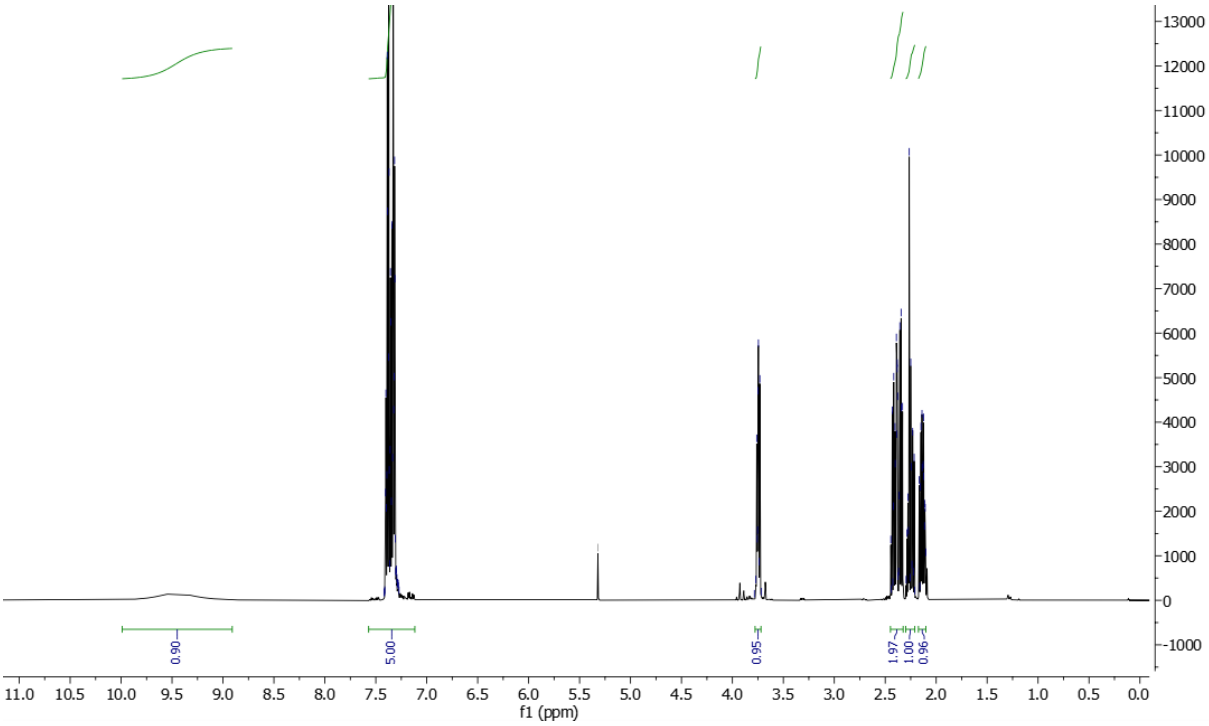

Figure 131. ^{1}H NMR spectrum of **157**

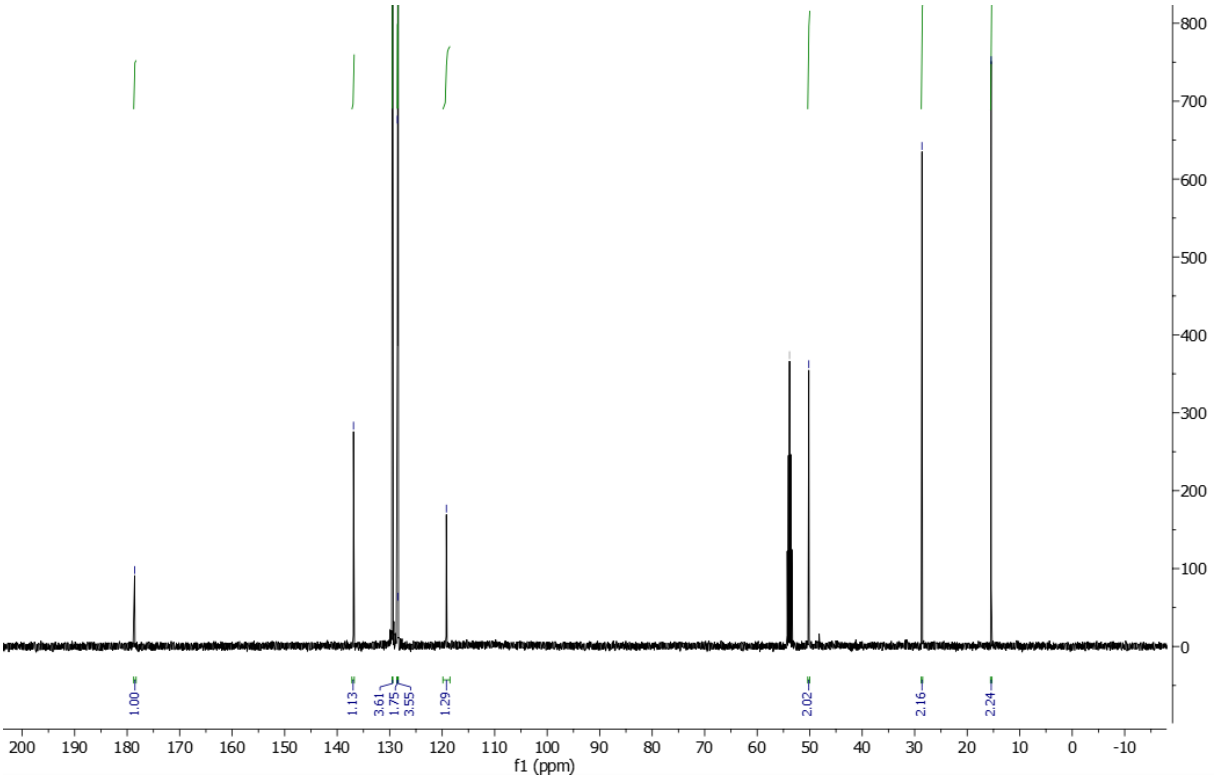

Figure 132. ^{13}C NMR spectrum of **157**

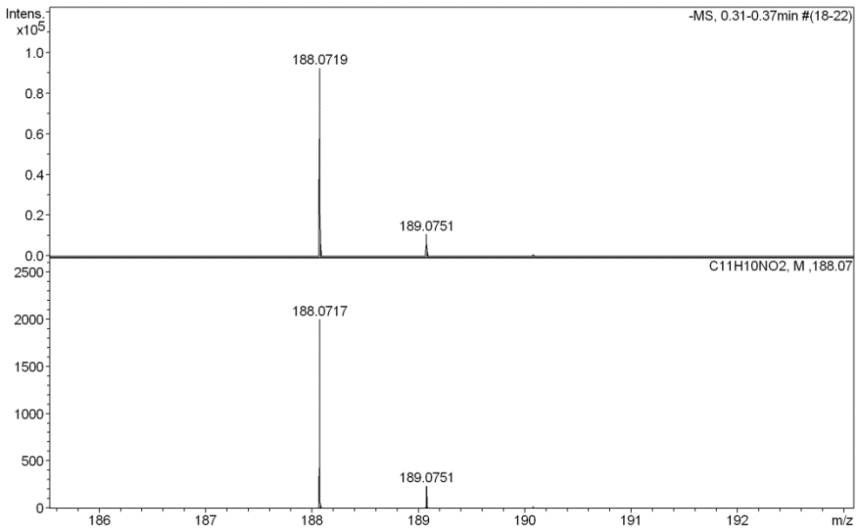

Figure 133. High resolution ESI spectrum of **157**

6-phenyl-4,5-dihydropyridin-2(3H)-one (**155**)

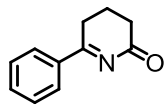

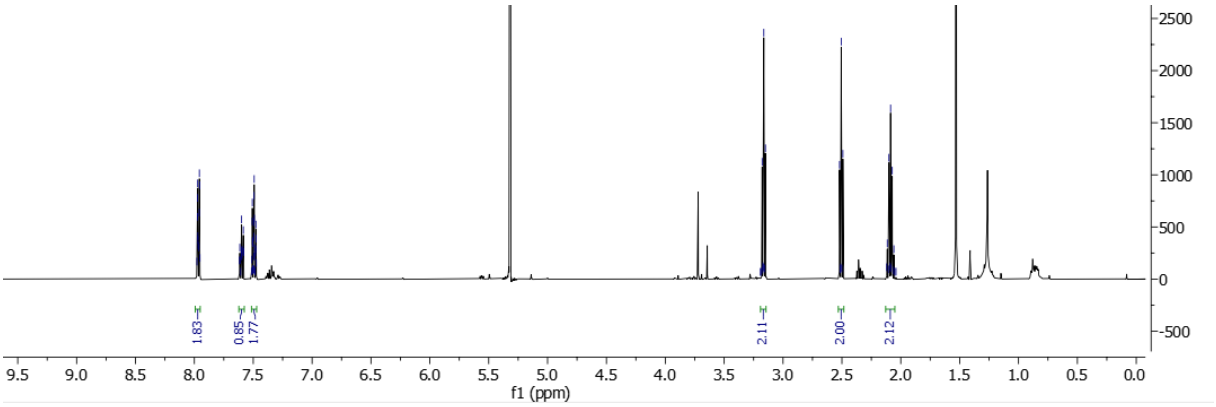

Figure 134. ^{1}H NMR spectrum of **155**

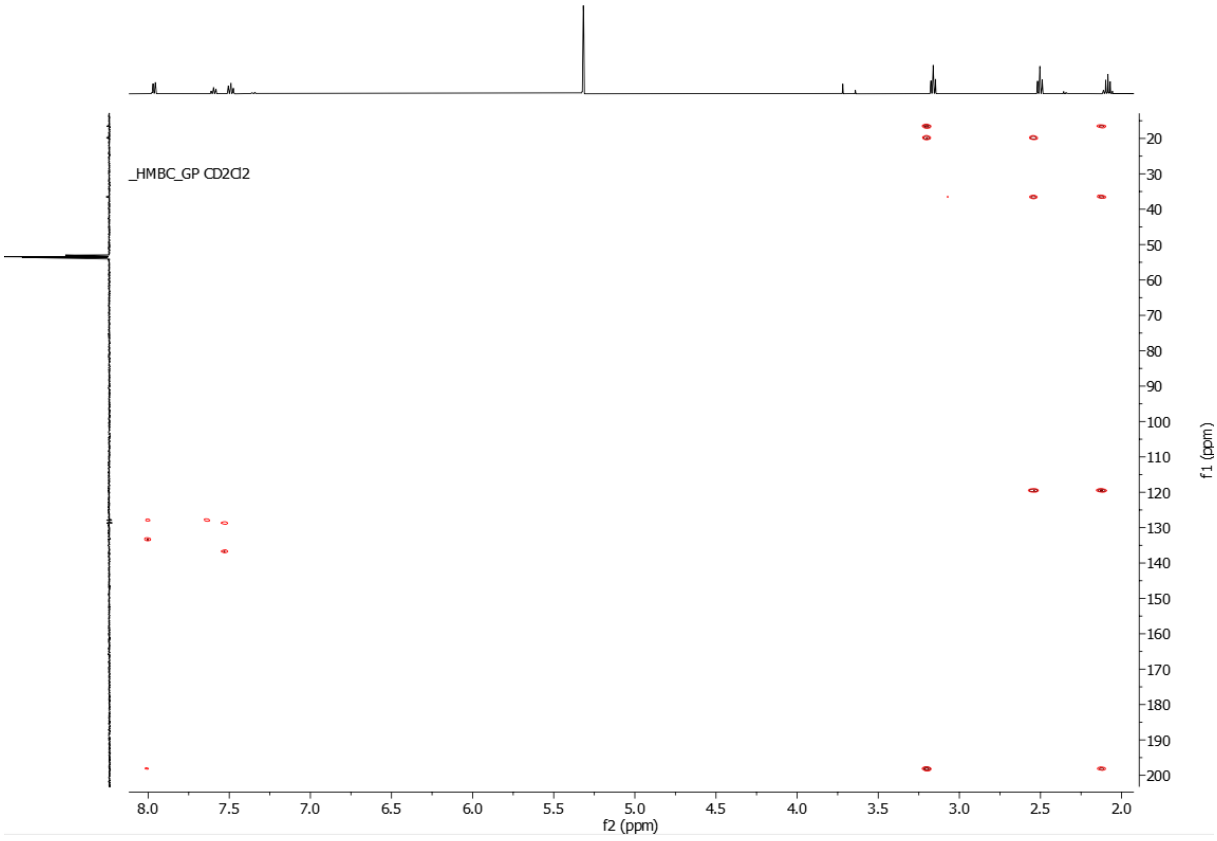

Figure 135. HMBC spectrum of **155**

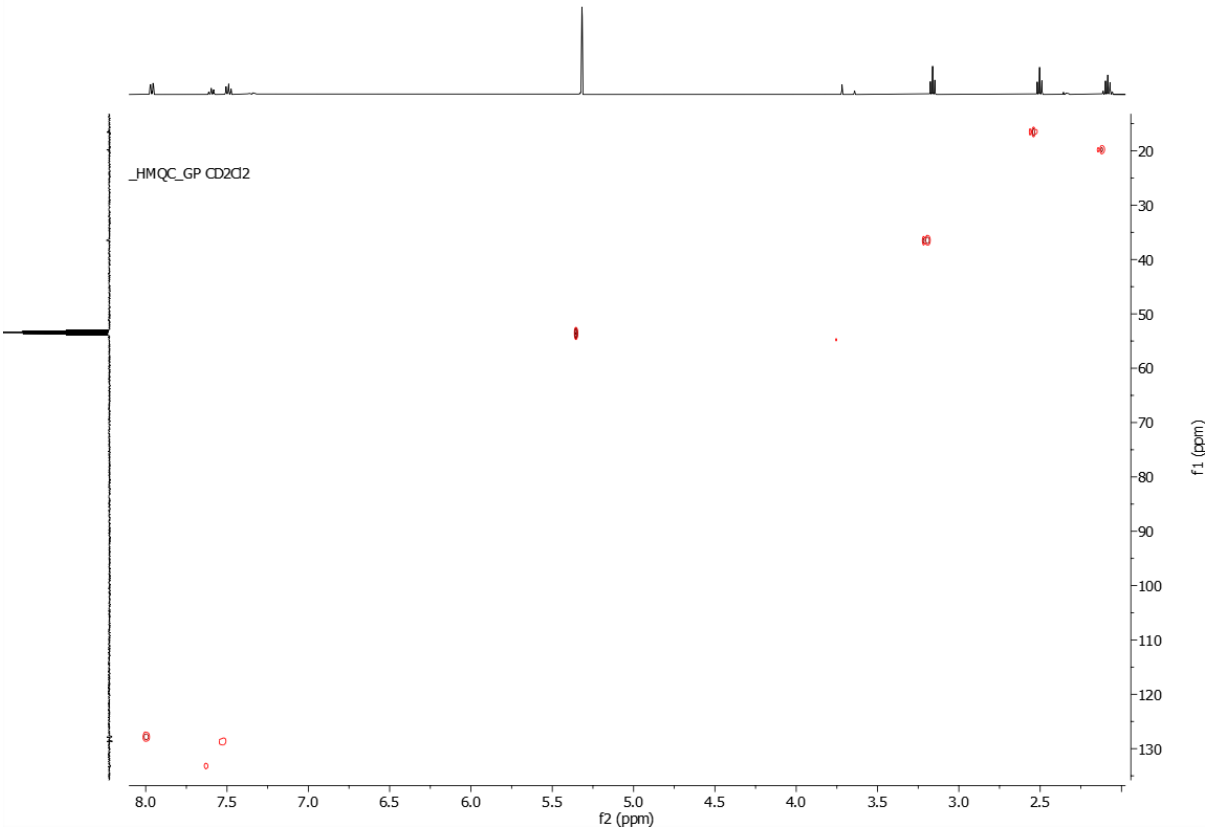

Figure 136. HMQC spectrum of **155**

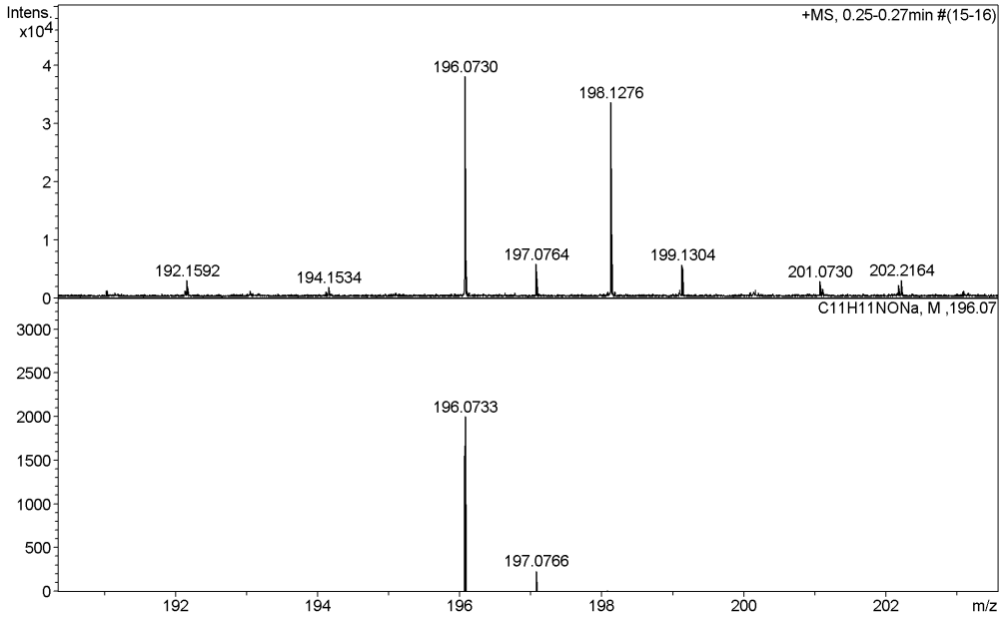

Figure 137. High resolution ESI spectrum of **155**

5-phenyl-3,4-dihydro-2H-pyrrol-2-one (**158**)

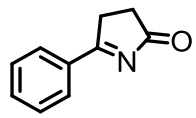

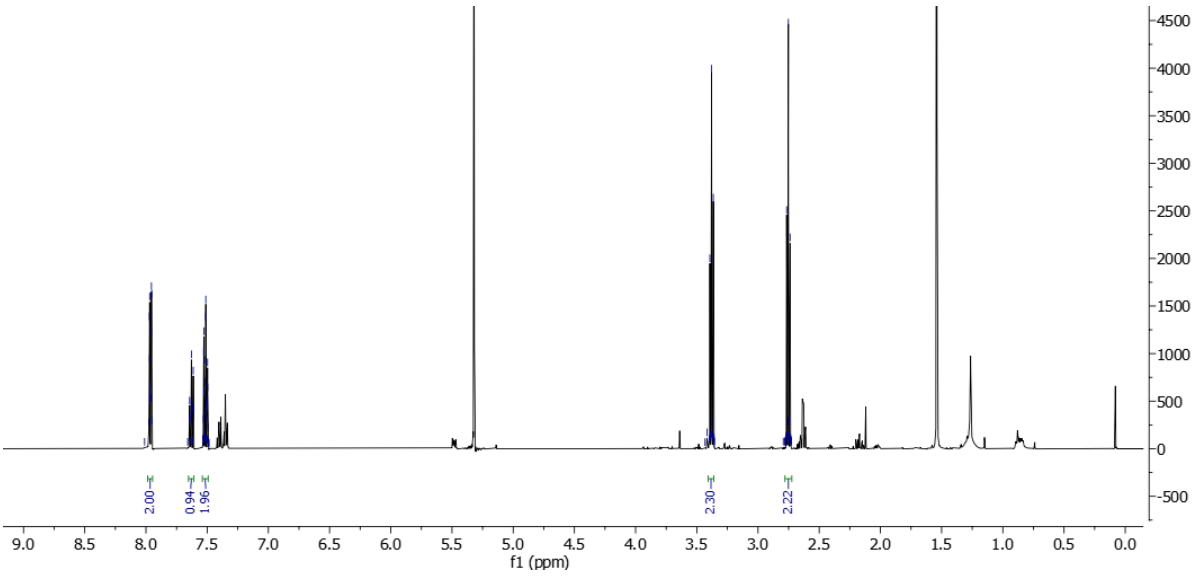

Figure 138. ^{1}H NMR spectrum of **158**

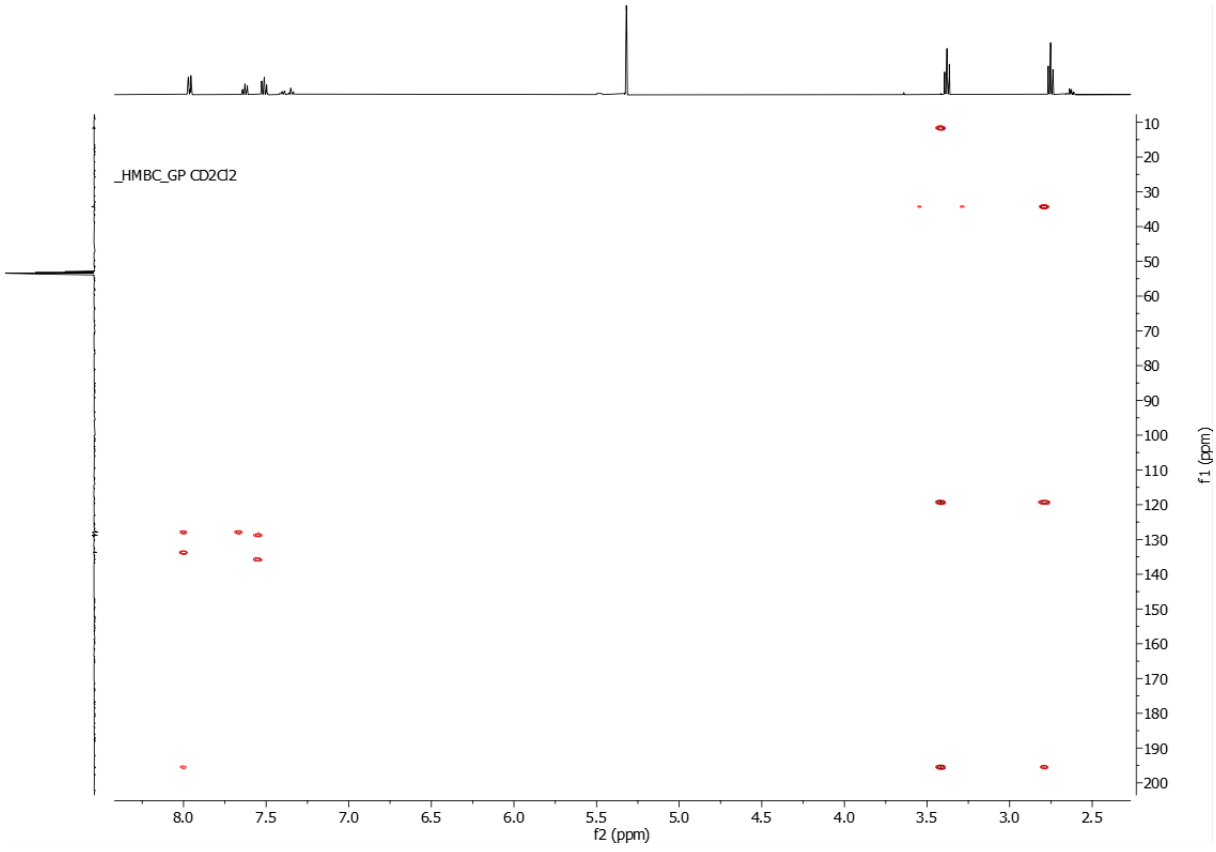

Figure 139. HMBC spectrum of **158**

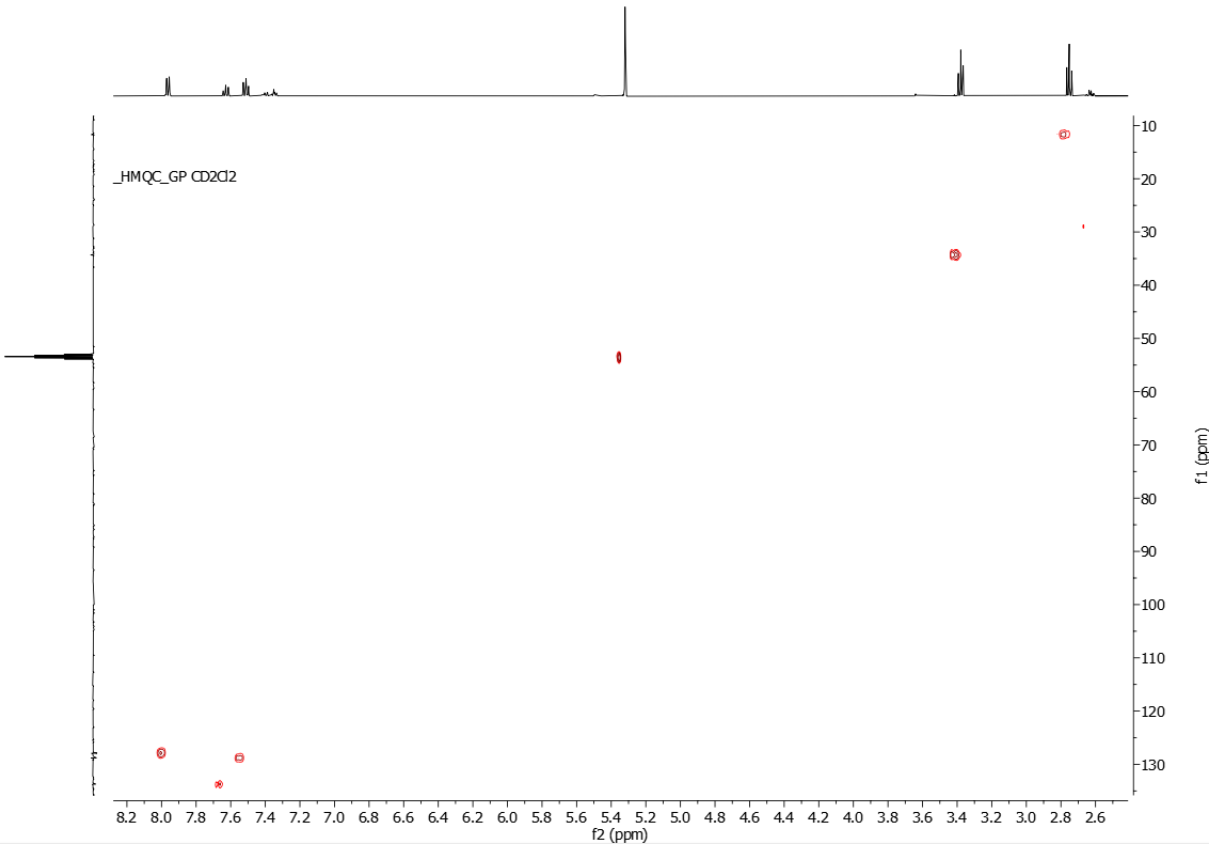

Figure 140. HMQC spectrum of **158**

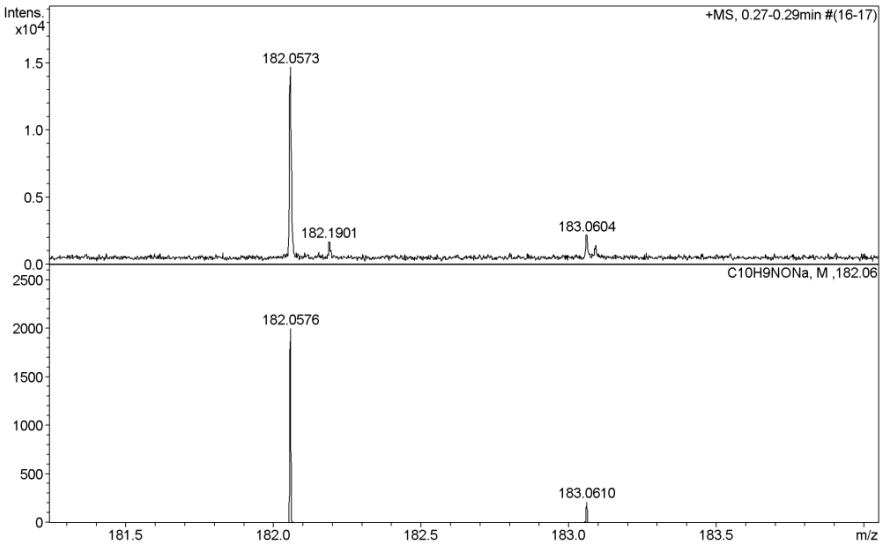

Figure 141. High resolution ESI spectrum of **158**

(methylenebis(2-hydroxybenzene-5,1,3-triyl))tetramethanol (**145**)

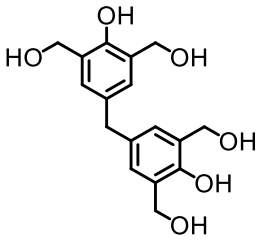

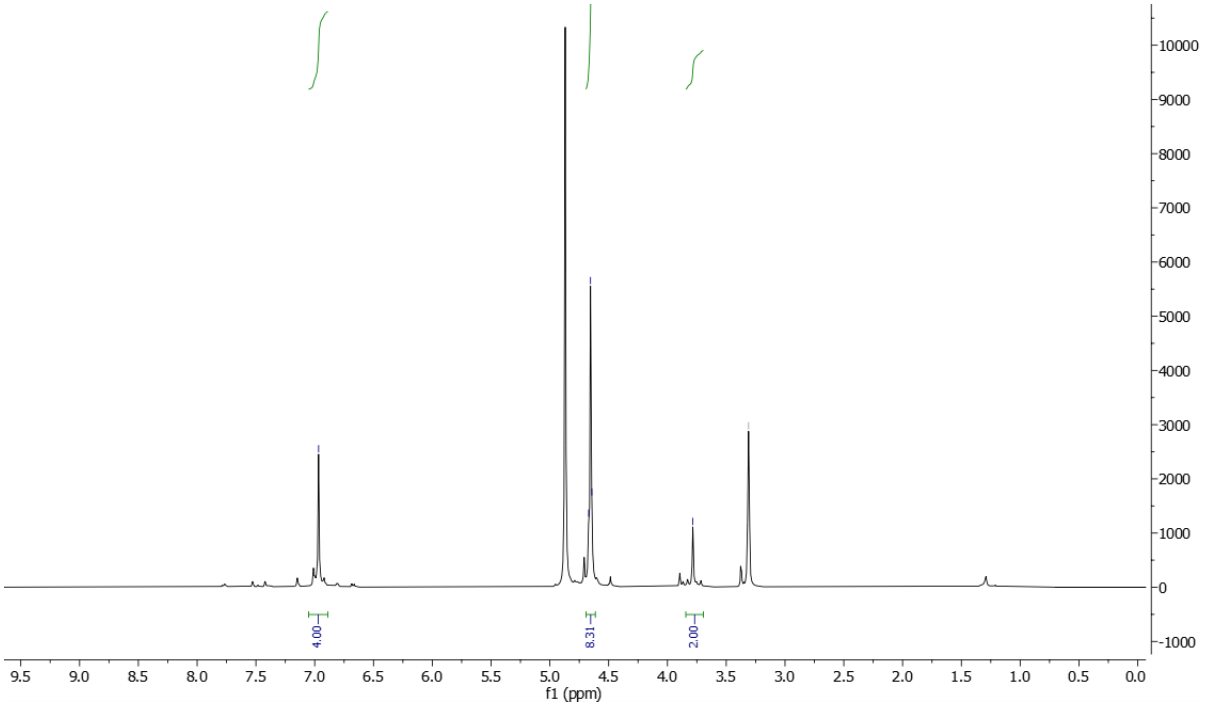

Figure 142. ^{1}H NMR spectrum of **145**

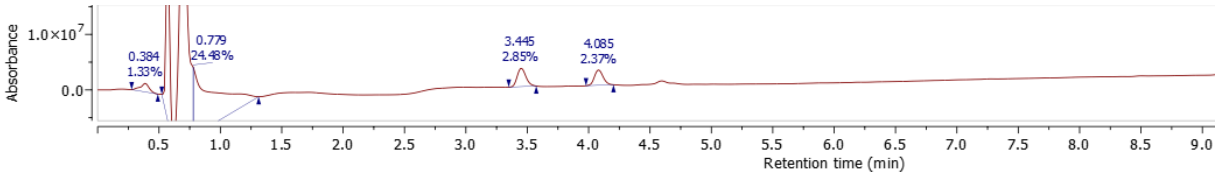

Figure 143. LC chromatogram of **145**

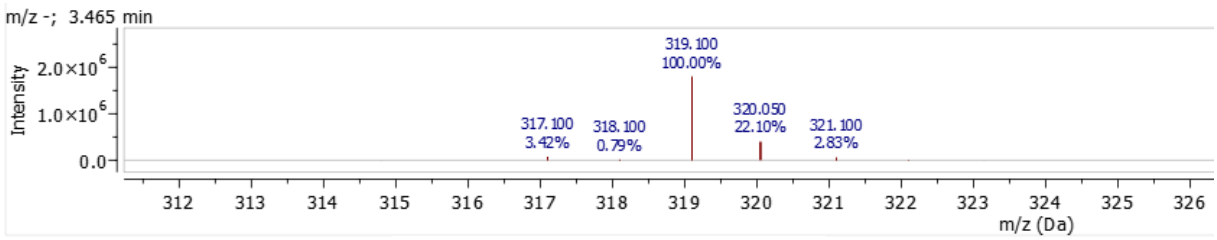

Figure 144. ESI spectrum of **145**

4,4'-methylenebis(2,6-dibromophenol) (**107**)

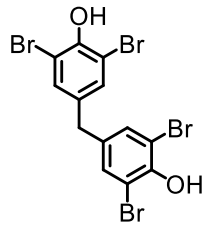

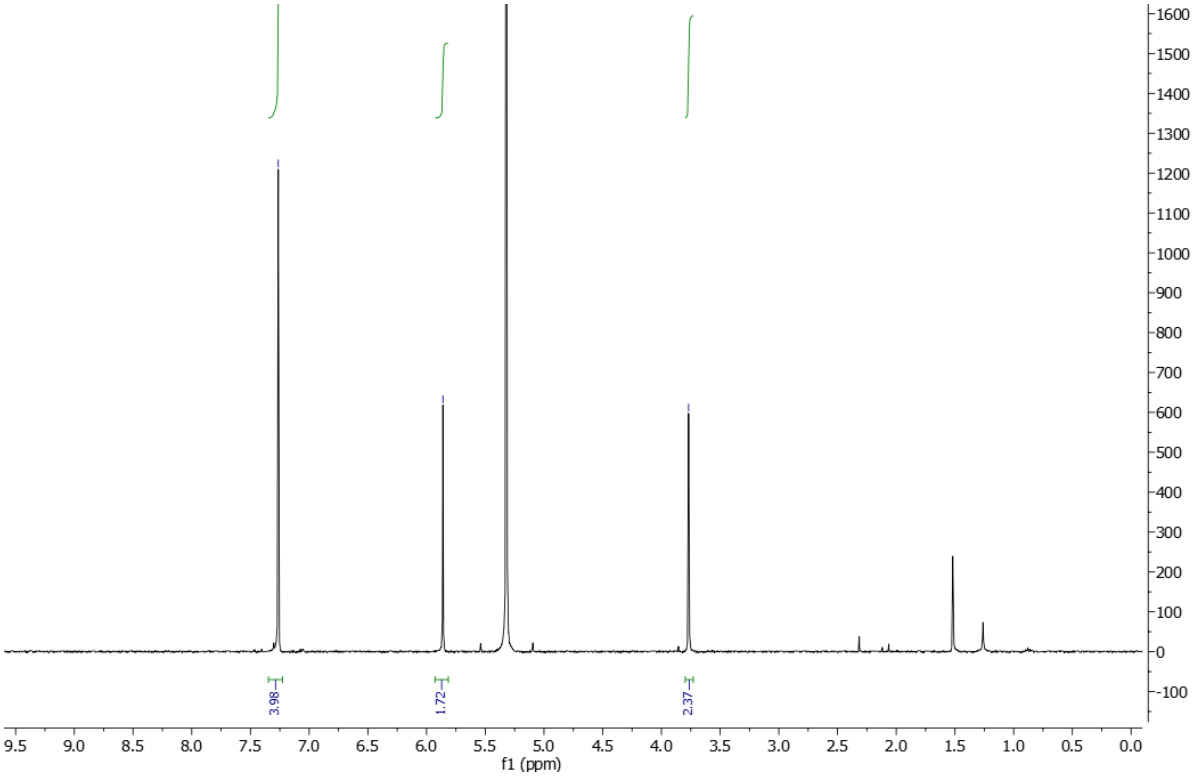

Figure 145. ^{1}H NMR spectrum of **107**

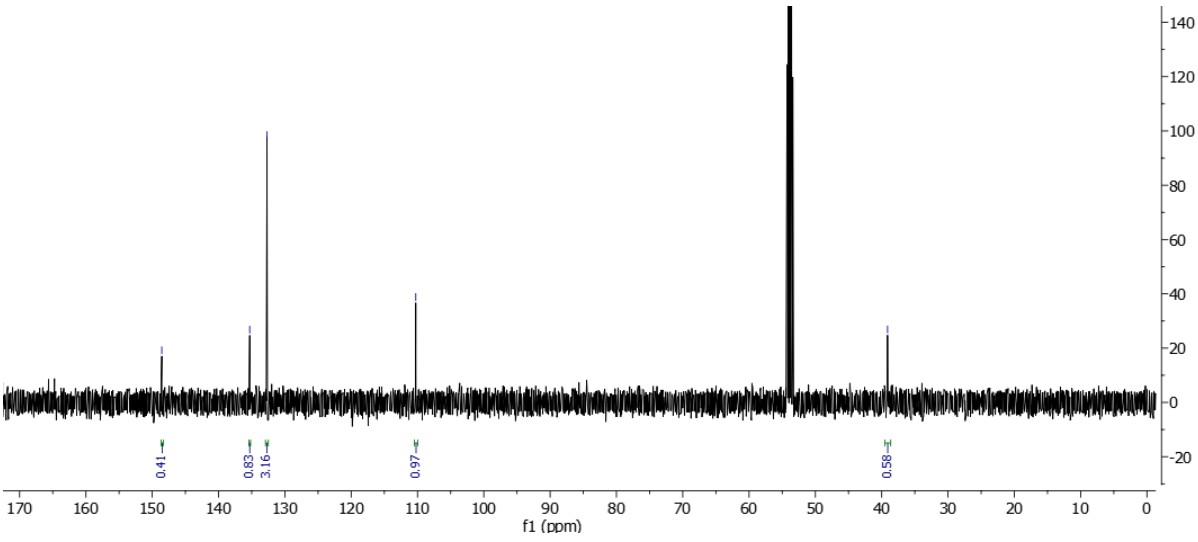

Figure 146. ^{13}C NMR spectrum of **107**

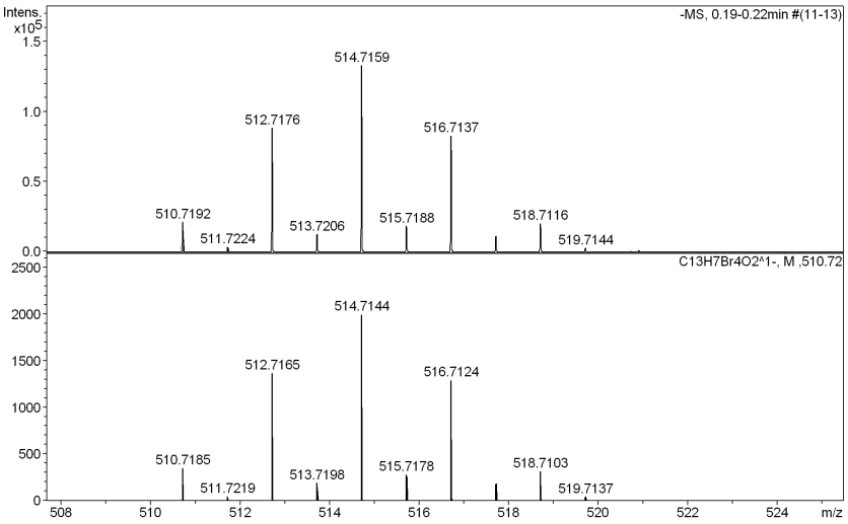

Figure 147. High resolution ESI spectrum of **107**

4,4'-methylenebis(2,6-dibromoaniline) (**143**)

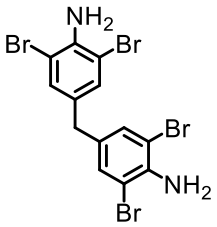

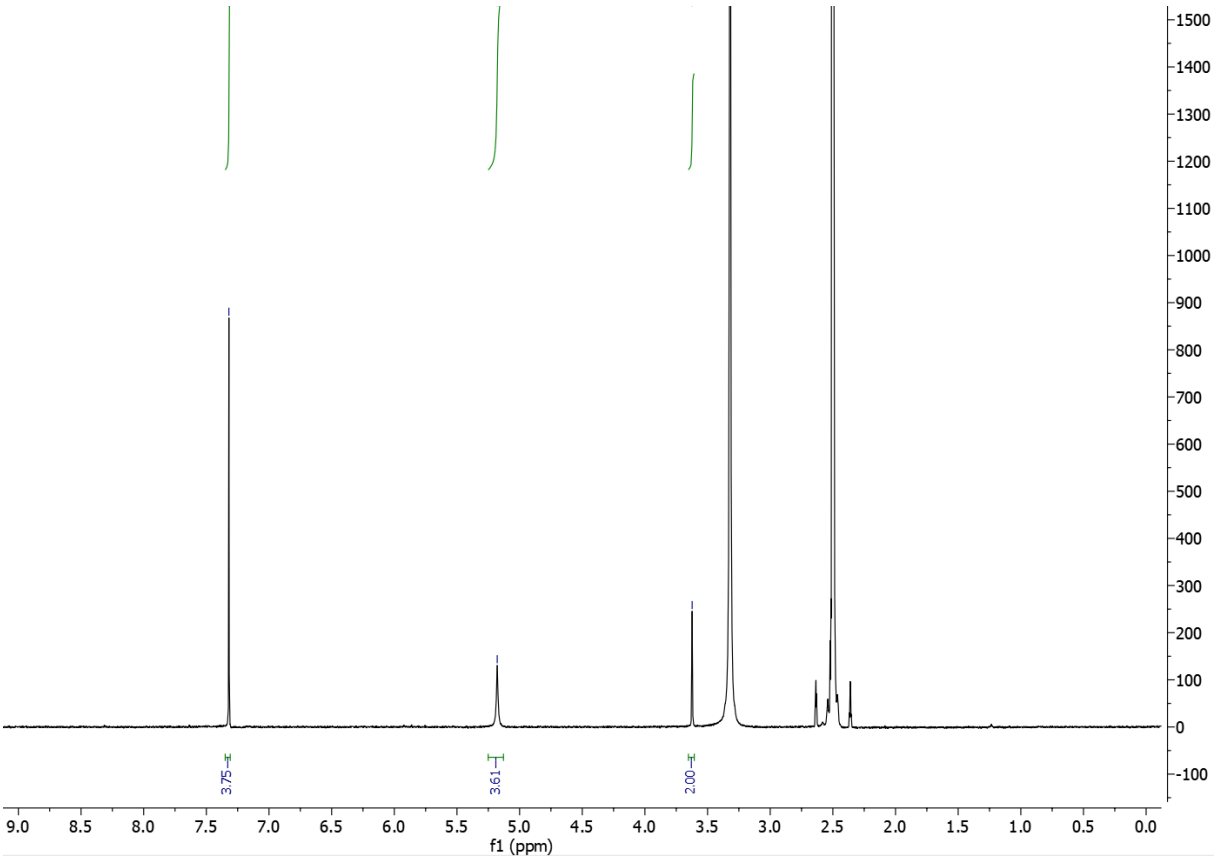

Figure 148. ^{1}H NMR spectrum of **143**

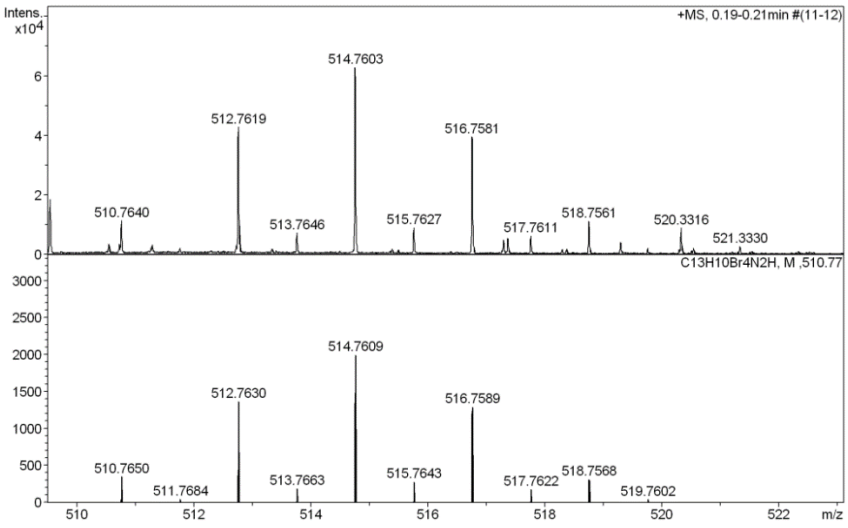

Figure 149. High resolution ESI spectrum of **143**

bis(3,5-dibromophenyl)methane (**144**)

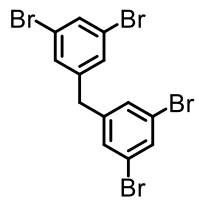

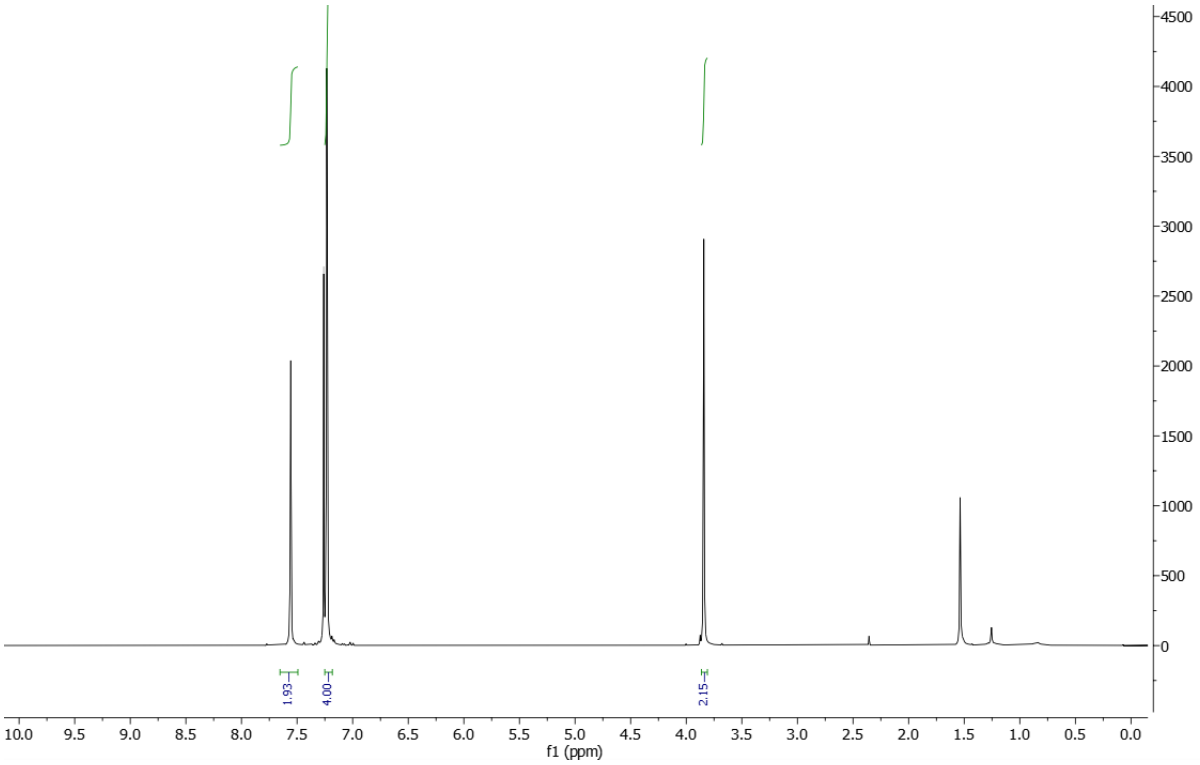

Figure 150. ^{1}H NMR spectrum of **144**

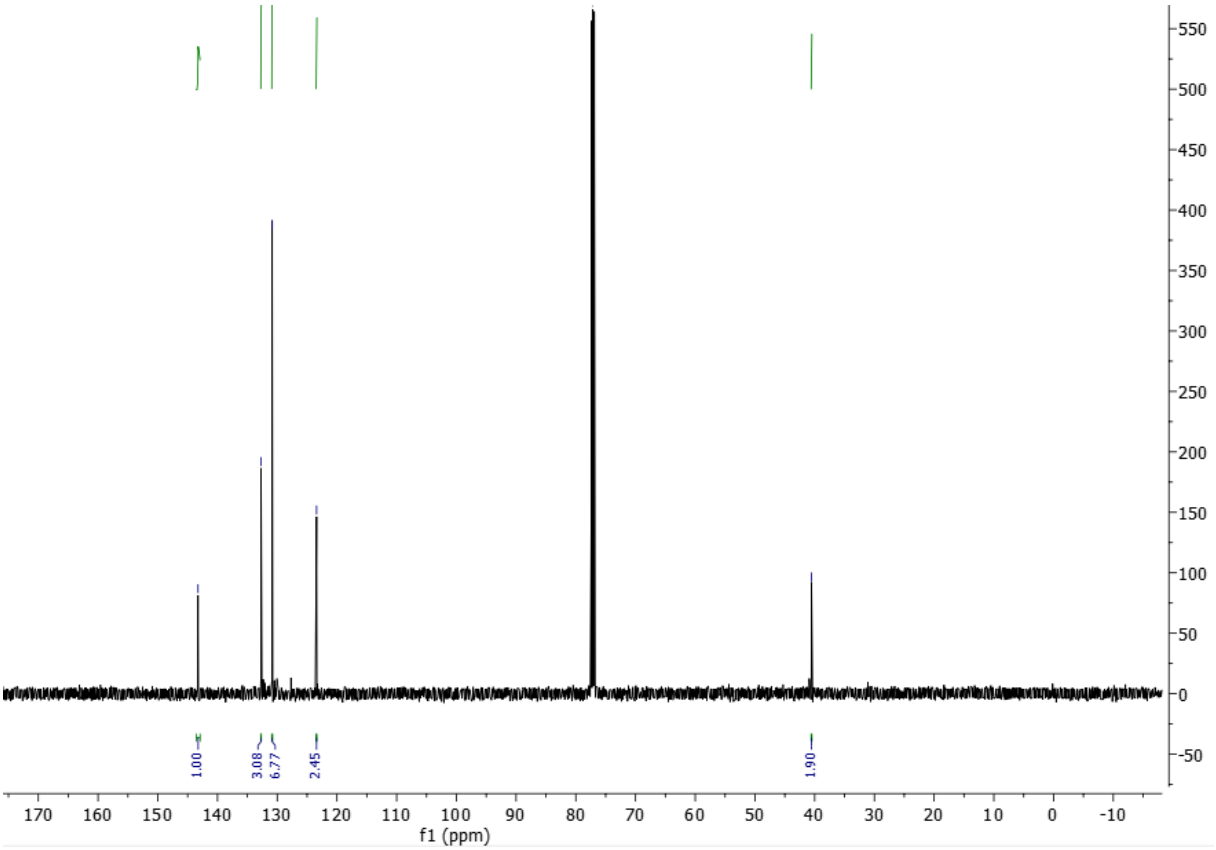

Figure 151. ^{13}C NMR spectrum of **144**

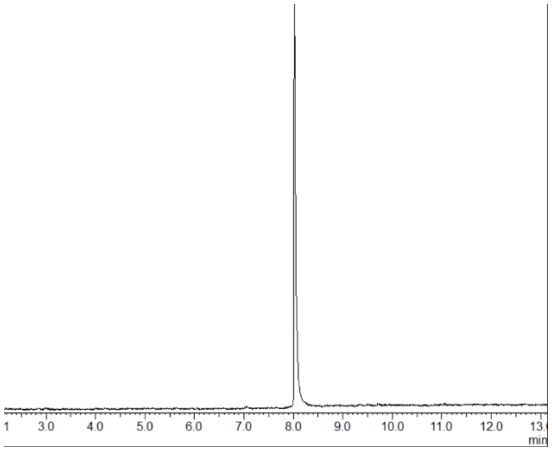

Figure 152. GC chromatogram of **144**

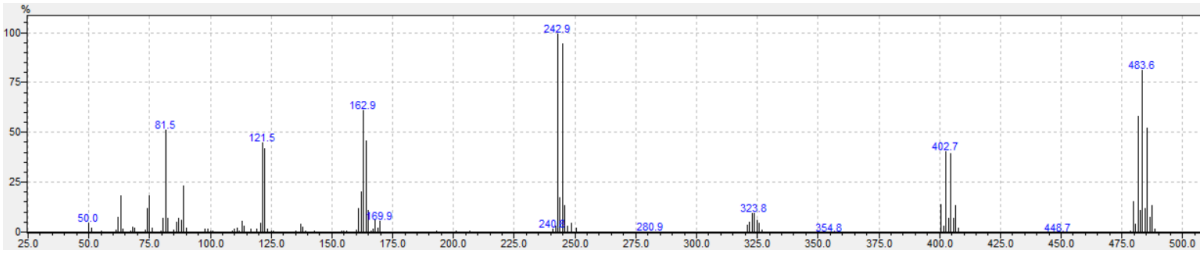

Figure 153. EI spectrum of **144**

5,5'-methylenebis(3-bromobenzaldehyde) (**105**)

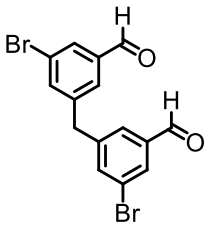

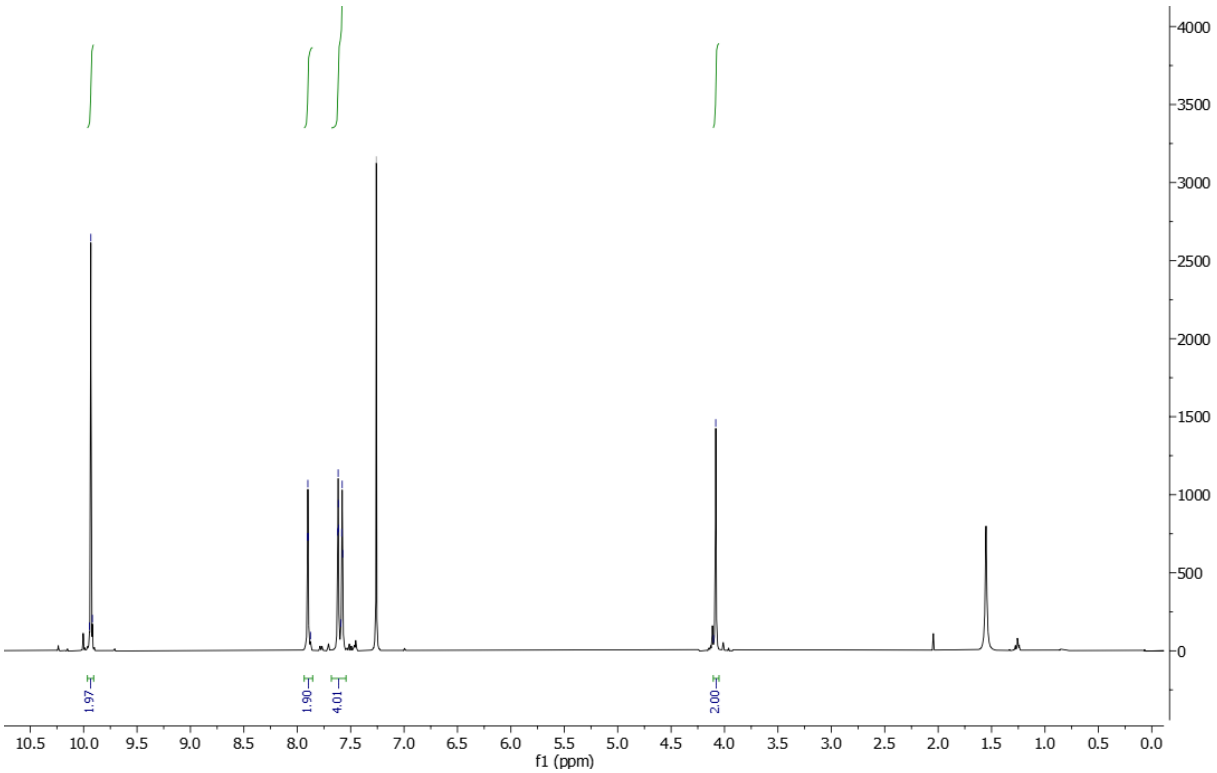

Figure 154. ^{1}H NMR spectrum of **105**

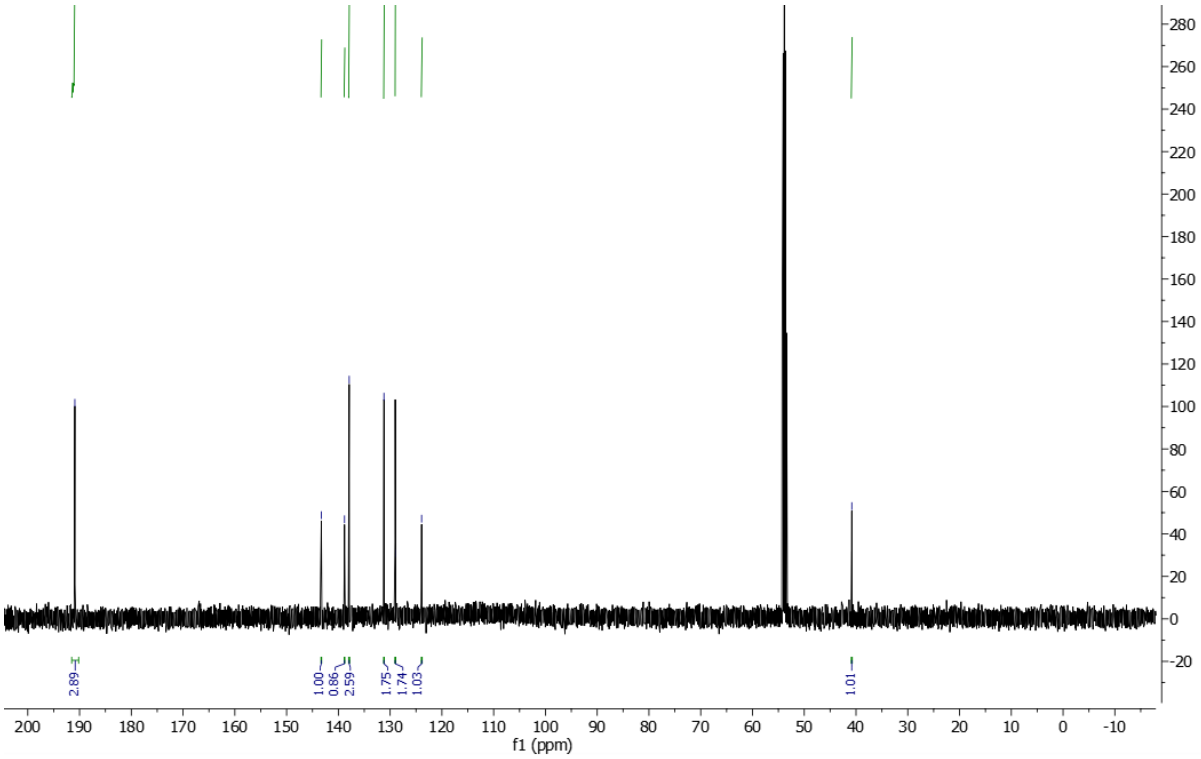

Figure 155. ^{13}C NMR spectrum of **105**

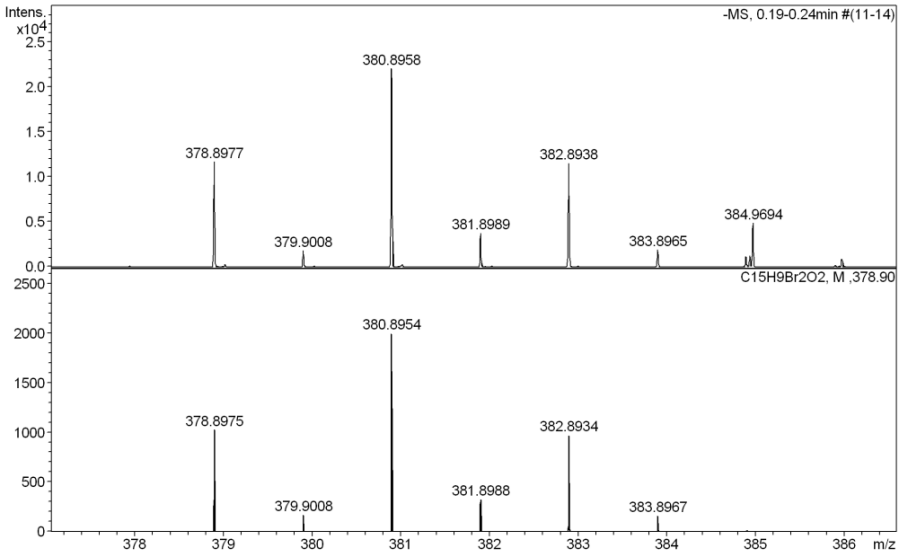

Figure 156. High resolution ESI spectrum of **105**

Methylenespherophane derivative (**88**)

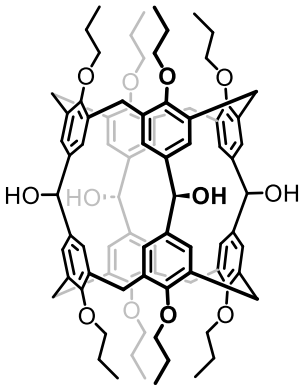

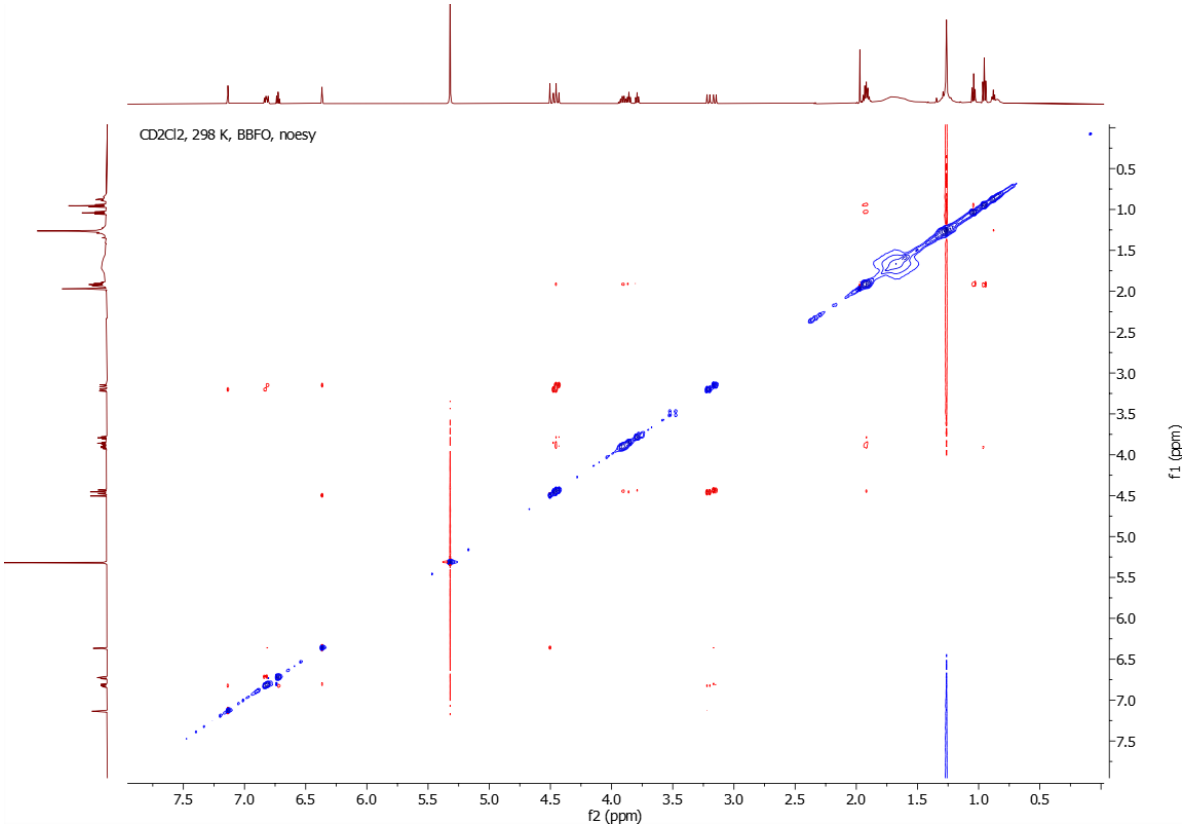

Figure 157. NOESY spectrum of **Table 2 entry 5**

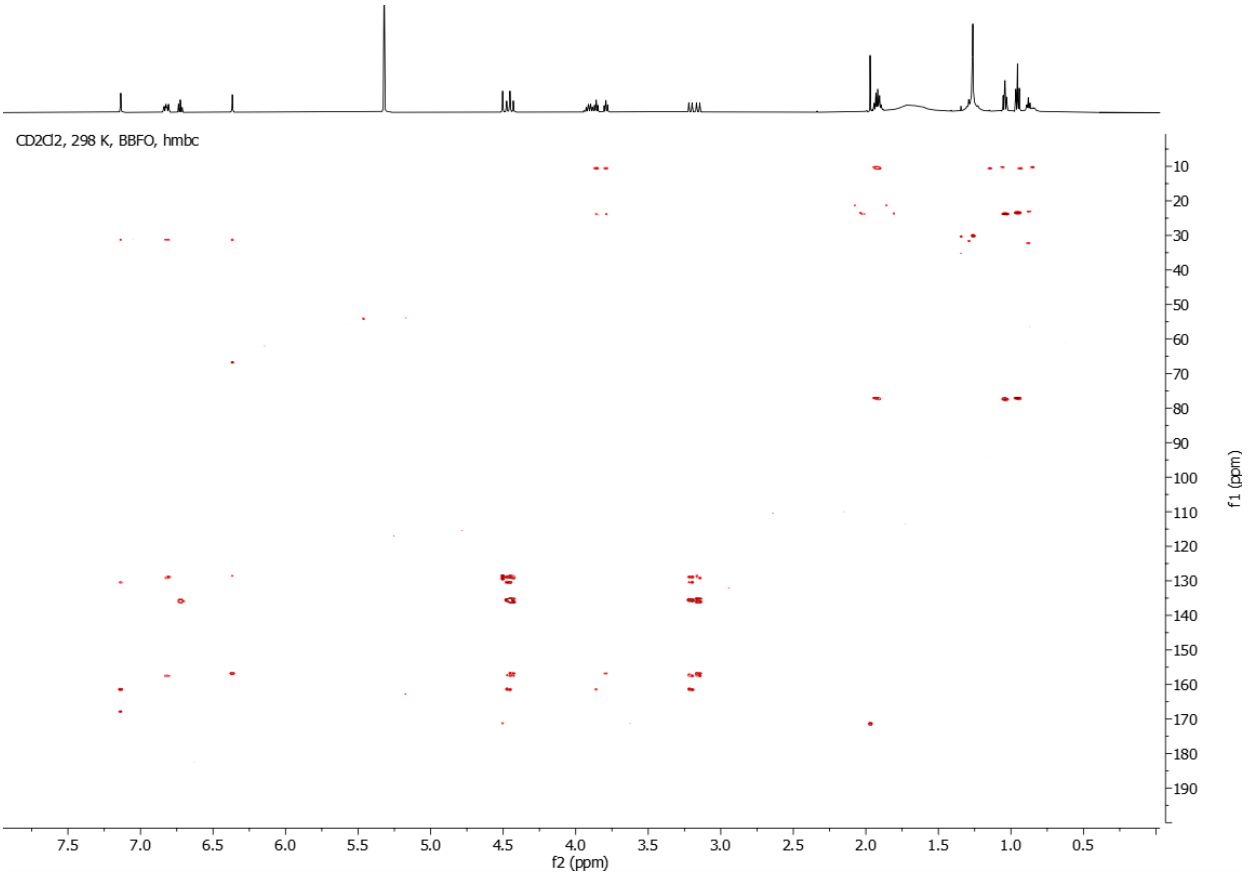

Figure 158. HMBC spectrum of **Table 2 entry 5**

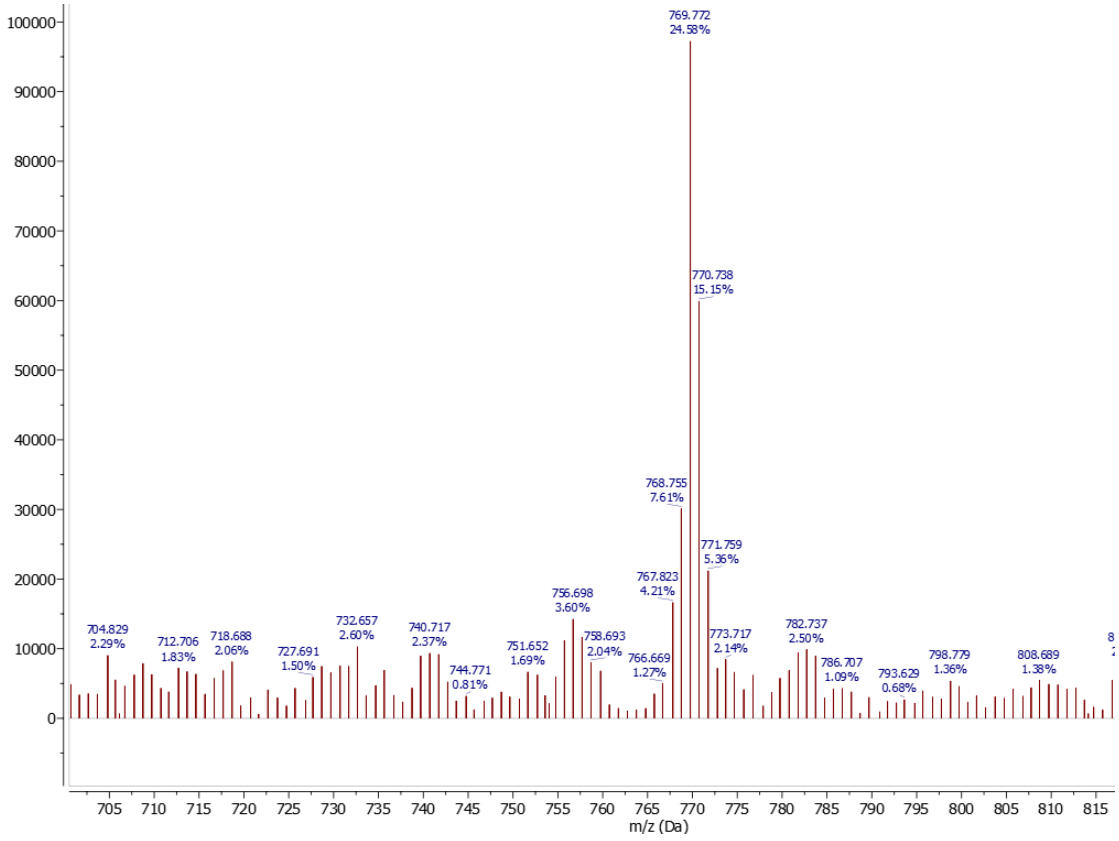

Figure 159. MALDI-TOF spectrum of reduction attempt **Table 2 entry 6**

small methylenespherophane precursor (**104**)

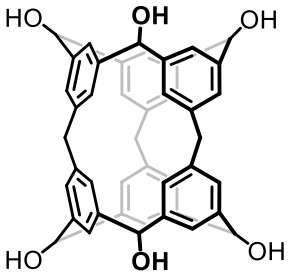

measurements in DMSO-d_6:

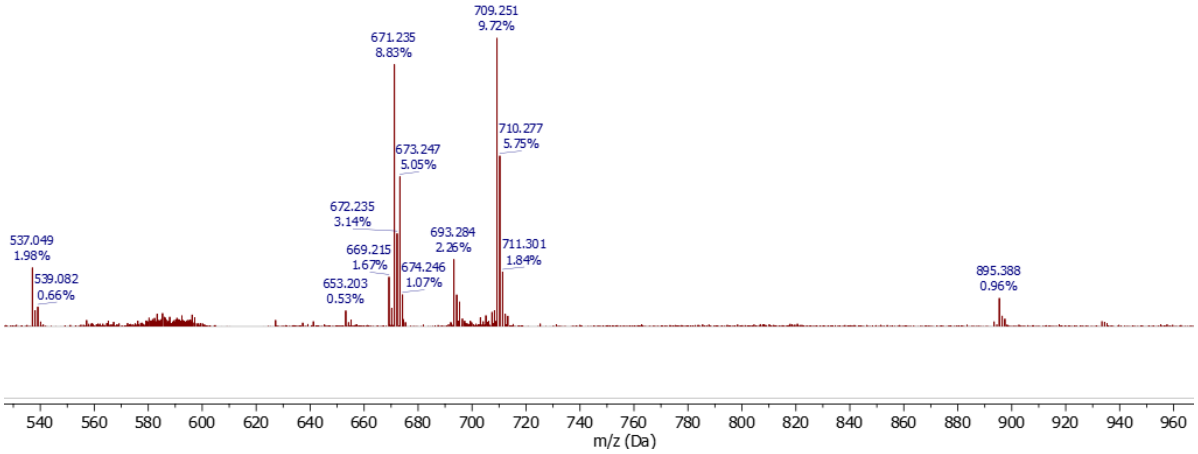

Figure 160. MALDI-TOF spectrum (mode: reflective negative) of inconclusive **104** fraction, measured in DMSO-d_6.

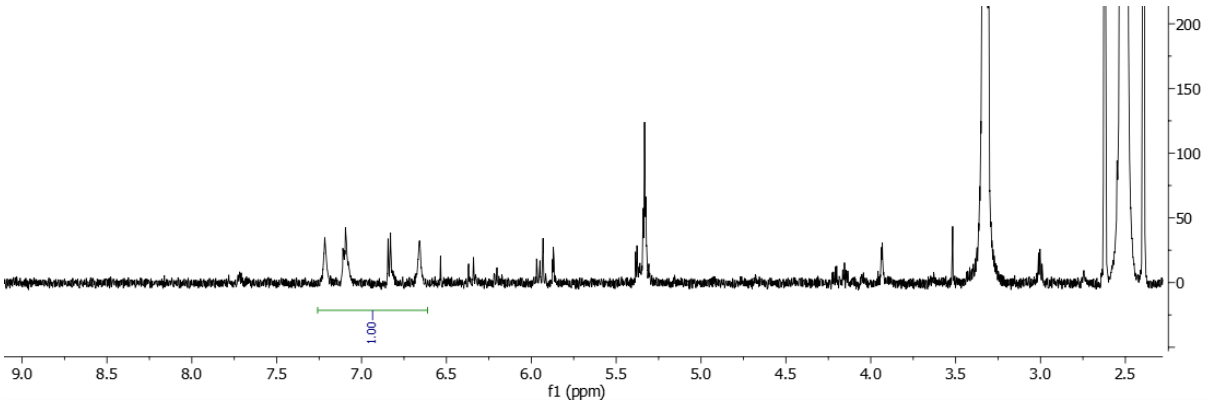

Figure 161. ^{1}H-NMR spectrum of inconclusive **104** fraction, measured in DMSO-d_6.

measurements in D_2O:

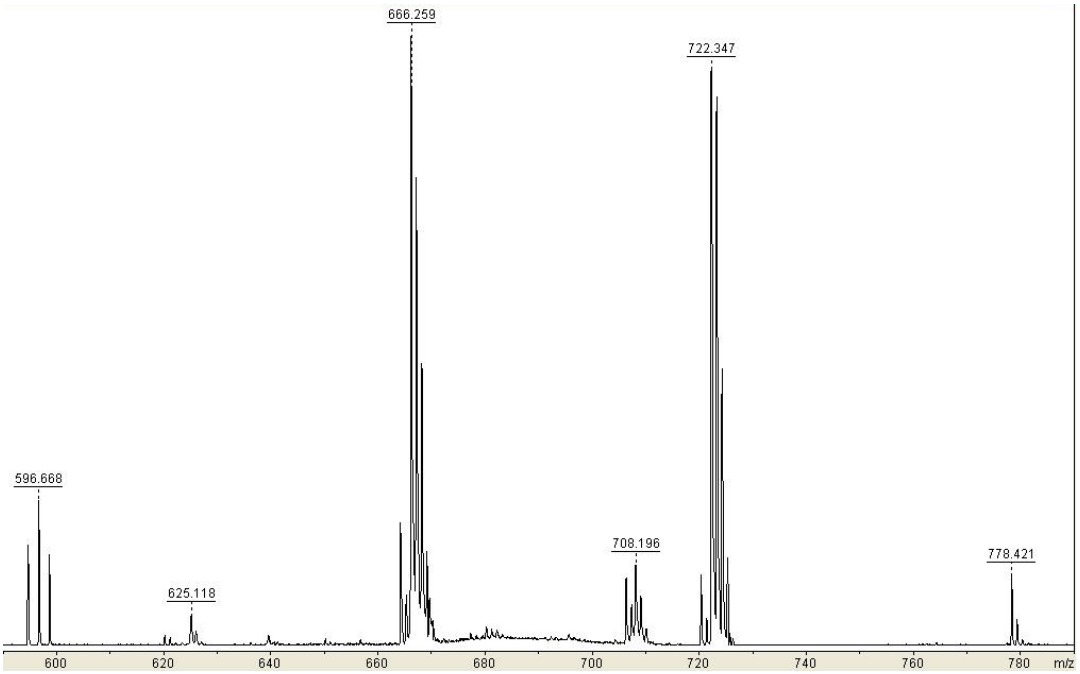

Figure 162. MALDI-TOF spectrum (mode: reflective negative) of inconclusive **104** fraction, measured in D_2O.

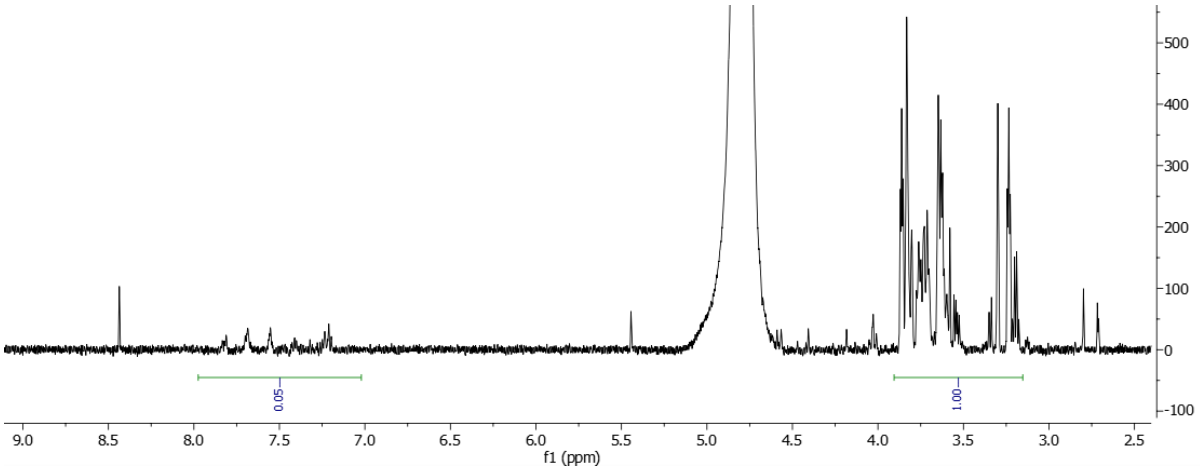

Figure 163. ^{1}H-NMR spectrum of inconclusive **104** fraction, measured in D_2O.

Square pyramidal shaped cage molecule, porphyrinogen (**109**)

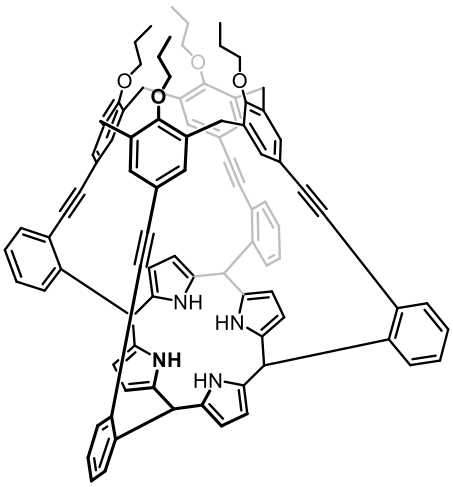

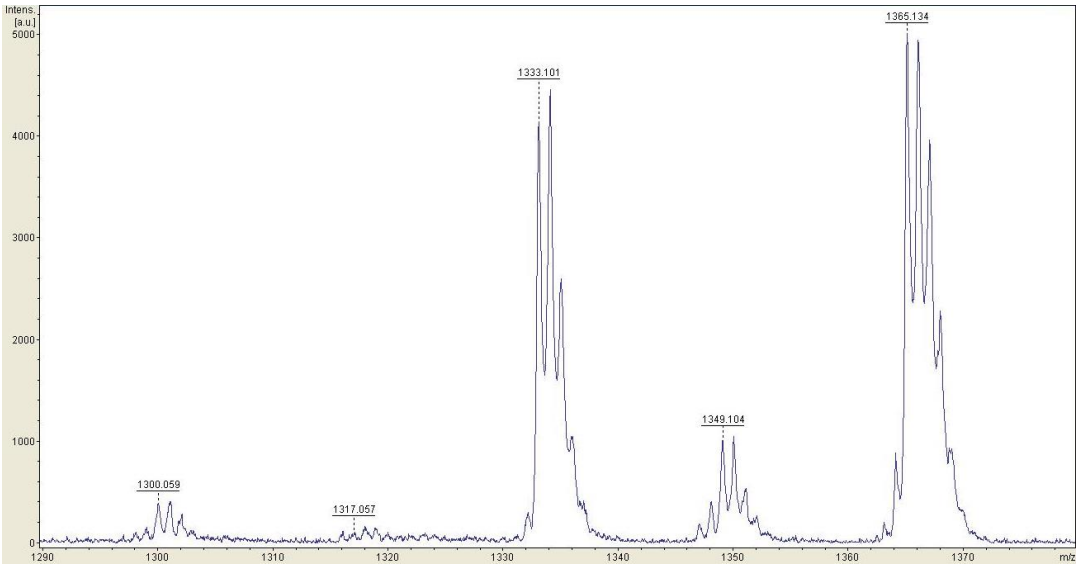

Figure 164. MALDI-TOF spectrum of fourfold oxygen loss.

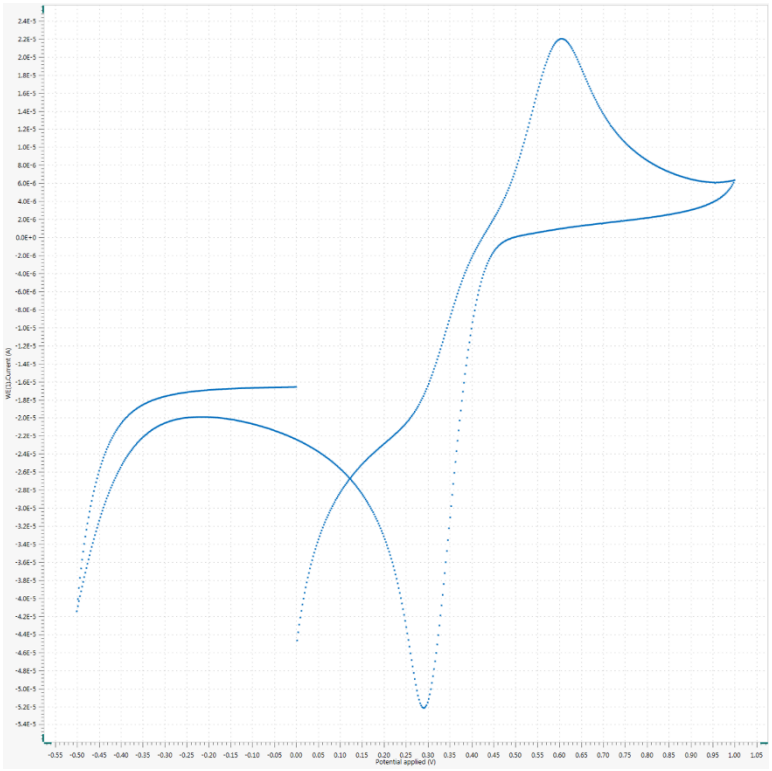

Figure 165. CV conditions **Table4 entry 2**

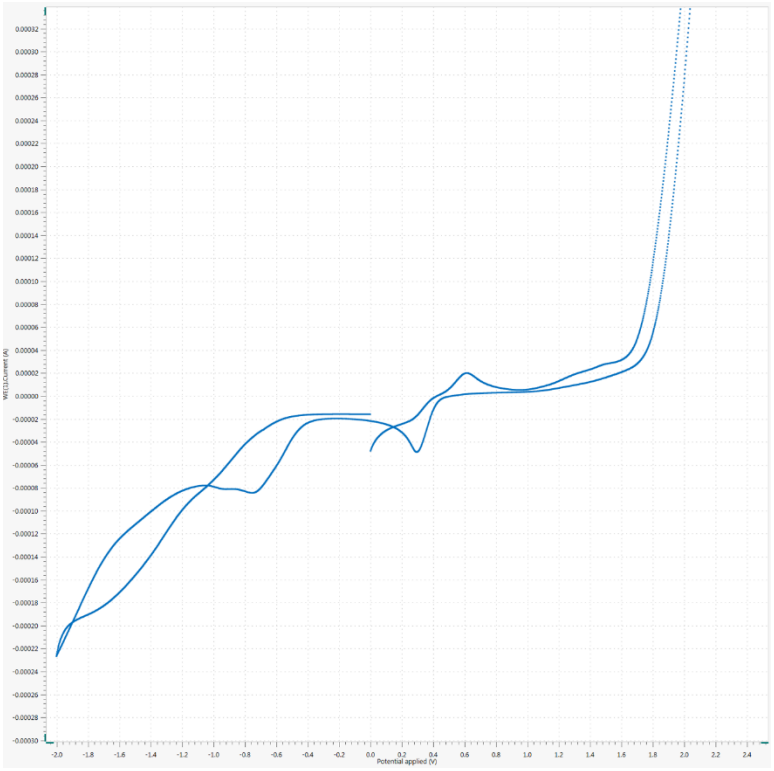

Figure 166. CV conditions **Table4 entry 4**